Tethered Axial Coordination as a Control Modality in Rhodium(II)-Catalyzed Carbene Transfer Reactions

A Dissertation Presented for the

Doctor of Philosophy

Degree

The University of Tennessee, Knoxville

Anthony Dean Abshire

December 2022

This dissertation is dedicated to my mother, Diane Abshire. Although you could not be here to see me finish, you always knew I could accomplish whatever I put my mind to.

Acknowledgments

Upon reflecting on my graduate experience, it is apparent that many people have helped me tremendously on this journey. No individual has help me on this journey more than my advisor, Dr. Ampofo Darko. Without his patience, understanding, and mentorship, completion of this journey would not have been possible.

I would also like to thank the members of my graduate committee: Dr. Michael Best, Dr. Konstantinos Vogiatzis, and Dr. Steven Chmely. The standards you all have set and advise you have given have been invaluable to my development throughout.

Additionally, I would like to thank the teachers and professors that helped me develop my passion for chemistry and as an individual capable of taking on the challenge of graduate school. I would like to begin by thanking Dr. Matthew Donahue, my undergraduate research advisor. He allowed me to travel around the country to discuss my undergraduate research and gave me the first insight into what graduate school would be like. Dr. Julia Pigza took the time to sit down and discuss elucidation techniques in-depth and never allowed me to hide from questions during group meetings during my undergraduate research experience. I would like to thank Dr. David Rankin, my organic chemistry professor, for helping me realize my passion for chemistry and all I could accomplish if pursued it as a career. Lastly, I would like to thank Bert Nokes for believing in me when I did not believe in myself. He still encourages me today to be the best person I can possibly be.

I would also like to thank the members of the Darko Research Group. Dr. Bradley Anderson, Dr. Derek Cressy, William Sheffield, and Dr. Cristian Zavala have been critical in helping me develop a thorough understanding of the many projects I have been a part of. Eric Fussell, Desiree Moore, and Caleb Garrett have been supportive and offered many

general chemistry discussions encompassing numerous topics. All of which were greatly appreciated.

I would also like to thank my family. My wife Dr. Erin Abshire has been nothing but supportive along this journey and I could not have completed this without her by my side. I would like to thank my mother, Diane Abshire, and my father, Mark Abshire, for always believing in me whether or not I believed in myself. I would like to thank my sister and brother-in-law, Theresa and Tarron Langston, for being more like my parents when my parents could not be. I would also like to thank my wifes mother and grandmother, Lisa Realini and Phyllis Beeching. Without their support, the transition to graduate school would have been impossible.

I would also like give a special acknowledgement to Dr. Justin Kirkland for our many discussions, his advice, and undying patience. He helped me develop my computational project and was also a great friend throughout graduate school. I know it was not easy to help a bench chemist with their understanding of computational chemistry.

Abstract

Dirhodium(II,II) paddlewheels, Rh(II), complexes are versatile carbene transfer catalysts that are broadly applied in insertion reactions, cycloadditions, and ylide transformations. The effects of axial coordination in Rh(II)-catalyzed carbene transfer reactions are still poorly understood due to compounding factors that are difficult to isolate. Traditionally, researchers study axial coordination by addition of Lewis base additives. To ensure interaction between the Lewis base and catalyst, high molar equivalents are often used. This can also have the undesired effect of hampering the activity of the catalyst and suppressing the yield of the reaction. We have developed ligands with a tethered thioether to overcome these issues. We found that the ligands with tethered thioethers can be selectively exchanged onto Rh_2OAc_4 to provide heteroleptic complexes with a thioether as the Lewis base. These compounds were then characterized by NMR, UV-vis, X-ray crystallography and cyclic voltammetry. The complexes were studied in cyclopropanation of olefins and silyl-hydrogen insertion reactions of donor/acceptor and donor diazo compounds. These results were compared to control catalysts to isolate the effects of the axially coordinating thioether. In cyclopropanations with ethyl diazoacetate, it was demonstrated that reactivity was affected by tether length and the substituent on the thioether. It was also found that complexes with the thioether tether afforded higher yields than the control catalysts. In silyl-hydrogen insertion reactions with methyl phenyl diazoacetate, it was found that the catalyst was selective toward diazo compounds with donating substituents and provided comparable yields otherwise. This result led us to study the catalyst in silyl-hydrogen insertions with hydrazone protected donor diazo compounds. It was found that the control catalyst outperformed the catalysts with thioether tethers. We proposed the catalyst is influenced by the axial coordination of

the dioxane solvent. Density functional theory calculations and geometry optimizations were performed to supplement the theoretical understanding of the role the tether has in reactivity. The calculations indicate donation of the axial ligand destabilizes the highest occupied molecular orbital of the catalysts and the resulting rhodium(II)-carbene intermediates.

Table of Contents

1 Introduction **1**

1.1 Silylation Reactions and the Significance of Organosilanes 1

1.2 Cyclopropanation Reactions and the Significance of Cyclopropanes 10

1.3 Introduction to Computational Methods Utilized 13

1.4 Research Question and Dissertation Organization 14

1.4.1 Research Question 14

1.4.2 Dissertation Organization 15

2 Heterolepticity and Axial Coordination as a Control Element in Rh(II)-Catalyzed Carbene Transfer Reactions **17**

2.1 Disclosure 17

2.2 Abstract 18

2.3 Introduction 18

2.3.1 Structural Features and Reactivity of Rh(II) Complexes 20

2.3.2 Ligand Environment 21

2.4 Synthesis of Heteroleptic Rh(II) Complexes 21

2.5 Rhodium(II) Paddlewheel Electronic Structure 36

2.6 Catalysts and Applications 45

2.6.1 Mixed Carboxylate Complexes 45

2.6.2 Ortho-metalated Phosphine Derived Complexes 53

2.6.3 Mixed Phosphate Complexes 57

2.6.4 Mixed Carboxylate/Carboxamidate Complexes 59

2.6.5 Immobilized Complexes . . . 65
2.6.6 Dirhodium Metallopeptide Complexes . . . 70
2.6.7 Complexes with Additives for Axial Coordination . . . 74
2.6.8 Mixed Complexes with Tethered Axial Coordination . . . 86
2.7 Conclusion . . . 90

3 Effect of Tethered, Axial Thioether Coordination on Rhodium(II)- Catalyzed Silyl–Hydrogen Insertion 93
3.1 Disclosure . . . 93
3.2 Abstract . . . 94
3.3 Introduction . . . 94
3.4 Results and Discussion . . . 98
3.4.1 Rh(II) Complex Synthesis . . . 98
3.4.2 UV-vis Complexes . . . 98
3.4.3 Si–H Insertion Optimization . . . 100
3.4.4 Si–H Insertion Substrate Scope . . . 102
3.4.5 Mechanistic and Computational Discussion . . . 102
3.5 Conclusions . . . 107
3.6 Experimental . . . 107
3.6.1 General Considerations . . . 107
3.6.2 Synthesis of Complex 89 . . . 108
3.6.3 Procedure for Si–H Insertion Reactions . . . 109
3.6.4 Silyl Product Yield Calculations . . . 109
3.6.5 Synthesis of Silane Products for Characterization . . . 109
3.6.6 Computational . . . 110

4 Rh(II)-Catalyzed Si–H Insertion of Nosyl Hydrazone Protected Donor Diazo Compounds 111
4.1 Disclosure . . . 111
4.2 Abstract . . . 111

4.3 Introduction . . . 112
4.3.1 Donor-type Diazo Compounds in Si–H and Related Group 14 Insertion Reactions . . . 118
4.4 Results and Discussion . . . 123
4.4.1 Si–H Insertion Optimization . . . 123
4.4.2 Si–H Insertion Substrate Scope . . . 125
4.4.3 Discussion . . . 127
4.5 Conclusion . . . 127
4.6 Experimental Procedures . . . 128
4.6.1 General Considerations . . . 128
4.6.2 Procedure for Silane Synthesis . . . 129
4.6.3 Silyl Product Yield Calculations . . . 129

5 Tuning Rh(II)-Catalyzed Cyclopropanation with Tethered Thioether Ligands 130

5.1 Disclosure . . . 130
5.2 Abstract . . . 131
5.3 Introduction . . . 131
5.4 Results and Discussion . . . 134
5.4.1 Microwave Ligation Optimization . . . 136
5.4.2 Microwave Ligation Scope . . . 138
5.4.3 Crystallography of Complexes . . . 138
5.4.4 UV-vis of Complexes . . . 141
5.4.5 Cyclopropanation Optimization . . . 141
5.4.6 Cyclopropanation Scope . . . 145
5.4.7 Cyclic Voltometry of Complexes . . . 145
5.4.8 Computational Study of Metal Carbenoids . . . 148
5.5 Conclusions . . . 157
5.6 Experimental . . . 158

5.6.1 General Considerations . . . 158
5.6.2 Ligand Synthesis . . . 158
5.6.3 General Microwave Conditions . . . 159
5.6.4 General Procedure for Microwave Reactions . . . 160
5.6.5 General Procedure for the Cyclopropanation of Olefin Substrates with 107 . . . 162
5.6.6 Computational . . . 162

6 Chiral Rh(II) Complexes with Tethered, Axially Coordinated Ligands (TACLs) Improve Asymmetric Cyclopropanation with Methyl Phenyldiazoacetate 164

6.1 Disclosure . . . 164
6.2 Abstract . . . 165
6.3 Introduction . . . 165
6.4 Results and Discussion . . . 169
6.4.1 Ligand Synthesis . . . 169
6.4.2 Complex Synthesis . . . 169
6.4.3 Asymmetric Cyclopropanation . . . 171
6.4.4 Discussion . . . 174
6.5 Conclusion . . . 174
6.6 Experimental Procedures . . . 175
6.6.1 General Considerations . . . 175
6.6.2 Ligand Synthesis . . . 175
6.6.3 Complex Synthesis . . . 176
6.6.4 Aysmmetric Cyclopropanation . . . 178

7 Conclusion 179

Appendices 216

Vita 241

List of Tables

3.1 Catalyst screening of Si–H insertion of methyl phenyl diazoacetate. 101

3.2 Si–H insertion substrate scope 103

4.1 Reaction optimization of Si–H insertion of hydrazone 104a with dimethylphenylsilane over a 24hrs. 124

5.1 Optimization of microwave synthesis parameters for Rh(II) complex synthesis 137

5.2 Catalyst screening for the cyclopropanation of styrene with 40. 144

5.3 Bond lengths and Natural Population Analysis of carbenoids 116 and 117. . 153

5.4 Natural Population Analysis and Wiberg index values for the calculated mechanism of N_2 extrusion of 40 with complexes 3, 87, and 89. 154

6.1 Asymmetric cyclopropanation of styrene with methyl phenyldiazoacetate. . . 173

List of Figures

1.1 a) Stabilization and activation of organosilanes due to orbital symmetry. b) Selective carbanion formation with organosilane reagent. c) Nonselective carbanion formation with resulting in mixed products. d) Utilization of organosilane reagent for a tetracyclic intermediate of progesterone in high yield. 3

1.2 First report of a Pd-catalyzed cross-coupling reaction with proposed mechanism. 4

1.3 Notable organosilane compounds and their activities. 6

1.4 More recently developed classes of reactions to form organosilanes. 7

1.5 General mechanism of Rh(II) catalyzed Si–H insertion reaction. 9

1.6 Notable examples of bioactive compounds featuring the cyclopropane moiety. 11

1.7 a) Common strategies to form cyclopropanes. b) General mechanism of the Rh(II)-catalyzed cyclopropanation reaction. 12

2.1 General structure of Rh(II) paddlewheel complexes. 19

2.2 Ligand arrangements of Rh(II) paddlewheel complexes. 22

2.3 General notation for heteroleptic Rh(II) complexes. Shown with heteroleptic carboxylate bridging ligands. 23

2.4 Mechanism of ligand exchange reactions of Rh(II) paddlewheel complexes. Shown with carboxylate ligands. 25

2.5 Possible products in the synthesis of heteroleptic complexes by ligand exchange. Shown with mixed carboxylate/carboxamidate ligands as an example. 26

2.6 Maximizing yields of heteroleptic Rh(II) complexes through multi-cycle sequences of ligand exchange reactions. 28
2.7 Ligand exchange with triphenylphosphine and $Rh_2(OAc)_4$ to produce orthometalated phosphine Rh(II) complexes. Two-fold exchange is preferred and the *cis-anti* isomer 4 or *cis-syn* isomer 5 can synthesized depending on conditions. 29
2.8 Examples of dicarboxylic acid ligands that preferentially form bis-chelated heteroleptic complexes. 30
2.9 Synthesis of heteroleptic complexes 8 and 9 via three-fold ligand exchange with *R*-TPCP ligand. 32
2.10 Ligand exchange reaction with pendant thioethers. 33
2.11 Synthesis of *cis* and *trans* isomers of $Rh_2(OAc)_2(tfa)_2$ 11. 34
2.12 Synthesis of partial paddlewheel complex 12, in which acetate ligands have been replaced with acetonitrile solvent (S = CH_3CN). 35
2.13 A qualitative molecular orbital diagram derived from the combination of the AOs of two square planar RhL_4 complexes to form $Rh_2(L–L)_4$ and further perturbation of the resulting energies by 2 axial ligands, L_{ax}. 38
2.14 a) The Lewis and molecular orbital depiction of H_2's bonding. b) The The Lewis structure and molecular orbital theory bonding models for the linear H_3^- anion. 40
2.15 a) The σ and π 3c/4e molecular orbitals for available for bonding with the Rh(II) carbenoid. b) Qualitative molecular orbital diagram for the Rh(II) carbenoid. 41
2.16 (a) Synthesis of heteroleptic dirhodium(II) carboxylates with phthaloylamino ligands. (b) Yields and selectivity of complex 1 versus $Rh_2(TCPTTL)_4$ in diazo-mediated cyclopropanation. (c) Non-covalent interactions on 1. 46
2.17 C–H insertion of 4-methyl-N-phenylindole with 17. 49
2.18 Cyclopropenation of trimethylsilylacetylene with 17. 50
2.19 C–H insertion of 4-methyl-*N*-phenylindole with 17. 51

2.20 Fox group synthesis of piperarborenine B using catalyst 21 in a tandem bicyclobutanation/homoconjugate addition as a key step. 52
2.21 Notable orthometalated phosphine Rh(II) catalysts. 54
2.22 Intramolecular selectivity studies with orthometalated phosphine complexes 24a and 24b compared to common homoleptic dirhodium (II,II) catalysts. . . 55
2.23 Selectivity for C–H insertion over β-elimination was best with monometalated complex 37. 56
2.24 Cyclopropanation with chiral orthometalated phosphine Rh(II) catalysts. . . 58
2.25 Synthesis of heteroleptic Rh(II) phosphate complexes (a) 43 and (b) 45. . . . 60
2.26 Tandem oxonium ylide/[2,3] sigmatropic rearrangement with homoleptic and heteroleptic Rh(II) phosphate complexes. 61
2.27 Cyclopropenation of alkynes using $Rh_2(DPTI)_3(OAc)$. 63
2.28 Features of mixed-ligand glycoluril/carboxylate Rh(II) complex 51. 64
2.29 (a) Synthesis and features of $Rh_2(R\text{-TPCP})_3(acam)$ (52). (b) Cyclopropanation of 4-methoxy styrene with stannylated diazo 53 using 52 as catalyst. . . 66
2.30 Immobilised chiral Rh(II) catalysts. 68
2.31 (a) Cyclopropanation of styrene with diazo 58 using immobilized catalyst 55. (b) Synthesis of diazo compounds and enantioselective C–H functionalization in flow. 69
2.32 (a) Synthesis of artificial metalloenzymes that incorporate complex 63. (b) Enantioselective cyclopropranation catalyzed by Rh(II) metalloenzyme POP-ZA4-HFF-63. 71
2.33 (a) Biotinylated Rh(II) complex 67 incorporated into a streptavidin scaffold. (b) Comparison of TON using Rh(II) catalysts alone and in the presence of wild type streptavidin (Sav WT). 73
2.34 Rh(II) peptide catalyst 68 and its use in enantioselective cyclopropanation of olefin. 75
2.35 Gram scale synthesis of ascomycin derivative. 77

2.36 Evaluation of the $Rh_2(TBSP)_4$ catalyzed cyclopropanation of methyl phenyldiazoacetate and styrene in SCF fluoroform. 78
2.37 The $Rh_2(TPA)_4$ catalyzed enantioselective O–H insertion of H_2O with 72. . . 79
2.38 a) $Rh_2(S\text{-NTTL})_4$ catalyzed cyclopropanation of α-cyano diazo 74 and styrene in toluene. b) $Rh_2(S\text{-NTTL})_4$ catalyzed cyclopropanation of α-cyano diazo 74 and styrene in DCE. c) Active Rh(II) adduct at different temperatures. . 81
2.39 Metallopeptide catalyzed Si–H insertion with triphenylphosphite additive. . . 82
2.40 a) Adduct 76 formed in solution from 2 equivalents of DMAP and CH_2Cl_2. . 84
2.41 a) Species of catalyst that exist in solution. b) $Rh_2(TCPTCC)_4$-catalyzed [3+6+3+6] macrocyclization on a 20g scale. 85
2.42 (a) Synthesis of complex 83 from ligand 82. (b) C–H insertion of 1-methyl indole with diazo 72 using 83 compared to 3. (c) Range of yields of C–H insertion of functionalized indoles using complex 83. 87
2.43 Heteroleptic complexes with tethered, axially coordinating thioether ligands (85, 87, and 88) and their control complexes (86 and 89). 89
2.44 a) Synthesis of complex 92 and 93 depending on equivalents of ligand 91. b) Synthesis of cyclopropane 95 using catalysts 92 and 93 compared to conventional Rh(II) catalysts 3 and 6. 91

3.1 Features of a dirhodium carboxylate complex. 95
3.2 (Top) Cyclopropanation with dirhodium complexes featuring tethered, axially coordinated thioether ligands. (Bottom) Investigating silyl–hydrogen insertion reactions using mixed oxazolidinate/carboxylate dirhodium complexes. . 97
3.3 Ligand exchange with ligand 97 to produce complex 89. 99
3.4 Frontier molecular orbital, HOMO-LUMO gap, and frontier orbital perturbation comparison for complexes 87 and 89 calculated at the M06-2X/def2-TZVPP level of theory. Hydrogens were removed for clarity. 104
3.5 Full molecular orbital diagram calculated for 87 and 89 calculated at the M06-2X/def2-TZVPP level of theory. Hydrogens were removed for clarity. 106

4.1 Classification of diazo compounds. 113
4.2 The reactivity trend of diazo compounds and metal carbenoids. 114
4.3 a) Rh(II) carbenoids 100 and 101 Fürstner published crystal structures of. b) Rh(II) carbenoid 102 studied spectroscopically be Davies. 115
4.4 a) Proposed mechanism of Bamford-Stevens reaction in polar aprotic solvent using a moderate base. b) Proposed mechanism of Bamford-Stevens reaction in polar protic solvent using a strong base. c) Proposed mechanism of the Shapiro reaction. 117
4.5 a) Silver(I) triflate catalyzed Si–H insertion of nosyl-protected hydrazones. b) Iron porphyrin catalyzed Si–H insertion of tosyl-protected hydrazones. 119
4.6 Palladium catalyzed Si-H insertion of tosyl-protected hydrazones with proposed mechanism. 120
4.7 a) First example of Rh(II)-catalyzed Si–H insertion of diaryl diazo compounds with chiral silanes. b) Enantioselective Si–H insertion diaryl diazo compounds with chiral Rh(II) spiro-phosphate complex 103. c) Enantioselective Si–H insertion of trisyl-protected alkynyl hydrazones with complex 103. 121
4.8 Hydrazone substrate scope of Si–H insertion 126

5.1 General structure of Rh(II) carboxylate (X = O) and carboxamidate (X = N) complexes. 132
5.2 Dirhodium complexes with tethered, axial coordination in diazo-mediated applications. 135
5.3 Complexes synthesized *via* microwave method. 139
5.4 X-Ray structure of complex 107 with thermal ellipsoids at 50% probability. Only two of the four molecules in the asymmetric unit is shown. Selected bond lengths and angles as an average of the four structures of the asymmetric unit: Rh–Rh 2.42 Å, Rh–S 2.50 Å, Rh–N_2 2.24 Å, Rh–Rh–S 175.5°. 140
5.5 UV-vis spectrum of complexes 87, 106, 107, and 108. 142

5.6 107-catalyzed cyclopropanation with 40. Yields are averaged over 2 runs and calculated by ^{1}H NMR except for compounds 109 and 114. Performed at 25 °C. 146
5.7 Cyclic voltammograms of complexes 87, 89, 106, 107, and 108. Electrolyte comprised of 0.1 M [TBA][PF6] in DCM (scan rate of 100 mV s^{-1}). 147
5.8 Molecular orbitals of complex 107 in comparison to 89 calculated at the M06-2X/def2-TZVPP level of theory. 149
5.9 Calculated orbitals and energies of 40 carbenoid species 116 and 117. Calculated at the M06-2X/def2-TZVPP level of theory. 150
5.10 Comparison of the coordination and transition state energy differences during the extrusion of N_2 of 40 with complexes 3, 87, and 89 calculated at the M06-2x/def2-TZVP level of theory. 155

6.1 a) General structure of chiral Rh(II) carboxamidate complex. b) General structure of Rh(II) carboxylate complex with phthalimide-protected amino acid ligands. c) General structure of Rh(II) carboxylate with chiral cyclopropyl ligands. 166
6.2 (Top) Cyclopropanation with achiral Rh(II)-carboxylate complex featuring a tethered, axially coordinating thioether ligand. (Bottom) Cyclopropanation Chiral Rh(II) complexes with chiral tethered, axially coordinating thioether ligands. 168
6.3 a) Synthesis of ligand 121. b) Synthesis of ligand 126. 170
6.4 a) Synthesis of complexes 127a/b. b) Synthesis of complex 128. 172

1 ^{1}H NMR of complex 89. 217
2 ^{13}C NMR of complex 89. 218
3 ^{1}H NMR of complex 104c. 219
4 ^{13}C NMR of complex 104c. 220
5 ^{1}H NMR of complex 105c. 221
6 ^{13}C NMR of complex 105c. 222
7 ^{1}H NMR of complex 105f. 223

8 ^{13}C NMR of complex 105f. . . . 224
9 ^{1}H NMR of compound 121. . . . 225
10 ^{13}C NMR of compound 121. . . . 226
11 ^{1}H NMR of complex 126. . . . 227
12 ^{13}C NMR of complex 126. . . . 228
13 ^{13}C NMR of complex 127a/b. . . . 229
14 ^{1}H NMR of complex 127a/b. . . . 230
15 ^{1}H NMR of complex 128. . . . 231
16 ^{13}C NMR of complex 128. . . . 232
17 Molecular orbital diagram of 3 . . . 233
18 Molecular orbital diagram of 89 . . . 234
19 Molecular orbital diagram of 87 . . . 235
20 Molecular orbital diagram of 107 . . . 236
21 Molecular orbital diagram of carbenoid formed from 3 and 40 . . . 237
22 Molecular orbital diagram of carbenoid formed from 89 and 40 . . . 238
23 Molecular orbital diagram of carbenoid formed from 87 and 40 . . . 239
24 Molecular orbital diagram of carbenoid formed from 107 and 40 . . . 240

Chapter 1

Introduction

1.1 Silylation Reactions and the Significance of Organosilanes

Silicon is one of the most abundant atoms in the earth's crust, commonly cited as 24.6% of its measured mass. Organosilanes are important reagents in organic chemistry and have been sought after due to their prevalence in industrial products. The lack of naturally occurring organosilanes has presented an opportunity for the synthetic chemist to fill this void. The original methods to form silanes involved utilizing Grignard reagents, organozinc reagents, and organolithium reagents with electrophilic silanes, greatly limiting its functional group tolerance with potential electrophiles, such as esters, aldehydes, and halides. With these methods, formation of inorganic salts, poor atom economy, and toxicity of byproducts are also drawbacks. The diversification of methodology has been of interest since the first C–Si bond formation reported by Friedel and Craft in 1863.[1] Metal-catalyzed carbene transfer reactions have greatly diversified the scope of organosilanes that can be achieved, although it is not the only newly developed methodology. This section aims to introduce organosilanes as reagents, their uses in bioactive molecules and other industrial applications, and modern methodologies developed to achieve these compounds.

The reactivity of organosilanes is driven by their ability to stabilize α-carbanions and β-carbocations, activate π-bonds β to the silicon, selectively form carbanions faster than corresponding C–H deprotonation, and replace more toxic, highly reactive transmetalation reagents for transition metal mediated cross-coupling reactions. Organosilanes also can act as a protecting group for a hydroxyl groups and reduce carbonyl groups.[2] Neither of these processes utilize tetra-carbo-substituted silanes and will be excluded from this discussion.

The stabilization of α-carbanions is a result of donation from the electron density in the empty α-Cp orbital into the Si–C σ^* antibonding orbital (Fig. 1.1a). This delocalizes the electron density from the Cp orbital of the α carbons and decreases its nucleophilicity.[2] Stabilization of β carbocations by silanes is also known as the β silicon effect. This is a result of the C–Si σ bond donating electron density into the empty β Cp orbital (Fig 1.1a). The third effect the favorable orbital geometry of C–Si bonds is the activation of π systems β to the silicon atom. Much like the β silicon effect, the C–Si σ orbital is aligned with the filled C–C π orbital and can donate electron density into the π system, making it more nucleophilic.[2] This effect is also driven by the stabilization of the resulting β-carbocation by the β-silicon effect described above.

A classic example of the selectivity that can be imparted by silane-directed carbanion formation, as opposed to traditional acid/base chemistry, was presented by Pearce and Fleming.[3] When the acetal with a silane carbanion directing group was treated with a Lewis acid, only one product was formed (Fig. 1.1b). A corresponding acetal without the silane to direct carbanion formation was treated with a Lewis acid and resulted in a mixture of 4 products (Fig. 1.1c). The concept of silane directed carbanion formation was then utilized by Johnson *et al.*to form a tetracyclic intermediate of progesterone in high yield (Fig. 1.1d).

The ability of tetracoordinate organosilanes to participate in Pd-catalyzed cross-coupling was disclosed by Hiyama *et al.*[4] The benefit of a silane cross-coupling reagent to replace the more traditional boron reagents are increased stability and decreased toxicity. The formation of a highly coordinated silicate is deemed necessary for transmetalation to occur. In Hiyama's disclosure, vinyl- and alkynyl-(trimethyl)silanes were coupled with aryl iodides in the presence of catalytic amounts of palladium, or Pd, in high yield (Fig. 1.2).[4] The

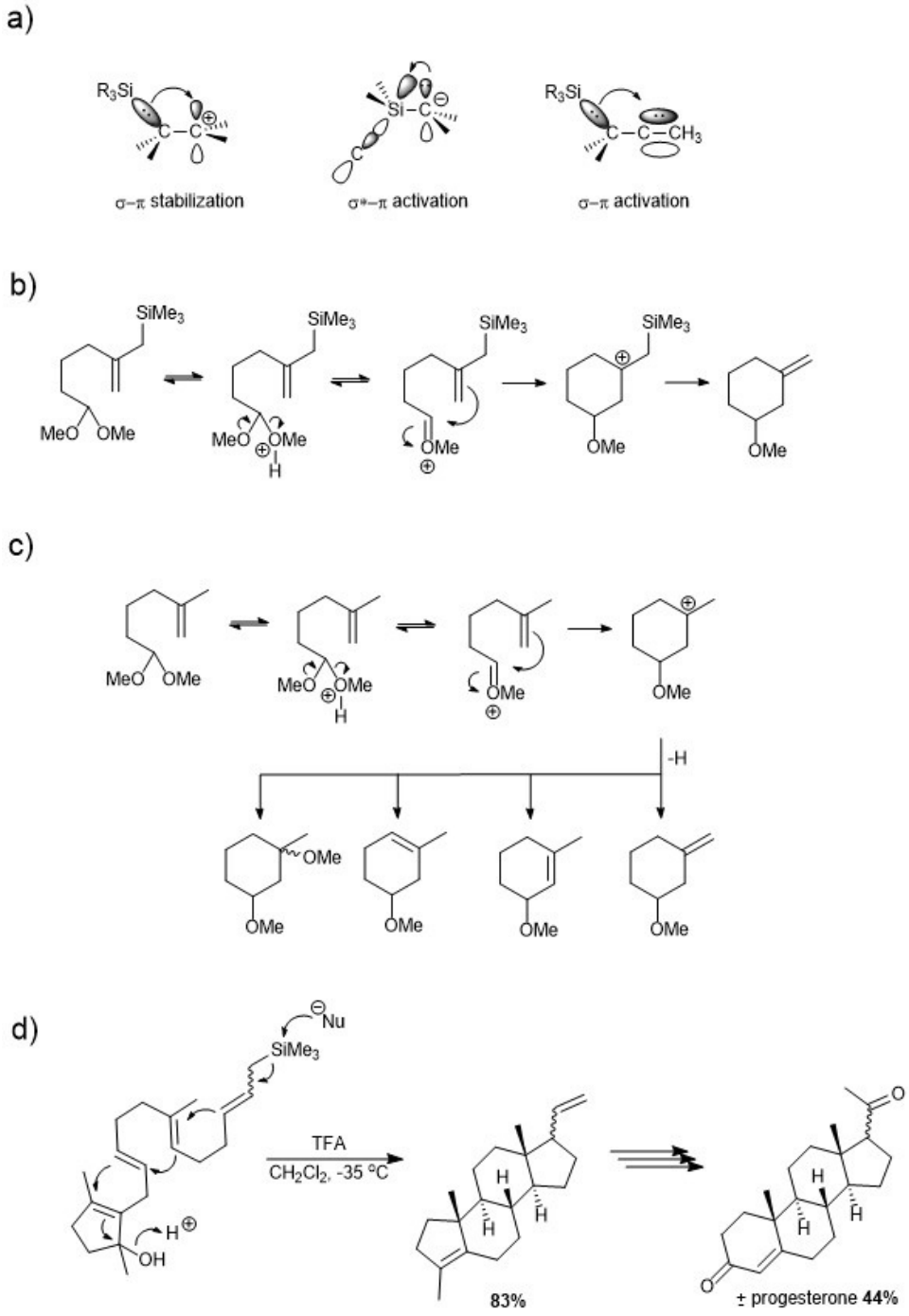

Figure 1.1: a) Stabilization and activation of organosilanes due to orbital symmetry. b) Selective carbanion formation with organosilane reagent. c) Nonselective carbanion formation with resulting in mixed products. d) Utilization of organosilane reagent for a tetracyclic intermediate of progesterone in high yield.

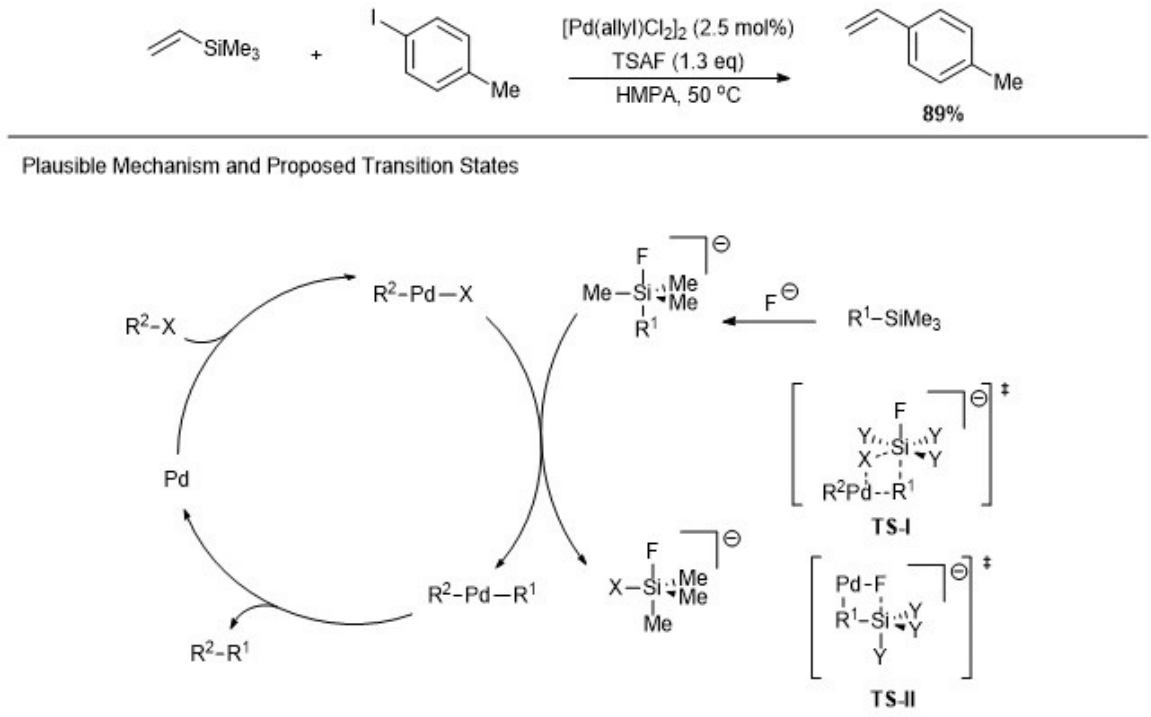

Figure 1.2: First report of a Pd-catalyzed cross-coupling reaction with proposed mechanism.

proposed mechanism of the cross-coupling reaction begins with the oxidative addition of R^2–X to the Pd(0). Then, transmetalation is of the hypervalent silicon species with the R^2–Pd(II)–X forms R^2–Pd(II)–R^1. This is followed by reductive elimination resulting in the R^2–R^1 product and Pd(0) catalyst. There are two proposed transition states for the transmetalation step of the Pd-catalyzed cross coupling reaction, TS-I and TS-II. TS-I is a more traditional transmetalation transition state and is supported by experimental evidence.[4] TS-II was proposed due to theoretical and electrochemical studies performed more recently.[5,6] Since this disclosure, many examples of organosilanes as coupling reagents in C–C bond forming cross-coupling reactions have been reported.[2]

The interest in organosilanes is also due to their ability to increase bioactivity and their application in other industrial products. The substitution of X = C with X = Si in the muscarinic receptor agonist resulted in increased activity at the receptor(Fig. 1.3).[7] Increased activity was also seen when the histamine antagonist Sila-terenadine, an isostere of Terfenadine, was tested.[7] Organosilanes have also been found to exhibit insecticidal and antifungal properties, as seen with Silafluofen and Flusilazoze respectively. Silane groups can also increase lipophilicity of molecules as seen with Camphothecin derivative Karenitecin. Organosilanes are also prevalent in material science. They can be incorporated into materials to increase temperature resistance, hydrophobicity, flame-retardance, and anti-aging properties. This allows them to be implemented broadly across materials in everyday use, such as, electronic devices, personal care, green energy, biomedical, construction, and aerospace industries.[1]

With the interest and utility of organosilanes high, many methods to form organosilanes have been developed (Fig. 1.4). There are five major classes of reactions to form organosilanes: transition metal mediated carbene Si–H insertion reactions, transition metal-catalyzed cross-coupling reactions, transition metal-catalyzed C–H silylation, transition metal-catalyzed hydrosilylations, and radical reactions. In transition metal-mediated carbene transfer reactions, a carbene precursor, most commonly a diazo compound, is thermally decomposed or decomposed by the metal center (Fig 1.4a).[8] This produces an electrophilic carbenoid intermediate that will electrophilically activate the Si–H bond,

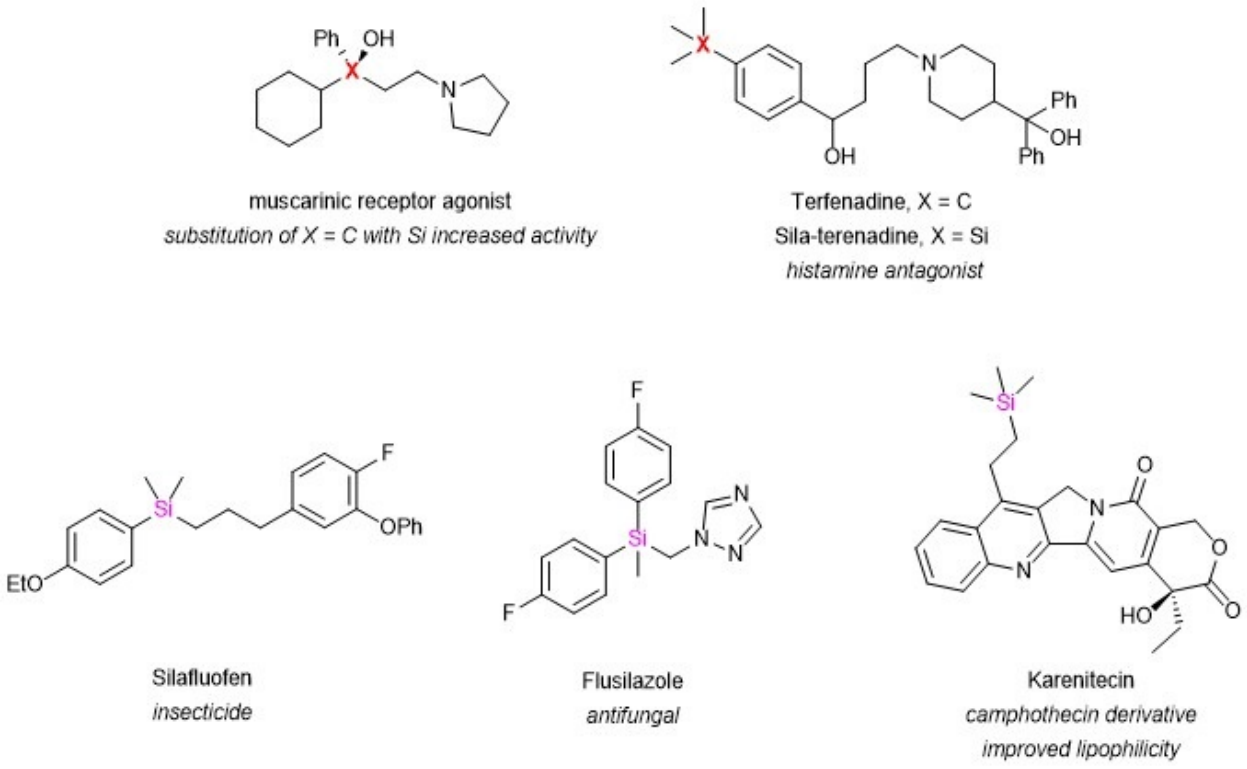

Figure 1.3: Notable organosilane compounds and their activities.

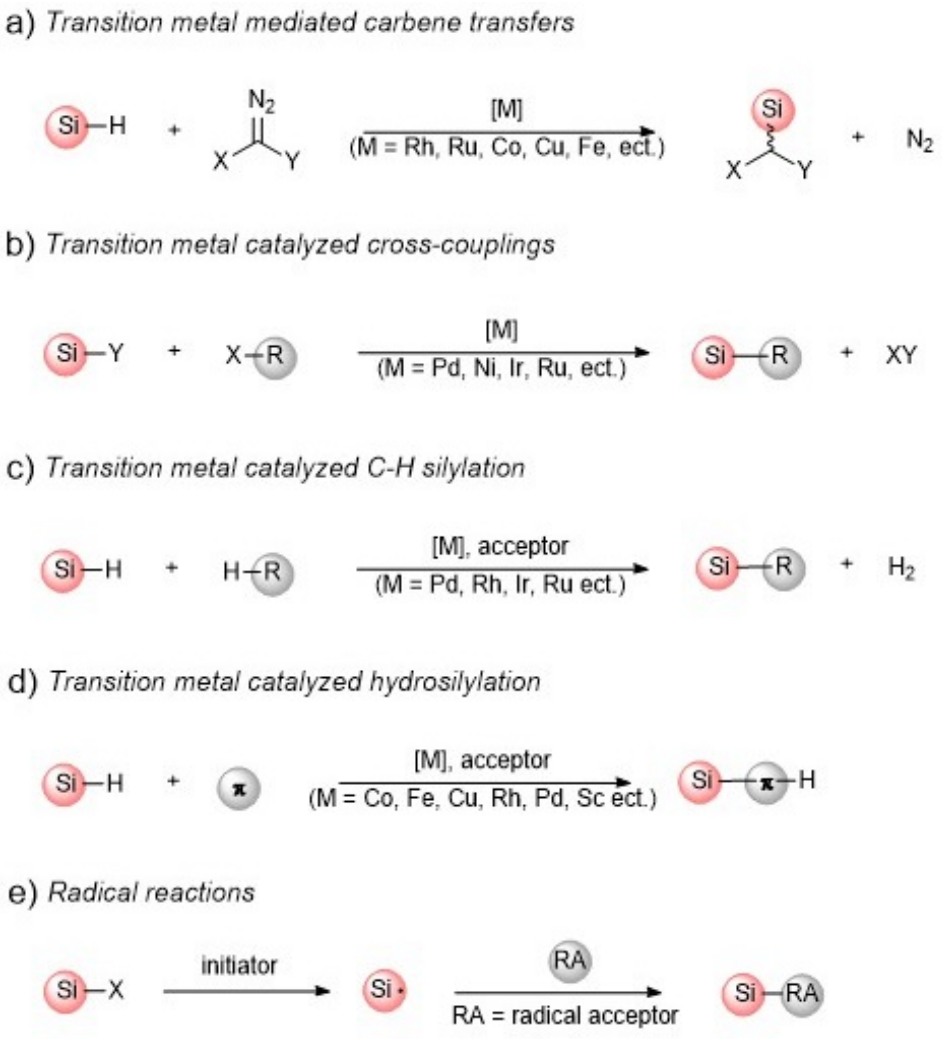

Figure 1.4: More recently developed classes of reactions to form organosilanes.

resulting in carbene insertion also known as Si–H insertion, followed by regeneration of the catalyst. Rh(II) paddlewheel complexes are considered a privileged class of catalysts in transition metal-mediated carbene transfer reactions due to the high turnover numbers, diverse reactivity of Rh(II) carbenoids, and diverse selectivity that can be achieved. The Rh(II)-mediated carbene Si–H insertion reaction proceeds through a similar mechanism as other transition metal mediated carbene Si–H insertion reactions (Fig 1.5). The first step of the mechanism is coordination of the diazo compound to a Rh axial site (Fig. 1.5, step I). This is followed by the extrusion of nitrogen (Fig 1.5, step II). Introduction of the silane (Fig. 1.5, step III) is followed by concerted asynchronous insertion into the Si–H bond (Fig. 1.5, TS) resulting in the desired organosilanes and regeneration of the catalyst (Fig 1.5, step IV). A potential competing reaction is homocoupling between the Rh(II) carbenoid and another equivalent of the initial diazo compound (Fig. 1.5, step V). Homocoupling, or dimerization, can be avoided by slow addition of the diazo compound to limit its concentration, or by adding excess silane reagent. An introduction to the general Rh(II) paddlewheel structure, the electronic structure of the Rh(II) paddlewheel complex and carbenoid, synthesis of Rh(II) paddlewheel complexes, and leveraging axial coordination in Rh(II) catalysis are presented in the Chapter 2.

Transition metal-catalyzed cross-coupling is another method to form organosilanes (Fig 1.4b).[9] However, these transformations suffer from unstable and toxic reagents, poor atom economy, and the need for pre-activation of substrates. The transition metal catalyzed C–H silylation is normally performed at stoichiometric amounts of reagent and have good atom economy, but suffer in terms of selectivity(Fig. 1.4c).[7] Transition metal hydrosilylations are atom economical, but the substrates must have an unsaturation to add across (Fig. 1.4d).[2] Multiple unsaturations can result in the formation of over-silylated products. Radical reactions are a broad set of transformation that can proceed by one of two pathways. The first pathway applies to most radical reactions[10] toward organosilanes (Fig 1.4e). First, the silane reagent is treated with an initiator, usually peroxides, light, or a combination of hypervalent iodide or metal, and a peroxide. The second pathway is an alkyl radical initiated silylation of a $R_3SiBpin$ reagent.

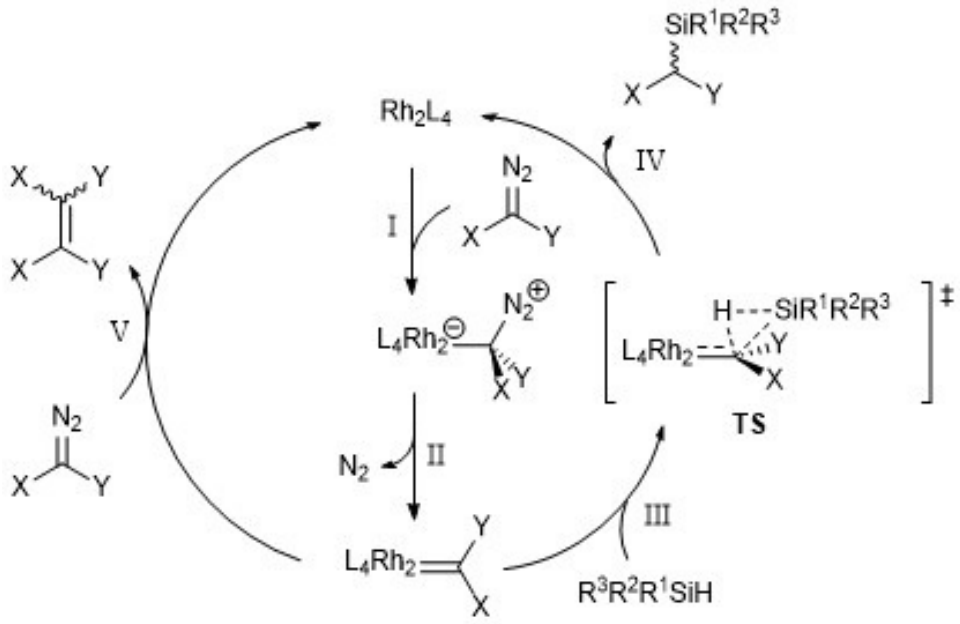

Figure 1.5: General mechanism of Rh(II) catalyzed Si–H insertion reaction.

1.2 Cyclopropanation Reactions and the Significance of Cyclopropanes

The interest in cyclopropanation reactions stem from their prevalence in pharmaceutical products and natural products. Their ability to impart structural rigidity, increase hydrophilicity, and potential to form a compact asymmetric scaffold allows for pharmaceutical therapies to be intelligently designed around this moiety. An example of this prevalence in pharmaceutical therapies is that 8.5 % of all new drugs approved by the Federal Drug Administration between 2012 and 2018 featured a cyclopropane moiety.[11] Cyclopropanes are featured in many pharmaceutical therapies with diverse bioactivities as well as other bioactive compounds (Fig. 1.6). Some notable examples are cancer inhibitor and anti-depressant, Lenvatinib and Tranylcypromine respectively.[12] The cyclopropane moiety also features in steroidal hormone therapeutic Drospirenone and fibromyalgia therapeutic Milnacipran.[12] Not all compounds featuring the cyclopropane moiety are pharmaceutical therapeutics. The insecticide *trans*-chrysanthemic acid is an example of the potential of these compounds in other industrial industries.[12]

There are multiple synthetic strategies to form cyclopropanes (Fig. 1.7a) The Simmons-Smith reaction utilizes alkyl zinc reagents formed from zinc metal and diiodomethane.[13] The $IZnCH_2I$ intermediate then cyclizes with retention of the *cis* and *trans* isomers. Cyclopropanation can also occur from cyclization between an olefin and a free carbene. Free carbenes are highly reactive species that lack selectivity in cyclopropanation reactions.[14] The Johnson-Corey-Chaykovsky reaction involves an addition of a sulfur ylide to an enone followed by subsequent cyclization to form a cyclopropane.[15] The product of this reaction favors *trans* substitution no matter the initial stereochemistry. The Kulinkovich reaction is another method to form cyclopropanes. The draw back to this reaction is the resulting cyclopropane has a hydroxyl substituent.[16] The most diverse method to form asymmetric cyclopropanes is the transition metal-catalyzed cyclopropanation reaction through a diazo-derived carbenoid intermediate.[17]

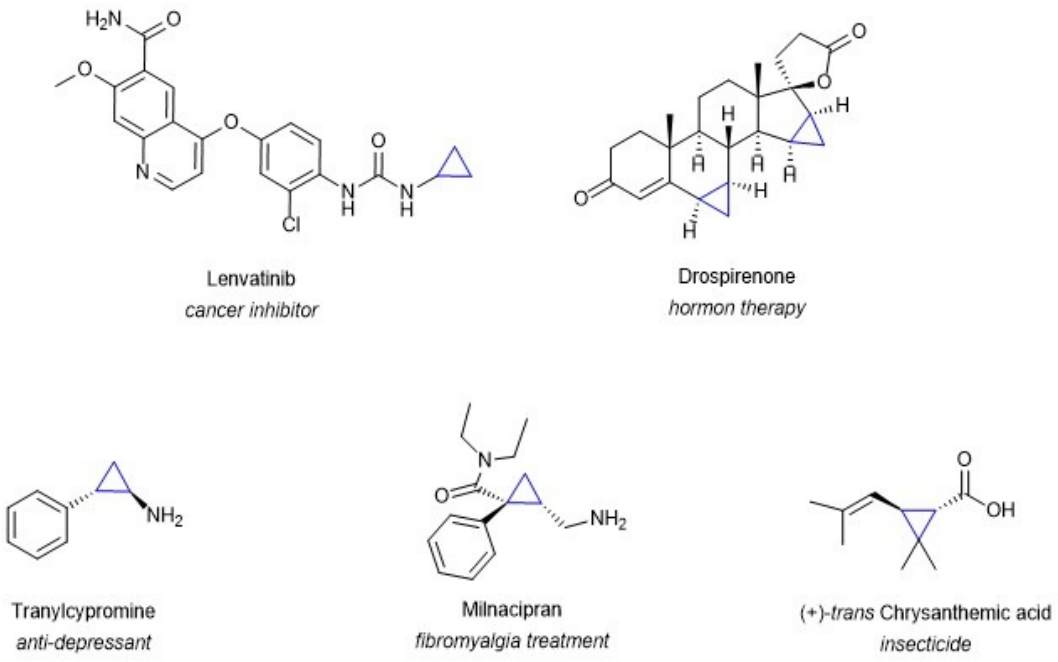

Figure 1.6: Notable examples of bioactive compounds featuring the cyclopropane moiety.

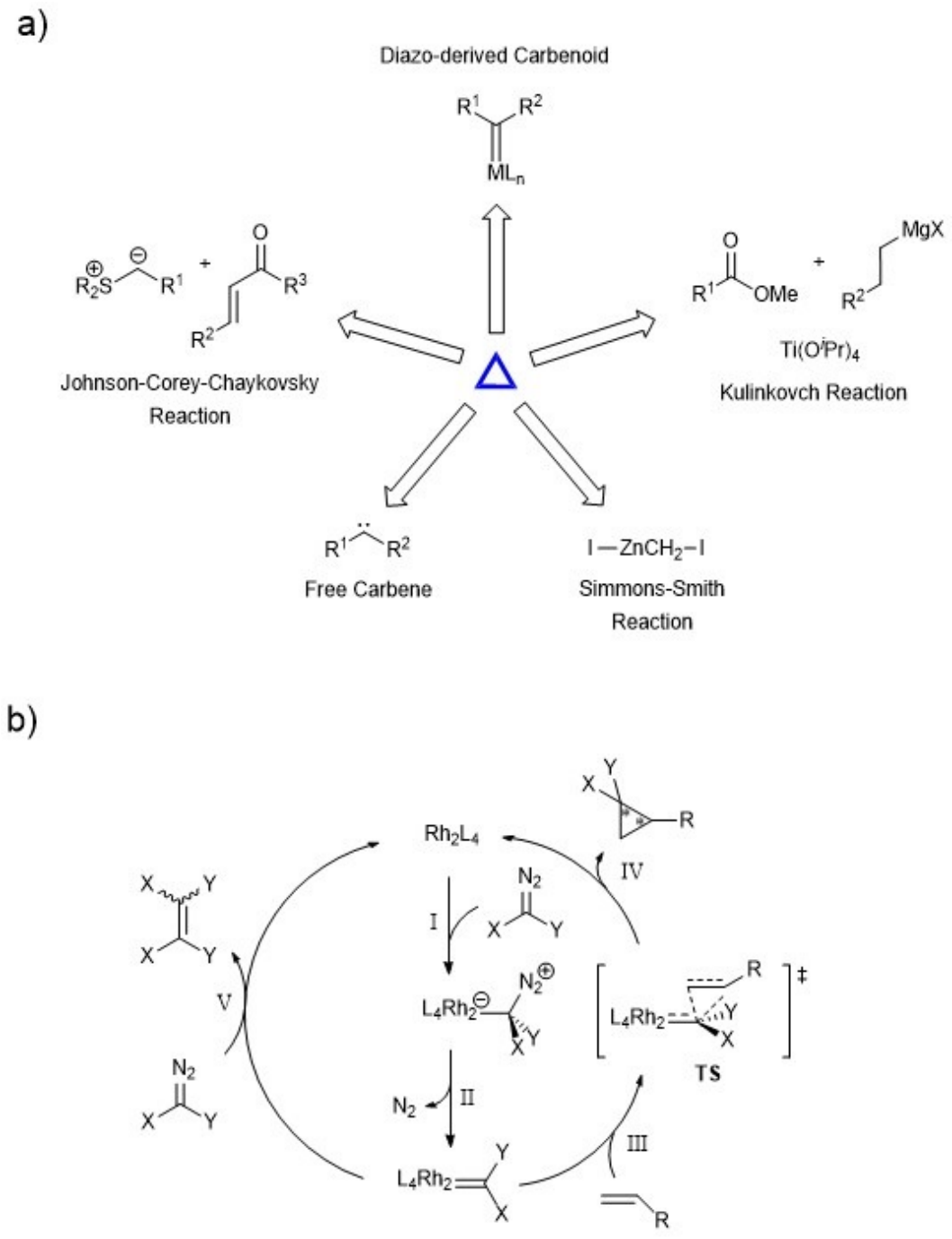

Figure 1.7: a) Common strategies to form cyclopropanes. b) General mechanism of the Rh(II)-catalyzed cyclopropanation reaction.

Rhodium and copper have become the most used transition metals for diazo-derived carbenoid cyclopropanation reactions, although the transformation can be mediated by other group 9 and 11 transition metals.[18] Copper complexes benefit from low cost, a large ligand library, and highly enantioselective reactions. The downsides of copper complexes are any excess olefin in solution can to coordinate to the catalyst and the limited diazo compounds it can form carbenoids with.[18] This constrains potential diversity with both substrates. Rh(II) paddlewheel complexes are efficient at decomposing all diazo compounds and are only limited due to the carbenoid formed being stable with some donor-type diazo compounds. The general mechanism for the Rh(II)-catalyzed cyclopropanation reaction is similar to other diazo-derived carbenoid cyclopropanations (Fig. 1.7b). The first step is the coordination of the diazo compound followed by extrusion of N_2 (Fig. 1.7b, steps I and II respectively). The next step is nucleophilic attack on the carbenoid by the incoming olefin substate immediately followed electrophilic cyclization. This is considered to be a concerted asynchronous transition state (Fig 1.7b, TS) that is followed by product formation and regeneration of the catalyst. Dimerization of the diazo compound is also a competing reaction and can be limited with slow addition and/or excess olefin reagent as mentioned above.

Asymmetric cyclopropanation reactions have predominantly been controlled by the development of bulky chiral ligands that form a "chiral crown" at one or both of the axial position. Highly efficient asymmetric Rh(II) paddlewheel complexes are thought to be symmetric at both axial sites or the bridging ligands create a chiral crown at one axial site while sterically crowding the other axial site to inhibit diazo compound coordination and decomposition.

1.3 Introduction to Computational Methods Utilized

The calculations presented herein were calculated with density functional theory using the M06-2x[19] functional developed by Zhao and Truhlar in 2008 and the valence triple-ζ def2-TZVPP[20] bases set, or def2-TZVP[20] due to resource constraints, with built in electronic

core potential. Density functional theory was developed by Kahn and Sham[21] on the basis of the Hohenberg–Kohn theorems.[22] All geometry optimizations were run on an ultrafine gradient with strict conversion criteria. The initial calculation performed were all geometry optimizations to inspect how axial coordination effects the frontier orbitals of our catalyst. It is also useful as a 3D modeling tool to inspect whether a ligand will have the required geometry to coordinate at the axial site and if that is a minima on the potential energy surface. My final computational project was to model the N_2 extrusion step and inspect how the electron density is modulated through the atoms and bonding framework. To calculate transition states of the complexes, a scan of the potential energy surface was performed. This was completed by systematically decreasing the Rh–C bond length and optimizing the structures utilizing a smaller basis set, def2-SVP.[20] The scan of the potential energy surface would identify a local maxima. This indicates the position of a saddle point on the potential energy surface indicating it was a transition state. I utilized the Wiberg Bond Indices identify the bond order.[23] Wiberg bond order is calculated by taking the summation of the atomic orbitals on two atoms and a corresponding density matrix. For population analysis, NBO3[24] Natural Population Analysis calculations were performed. Natural population analysis was developed by Weinhold and Reed.[25] Natural population analysis was developed to calculate atomic and orbital populations of molecular wave functions in general atomic orbital sets. This results in the natural charge of the atom.

1.4 Research Question and Dissertation Organization

1.4.1 Research Question

The hypothesis studied herein is, *axial coordination can be leveraged to impart an increase in activity and selectivity.* It is our intent to probe the role of axial coordination in Rh(II)-catalyzed carbene transfer reactions by designing tethered axial coordinating ligands, or TACLs. The tether keeps the LB in proximity of the axial site allowing us to study the effects of this interaction on activity and selectivity. The ability to adjust the activity and

selectivity of the Rh(II) paddlewheel catalyst is traditionally accomplished through exchange of the bridging ligands, with interactions at the axial site often being overlooked as a mode to tune the electronics of the catalyst. Coordination at the axial site can hinder the activity of the catalyst, or completely shut it down, by coordinating to both axial sites where the coordination must be out competed by the diazo substrate, although this is not always the case. Leveraging a tether to mitigate this potential poisoning of the catalyst allows us to form mono- and bis-complexes without having to overcome the equilibrium between mono-, bis- and free complex that occurs when exogenous additives are used as a control mode. It also keeps the LB in proximity to the axial site allowing us to remove the adjustment of dielectric constant that comes with polar additives in high concentrations. Adding a tether to one or two of the ligands on the Rh paddlewheel structure inherently forms a heteroleptic complex. This allows us to selectively change one or two ligands, as described above, resulting in an added tuning method of this class of catalyst when other hetero atoms are used.

1.4.2 Dissertation Organization

Chapter two is an adaptation of our manuscript "Heteroleptic Dirhodium(II,II) Paddlewheel Complexes as Carbene Transfer Catalysts" and introduces the structure and syntheses of the Rh(II) paddlewheel as well as provides comprehensive review at the past use of heteroleptic complexes, axial coordination, and the combination of both as a control mode in carbene transfer reactions. Chapter three is an adaptation of our manuscript "Effect of Tethered, Axial Thioether Coordination on Rhodium(II)-catalyzed Silyl–hydrogen Insertion." This chapter introduces the silyl-hydrogen insertion reaction and describes our testing of the TOX series of catalyst in the reaction. Chapter four provides a comprehensive review of donor diazos in silyl–hydrogen insertion reactions and the work completed toward a manuscript in progress. Chapter four descibes our efforts to implement Rh(II) catalyst in Si–H insertion reactions with hydrazone protected donor diazo precursors. Chapter five is an adaptation of our manuscript "Tuning Rh(II)-catalyzed Cyclopropanation with Tethered Thioether Ligands" and introduces the cyclopropanation reaction, ethyl diazoacetate as a substrate, and describes our efforts toward testing our oxazolidinone mixed ligand catalyst with tethered

thioether moieties and computational analysis to aid in our understanding of the system. Chapter 6 is a manuscript in progress on Rh(II)-catalyzed asymmetric cyclopropanation. Included are our efforts to design chiral tethered axially coordinating ligands (TACLs), form heteroleptic complexes with the ligands, and test their activity and selectivity in asymmetric cyclopropanations. Chapter 7 presents a summation of the conclusions drawn from Chapters 3-6.

Chapter 2

Heterolepticity and Axial Coordination as a Control Element in Rh(II)-Catalyzed Carbene Transfer Reactions

2.1 Disclosure

The following chapter is an adaptation of the journal article A. Abshire, D. Moore, J. Courtney, and A. Darko. Heteroleptic dirhodium(II,II) paddlewheel complexes as carbene transfer catalysts. Org. Biomol. Chem., 19(41):8886–8905, 2021. Dr. Ampofo Darko wrote the introductory sections, compiled and edited the document, and helped make figures. I performed an exhaustive literature search, wrote the excerpts on Ball, Charette, Davies, Fox, and Laureta's work, made figures, and helped complete the final edits. Desiree Moore wrote excerpts on Corey, Doyle, Bera and Ward's work. Jobe Courtney wrote excerpts on Lewis, Corey, and Darko' works. Desiree Moore and Jobe Courtney also helped edit their sections.

2.2 Abstract

This chapter highlights the applications of dirhodium(II,II), Rh(II), paddlewheel complexes with a heteroleptic scaffold. Rh(II) paddlewheel complexes are well-known as highly efficient and selective carbene transfer catalysts. While the majority of described complexes are homoleptic, comparatively fewer studies have concerned heteroleptic complexes. Here, we emphasise the use of heteroleptic complexes in order to highlight their benefits as carbene transfer catalysts and spur future research. Methods to synthesize heteroleptic Rh(II) paddlewheel complexes are discussed as well as a categorical review of their types of heteroleptic complexes and the carbene reactions in which they have been used.

2.3 Introduction

Rh(II) paddlewheel complexes (Fig. 2.1) are well known for mediating effective, highly enantioselective carbene transfer reactions in synthetic organic chemistry through the *in situ* generation of rhodium carbenoids from α-diazocarbonyl precursors.[26–29] The rhodium carbenoids that form then undergo a variety of transformations such as cyclopropanation,[14,30–32] C–H insertion,[33–37] Si–H insertion,[38–40] and ylide formation.[41,42] Modifying bridging ligands around the Rh(II) core and changing the carbene structure are key to developing selective transformations.[27,43–45] Carboxylates and carboxamidates make up a significant portion of bridging ligands and their design has been largely focused on homoleptic complexes, in which all four bridging ligands are the same.[45] The most successful ligands have equivalent environments on each Rh atom in the bimetallic core and their spatial arrangements around the rhodium axial sites allow for selective, diazo-mediated transformations.[35,45] While homoleptic complexes dominate reported Rh(II) paddlewheel complexes, there are relatively few reports that feature heteroleptic Rh(II) paddlewheel complexes. Here, we highlight the reports that show that there are opportunities associated with heteroleptic Rh(II) paddlewheel complexes that can be leveraged in rhodium carbenoid chemistry. These include the ability to fine-tune properties of catalysts, the opportunity for

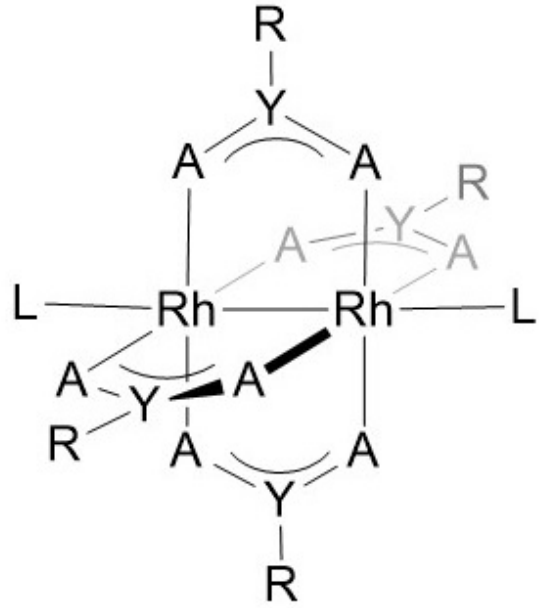

Figure 2.1: General structure of Rh(II) paddlewheel complexes.

interesting ligand interactions that lead to catalytic improvements, and ways to heterogenize complexes.[46] Heteroleptic scaffolds have also allowed a gateway to the design of artificial rhodium metalloenzymes.[47] There are very few examples of asymmetric transformations with heteroleptic Rh(II) complexes, making this an untapped strategy for more diversity in catalyst design.

2.3.1 Structural Features and Reactivity of Rh(II) Complexes

Several reviews have been written on the subject of Rh(II) complexes,[26,43,48–50] with the most comprehensive review on their structural aspects and applications appearing in the book by Cotton *et al.* in 2005[51] in chapters by Chifotides *et al.*[50] and by Doyle *et al.*[52] In this review, we will provide a brief overview of the most relevant concepts with an emphasis on heteroleptic Rh(II) complexes. The Rh–Rh bond is formally a single bond, with a simplified molecular orbital description involving 14 electrons in a $\sigma^2\pi^4\delta^2\delta^{*2}\pi^{*4}$ configuration.[50] Rh(II) paddlewheel complexes are surrounded by four bridging ligands that donate varying degrees of charge to the Rh_2^{4+} core (Fig. 2.1). The possibilities of combinations for bridging atoms include oxygen, phosphorus, carbon, nitrogen, and sulphur atoms and the nature of bridging ligands allows the control of the catalytic performance of the complex.[50] As a demonstration, perfluorobutyrate ligands render the rhodium center more electrophilic, while ligands such as amidates result in more electron rich Rh(II) complexes.[53] As a result, amidate ligands are generally less reactive in reactions involving carbene transfer, but are often more selective.[54,55]

The two axial sites of the Rh(II) catalysts are the electrophilic reaction sites and are often occupied by labile axial ligands (L, Fig. 2.1) that establish weaker bonds compared to the bridging ligands.[50] The identity of the axial ligand impacts the electronic spectra of Rh(II) complexes due to the perturbation of the Rh–Rh π^* to σ^* HOMO–LUMO transition.[56] Axial ligands can also impact catalytic activity of Rh(II) catalysts. For example, coordinating solvents like acetonitrile (CH_3CN) and tetrahydrofuran (THF) can completely inhibit formation of the metallocarbenoid in carbene transfer reactions.[57] Lately, efforts to

tune properties of Rh(II) catalysts have also included modification of axial coordinating groups.[58–61]

2.3.2 Ligand Environment

Rh(II) paddlewheel complexes are unmatched in their enantioselectivity and the ligand environment about the rhodium faces play an important role in stereoinduction. In classic models, the possible arrangements of the ligands can lead to four possible symmetries (Fig. 2.2),[49] but their methods of selectivity and ligand environment are still an area of intense research. The models for asymmetric induction of chiral dirhodium complexes are based on analysing x-ray structures, however, it was found that catalyst conformations can be flexible in solution.[62] Thus, it is not always clear that a Rh(II) paddlewheel complex will be a selective catalyst solely based on solid-state models. Models explaining asymmetric induction have become more nuanced as a result of a better understanding of the dirhodium paddlewheel ligand environment. Initially it was suggested that only catalysts possessing C_2 or D_2 symmetry are likely = be the most enantioselective complexes since they will have equivalent rhodium faces.[49] However, with adequate blocking of one Rh site, highly enantioselective rhodium(II,II) complexes now include those with C_4 symmetry.[63,64] Heteroleptic complexes (Fig. 2.3) introduce C_1 complexes as possible sources of asymmetric induction,[65] thereby adding to the possibilities of asymmetric Rh(II) paddlewheel complexes to those of lower symmetry.

2.4 Synthesis of Heteroleptic Rh(II) Complexes

The main method of synthesizing Rh(II) complexes involves ligand exchange with dirhodium (II,II) tetraacetate ($Rh_2(OAc)_4$), dirhodium (II,II) tetrakis(trifluoroacetate) ($Rh_2(tfa)_4$), or dirhodium (II,II) carbonate under refluxing conditions.[50] The conditions for ligand exchange typically involve an excess of the new ligand (at least 4 molar equivalents) in high boiling solvents such as chlorobenzene. Exchange reactions of Rh(II) carboxylates ($Rh_2(O_2CR)_4$) proceed by stepwise replacement of the RCO_2^- ligand by the new ligand, retaining the Rh–Rh

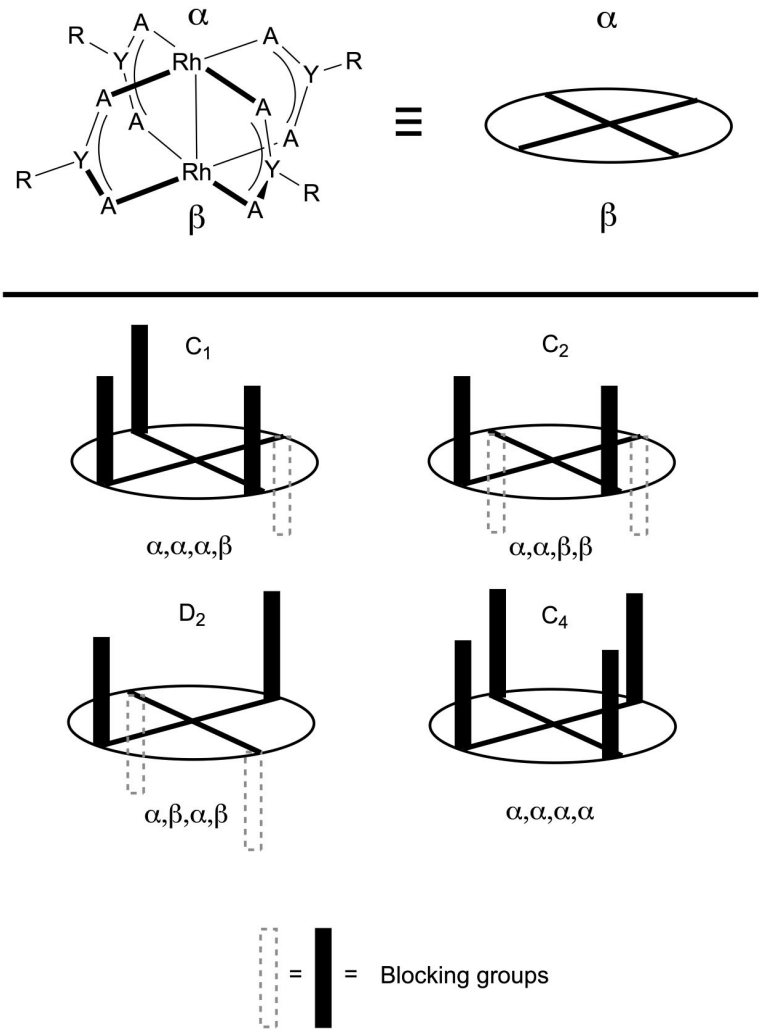

Figure 2.2: Ligand arrangements of Rh(II) paddlewheel complexes.

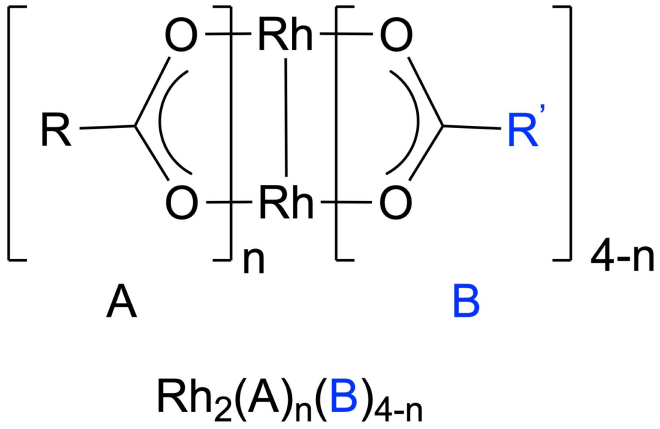

Figure 2.3: General notation for heteroleptic Rh(II) complexes. Shown with heteroleptic carboxylate bridging ligands.

bond in the process. The process begins with coordination of the incoming ligand to the axial site, which facilitates displacement of the incumbent ligand (Fig. 2.4). The process repeats until all four RCO_2^- ligands are replaced with the new ligand. The ratio of the partial substitution products can differ depending on the nature of the incoming ligand. The ligand exchange reaction of $Rh_2(OAc)_4$ with trifluoroacetic acid was monitored by NMR spectroscopy and the relative rates of the sequential substitution was found to be approximately $1 : 2 : 0.1 : 0.025$ for the first, second, third, and fourth substitution.[66] Heating $Rh_2(OAc)_4$ in molten acetamide resulted in a distribution of $1 : 3 : 1 : 1$, while the same reaction with molten *N*-phenylacetamide provided ratios of $1 : 2 : 2 : 2$ of sequential acetamide substitution.[67] If complete substitution is desired, then removal of the released ligand from the reaction mixture will drive the equilibrium towards complete ligand exchange. In ligand substitutions with $Rh_2(OAc)_4$, tetra-substituted complexes may be maximized by using a Soxhlet extractor in which the thimble is filled with an inorganic base to trap released acetic acid.[68]

Because of the complex mixture of substitution products in Rh(II) ligand exchange reactions, the synthesis of heteroleptic complexes is difficult to control, and this has undoubtedly limited their use. The mixture of products is further complicated when bridging atoms are not the same. In ligand exchanges with achiral amidate bridging ligands for example, up to 14 different isomers of mixed-substitution products are possible due to geometric isomers when bridging ligands contain two or more amidate ligands (Fig. 2.5).[67,69,70] The difference in connectivity also affects reactivity, as it renders each Rh atom non-equivalent. There are, however, some methods to efficiently access heteroleptic Rh(II) complexes.

In the pursuit of isolating heteroleptic Rh(II) carboxylate complexes, Charette *et al.* mitigated the separation of complex mixtures of partial ligand exchange products by using chloro-substituted bridging ligands as "polarity-control groups."[65] The presence of the chloride groups on the ligands dramatically affected the R_f of the compounds such that the number of chloro-substituted bridging ligands were the defining factor for retention on silica. Well-defined chromatographic separation could then be achieved in order to isolate

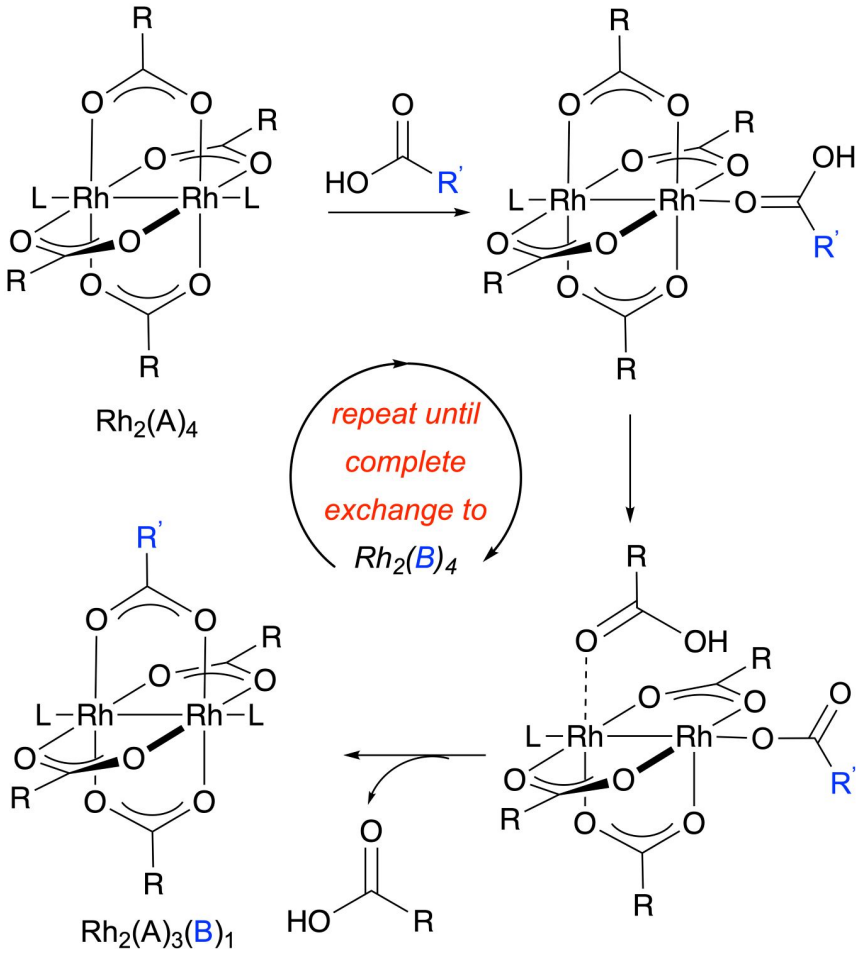

Figure 2.4: Mechanism of ligand exchange reactions of Rh(II) paddlewheel complexes. Shown with carboxylate ligands.

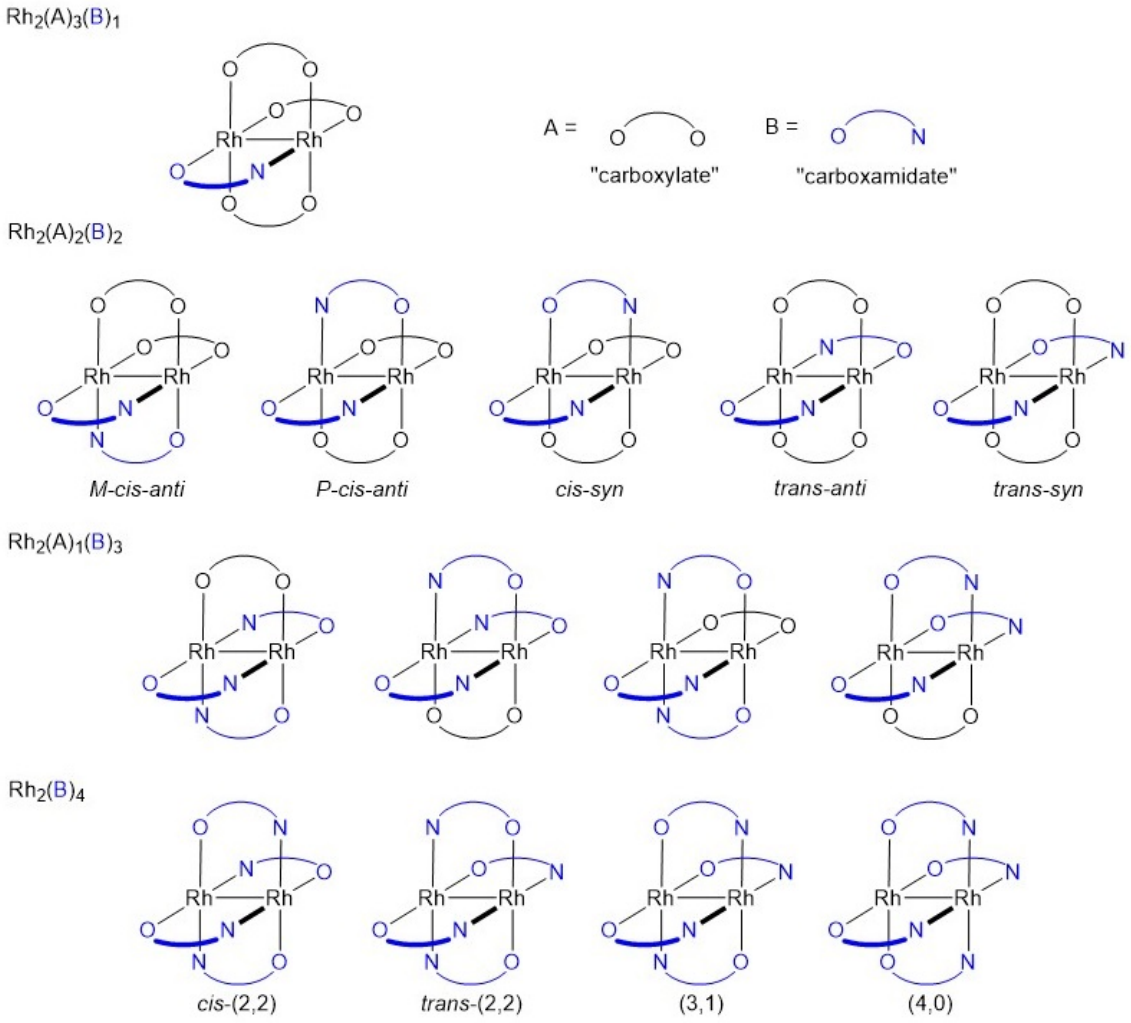

Figure 2.5: Possible products in the synthesis of heteroleptic complexes by ligand exchange. Shown with mixed carboxylate/carboxamidate ligands as an example.

heteroleptic complexes such as complex 1.[65] They further increased yields of 1 by separating and resubmitting any undesired complexes and unreacted exchange ligand to the reaction conditions in multi-sequence reactions (Fig. 2.6). Hashimoto also utilized such a recycling procedure to maximize yields of heteroleptic complex 2 with a functionalizable bridging ligand.[71]

There are ligands that have a propensity to be selective for certain bridging ligand substitution. Aryl phosphines can be substituted as bridging ligands through orthometalation onto Rh(II) carboxylates, which preferentially produces complexes with the formula $Rh_2(O_2CCR_3)_2(PC)_2$ (PC = orthometalated aryl phosphine).[72–74] The first example was the reaction with triphenylphosphine (PPh_3) and $Rh_2(OAc)_4$ in refluxing acetic acid, which produced complex 4 (Fig. 2.7).[72,73] Using similar conditions, a number of orthometalated phosphine Rh(II) complexes have been prepared with different variations of arylphosphine and carboxylate ligands with different variations of arylphosphine and carboxylate ligands.[75–78] The complexes preferentially form with *cisoid* carboxylate and phosphine bridging ligands with one phosphorus atom coordinated to each rhodium center, which can be classified as a *cis-anti* or head-to-tail arrangement.[50,69] Head-to-head, or *cis-syn*, arrangements are also known and can synthesized using an excess of arylphosphine in refluxing toluene such as for the synthesis of complex 5 (Fig. 2.7).[79,80]

Using chelated carboxylate bridging ligands is another way to control substitution. Taber *et al.* were the first to try this with a dicarboxylic acid specifically designed to fill the gap between carboxylate ligand positions on the paddlewheel scaffold.[81] With $Rh_2(tfa)_4$ 6 as the precursor with the benzenedipropanoic acid ligand in 1,2-dichloroethane at 105 °C, 7 was obtained as the only product along with unreacted $Rh_2(tfa)_4$ (Fig. 2.8). In another example, Bonar-Law *et al.* used dicarboxylates derived from 1,3-benzenediols to synthesize molecular architectures.[82–84] The ligands preferentially substituted two bridging ligands of the Rh(II) carboxylate precursors in *N*,*N*-dimethylaniline at 140 °C to produce complexes like 8 (Fig. 2.8). The remaining two bridging ligands could be further exchanged without loss of the bis-chelated bridging ligand and this modularity allowed for the linking of the remaining carboxylate ligands in an intermolecular fashion to synthesize of a variety of square

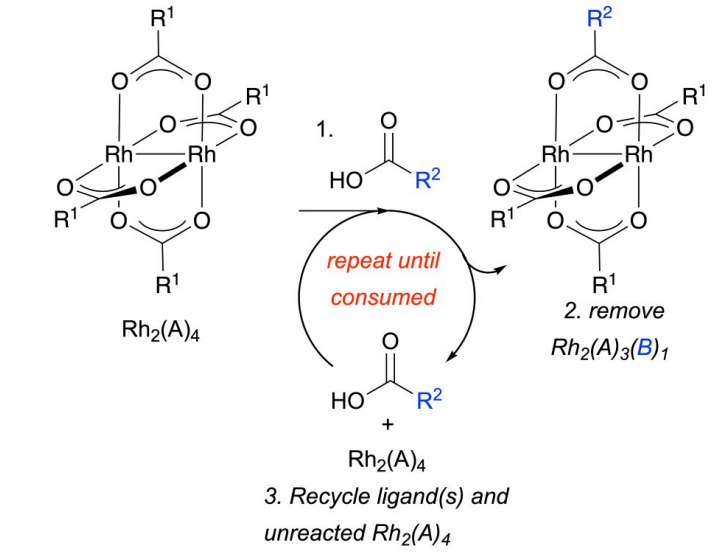

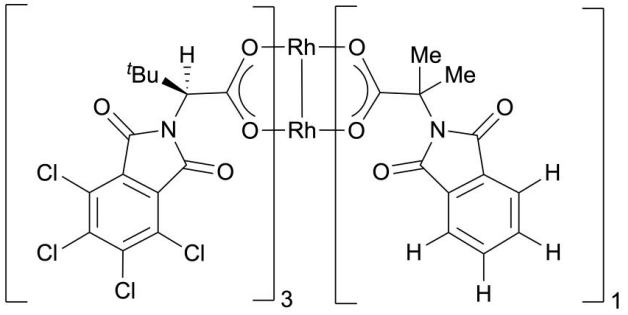

1, Rh_2(*S*-TCPTTL)$_3$(PTAiB)
61% yield after 3 cycles

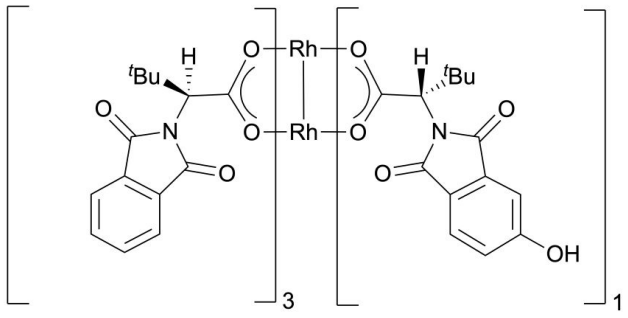

2, Rh_2(*S*-PTTL)$_3$(*S*-OHPTTL)
74% yield after 3 cycles

Figure 2.6: Maximizing yields of heteroleptic Rh(II) complexes through multi-cycle sequences of ligand exchange reactions.

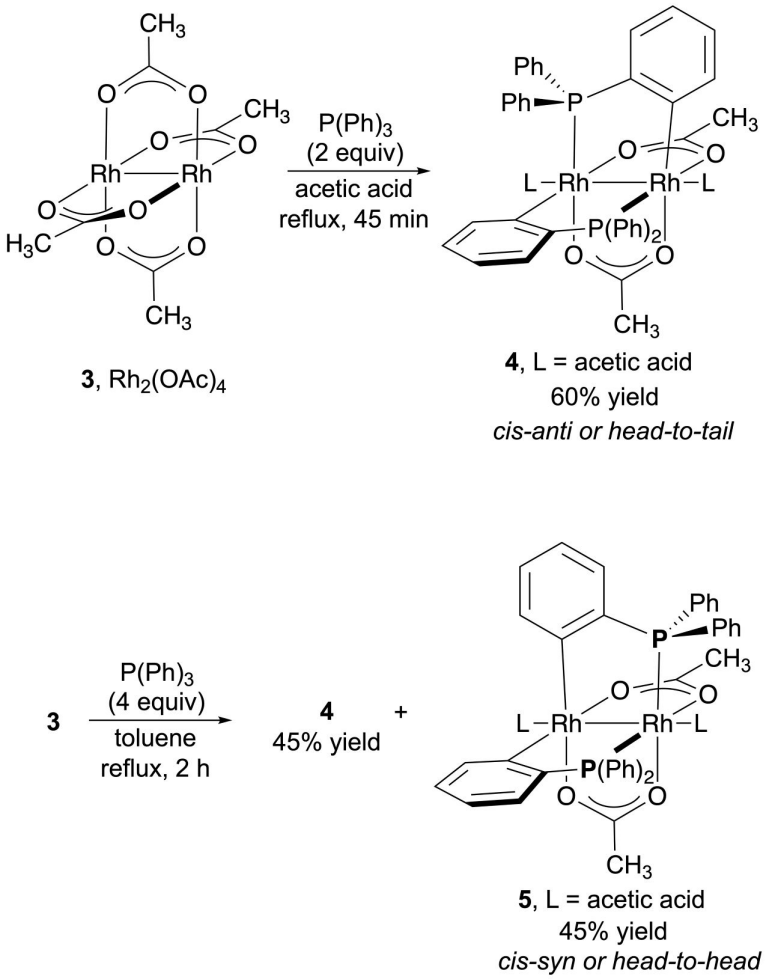

Figure 2.7: Ligand exchange with triphenylphosphine and $Rh_2(OAc)_4$ to produce orthometalated phosphine Rh(II) complexes. Two-fold exchange is preferred and the *cis-anti* isomer 4 or *cis-syn* isomer 5 can synthesized depending on conditions.

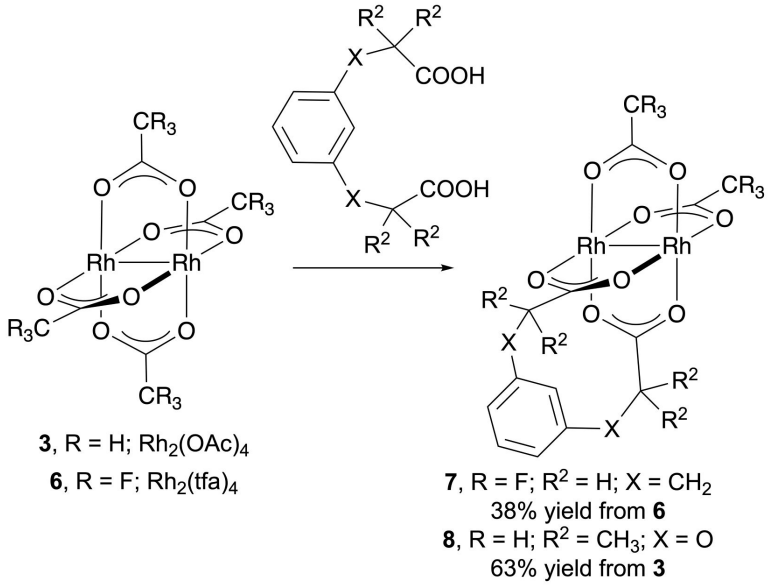

Figure 2.8: Examples of dicarboxylic acid ligands that preferentially form bis-chelated heteroleptic complexes.

macrocycles.[83] Very recently, Fürstner and Caló found that the synthesis of trisubstituted heteroleptic complexes $Rh_2((R)\text{-TPCP})_3(A)$ (TPCP = triphenylcyclopropane carboxylate, A = tfa or OAc) was straightforward and high yielding when starting from $Rh_2(tfa)_4$ or $Rh_2(OAc)_4$ as the parent complex in high boiling solvents (Fig. 2.9).[85] Presumably, the steric bulk associated with TPCP helped to control the exchange process.

Recently, our group has shown that the incorporation of axial coordination can prevent further ligand exchange to tri- and tetra-complexes.[86] When thioether ligands were tethered to carboxylate or carboxamidate bridging ligands, the only products were those of mono- and di-substitution when $Rh_2(OAc)_4$ was used as the starting material, with mono-substitution being favoured. Although, the mixture of products was somewhat complicated by *cis* and *trans* isomers of the di-substituted complexes (Fig. 2.10).

One can also start with a complex with ligands of differing lability in which the more labile ligand can be preferentially exchanged. Mixed acetate/trifluoroacetate complexes $[Rh_2(OAc)_n(tfa)_{(4-n)}]$ have been used as the starting material in this strategy. Conveniently, *cis* and *trans* isomers of $[Rh_2(OAc)_2(tfa)_2]$ 11 can be selectively synthesized depending on the reaction conditions (Fig. 2.11) and Corey *et al.* used this method to control for the synthesis of the isomers of $[Rh_2(DPTI)_2(OAc)_2]$ complexes.[69] Ball has also used *cis*-11 and $[Rh_2(OAc)_3(tfa)]$ to synthesize a variety of heteroleptic Rh(II) peptide complexes.[47,87]

Garner, Clegg, *et al.* found that treatment of Rh(II) paddlewheel compounds with trimethyloxonium tetrafluoroborate in acetonitrile (CH_3CN) produced complex 12 (Fig. 2.12).[88] These partial paddlewheel compounds possessed two bridging acetates and six CH_3CN ligands at the remaining equatorial and axial coordination sites. The acetonitrile ligands can be easily displaced by new ligands, resulting in di-substituted heteroleptic complexes $Rh_2(OAc)_2(L)_2$. This strategy is particularly useful for incorporating neutral complexes[89–91] and for studying the anti-tumour activity of Rh(II) complexes.[92,93]

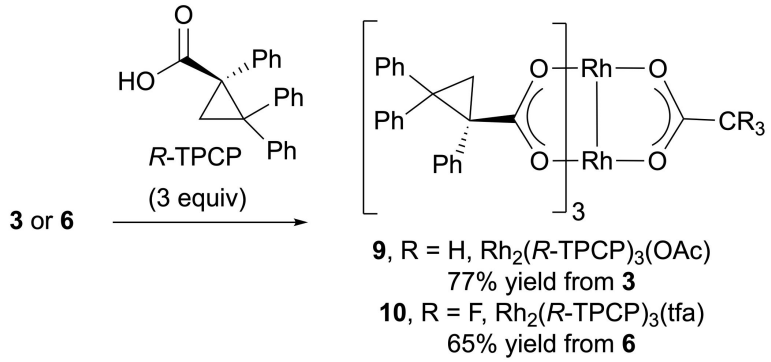

Figure 2.9: Synthesis of heteroleptic complexes 8 and 9 via three-fold ligand exchange with *R*-TPCP ligand.

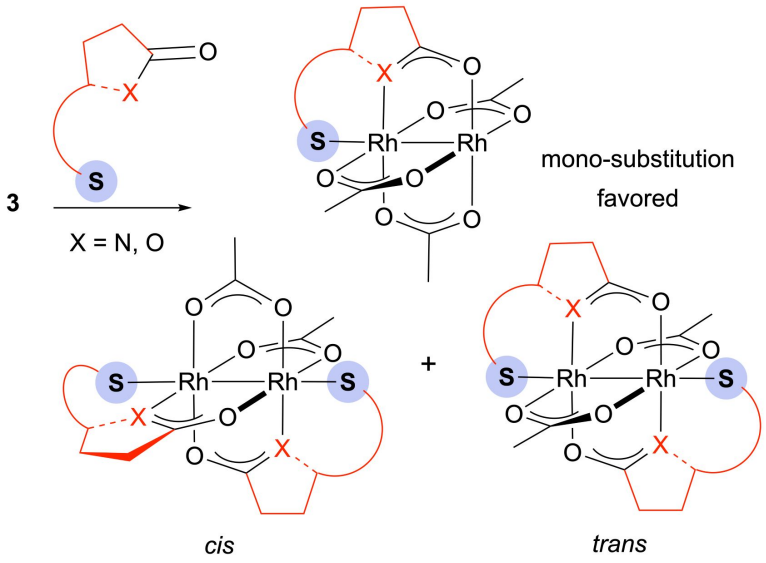

Figure 2.10: Ligand exchange reaction with pendant thioethers.

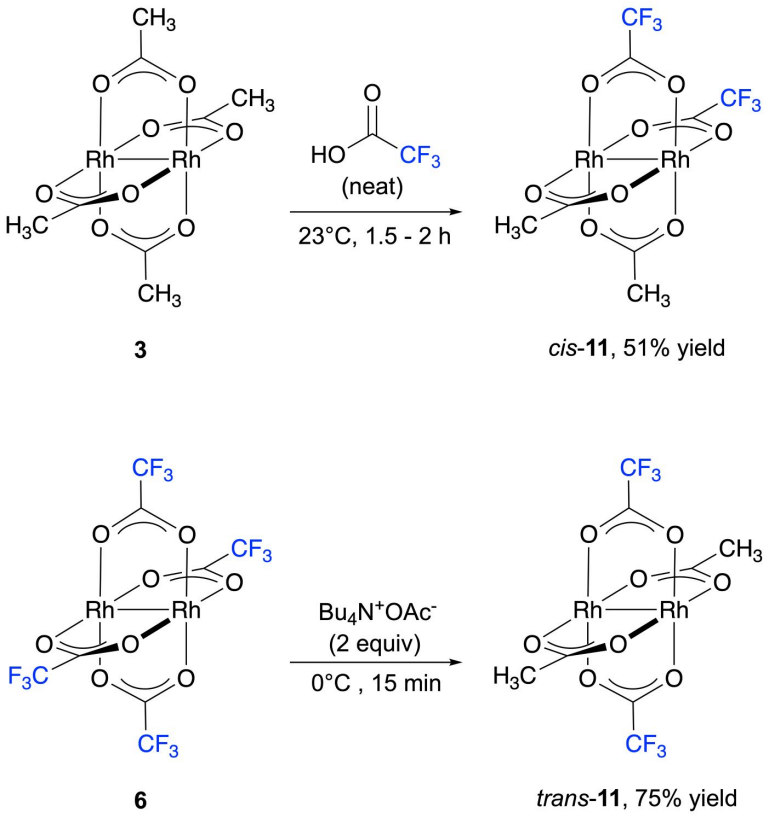

Figure 2.11: Synthesis of *cis* and *trans* isomers of $Rh_2(OAc)_2(tfa)_2$ 11.

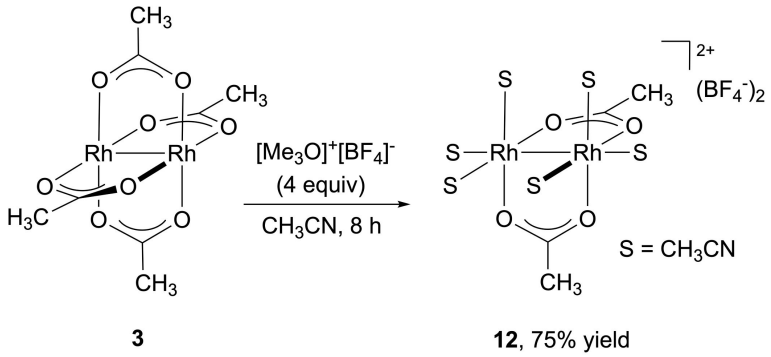

Figure 2.12: Synthesis of partial paddlewheel complex 12, in which acetate ligands have been replaced with acetonitrile solvent (S = CH_3CN).

2.5 Rhodium(II) Paddlewheel Electronic Structure

The physical structure of the Rh(II) paddlewheel complex is characterized by four bridging ligands, two Rh centers connected by a single bond, and two axial positions which can be occupied by labile coordinating ligands. The physical structure of the Rh(II) complex is often perturbed to enact differing enantioselectivity by way of bridging ligand modifications. The equatorial bridging ligands are kinetically inert and usually require harsh conditions to substitute. However, the axial ligands are kinetically labile, a property that is proposed to be due to the *trans* effect. The *trans* effect and *trans* influence are commonly regarded as the same phenomena. The difference between the *trans* effect and *trans* influence is the *trans* influence is a thermodynamic effect. The impact of a ligand on the bond length of an atom *trans* is considered the *trans* influence. When an atom effects the rate of substitution this is considered the *trans* effect. The two are often confused because historically they have both been referred to as the *trans* effect but the *trans* effect was referred to as the kinetic *trans* effect and the *trans* influence was referred to as the thermodynamic *trans* effect. The axial sites on the Rh(II) paddlewheel complex have been established to be the site of catalysis for carbene and nitrate transfer reactions through rigorous computational and experimental efforts.[94–100] Therefore, the efficient catalytic properties of the Rh(II) paddlewheel complex are also proposed to be due to the *trans* effect, or the ability of the *trans* rhodium atom to the carbene to increase the rate at which the carbene reacts.

The indication that the *trans* effect is responsible for the efficient catalytic activity of the Rh(II) paddlewheel complex makes the understanding of the Rh–Rh bond's electronic structure integral to understanding its reactivity. Cotton developed a convention to describe these metal–metal bonding events with the x and y axes pointing toward the equatorial bridging ligands and the z axis along the Rh–Rh bond.[51] A single Rh in a square planar geometry, or D_{4h} symmetry, consists of five valence d atomic orbitals, or AOs. These AOs have their own symmetry notation: a_{1g}, b_{1g}, b_{2g}, and e_g for the d_{z^2}, $d_{x^2-y^2}$, d_{xy}, and the energetically degenerate d_{xz} and d_{yz}, respectively. The combining of two of these AOs of the RhL_4 D_{4h} square planar complex to form the Rh(II) paddlewheel complex also with

D_{4h} symmetry. The resulting molecular orbital, or MO, diagram consists of combinations of the AOs of the individual RhL_4 to form MOs that describe the electronic structure of the Rh–Rh bond (Fig. 2.13). The d_{z^2} orbitals combine to give a filled σ bonding orbital, of a_{1g} symmetry, and an unfilled σ^* antibonding orbital, of a_2u symmetry, combinations. The degenerate d_{xz} and d_{yz} orbitals overlap with themselves to form a degenerate set of π bonding orbitals, of e_u symmetry, and a set of π^* antibonding orbitals, of e_g symmetry. A δ-type overlap is the result of the combination of the d_xy and $d_{x^2-y^2}$ orbitals. The MOs formed from these combinations are two δ bonding orbitals, of b_2g and b_1g symmetry respectively, and two δ^* antibonding orbitals, of b_{1u} and b_{2u} symmetry respectively. The b_2g and b_1u orbitals resulting from the combination of the $d_{x^2-y^2}$ orbitals are too high in energy to be filled so they are not relevant to the discussion as it relates to the reactivity of the system. Some consequences that result from these combinations are the Rh–Rh bond order is one and the π^* and δ^* are similar in energy. Extensive computational modeling has been conducted to answer the question of whether the HOMO consist of either the π^* or δ^* orbitals since the result is not apparent from experimental evidence (*vide infra*).

An L_{ax} may not be purely a σ donor but may also have π-accepting properties. If it has an empty p or d orbital, or antibonding orbitals with matching symmetry to the Rh–Rh π^* orbital, π-backbonding can occur. This is a plausible explanation for the exceptional rate that Rh(II) complexes decompose diazo compounds. Not only does the diazo compounds have σ-donation from the negatively polarized C atom into the Rh–Rh σ^* orbital, a filled Rh–Rh π^* orbital is capable of π-backbonding with the C–N antibonding orbital. This interaction would further weaken the C–N bond and increase the rate of nitrogen extrusion to for the metal carbene. The increased rate of the reactivity of the group *trans* to the rhodium is the it is classified as a kinetic *trans* effect. A demonstration of its superelectrophilicity is that the carbenoid can activate C–H bonds. This "superelectrophilic" phenomena has been eloquently described by Berry in his three-center/four-electron (3c/4e) bonding model.[56] Berry took inspiration from the three-center bonding description of the Rh(II) carbenoid intermediate proposed by Nakamura *et al.* as a result of a comprehensive density functional theory (DFT) study of the Rh(II)-catalyzed C–H functionalization mechanism.[101] In its

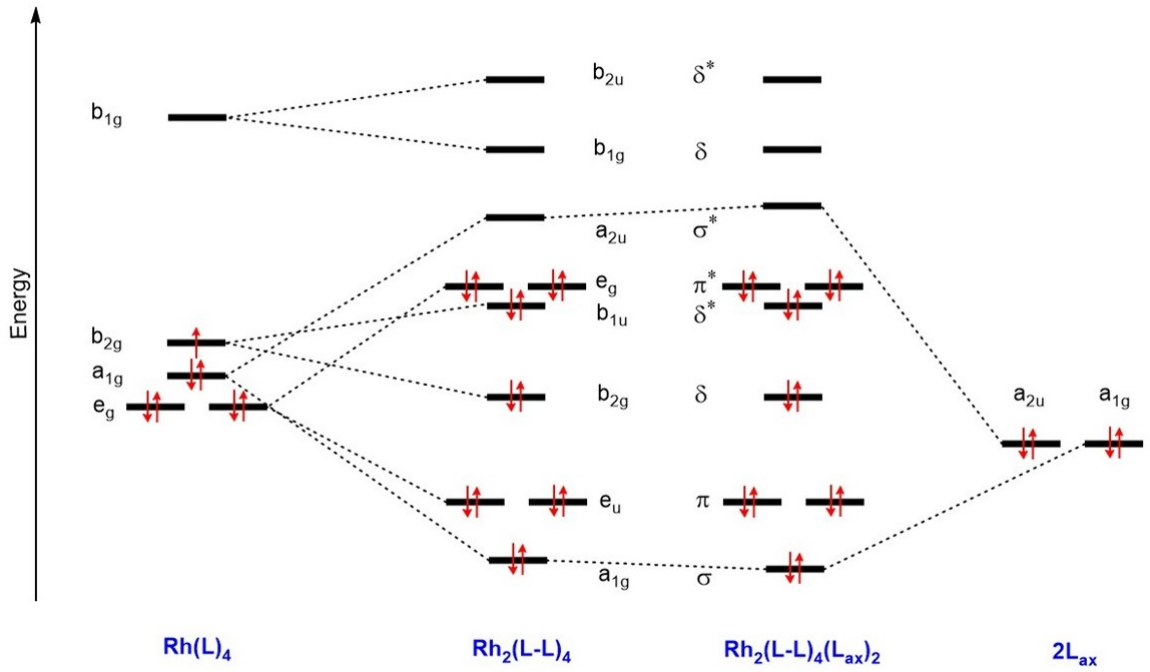

Figure 2.13: A qualitative molecular orbital diagram derived from the combination of the AOs of two square planar RhL_4 complexes to form $Rh_2(L–L)_4$ and further perturbation of the resulting energies by 2 axial ligands, L_{ax}.

simplest form, the 3c/4e model can be implemented to describe the H_3^- system and explain the divergence from the two-center/two-electron system of molecular hydrogen (H_2, Fig. 2.14a). As described in DFT studies, the donation of the lone pair of the H^- into the H–H antibonding orbital increases the original bond length of H_2 from 0.74 to 1.08 Å, which is a 40% increase (Fig. 2.14b).[102] The interaction between the H lone pair and the H–H antibonding orbital are greatest when the geometry is linear (180°). Not only are there physical differences between the 2c/2e H_2 and the 3c/4e H_3^- anion, there are energetic differences as well. Berry demonstrates that the H_3^- anion has nine electronic states while H_2 only has four. The lowest singlet to singlet excited state of the H_3^- takes roughly two-fold less energy to access as the lowest H_2 excited state. This transition is the promotion an electron from the HOMO to the LUMO. The Pearson model states that chemical reactivity of a molecule is related to the lowest energy excitation of a molecule,[103] so the 3c/4e molecule should be more reactive. Also, the increased number of excited states should mean the 3c/4e system will be more diverse in reactivity.

Berry also demonstrates how the 3c/4e model is applicable to the Rh(II) carbenoid intermediate. It is important to define the electronic structure of the Rh(II) carbenoid to understand the implications of the 3c/4e bonding model on reactivity. The Rh(II) carbenoid is a Rh_2^{4+} dimer with a singlet carbene axially coordinated. The orbitals that appear in the bonding framework are one set of three-centered σ orbitals, one set of three-centered π orbitals, and two-center $Rh_2\pi$ and δ orbitals (Fig. 2.15a). The bonding framework consists of 16 valence electrons; 14 electrons from the Rh–Rh framework and the two electrons donated into a Rh from the carbene. The molecular orbitals have been qualitatively ordered by energy as $\sigma < \pi < \mathrm{Rh_2}\text{-}\pi < \delta < \sigma_{nb} \sim \pi_{nb} < \delta^* \sim \mathrm{Rh_2}\text{-}\pi^* < \pi^* < \sigma^*$ and filling these with the 16 electrons produce an electronic configuration of $\sigma^2\pi^2\mathrm{Rh_2}\text{-}\pi^2\delta^2\sigma_{nb}^2\pi_{nb}^2\delta^{*2}\mathrm{Rh_2}\text{-}\pi^{*2}$(Fig 1.15b).[56] This indicates the HOMO of the carbenoid intermediate is non-bonding regarding the Rh–C bond and the LUMO is the three-centered π^* orbital that predominantly features the empty C p orbital. The presence of occupied $\sigma^2\sigma_{nb}^2$ and $\pi^2\pi_{nb}^2$ indicate both a 3c/4e σ and 3c/4e π bond are present in the electronic structure of the Rh–Rh–C bonding framework of the carbenoid intermediate. Also, the Rh–Rh and Rh–C bonds having both σ and π components

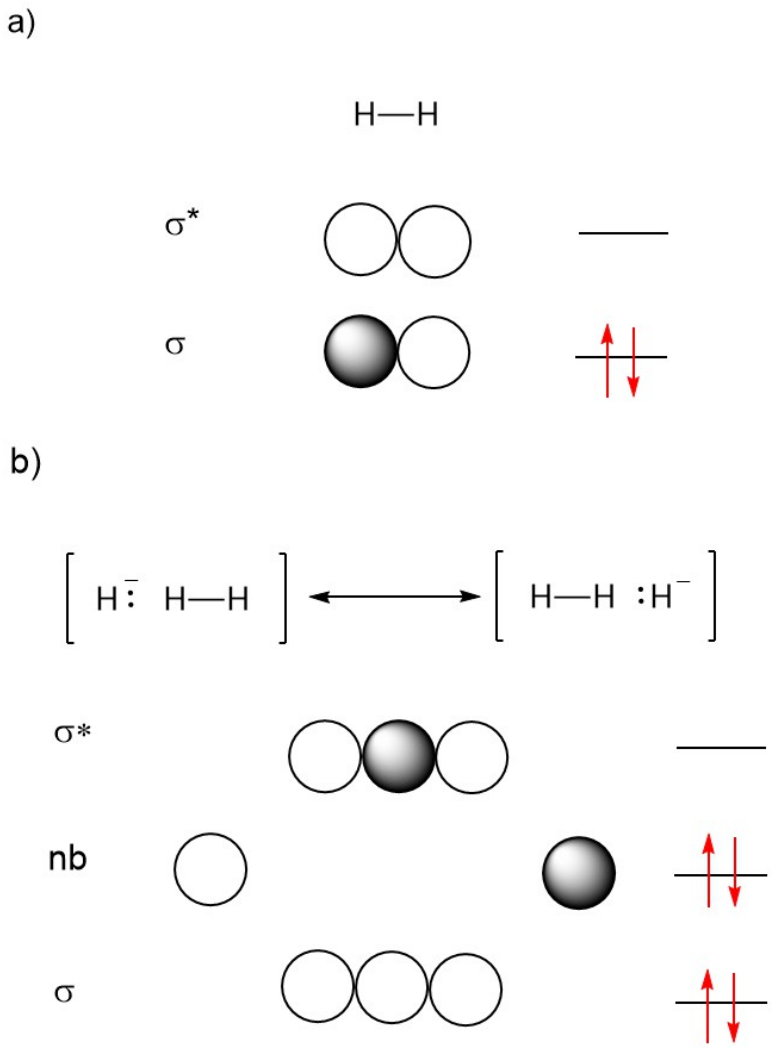

Figure 2.14: a) The Lewis and molecular orbital depiction of H_2's bonding. b) The The Lewis structure and molecular orbital theory bonding models for the linear H_3^- anion.

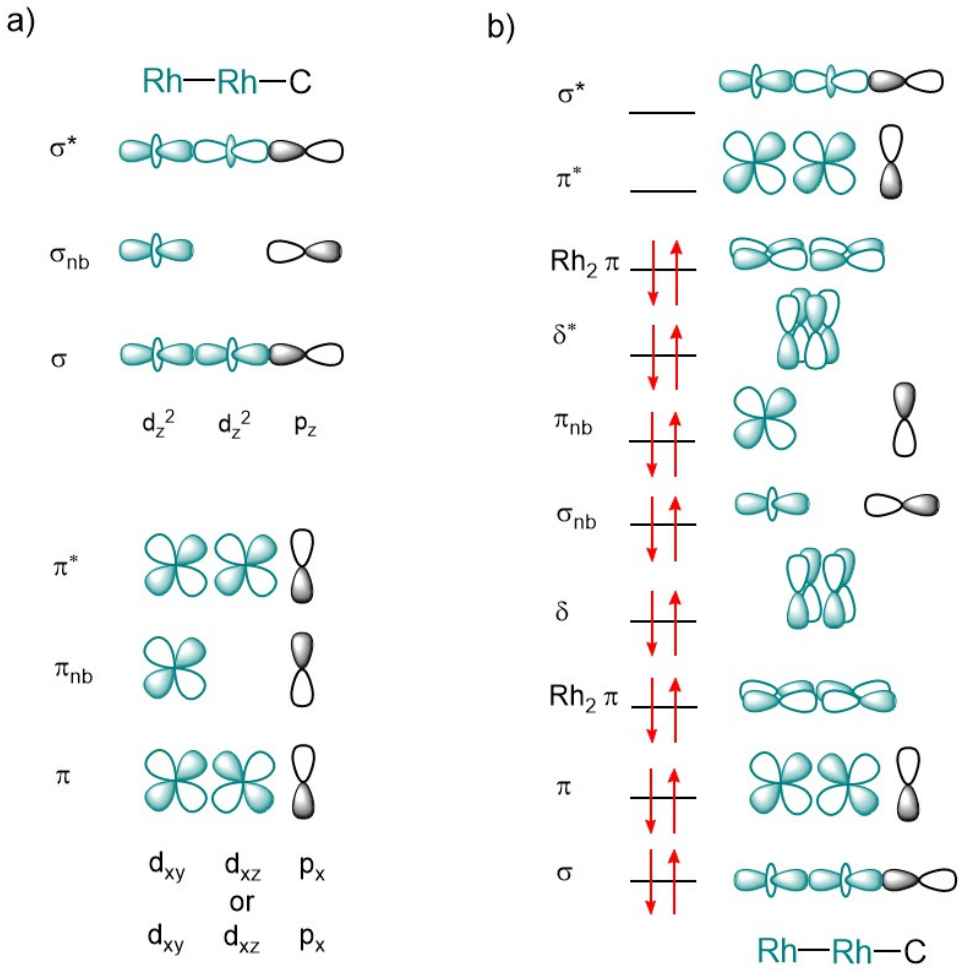

Figure 2.15: a) The σ and π 3c/4e molecular orbitals for available for bonding with the Rh(II) carbenoid. b) Qualitative molecular orbital diagram for the Rh(II) carbenoid.

would indicate they both have double bond character. Although both the Rh–Rh and Rh–C bonds have double bond character, neither contain true double bonds. The consequence of the 3c/4e σ and π bonds are a weakening of the interaction between the Rh–Rh and Rh–C bonds. This can be seen in the calculated Mayer bond orders for the Rh_2(formate)$_4$ carbenoid from decomposed from diazomethane, which have Rh–Rh and Rh–C bonds of 0.79 and 1.35 respectively.[56]

As mentioned above, the symmetry of the HOMO has been of much discussion in the literature. Groups have probed the valence structure with multiple spectroscopic and computational methods to provide a clearer picture of the electronic structure of the Rh–Rh bond. Dubick and Marten performed the earliest calculations to address this this problem. They utilized H*ü*ckel calculations in their initial disclosure on model complex $Rh_2(O_2CH)_4$ to determine the electronic configuration to be $\sigma^2\pi^4\delta^2\delta^{*2}\pi^*{}_4$.[104] In a subsequent disclosure, Norman and Kolari utilized SCF-α calculations to determine the electronic configuration of $Rh_2(O_2CH)_4$ to be $\sigma^2\pi^4\delta^2\pi^{*4}\delta^{*2}$.[105,106] The first experimental indication of the symmetry of the HOMO was an EPR study of the cationic $[Rh_2(O_2CH_3)_4{\cdot}(H_2O)_2]^+$ complex in which the HOMO was determined to be the degenerate π^* orbitals.[107,108] Mougnet *et al.* disclosed an *ab initio* SCF/CI computational study that supported the result of the EPR study.[109] Interestingly, *ab initio* calculations of the $Rh_2(O_2CH_3)_4{\cdot}(PH_3)_2$ complex by Nakatsuji *et al.* determined the HOMO to be the σ^2 orbital while the $Rh_2(O_2CH_3)_4$, $Rh_2(O_2CH_3)_4{\cdot}(H_2O)_2$, and $Rh_2(O_2CH_3)_4{\cdot}(NH_3)_2$ complexes were all calculated to be the δ^{*2} orbital.[110] A subsequent *ab initio* SCF-Xα-SW study of the $Rh_2(O_2CCF_3)_4$ complex agreed with the previously mentioned SCF-Xα calculations that $\sigma^2\pi^4\delta^2\pi^{*4}\delta^{*2}$ represents the electron configuration. A difference in energy was calculated between the π^{*4} and δ^{*2} orbitals and their ionization potentials to be 0.48 eV and $\sim$0.75 eV, respectively.[111]

Lichtenberger *et al.* reported He I and He II gas-phase photoelectron spectra that determined the electron configuration of $Rh_2(O_2CCF_3)_4$ it be $\sigma^2\pi^4\delta^2\delta^{*2}\pi^{*4}$ agreeing with DFT calculations they performed.[112] The energy separation between the calculated π^{*4} and δ^{*2} ionization energies was only 0.14 eV. In a later computational study, Sizova and Ivanova used the DFT functional B3LYP with multiple basis sets and found the

$Rh_2(O_2CH)_4$, $Rh_2(O_2CCH_3)_4$, $Rh_2(O_2CC_6H_5)_4$, and $Rh_2(O_2CCF_3)_4$ electron configurations to be $\sigma^2\pi^4\delta^2\pi^{*4}\delta^{*2}$ regardless of basis set used. It is noteworthy that all orbital energies calculated for $Rh_2(O_2CCF_3)_4$ were much lower than the rest of the series. Elucidation of the orbitals that truly make up the HOMO of the Rh(II) paddlewheel complex will need more refined tools that can separate the degeneracy. It does seem to be agreed upon in recent literature that it consist of either the π^* or the δ^*.

The Rh(II) carbenoid's electronic structure has been investigated computationally and experimentally. Computational studies of the Rh(II) carbenoid are essential due to their transient nature. Spectroscopic data and x-ray crystal structures have only recently been obtained.[113] Most computational studies of the Rh(II) carbenoid complex focus less on the electronic structure and more on the potential energy surface, Natural Bond Order, or NBO, calculations and Natural Population Analysis, or NPA, calculations coupled with structural elements to inform on the system. Since there are few examples of Rh(II) carbenoids isolated or ways to broadly probe this fleeting intermediate, the discussion on the Rh(II) carbenoid will be narrowed to a discussion of how axial coordination is to affects the Rh(II) carbenoid structure and how this relates to reactivity of the metal carbene.

Davies *et al.*, the experimentally and computationally investigated the Bi–Rh paddlewheel complex and its performance in relation to Rh_2(formate)$_4$.[100] In their computational studies they calculated the reaction potential energy surface at the B3LYP/6-311G(2d,2p)[Rh-RSC+4f][Bi-RLC]//B3LYP/631G*[Rh-RSC+4f][Bi-RLC] level or theory for both catalyst in the cyclopropanation of styrene with methyl phenyldiazoacetate. The rate calculated rate of the reaction, 19 kcal/mol versus 11.3 kcal/mol with the Bi–Rh complex and Rh_2(formate)$_4$ respectively, did not agree with the observed rates of reaction. This led Davies and coworkers to investigate the axially coordinating species effect on the cyclization reaction. They reasoned the choice of acetone as an axial coordinating group due to the carbonyl functional groups prevalence in the products of these reactions. Axial coordination of acetone on the Rh_2(formate)$_4$ during the cyclopropanation reaction was found to have a large impact on the on the barrier for N_2 extrusion in the rate determining step, an increase of 4.7 kcal/mol.[100] This phenomenon was much less pronounced on this barrier when acetone

was axially coordinated to the Bi–Rh complex and the resulting calculated rates agreed with experimental results. A charge distribution analysis, utilizing Mulliken charges, was performed throughout the reaction pathway. It was concluded that both the Rh and Bi could act as a redox pool, but the event happened at different points in the reaction. The distal Rh was oxidized upon coordination of the diazo compound while the Bi was not oxidized until the carbenoid formation event.

In 2015, Kisan and Sunoj studied the effects of axial coordination by a chiral spinol phosphoric acid used in a cooperative catalyst system in their pursuit of enantiopure amino esters.[114] The uncertainty of the dynamical system led them to investigate other additives as well. They calculated the potential energy surface at the SMD($CHCl_3$)-M06/LANL2DZ[6-31G(d,p)]//B3LYP/ LANL2DZ[6-31G(d)] level of theory) in which axial solvent ($CHCl_3$) level of theory along the reaction coordinate diagram and found the axial coordination of the additives did not have a profound effect on the energy barrier for any transformation other than the cooperative catalysis step where the chiral spinol phosphoric acid's axial coordination stabilized the desired transition state.

The most thorough computational study of the effect axial coordination has on the Rh(II) catalyst, Rh(II) carbenoid, and its relationship to reactivity was conducted by Tanillo *et al.* in 2021.[115] They systematically investigated the effects of axial coordination of solvents with varying degrees of σ donation on the decomposition of acceptor-acceptor, donor-acceptor, and donor-donor diazo compounds with Rh_2(formate)$_4$ at the M06/SDD[6-11+G(d,p)]//B3LYP/LANL2DZ[631G(d)] level of theory. They sought to answer whether axial coordination had a notable impact on reactivity and selectivity in C–H insertion reactions. They also sought to reveal if it was possible to rationally tune reactivity with solvent. The results of their study on the perturbation of frontier molecular orbital agreed with Berry's demonstration of the σ donation increasing the energy of the LUMO, resulting in an increased HOMO-LUMO gap. The effect of axial coordination on the Rh(II) carbenoid frontier orbitals was found to have a greater destabilization effect on the HOMO.[56,115] They then turned their attention toward the N_2 extrusion step. They found that increasing the σ donation of the axial coordinating solvent would not only reduce the exothermic

nature of the diazo coordination step but could create an energetic barrier. This increased barrier was also present in the nitrogen extrusion step. When Tantillo *et al.* studied effects of axial coordination on regioselectivity in the C–H insertion of propane they found isopropanol had the greatest effect with donor/donor and donor/acceptor diazo compound. The increased σ donation had a negative impact on regioselectivity with acceptor/acceptor diazo compounds. When studying axial coordination's impact on structural characteristics, it was found that the bond distance resisted dramatic increase in Rh–Rh bond distance throughout the catalytic cycle. This resistance happened regardless of the calculated bond order as described by the Wiberg Bond Indices. The conclusion of their study is iteratively the impacts seem quite small but could have a profound effect in the flask.

2.6 Catalysts and Applications

2.6.1 Mixed Carboxylate Complexes

In 2012, Charette *et al.* disclosed a method for incorporating a tetrachlorophthaloyl group on the bridging ligand scaffold to control the polarity of heteroleptic complexes.[65] The markedly different polarity when chlorinated ligands were incorporated eased the chromatographic purification of the product mixtures, which contained a statistical mixture of four to six products (Fig. 2.16a). The introduction of the halogens increased structural rigidity in the complexes *via* intramolecular halogen bonds between ligands. Charette *et al.* al. produced 10 examples of the ligand substitution resulting in overall yields ranging from 58% to 87%. In most cases, the $Rh_2(A)_3(B)_1$(A = chlorinated phthalolyamino ligand, B = non-chlorinated carboxylate ligand), *cis* and *trans* $Rh_2(A)_2(B)_2$, and $Rh_2(A)_1(B)_3$ were all isolable by flash chromatography. In a few cases, *cis* and *trans* isomers of the $Rh_2(A)_2(B)_2$ could not be separated. The method was further applied to the production of a phosphate-carboxylate complex that was also separable by column chromatography.

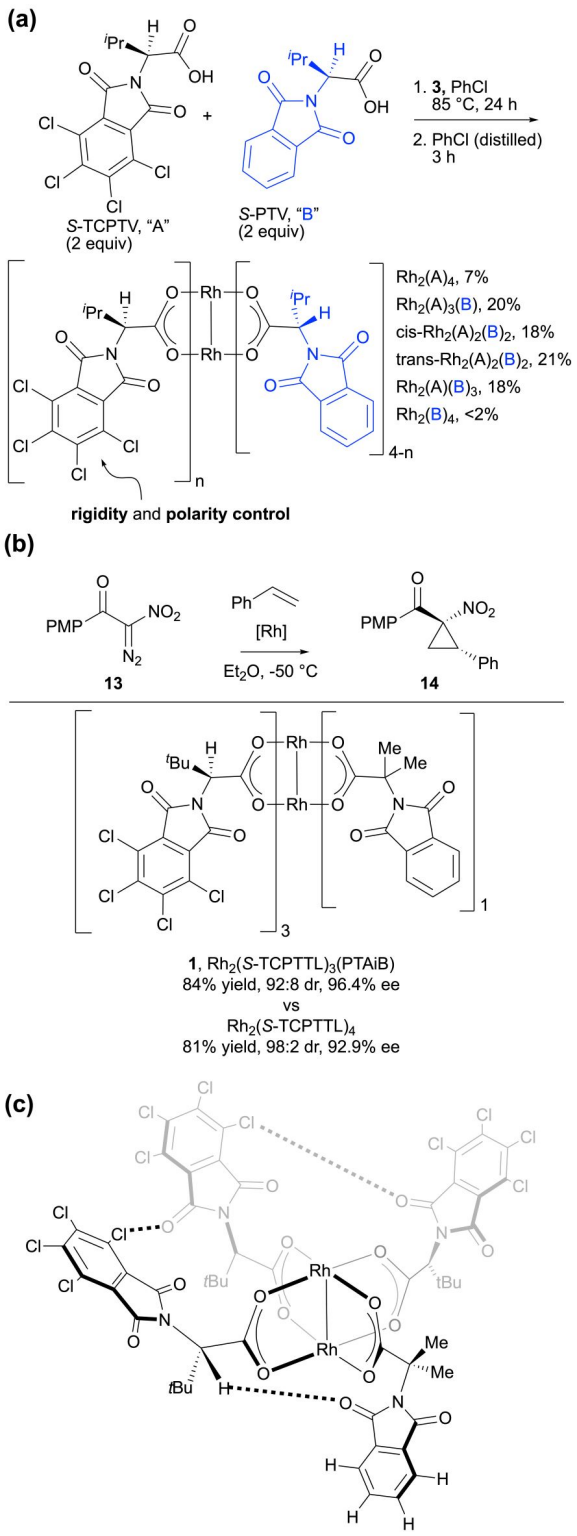

Figure 2.16: (a) Synthesis of heteroleptic dirhodium(II) carboxylates with phthaloylamino ligands. (b) Yields and selectivity of complex 1 versus $Rh_2(TCPTTL)_4$ in diazo-mediated cyclopropanation. (c) Non-covalent interactions on 1.

Complexes with $Rh_2(A)_3(B)_1$ substitution were chosen as interesting candidates to investigate the effects of halogen bond rigidification in the cyclopropanation of styrene with α-nitro diazoacetophenone. In particular, when the achiral PTAiB (PTAiB = *N*-phtalimido-2-aminoisobutyric acid) ligand was substituted as the non-chlorinated ligand, enantioselectivity was increased (Fig. 2.16b). This was reasoned by the 60-75° conformational twist in the ligand from the "all up" crown conformation because of the *gem*-dimethyl groups (Fig. 2.16c). Interestingly, a C–H$\cdots$O hydrogen bond between the achiral ligand and an adjacent TCPTTL (TCPTTL = *N*-tetrachlorophthaloyl-*tert*-leucinate) ligand provided another mode of stabilization not typically seen on rhodium paddlewheel complexes (Fig. 2.16c). Thus, Rh_2(*S*-TCPTTL)$_3$(PtAiB) complex 1 provided an entry into the viability of the α,α,α,β conformation as effective Rh(II) paddlewheel platforms for asymmetric rhodium carbenoid reactions.

Just before Charette's findings with Rh_2(*S*-TCPTTL)$_3$PtAiB, Fox *et al.* disclosed the heteroleptic Rh(II) complex, Rh_2(*S*-PTTL)$_3$TPA 17 (PTTL = *N*-phthaloyl-*tert*-leucinate, TPA = triphenylacetate).[116] Catalyst 17 was synthesized in 40% yield by direct ligand exchange with $Rh_2(OAc)_4$ using 3 equivalents of *N*-phthaloyl-(*S*)-*tert*-leucinate and one equivalent of triphenylacetic acid in refluxing chlorobenzene in a Soxhlet-type apparatus. The product mixture also contained 40% yield of the homoleptic complex Rh_2(*S*-PTTL)$_4$ and 20% yield of the disubstituted complex Rh_2(*S*-PTTL)$_2$(TPA)$_2$. Like Rh_2(*S*-PTTL)$_4$, the *N*-phthalimide groups on 17 were on the same face of the molecule, conserving the "chiral crown" conformation that was hypothesized to be the source of high enantioinduction.

The heteroleptic catalyst 17 was particularly useful for selectivity over side products from β-hydride migration that plague carbene reactions involving α-alkyl diazoacetates.[117] In the cyclopropanation of styrene by ethyl-α-diazobutanoate 15, catalyst 17 gave the best enantioselectivity when compared with the parent catalyst Rh_2(*S*-PTTL)$_4$. The heteroleptic complex compared favourably to the homoleptic variant, providing similar or increased enantioselectivity across the substrate scope. The diastereoselectivity and yields were comparable to Rh_2(*S*-PTTL)$_4$ for all substrates tested other than the 3-methoxystrene, in

which diastereoslectivity was better with 17 as catalyst (83:17 with Rh_2(S-PTTL)$_4$ compared to 99:1 with 17, Fig. 2.17).

Catalyst 17 was also successful in the cyclopropenation of α-n-alkyl-α-diazoesters with trimethylsilyl acetylene and 1-hexyne. Silylacetylenes, in particular, have failed to be an effective substrate in cyclopropenation reactions. Despite this difficult substrate, Rh_2(S-PTTL)$_3$TPA 17 outperformed all the chiral homoleptic catalysts surveyed, improving both yields and enantioselectivity of the silylcyclopropene product (Fig. 2.18). β-Hydride migration products were the major products with Rh_2(S-PTTL)$_4$ and other homoleptic catalysts tested in this system.

Fox *et al.* also used catalyst 17 in the C–H insertion of 4-substituted indoles.[116] At the time, the highest enantioselectivity achieved for 4-substituted indoles was with Hashimoto's Rh_2(S-PTTEA)$_4$ catalyst (PTTEA = N-phthaloyltriethylalaninate), which provided up to 86% ee of α-methyl-3-indolylacetates.[118] Complex 17 gave improved results in both yield and enantioselectivity, giving 80% yield and 81% ee of the C–H insertion of 4-methyl-N-phenylindole with α-diazobutanoate (Fig. 2.19).

Fox followed up his group's work on Rh_2(S-PTTL)$_3$TPA 17 with a report that featured heteroleptic complex Rh_2(S-NTTL)$_3$dCPA (NTTL = N-naphthaloyl-*tert*-leucinate, dCPA = dicyclohexylphenylacetate) 21 in an elegant synthesis of piperarborenine B, a cyclobutene-containing compound that has shown anti-cancer activity.[119] The 3 S-NTTL ligands are oriented on the top face creating a chiral crown while the bulky dCPA ligand serves to reinforce rigidification. Complex 21 was the optimal catalyst in the key bicyclobutanation/homoconjugate step for the synthesis of piperarborenine B. Synthesis of the cyclobutane 23 was achieved *via* a one-pot procedure with reaction of the diazoester 20 with 0.1 mol% of 21 to produce bicyclobutane intermediate 22, followed by cuprate addition and kinetic protonation to afford the trisubstituted cyclobutane 23 in 69% yield, 92% ee and 4:1 d.r. This was a significant improvement when compared to enantioselectivity obtained with homoleptic complexes (Fig. 2.20).

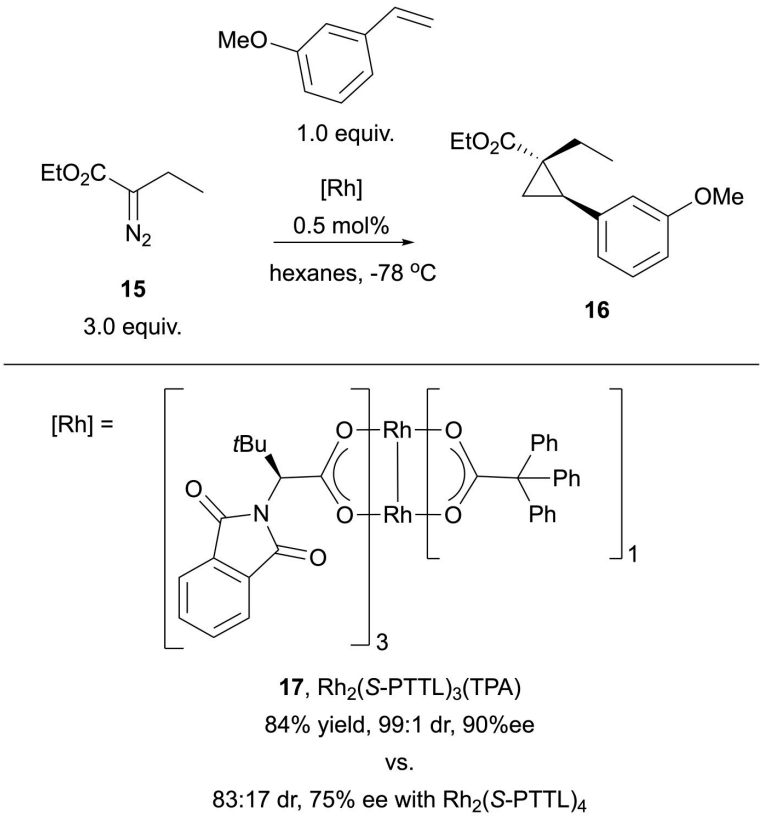

Figure 2.17: C–H insertion of 4-methyl-N-phenylindole with 17.

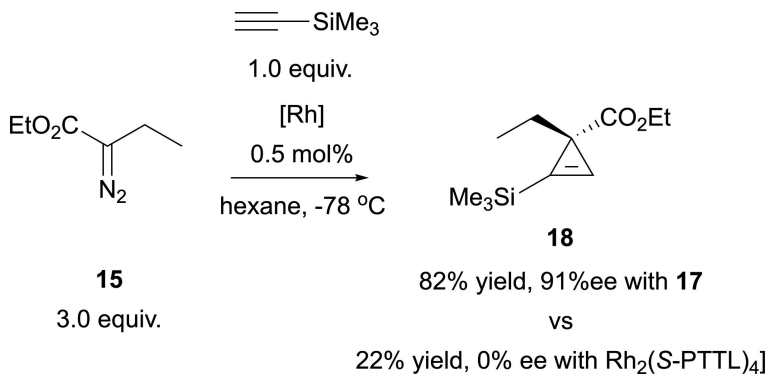

Figure 2.18: Cyclopropenation of trimethylsilylacetylene with 17.

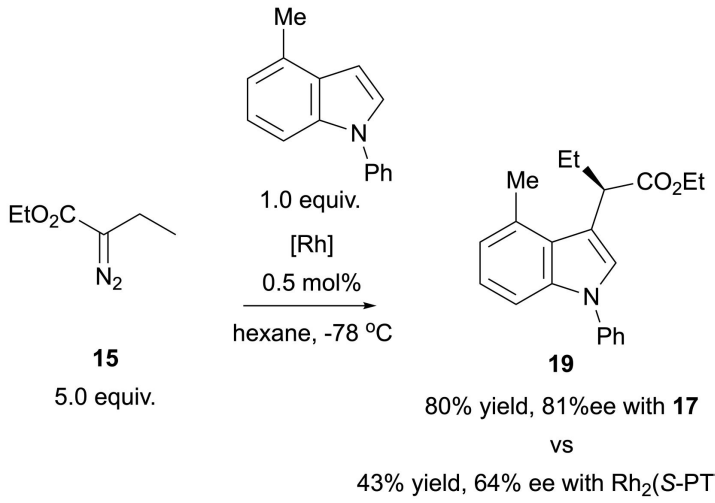

Figure 2.19: C–H insertion of 4-methyl-*N*-phenylindole with 17.

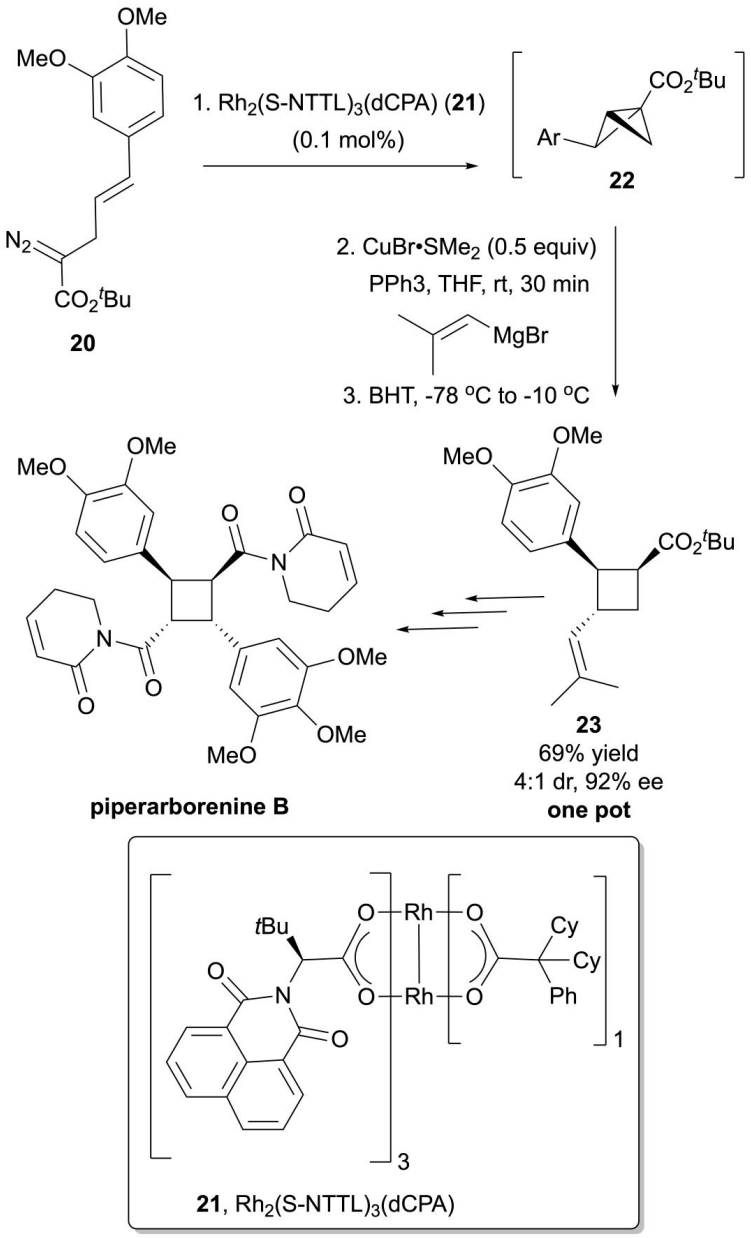

Figure 2.20: Fox group synthesis of piperarborenine B using catalyst 21 in a tandem bicyclobutanation/homoconjugate addition as a key step.

2.6.2 Ortho-metalated Phosphine Derived Complexes

Between 1995-2005, Lahuerta *et al.* intensively studied many derivatives of heteroleptic Rh(II) complexes with orthometalated phosphine and carboxylate bridging ligands (Fig. 2.21).[74,75,77,120–126] The complexes were prepared by normal ligand exchange conditions, but the orthometalated phosphine ligands had the added convenience of preferentially exchanging two acetate ligands in a *cis* fashion and a head-to-tail arrangement when 2 equivalents of arylphosphine was used.[72,73] Initially, the complexes were used as racemic mixtures, though enantioenriched *P* and *M* isomers could be isolated by chiral resolution (*vide infra*).[122]

In competitive intramolecular reactions, the racemic complexes were highly selective for cyclopropanation products over competing C–H insertion or aromatic substitution reactions, outperforming $Rh_2(OAc)_4$ in selectivity and the electron rich $Rh_2(cap)_4$ (cap = caprolactamate)[127] in yield (Fig. 2.22, shown with 24a).[74,75] Complexes with orthometalated phosphines and fluorinated carboxylate bridging ligands like 24b were the only derivatives to be selective for C–H insertion product 30 over aromatic substitution compared to common homoleptic Rh(II) complexes (Fig. 2.22). It was postulated that the π-backbonding ability of the metalated ring stabilizes the carbene for improved selectivity, while ligand field effects of the fluorinated carboxylate ligands stabilize the σ bond to result in a more electrophilic carbene.[75]

Methyl-2-diazoundecanoate 34 was chosen as the substrate to study the ability of the orthometalated phosphine catalysts to discern between intramolecular C–H insertion vs β-hydride migration of α-alkyl diazoesters.[77] At the time, previous studies of Rh(II) tetracarboxylates showed that β-hydride migration products were highly competitive to their 1,5-insertion counterparts at room temperature. Initially, upon extension to orthometalated phosphine complexes, doubly metallated complexes led only to migration product 36 in high yield. Ultimately, monometalated complex 37 with fluorinated aryl groups were much more selective for C–H insertion than doubly metalated complexes despite the expected increase in Rh-carbenoid electrophilicity due to the fluorinated phosphine (Fig. 2.23). Preference for product 35 *versus* migration product 36 was partly explained by an intermediate in which

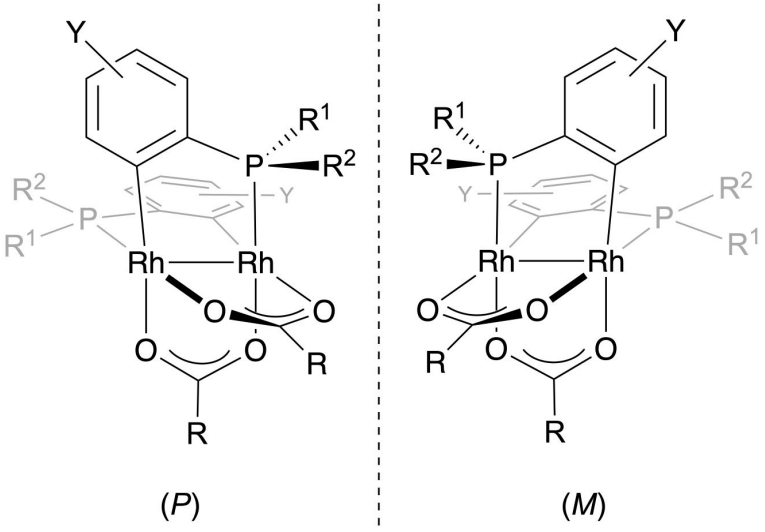

24, $Rh_2(O_2CR)_2(PC)_2$

24a, R^1, R^2 = *p*-FC_6H_4; R = CH_3; Y = *p*-F

24b, R^1, R^2 = C_6H_5; R = C_3F_7; Y = H

24c, R^1, R^2 = *p*-$CH_3C_6H_4$; R = CF_3; Y = *p*-CH_3

24d, R^1, R^2 = *m*-$CH_3C_6H_4$; R = CF_3; Y = *m*-CH_3

24e, R^1, R^2 = *p*-Me_3Si-C_6H_5; R = CF_3; Y = *p*-Me_3Si

24f, R^1, R^2 = C_6H_5; R = CF_3; Y = H

Figure 2.21: Notable orthometalated phosphine Rh(II) catalysts.

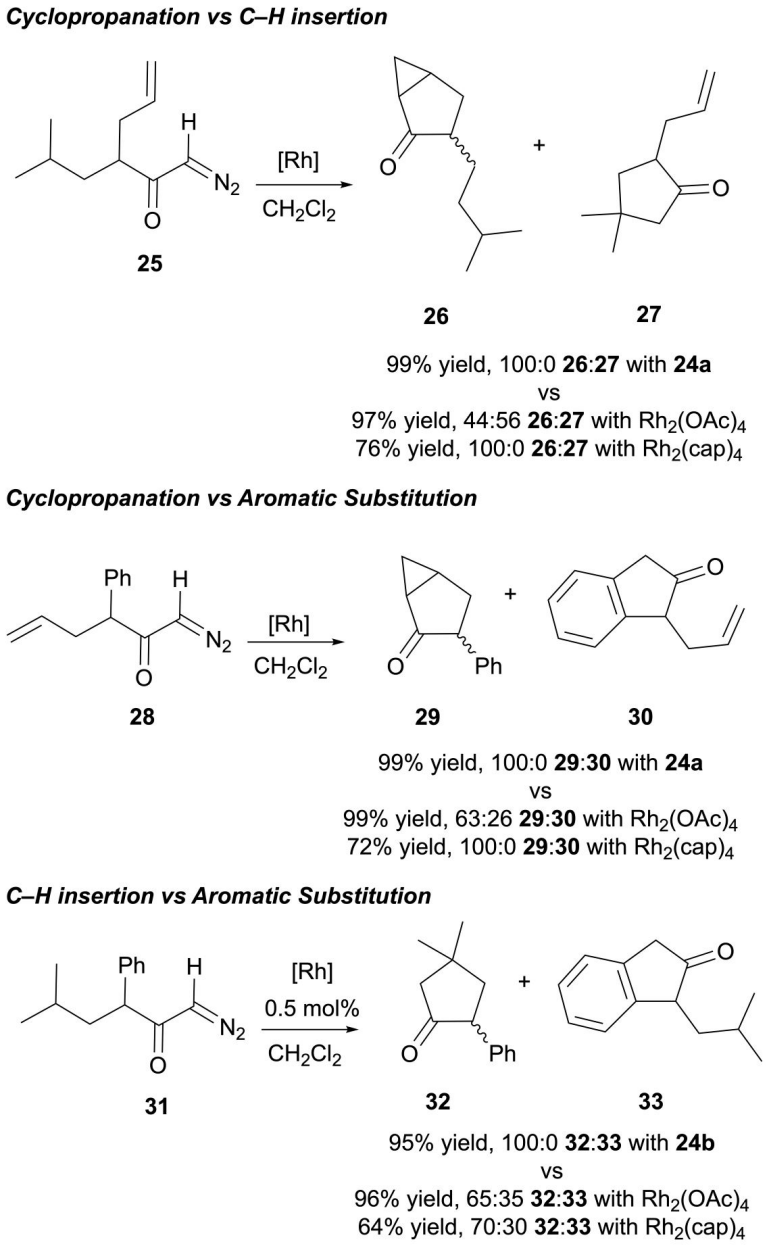

Figure 2.22: Intramolecular selectivity studies with orthometalated phosphine complexes 24a and 24b compared to common homoleptic dirhodium (II,II) catalysts.

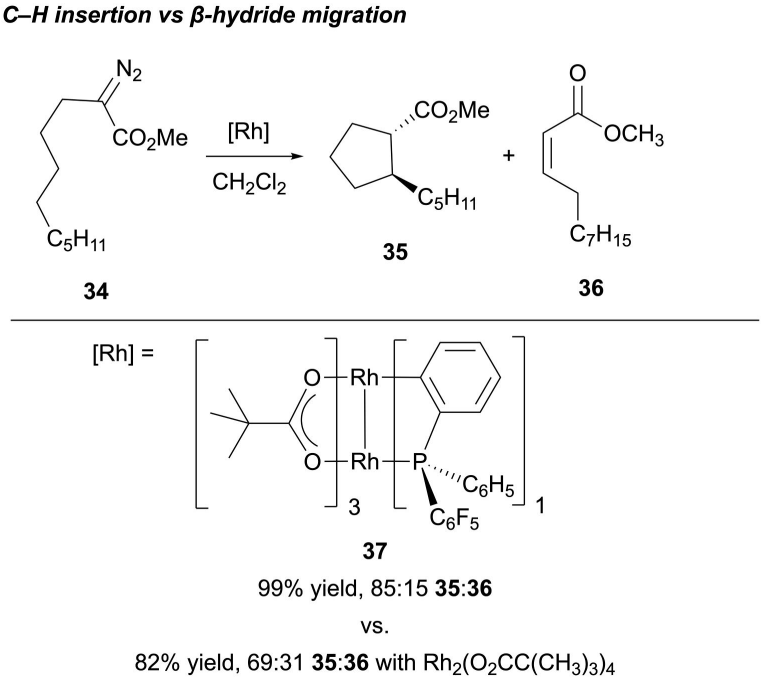

Figure 2.23: Selectivity for C–H insertion over β-elimination was best with monometalated complex 37.

the fluorine stabilizes the Rh-carbenoid, making the migration process slower and favouring cyclization.[77]

Pure enantiomers of the complexes were separated by chiral resolution strategies.[122,125] The racemic mixture of the *P* and *M* enantiomers were separated by exchanging the acetate groups with the chiral auxiliary, protosH (protosH = *N*-((4-methylphenyl)sulfonyl)-*L*-proline), followed by chromatographic separation of the resulting diastereomers. Exchange of the protos ligands with trifluoroacetic acid provided enantiomerically enriched heteroleptic Rh(II) complexes that gave products with up to 90% ee in the intramolecular cyclopropanation of α-diazo ketones such as 38. The results compared favourably with $Rh_2(5S\text{-MEPY})_4$[128] (MEPY = methyl pyrrolidone-5-carboxylate) which produced 39 in 6% ee (Fig. 2.24, shown with results from (*M*)-24c.[125] Notably, the chiral complexes provided excellent diastereoselectivity and enantioselectivity for the cyclopropanation of styrene with ethyl diazoacetate (40, Fig. 2.24). The presence of bulky trimethylsilyl substituents on the phenyl rings of the metalated phosphine ligands in catalyst (*M*)-24e was a key difference that further improved diastereocontrol between products 41 and 42.[76,125] These results are particularly notable as few Rh(II) catalysts are capable of diastereo- and enantiocontrol in cyclopropanation reactions with ethyl diazoacetate.[129,130]

In orthometalated phosphine catalysts, sterics and ligand basicity were found to be a large factor in predicting the behaviour of the complexes. In general, the less electrophilic complexes naturally had decreased catalytic activity but were associated with enhanced selectivity. More bulky substrates and catalysts also forced greater selectivity by limiting the possible orientations of the metal carbenoid. Of late, structural and kinetic studies have characterized research related to this series of complexes.[78,126,131]

2.6.3 Mixed Phosphate Complexes

One of the first Rh(II) paddlewheel complexes containing phosphate equatorial groups was prepared by McCann, McKervey, *et al.* as a heteroleptic system.[132,133] Complex $Rh_2(HCO_3)_2((+)\text{-Phos})_2$ 43 was synthesized in 15% yield via ligand exchange of sodium

Intramolecular Cyclopropanation

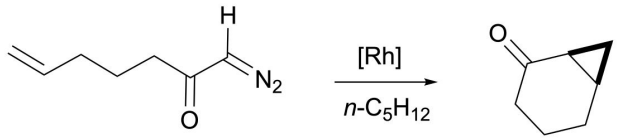

38 **39**

96% yield, 90% ee with (***M***)-**24c**

vs

96% yield, 6% ee with Rh_2(5*S*-MEPY)$_4$ in CH_2Cl_2

Intermolecular Cyclopropanation

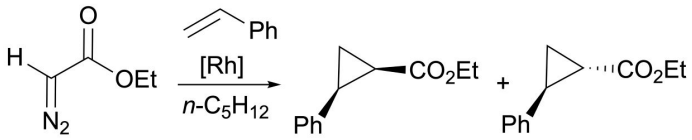

40 **41** **42**

[Rh]	yield (%)	**41**:**42**	% ee **41**	% ee **42**
(***M***)-**24c**	57	57:43	95	84
(***M***)-**24d**	60	44:56	95	92
(***M***)-**24e**	39	90:10	91	7
(***M***)-**24f**	55	48:52	91	87

Figure 2.24: Cyclopropanation with chiral orthometalated phosphine Rh(II) catalysts.

Rh(II) carbonate hydrate ($Na_4Rh_2(CO_3)_4 \cdot 2.5H_2O$) with an excess of the ligand (*S*)-(+)-PhosH (PhosH = 1,1'-bi-2-naphthyl-2,2'-diyl hydrogen phosphate) (Fig. 2.25). The complex was then tested for its ability to facilitate 2,3 sigmatropic arrangement, aromatic cycloaddition, and C–H insertion reactions. The catalyst was able to perform all the reactions in good yields (80-93%) with enantiomeric ratios ranging from 9% to 60% ee.[132] In pursuit of homoleptic dirhodium (II,II) phosphate complexes, Lacour *et al.* discovered conditions that resulted in improved yields of disubstituted heteroleptic phosphate complexes.[134] Using $Rh_2(tfa)_4$ 6 as a precursor, the exchange reaction with (*R*)-3,3'-dibromo-1,1'-binaphthyl hydrogen phosphate 44 in refluxing toluene provided complex 45 in 78% yield.[134]

Hodgson *et al.* aimed to access hyperolactone C, which has shown anti-HIV activity, through a key tandem oxonium ylide–[2,3]-sigmatropic rearrangement. To address the improvement of diastereoselectivity from previous studies of the reaction,[135] ylide precursor compound 46 was used as a model substrate to produce spirolactones 47 and 48. It was shown that $Rh_2(OAc)_4$ 3 in CH_2Cl_2 allowed for a highly *endo*-diastereoselective rearrangement (Fig. 2.26). A variety of chiral catalysts were then screened to explore the potential for a catalytic enantioselective path to norphenyl hyperolactone C. In particular, the binaphtholphosphate-derived catalyst Rh_2(*R*-BNP)$_4$ (BNP = binaphtholphosphate) had promising enantiomeric ratios (69:31 er) for the desired diastereomer 47 but with a loss of diastereoselectivity (84:41 dr) compared to 3. It was hypothesized that the bulky BNP ligands were contributing to the decrease in dr which warranted the exploration of the heteroleptic catalyst *cis*-Rh_2(R-BNP)$_2(OAc)_2$ 49. Complex 49 subsequently led to a recovery of the dr (92:8) and only a slight loss in er (61:39), highlighting the potential for heteroleptic dirhodium (II, II) binaphtholphosphate catalysts.

2.6.4 Mixed Carboxylate/Carboxamidate Complexes

Corey *et al.* explored the use of Rh(II) heteroleptic complexes of carboxylates and *R*,*R*-diphenyl-*N*-triflylimidazolidinone (DPTI) ligands for enantioselective cycloaddition reactions. The heteroleptic complex $Rh_2(DPTI)_3(OAc)$ 50 led to highly efficient and enantioselective synthesis of cyclopropenes and cyclopropanes and was more effective than

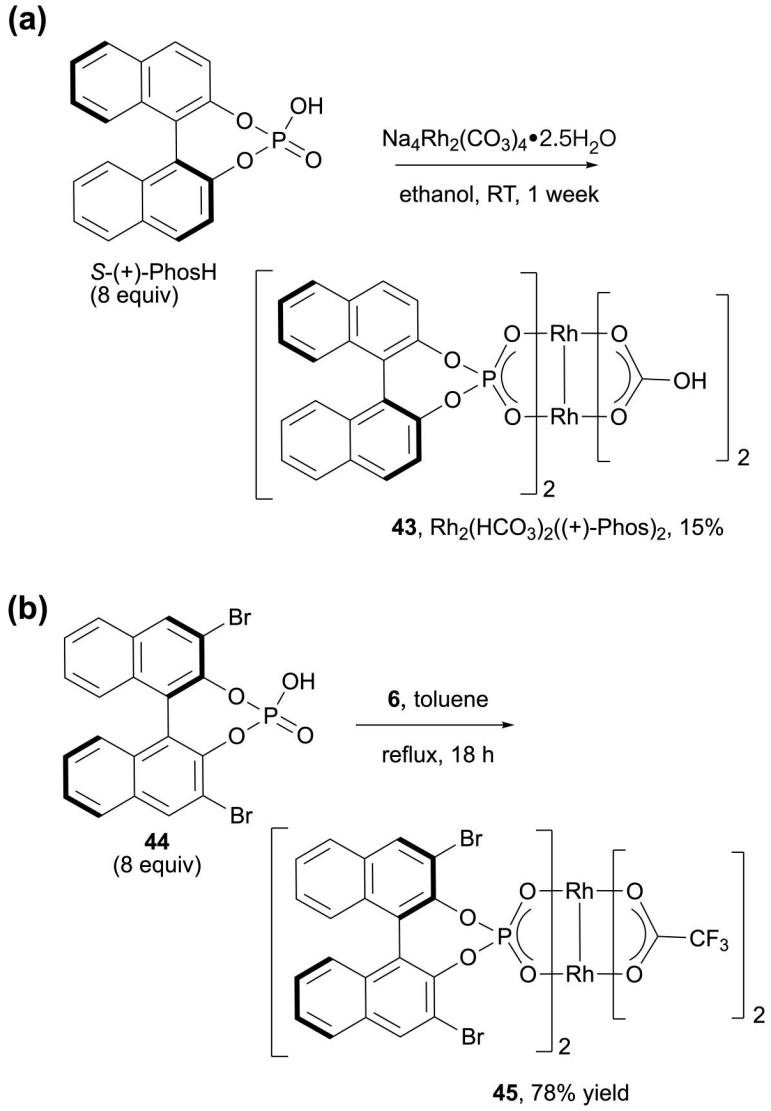

Figure 2.25: Synthesis of heteroleptic Rh(II) phosphate complexes (a) 43 and (b) 45.

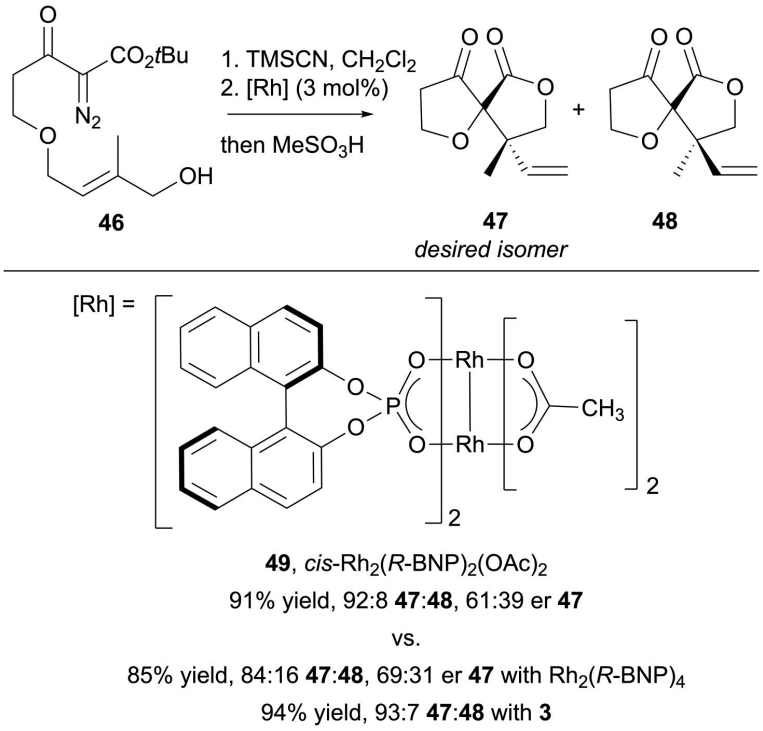

Figure 2.26: Tandem oxonium ylide/[2,3] sigmatropic rearrangement with homoleptic and heteroleptic Rh(II) phosphate complexes.

its homoleptic counterpart, $Rh_2(DPTI)_4$ (Fig. 2.27).[69,129] They tested the ability of $Rh_2(OAc)(DPTI)_3$ to catalyse the addition of ethyl diazoacetate (40) to a series of terminal alkynes in which the complex provided high yields (62-90%) and enantioselectivity (92-95% ee) of cyclopropenes. Additionally, it was shown that the reaction is acetylinically selective, reacting only with the terminal alkyne in substrates containing an alkene. The synthetic ability of the formed cyclopropenes was showcased by the first enantioselective synthesis of the naturally occurring fatty acid (9*R*,10*S*)-dihydrosterculic acid, a common cyclopropyl fatty acid of microorganisms and subtropical plants. Catalyst 50 was notable in that it provided evidence that Rh(II) paddlewheel complexes with C_1 symmetry were viable candidates for asymmetric carbenoid reactions.

Doyle *et al.* explored the use of the glycoluril derivative 1,6-bis-(*N*-benzyl)-diphenyl-glycoluril (1,6-BPGlyc) as a ligand for Rh(II) paddlewheel complexes in cyclopropanation reactions of styrene with ethyl diazoacetate and methyl phenyldiazoacetate.[136] Glycoluril compounds had been explored as moieties in phosphine and amine-based ligands, but this research was among the few examples that studied the structural advantages of glycoluril derivatives as a ligand.[137–139] Single crystal X-ray analysis of $Rh_2(OAc)_2$(1,6-BPGlyc)$_2$ 51 showed that the glycoluril ligand had potentially beneficial features such as a hydrogen-bond donor/acceptor group and possible interactions near the axial site through the aryl group (Fig. 2.28). However, their catalytic activity in cyclopropanation reactions of styrene and diazoacetates proved to be only comparable with other homoleptic Rh(II) paddlewheel complexes. Nevertheless, their added structural features increased the diversity of Rh(II) paddlewheel complexes.

Very recently, Fürstner and Caló investigated heteroleptic complexes for the enantioselective cyclopropanation using stannylated diazo esters. The authors sought to use the stannyl portion for subsequent Stille coupling after cyclopropanation.[85] They used mixed ligands with cyclopropyl acetate and either tfa, acetate, or acetamide. The best method they found for making their complexes involved treating either 3 or 6 with 3 equivalents of cyclopropyl ligand *R*-TPCP to furnish the trisubtituted complexes 9 and 20 in good

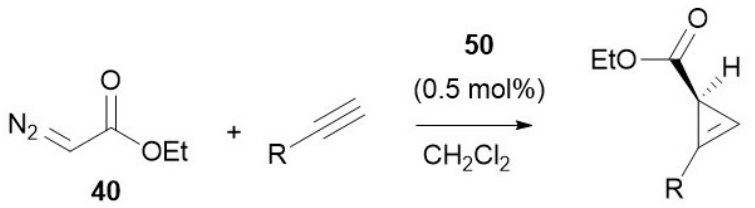

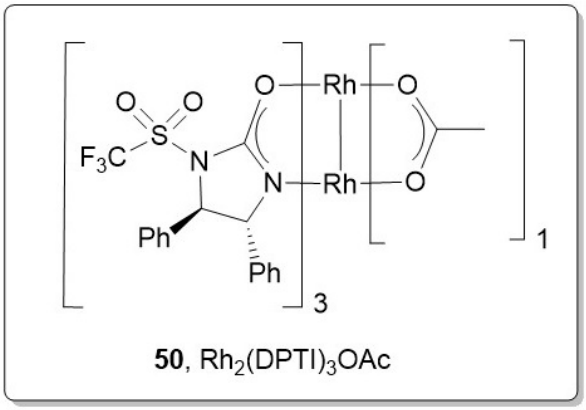

R	yield, %	ee, %
$CH_3(CH_2)_4$	90	95
$CH_3(CH_2)_5$	90	93
t-Bu	81	92
$CH_3(CH_3CH_2O)_2CH$	64	92
$BnOCH_2$	86	92
$MeOCH_2$	78	92
$BrOCH_2$	62	95

Figure 2.27: Cyclopropenation of alkynes using $Rh_2(DPTI)_3(OAc)$.

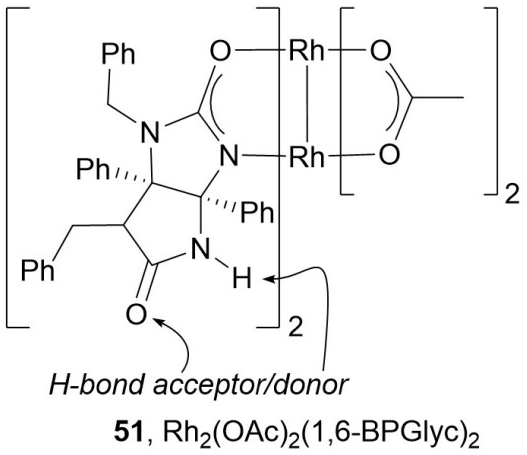

Figure 2.28: Features of mixed-ligand glycoluril/carboxylate Rh(II) complex 51.

yields. The complexes were then treated with acetamide ligand acam to obtain mixed carboxylate/acetamidate complex 51, though this was in low yields (Fig. 2.29a).

In the cyclopropanation reaction of diazo 52 with 4-methoxystyrene, it was found that the hetroleptic complex 51 outperformed it's homoleptic complex variant (no reaction with Rh_2(*R*-TPCP)$_4$) and heteroleptic complexes 9 and 10 in activity and enantioselectivity (Fig. 2.29b).[85] A broad scope of stannylated derivatives, germylated, and silylated products, as well as standard donor/acceptor carbenoid precursors were provided in excellent enantioselectivity (82-97% ee). Enantioselectivity was low when using ethyl diazoacetate (40) as the diazo compound, suggesting that moderately bulky substituents are needed at the carbenoid site. A critical importance was placed on the protic acetamide ligand as the source of enantioinduction. The effects are not completely understood, but the authors propose that reactivity selectively occurs on the Rh face with the N–H portion (Rh1, Fig. 2.29a), possibly hydrogen-bonding with the carbonyl of the carbenoid. This locks the carbenoid in a chiral pocket and also serves to bias the reactive site to one Rh center. When the N–H was replaced with N–Me, enantioselectivity was much lower, lending credence to the proposal.

2.6.5 Immobilized Complexes

A way to heterogenize Rh(II) complexes is via covalent linkage to at least one of the bridging ligands on the Rh(II) complex, creating a heteroleptic complex as a result. The goals here were to immobilize catalysts to maximize catalyst recyclability without loss of reactivity and selectivity. This is especially useful given the high cost of homogenous rhodium catalysts. Of the platinum metals group—platinum, palladium, rhodium, ruthenium, iridium, osmium—rhodium is currently the most expensive. Bergbreiter *et al.* were the first to report on the reusability and activity of polymer bound Rh(II) carboxylate catalysts,[140] followed by a collaboration with Doyle *et al.* to apply the strategy to chiral Rh(II) catalysts.[141] Since these seminal reports, a number of groups have investigated immobilized dirhodium(II, II) catalysts. These reports are covered in an excellent review article on methods to recycle Rh(II) catalysts.[46] Many of the methods to immobilize Rh(II) paddlewheel catalysts that are summarized in the review article involve immobilized

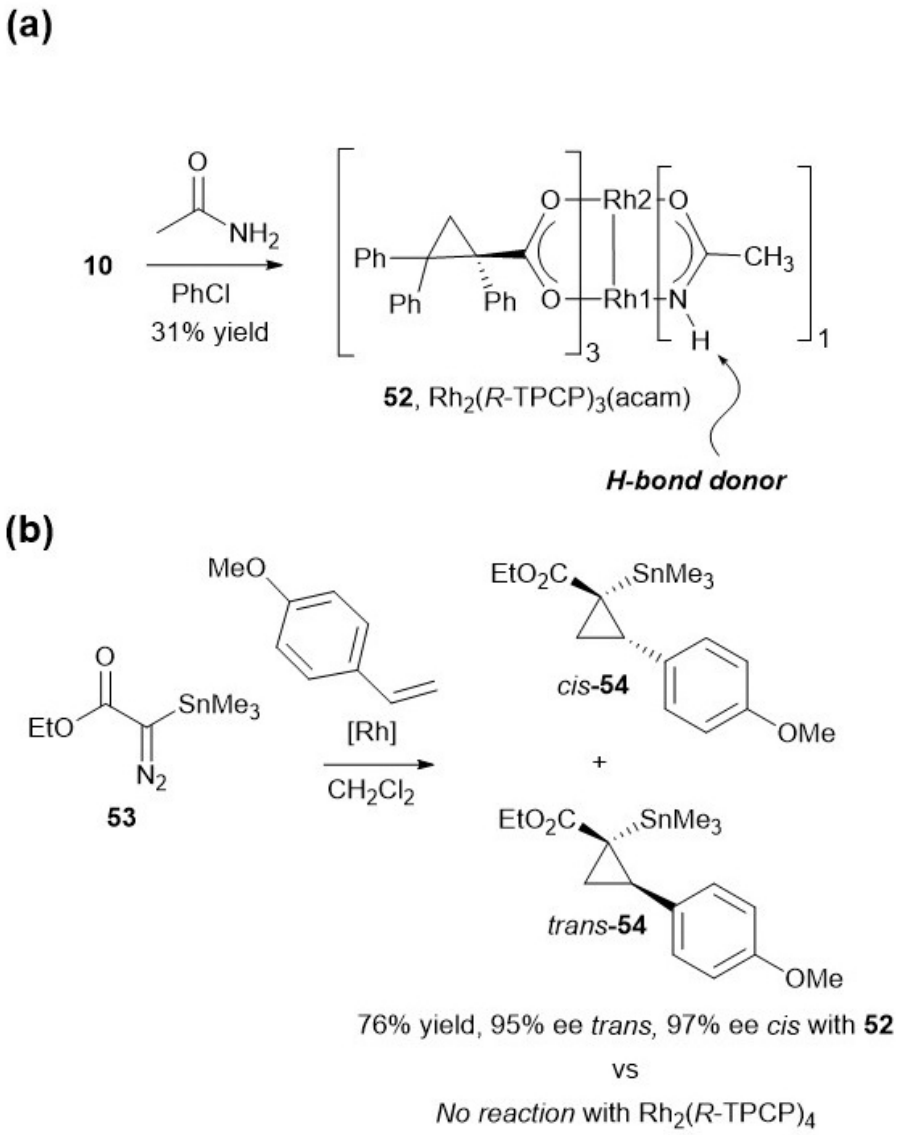

Figure 2.29: (a) Synthesis and features of Rh_2(*R*-TPCP)$_3$(acam) (52). (b) Cyclopropanation of 4-methoxy styrene with stannylated diazo 53 using 52 as catalyst.

heteroleptic complexes,[46] so only reports after the review was published will be discussed here.

Recently, the Davies and Jones groups have collaborated to develop immobilised Rh(II) catalysts for a variety of carbenoid transfer reactions. In 2013, they reported on the immobilisation of Rh_2(*S*-DOSP)$_4$ (DOSP = *N*-(dodecylbenzenesulfonyl)prolinate) by appending a silica support on one of the bridging ligands.[142] Rh_2(*S*-DOSP)$_4$ has historically been a versatile catalyst that routinely furnishes products with high enantioselectivity in transformations with donor/acceptor carbenoid intermediates across many diazo-mediated transformations.[143–147] Although the catalyst utility is widely demonstrated in literature, a recovery method was still elusive. Davies and Jones *et al.* envisioned solving this issue through immobilising the Rh_2(*S*-DOSP)$_4$ covalently to a solid support to avoid the leaching and restriction of catalytic activity seen in previous attempts at recovery.

The solid supported catalyst, Rh_2(*S*-DOSP)$_3$(*S*-silicaSP) 55 (Fig. 2.30), was compared to its homoleptic parent catalyst, Rh_2(*S*-DOSP)$_4$, in a series of diazo-mediated carbenoid transfer reactions.[142] The solid supported catalyst 55 improved on the yield of its homogeneous counterpart in the cyclopropanation of styrene with styryl diazoacetate 58 (92% versus 69% yield), while maintaining comparable enantioselectivity (98% versus 96% ee respectively, Fig. 2.31a). Other highlighted cycloaddition reactions saw only slightly lower yields and enantioselectivity of desired products when immobilized catalyst 55 was used. It was found that 55 could be used for 5 consecutive reactions of the cyclopropanation of styrene with phenyl diazoacetate without significant variance in yield or enantioselectivity.

Immobilized Rh(II) complexes developed by Davies and Jones *et al.* were also adapted for use as a C–H functionalization catalyst in continuous flow.[148,149] Sustainability and safety were maximized by combining the flow synthesis of diazo compounds from hydrazones, such as 60 (Figure 1.31b), in cascade reactions with flow C–H functionalization. In these reports, the immobilized complexes were embedded into hollow composite fibers in which reaction components were passed through. The immobilized complexes in flow compared well to batch processes in a number of cyclopropanation and C–H functionalization reactions. In one particular example, the C–H functionalization of *tert*-butyl ether 62 in flow compared

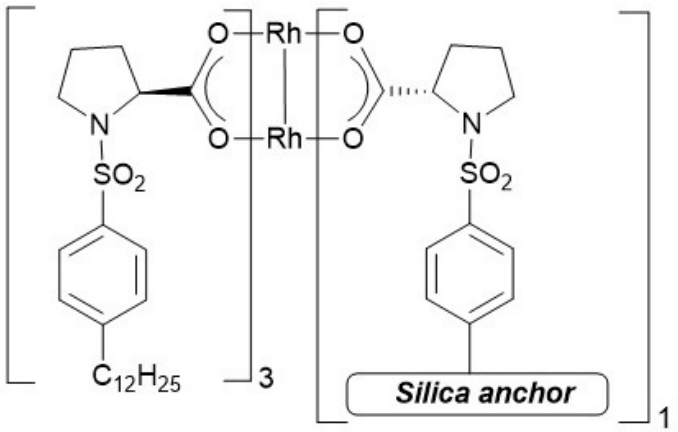

55, Rh_2(*S*-DOSP)$_3$(*S*-silicaSP)

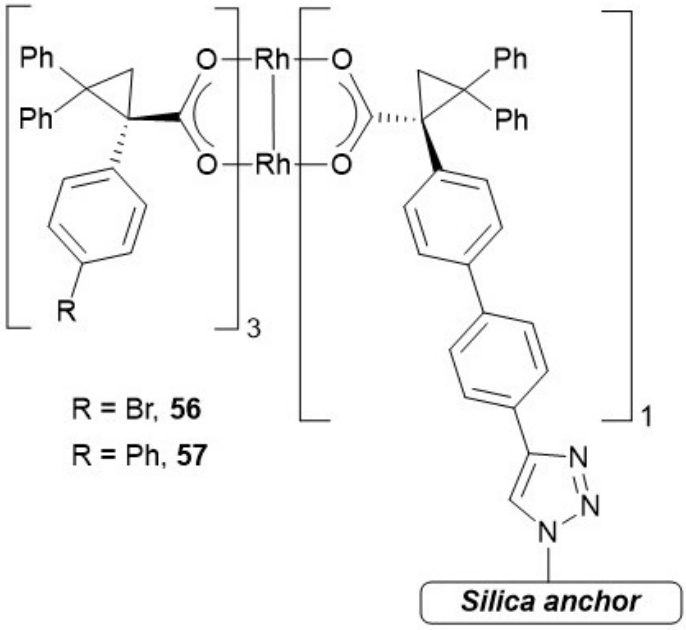

R = Br, **56**

R = Ph, **57**

Figure 2.30: Immobilised chiral Rh(II) catalysts.

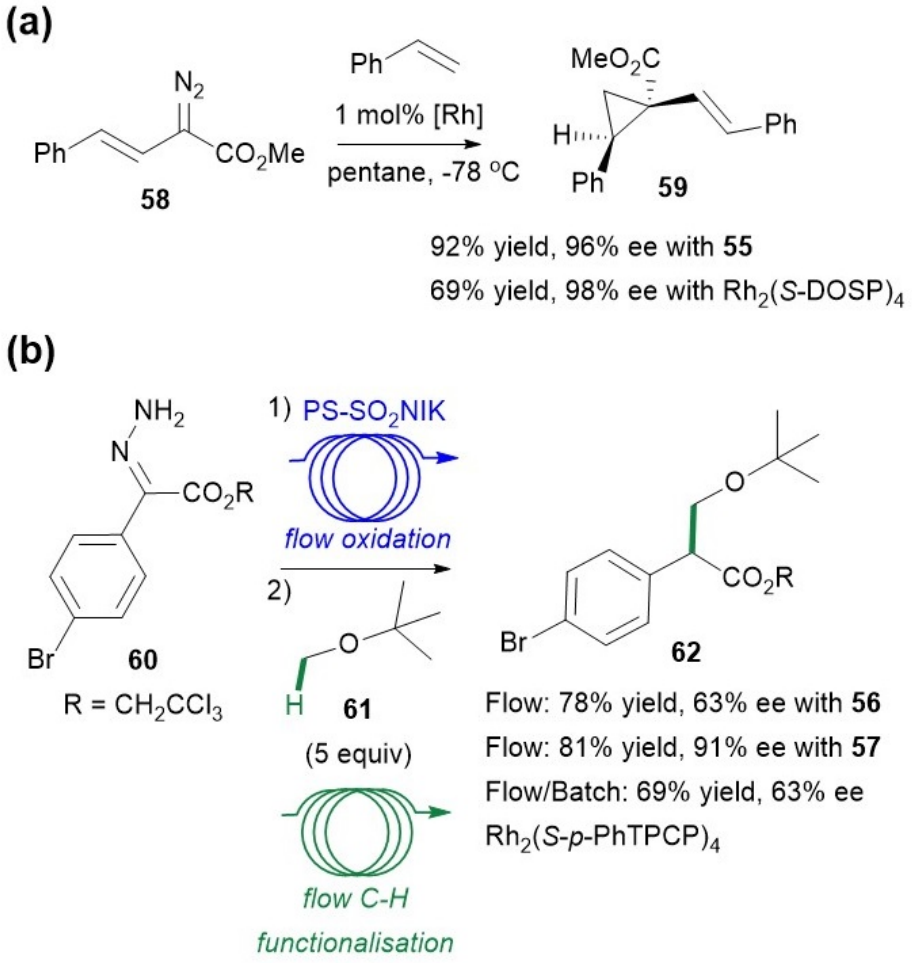

Figure 2.31: (a) Cyclopropanation of styrene with diazo 58 using immobilized catalyst 55. (b) Synthesis of diazo compounds and enantioselective C–H functionalization in flow.

favourably with the batch method (Figure 1.31b). Of the catalysts tested, immobilized complex 57 improved on yield and enantioselectivity compared to 56 and the batch reaction using Rh_2(*S*-*p*-PhTPCP)$_4$.[150] Further, the immobilized-rhodium hollow-fiber flow system could be recycled 10 times without any appreciable loss in yield or enantioselectivity in a benzylic C–H functionalization reaction.[149]

2.6.6 Dirhodium Metallopeptide Complexes

Heteroleptic Rh(II) complexes have been instrumental in the development of artificial metallopeptide scaffolds. The ability to synthesize different bridging ligands allows for functional handles on which to append peptides of interest. Unique structures and reactivity have resulted from this area of research.

Lewis *et al.* developed of a new class of artificial metalloenzymes (ArMs) based on a prolyl oligopeptidase (POP) scaffold.[151,152] Using enzymes as an inspiration, the authors sought to use a protein scaffold to improve the ability of a synthetic catalyst to the levels of their biological counterparts in respect to yield and selectivity. Rh(II) complexes were a good choice for the scaffold because of their ability to catalyse a multitude of reactions. Lewis selected to use cyclopropanation reactions to identify active ArMs because of its facile nature. Heteroleptic dirhodium cofactor 78 was synthesized with a functional handle on its bridging ligands, which were then used to link to proteins containing cysteine or *p*-azido-*L*-phenylalanine (AzF) residues.[151] The best approach of linking Rh(II) complex to the protein was *via* strain-promoted azide-alkyne cycloaddition (SPAAC) in which the Rh(II) complex contained a bicyclo[6.1.0]nonyne substitution (Fig. 2.32a).[153] The resulting ArMs were able to catalyze enantioselective cyclopropanation reactions and Si–H insertion reactions.[152] Initially, racemic products were obtained in cyclopropanation reactions, but improved interaction between the scaffold and cofactor was accomplished by linking the cofactors to the POP family of enzymes, which contain a cavity large enough to fit the cofactor. Targeted mutagenesis eventually resulted in the incorporation of histidine residues into the scaffold. One variation called HFF was found to catalyze styrene cyclopropanation with high enantioselectivity (92% ee) and high selectivity for product 65 over the competing

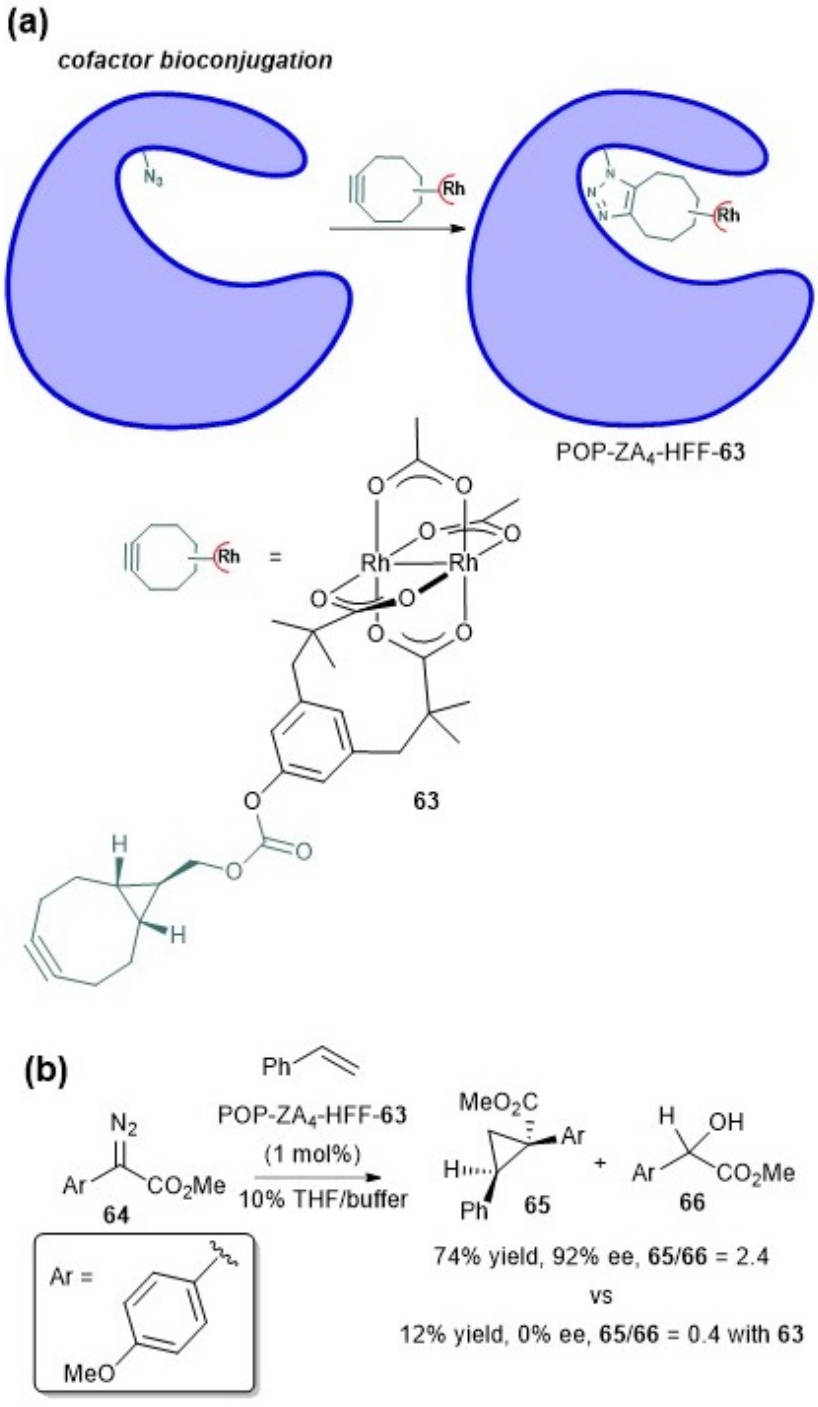

Figure 2.32: (a) Synthesis of artificial metalloenzymes that incorporate complex 63. (b) Enantioselective cyclopropranation catalyzed by Rh(II) metalloenzyme POP-ZA4-HFF-63.

O–H insertion product 66 (Fig. 2.32b).[151] The histidine mutations were proposed to improve enantioselectivity by binding to the proximal rhodium center of the cofactor and create a single active site at the distal center. It is important to note that high selectivity was dependent on conducting the reaction in a > 0.5M solution of NaBr or NaCl. It was believed that the halogen ions may interact with the secondary sphere. Control reactions catalyzed by complex 63 unbound to a protein scaffold led to low yield and dominant percentage of O–H insertion side product 66. Thus, by incorporating the complex into the protein scaffold, the selectivity for organic substrates was greatly improved.

Ward *et al.* leveraged the well-known biotin-streptavidin interaction to develop an ArM that contains Rh(II) complexes for carbenoid transformations. Protein wild-type streptavidin (Sav WT) was engineered to anchor bulky biotinylated Rh(II) complexes like 67 (Fig. 2.33a).[154] They successfully synthesized 6 biotinylated Rh(II) complexes in which they found that complex 67 in the absence of Sav outperformed the others in terms of TON in the cyclopropanation reaction of ethyl diazoacetate 40 and styrene (Figure 1.30b). Further, they tested Sav mutants to genetically optimize their catalyst. The results among the varying mutants incorporating Lewis-basic amino acids were similar to 67·Sav WT. Additionally, there was no influence on the diastereoselectivity and enantioselectivity of the cyclopropanation products 41 and 42. 67·Sav WT and mutants were also investigated for their influence in the C–H insertion of trifluoroethylphenyl diazoacetate with 1,4-cyclohexadiene. Here, the mutants 67·Sav S112E and K121E performed greater than cofactor 67 and 67·Sav WT.

In 2014, Ball *et al.* reported their development of a tripodal peptide ligands for Rh(II) catalysis of asymmetric cyclopropanations.[155] They disclosed an effective process of identifying immobilized metallopeptide catalyst through on bead testing for activity in a 96-well format. Ball et al. have previously reported that peptides with two side chains, either glutamate or aspartate, could serve as bidentate equatorial ligands for Rh(II) paddlewheel complexes.[47,156] Polypeptides had proved to be readily optimizable and the amino acid backbone of the ligand provided chirality as well as the potential of immense structural diversity. Initial screening of the 200 monopeptide bidentate catalyst did not

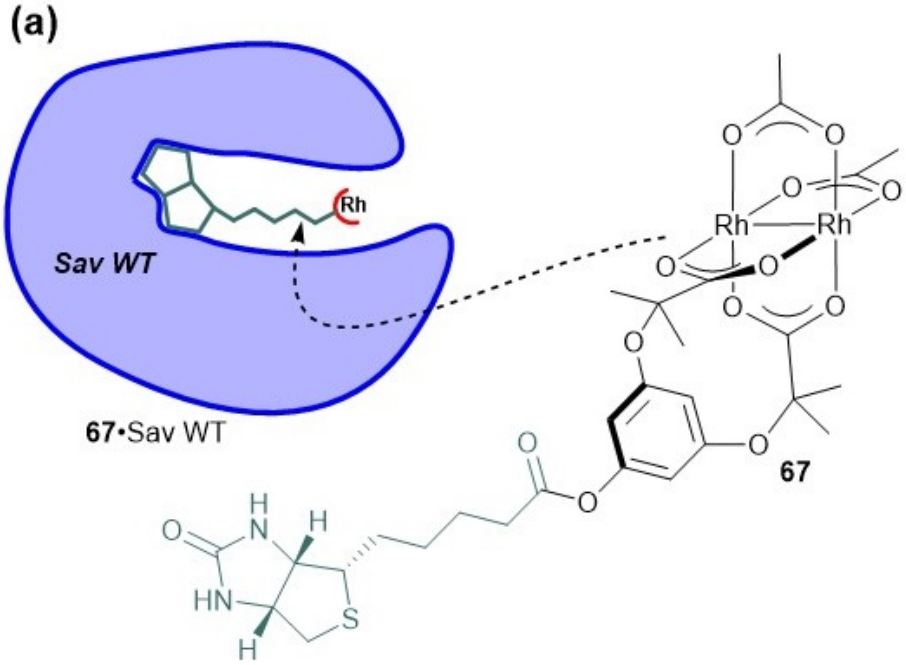

TON = 2 with **3**, 1.5/1 dr **41/42**
TON = 79 with **67**, 1.3/1 dr **41/42**
TON = 54 with **67**•Sav WT, 1.5/1 dr **41/42**
TON = 2 with **3**•Sav WT, 1.5/1 dr **41/42**

Figure 2.33: (a) Biotinylated Rh(II) complex 67 incorporated into a streptavidin scaffold. (b) Comparison of TON using Rh(II) catalysts alone and in the presence of wild type streptavidin (Sav WT).

provide any cyclopropanation product in greater than 55% yield. This result, coupled with recent literature and modelling studies elucidating one chiral rich rhodium environment,[157] led Ball *et al.* to reconsider the design of the ligand to bias the rhodium centers by axial coordination. They postulated that incorporation of a residue, such as histidine or methionine, could protect against bis-coordination, resulting in the quenching of the catalyst, and could block axial ligation of the substrate from the less desired rhodium center. After three iterations of 96 well libraries, it was found that histidine the most effective axial ligating ligand when compared to methionine-containing peptides. The Rh(II) complex 68, with a histidine residue in the i + 5 position was optimized to afford cyclopropane products in high yields and high enantioselectivity (89-99% ee, Fig. 2.34). With these results in hand, Ball showcased the importance of the histidine residue by testing a nearly isosteric phenylalanine and reported a 22% drop in enantioselectivity. They also synthesized the histidine containing catalyst in a solution phase procedure and found a diminished enantioselectivity of 37% ee, demonstrating the importance of the solid phase synthetic approach developed by the group.[155]

2.6.7 Complexes with Additives for Axial Coordination

The first report of an additive improving the outcome of Rh(II)-catalyzed carbene transfer reaction was in 2000 by Nelson et al. en route to an ascomycin derivative, a potential immunosuppressant.[158] The initial attempt of the O–H insertion of diazo 69 and ascomycin 70 utilized $Rh_2(oct)_4$, oct = octanoate, and was low yielding, 25-30% of 71. It was also noted that the HPLC trace indicated many side products formed. The yield of 71 was increased to 36% upon catalyst screening and parameter optimization. Nelson then went on to test weakly coordinating cosolvents and found additives tetramethyl urea and Hunig's base could increase the reactivity of the catalyst. Interestingly, a 1:1 CH_2Cl_2 /Hunig's base ratio made insertion immediate while 1:1 CH_2Cl_2 /TMU shut down reactivity completely. Adjusting the ratio of CH_2Cl_2/TMU to 1:125 allowed for a similar result to the 1:1 CH_2Cl_2/Hunig's base. It was postulated that the electron donating efficiency was directly correlated to the concentration of additive needed. The final conditions with Rh_2(1-adaman)$_4$, 1-adaman =

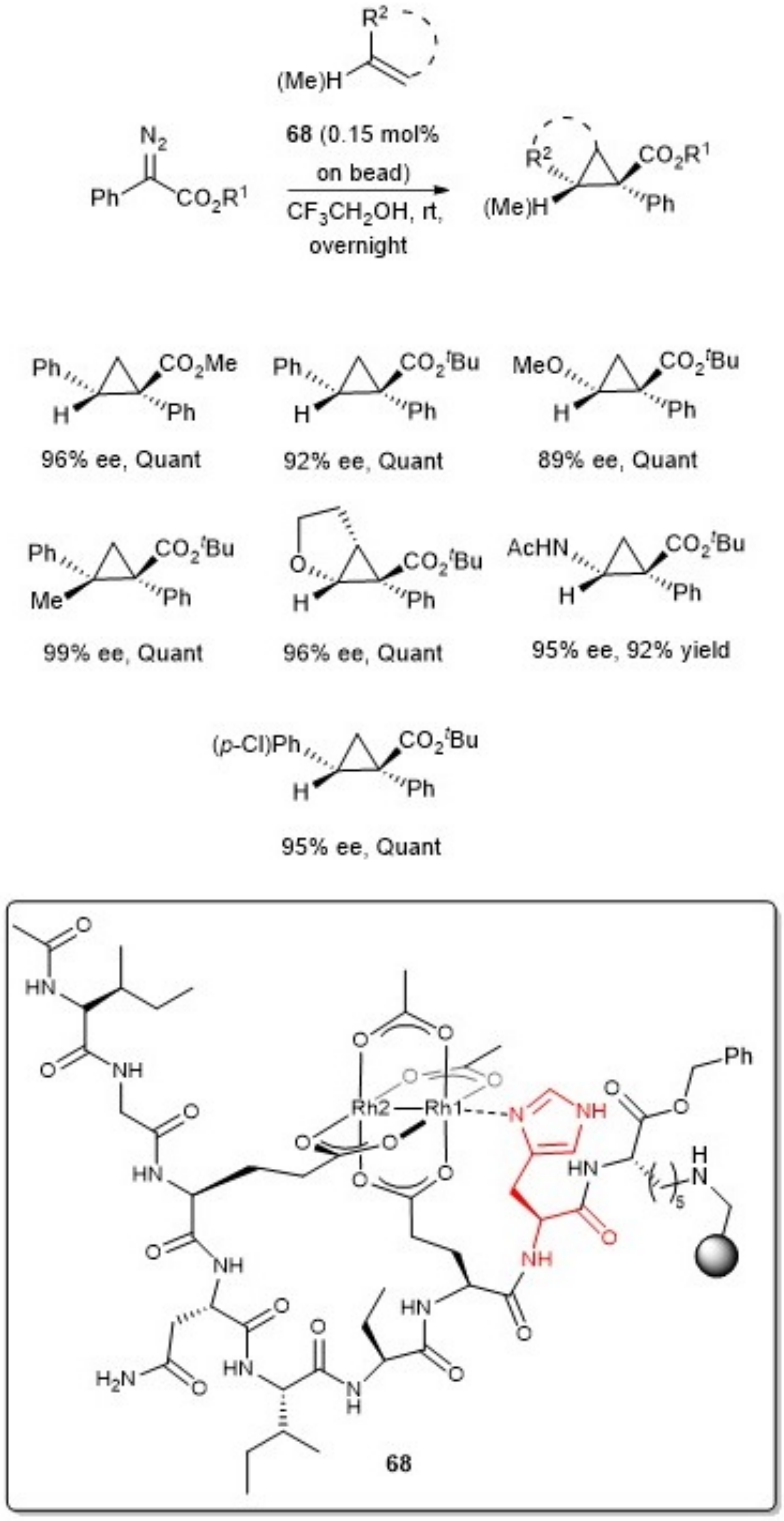

Figure 2.34: Rh(II) peptide catalyst 68 and its use in enantioselective cyclopropanation of olefin.

adamantane carboxylate, and 1:125 CH_2Cl_2/TMU increased the yield to 60-65% by HPLC. It was further shown that while increasing the scale to 20 grams the desired ether 71 was afforded in 55% yield after purification (Fig. 2.35).

In the same year Jessop *et al.* studied the effects of axial coordination on enantioselectivity.[159] They accomplished this by running a $Rh_2(TBSP)_4$, TBSP = 1-[phenylsulfonyl]-(2*S*)-pyrrolidinecarboxylate, catalyzed cyclopropanation of 72 and styrene in super critical fluid (SCF) fluoroform (Fig. 2.36). This allowed them to change the dielectric constant of the solution by adjusting the pressure as opposed to increasing the polarity of the solvent, therefore the ability to axial coordinate. This is possible due to the dielectric constant of SCF fluoroform being pressure dependent. It was disclosed that above 100 bar a 40% ee was achieved. When the fluoroform was brought near its critical point the ee increased to as high as 78%. However, the study of the effects of the axial coordination on ee were not conclusive. The authors indicated that it influenced the ee in some way. In most cases, the reactions using axial coordinating solvents would produce higher ee than would be expected due to the dielectric constant of the solution. Attempts at correlating these effects to physical parameters, such as cone angle, donor ability, and acceptor ability, proved futile. This suggested that no one parameter was responsible for the increase in ee but did provide and exciting new avenue to tune a catalyst to improve the result.

In 2010, Saito *et al.* sought to resolve the issue of low enantioselectivity in Rh(II)-catalyzed O–H insertions by addition of cinchona alkaloid additives.[160] Rh(II)-catalyzed enantioselective O–H insertions have failed to match the success of other insertion reactions with the highest ee obtained to this point being 8%. Utilizing their optimal catalyst and additive, $Rh_2(TPA)_4$,TPA = triphenyl acetate, and 2 mol% of quinine 73 respectively, 38% ee was obtained. This result was further improved to 50% ee by addition of silica gel and the reduction of temperature to -10 °C (Fig. 2.37). Increasing the additive loading to 5% or 10% dampened the activity of the catalyst and lowering the temperature to -20 °C reduced the ee to 46%.

A year before Saito's disclosure, Charette *et al.* reported an unprecedented positive effect of an achiral H-bond donor on diastereo- and enantioselective Rh(II)-catalyzed

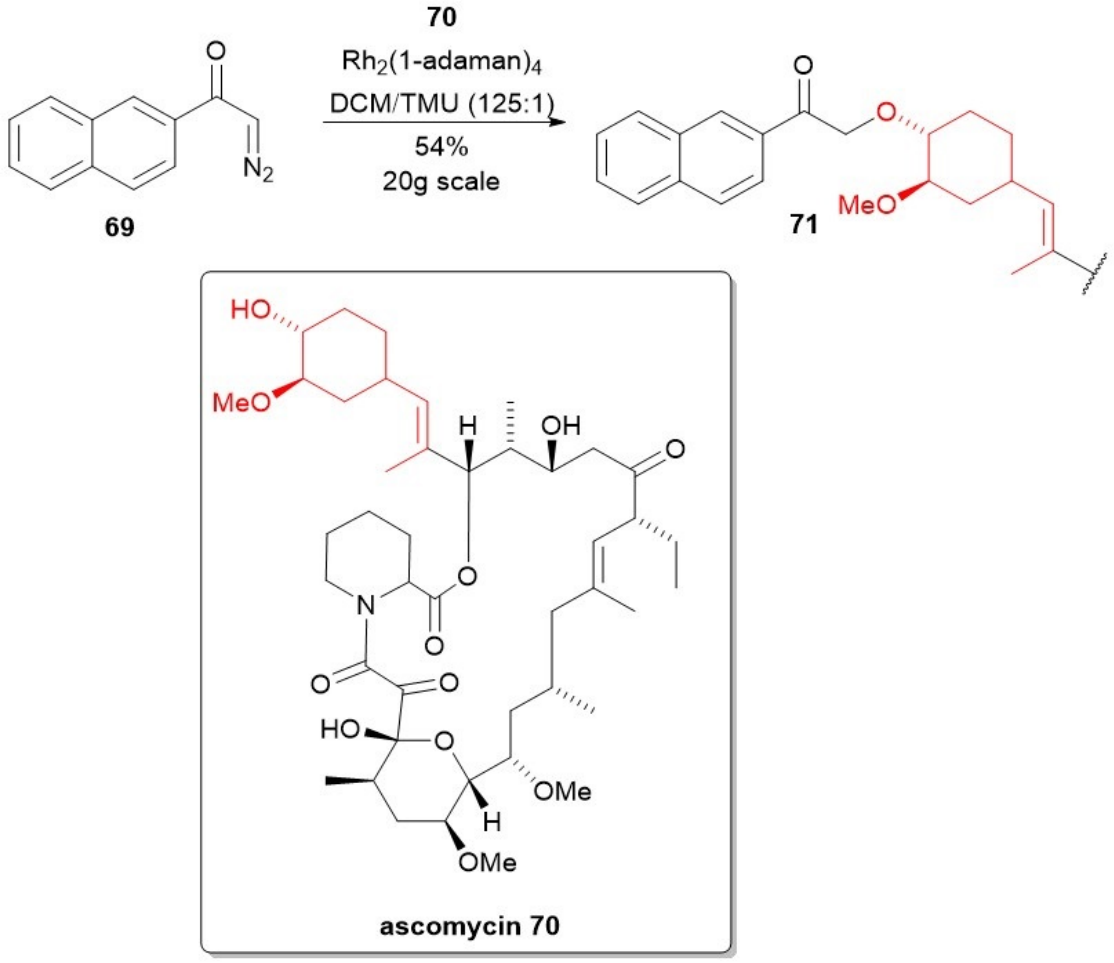

Figure 2.35: Gram scale synthesis of ascomycin derivative.

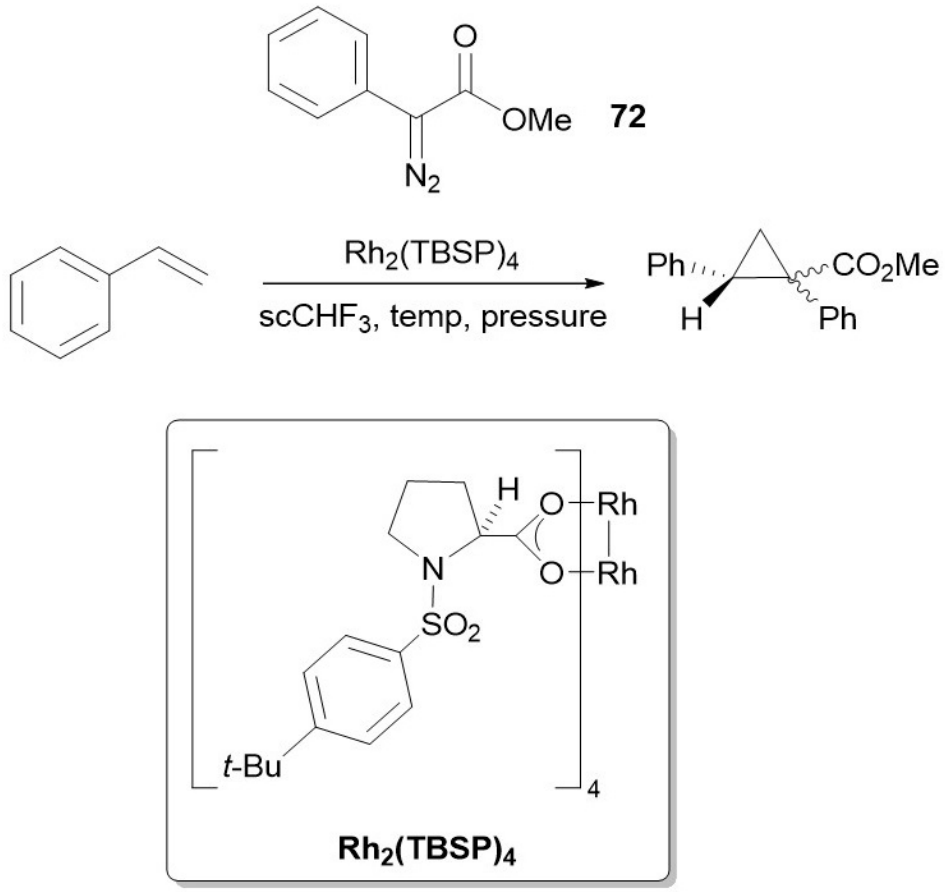

Figure 2.36: Evaluation of the $Rh_2(TBSP)_4$ catalyzed cyclopropanation of methyl phenyldiazoacetate and styrene in SCF fluoroform.

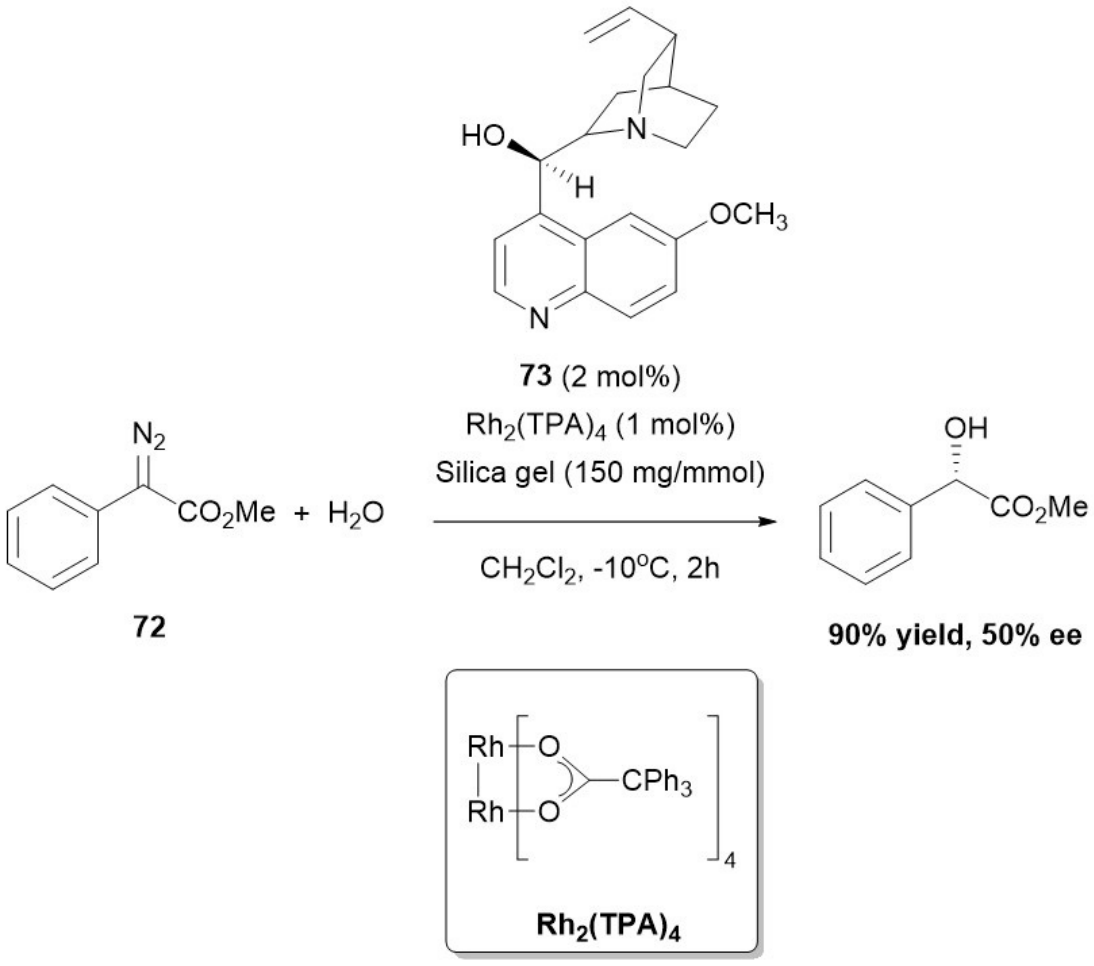

Figure 2.37: The $Rh_2(TPA)_4$ catalyzed enantioselective O–H insertion of H_2O with 72.

cyclopanations of α-cyano diazos and styrene. The optimal conditions were 5 equivalents of styrene and 1 mol % of $Rh_2(S\text{-NTTL})_4$, at -78 °C in toluene for 16 hours. The optimal additive was $TfNH_2$, Tf = $CF_3SO_2^-$, at 10 mol% (Fig. 2.38a).[161] The optimal conditions were applied across a 29 olefin substrate scope yielding up to 85%, 99:1 dr, and 98% ee.

The effect of various achiral additives on diastereoselective/enantioselective Rh(II)-catalyzed cyclopropanations of acceptor/acceptor diazos was also investigated by Charette *et al.* in 2010.[61] Lewis bases, LBs, that doubled as Bronsted acids were found to be successful. The enantioselectivity of the $Rh_2(S\text{-NTTL})_4$ catalyzed cyclopropanation of diazo 74 and styrene was increased by sulphonic amide additives in dichloroethane at 25 °C, with $TfNH_2$ performing best at 57:1 er, compared to 49:1 er achieved without any additive (Fig 1.38b). Subsequent studies found that DMAP as additive was responsible for making the catalyst less active but more selective. The active adduct is better controlled with temperature (Fig. 2.38c). It was proposed this effect on the catalyst makes the catalyst favor a later transition state as per the Hammond postulate. In a subsequent disclosure Charette *et al.* sought to utilize achiral LBs to enhance the diastereoselectivity.[62] Interestingly, they found that the results were diazo dependent. In the cases of the α-cyano and α-methylacetate diazos the enantioselectivity greatly diminished while improving with the enantioselectivity α-nitro diazo 2-3% across all reactions.

Ball and Zaykov sought to use a LB additive to increase the enantioselectivity of their metallopeptide, $Rh_2(pep)_2(OAc)_2$, catalyzed Si–H insertions (Fig. 2.39).[156] Upon screening the LBs, it was found that triphenylphosphite was the optimal additive. The enantiomeric excess of the Si–H insertion of diazo 72 and dimethylphenylsilane was increased from 50% with no additive to 66% with triphenylphosphite and complex 75. Next, they studied this additive with four other peptide ligands. In all cases, an increase in ee was obtained. With this result in hand, they studied the kinetics of the system. A plot of -log([diazo]/[diazo]$_0$) versus time was linear and indicated the kinetics were first order in substrate. The kinetic data also provided evidence that phosphite–75 adduct was kinetically competent due to a measured γ, a constant describing catalytic power, of 0.013. If the adduct was not kinetically

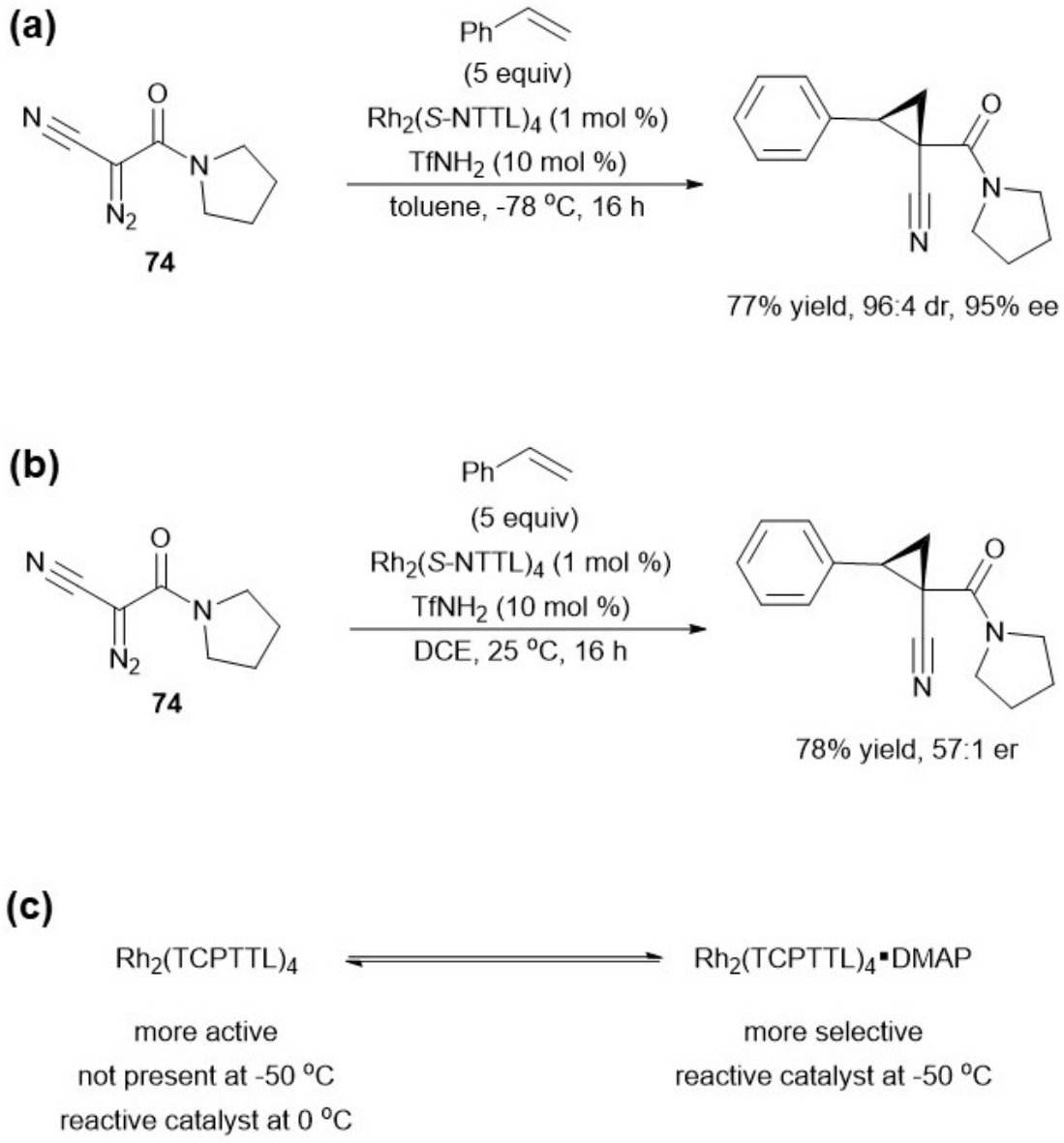

Figure 2.38: a) Rh_2(*S*-NTTL)$_4$ catalyzed cyclopropanation of α-cyano diazo 74 and styrene in toluene. b) Rh_2(*S*-NTTL)$_4$ catalyzed cyclopropanation of α-cyano diazo 74 and styrene in DCE. c) Active Rh(II) adduct at different temperatures.

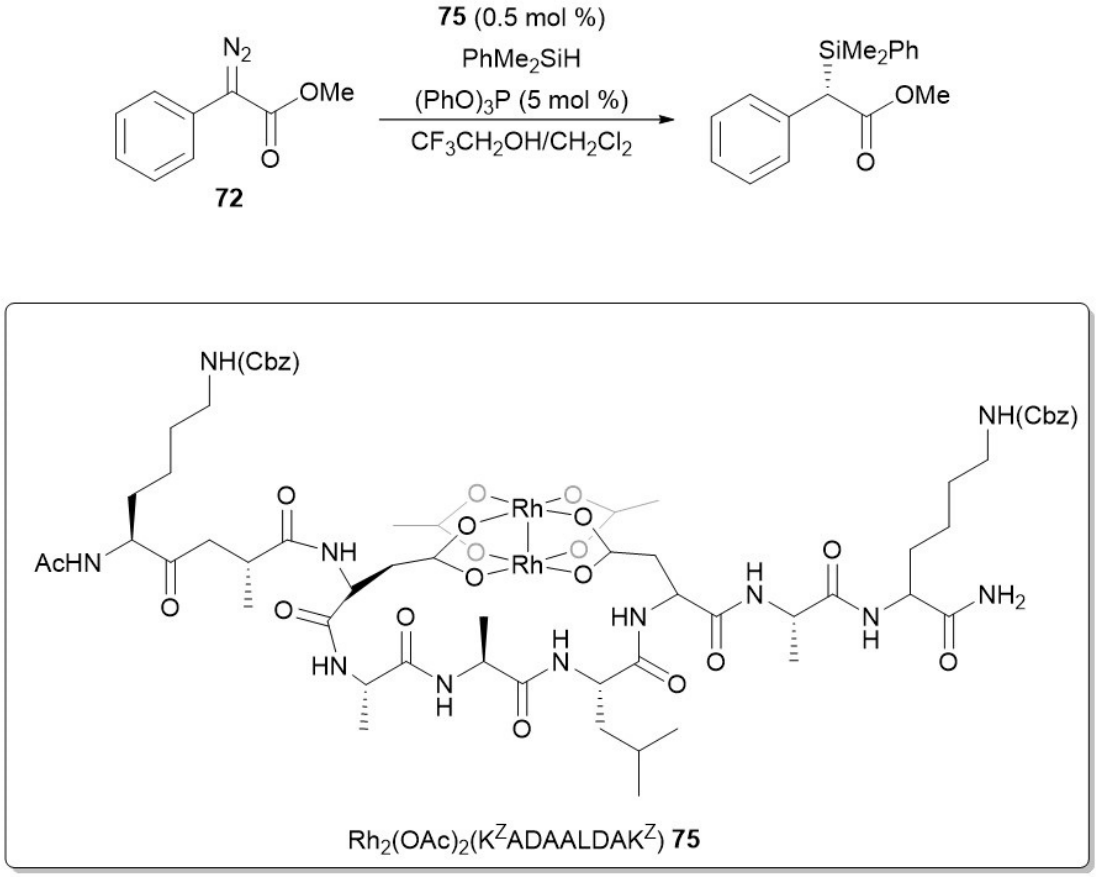

Figure 2.39: Metallopeptide catalyzed Si–H insertion with triphenylphosphite additive.

competent then γ would measure 0, as was found when measuring weak oxygen donor ligands in a previous study.

In 2014, Lebel *et al.* also found success increasing the activity and selectivity of Rh(II)-catalyzed amidation with thioethers by addition of additives.[162] In this study, DMAP alone was found to work best in cooperation with CH_2Cl_2 forming a bis(DMAP)CH_2Cl_2 compound 76 (Fig. 2.40a). The addition of 5 mol% of DMAP in CH_2Cl_2 solvent increased the yield to 92% and the dr to 88:12 of 77, from 82% yield and 80:20 dr without DMAP respectively. When the solvent was changed to isopropyl acetate without an additive, the yield and dr of 77 were both suppressed. This was rectified by adding 2.5 mol% of bis(DMAP)CH_2Cl_2 and 7 mol% of DMAP in the isopropanol solvent resulting in the optimal conditions, yielding 87% of the desired product 77 with a dr of 95:5 (Fig. 2.40b). It was proposed that the DMAP, as well as the thioether reagent, could activate the catalyst. UV-vis studies elucidated that the addition of 20 equivalents of thioanisole forms a 1:1 adduct with the Rh_2(*S*-NTTL)$_4$, λ_{max} of 560 nm. DMAP was shown to make a 1:1 and 2:1 DMAP/Rh complex upon addition of 1.4 and 2.8 equivalents of DMAP, respectively. The 1:1 DMAP/Rh complex resulted in the same λmax as the thioanisole/Rh complex while the 2:1 DMAP/Rh complex λmax was found at 530 nm. Formation of a thioanisole–Rh–DMAP adduct also resulted in a λmax of 530 nm indicating this is also a possible active catalytic species in solution.

In a study conducted by Lacour *et al.* it was seen that 1,4-dioxane acted as both a reagent and an axial ligand in their Rh(II)-catalyzed [3+6+3+6] synthesis of macrocycles.[163] This was elucidated though *in situ* IR experiments coupled with UV-vis titration experiments used to define the kinetics of the system. The kinetics calculated for the coordination events of dioxane greatly favored the bis-adduct 80 with 97.7 to 99.6% existing in solution at 6 equivalents of dioxane (Fig. 2.41a). The mono-adduct 79, or proposed catalytically active adduct, only made up 0.4 to 2.3% of material in solution. Complex 78 without 1,4-dioxane coordinated existed at <0.003%. A study was then conducted varying the concentrations

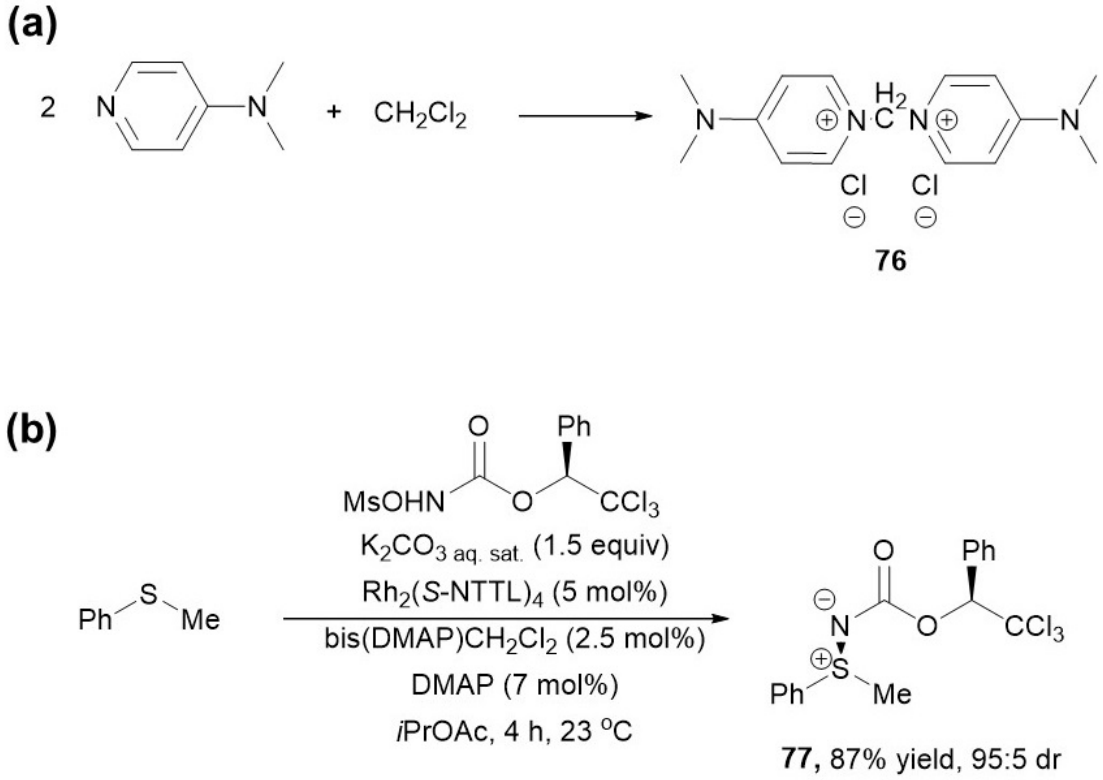

Figure 2.40: a) Adduct 76 formed in solution from 2 equivalents of DMAP and CH_2Cl_2.

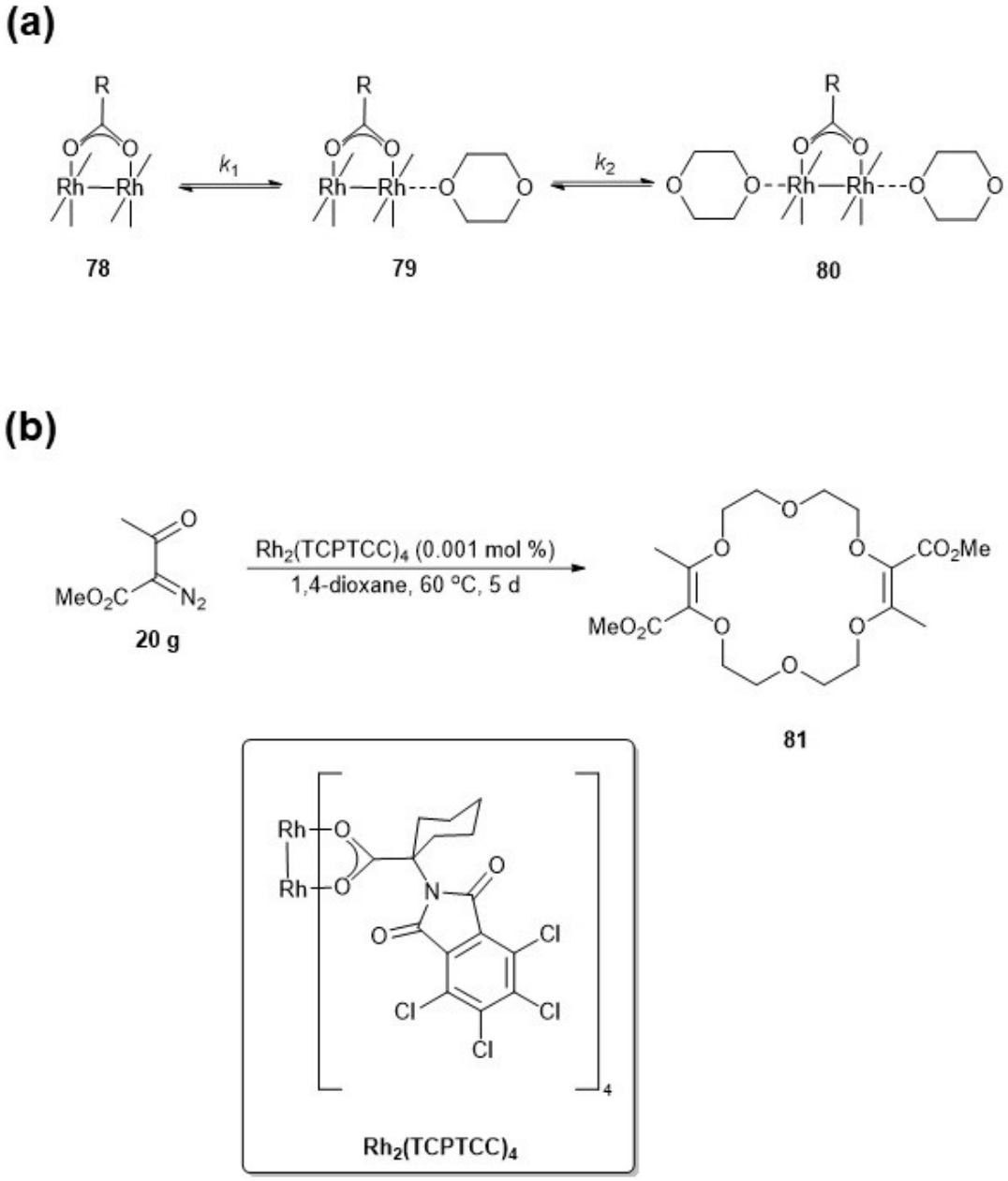

Figure 2.41: a) Species of catalyst that exist in solution. b) $Rh_2(TCPTCC)_4$-catalyzed [3+6+3+6] macrocyclization on a 20g scale.

of the dioxane in solution to study rate of diazo decomposition versus the amount of mono-adduct 79. A direct correlation was found between the calculated amount of the mono-adduct 79 in solution and the rate of dinitrogen extrusion measured. The reaction was then performed on a 20 gram scale yielding 76% of macrocycle 81 (Fig. 2.41b).

2.6.8 Mixed Complexes with Tethered Axial Coordination

Heteroleptic complexes have been used to study the effects of axial coordination in Rh(II) complexes. Historically, the study of axial ligands is performed by adding exogenous ligands and evaluating their effects on transformations.[58,61,156,158–160,162–164] However, the relatively weak coordination of axial ligands compared to bridging ligands makes this study difficult due to the rapid, equilibrium nature of the interaction.[165,166] Either adding an excess of exogenous ligands[156,167] or using a strongly coordinating axial ligand[168–171] have been used as strategies to circumvent the issue of weak axial binding, but each strategy introduces another set of issues: excess ligand leads to a higher probability that both axial sites are blocked, and a strongly coordinating ligand effectively dampens activity at the distal Rh site.[168] Tethering the axial coordinating ligand to the bridging ligand has recently been investigated as an effective means of studying axial ligation on Rh(II) complexes.

Bera *et al.* explored the effects of having bulky tethered ligands on the catalytic activities of Rh(II) complexes.[89] They utilized ferrocene-amide functionalized napthyridine ligands where weak axial coordination of the amide's carbonyl oxygen allowed catalytic activity to occur at the rhodium active site. Upon synthesis and characterization of seven functionalized napthyridine-based ligands, they studied their catalytic C–H functionalization of indoles in comparison to that of $Rh_2(OAc)_4$ 3.

Their preliminary results demonstrated that complex 83, containing two axially coordinated amide components from ligand 82 had the most promise for improved catalytic activity.[89] Complex 83 was synthesized through ligand exchange of partially solvated 11 with 2 equivalents of ligand 82 (Fig. 2.42a). The C–H insertion of 1-methyl-1*H*-indole with methyl phenyldiazoacetate 64 and 1 mol % of 83 resulted in a 92% yield of functionalized product 84 (Fig. 2.42b). This was a slight increase from a 90% yield achieved by 3. Similarly,

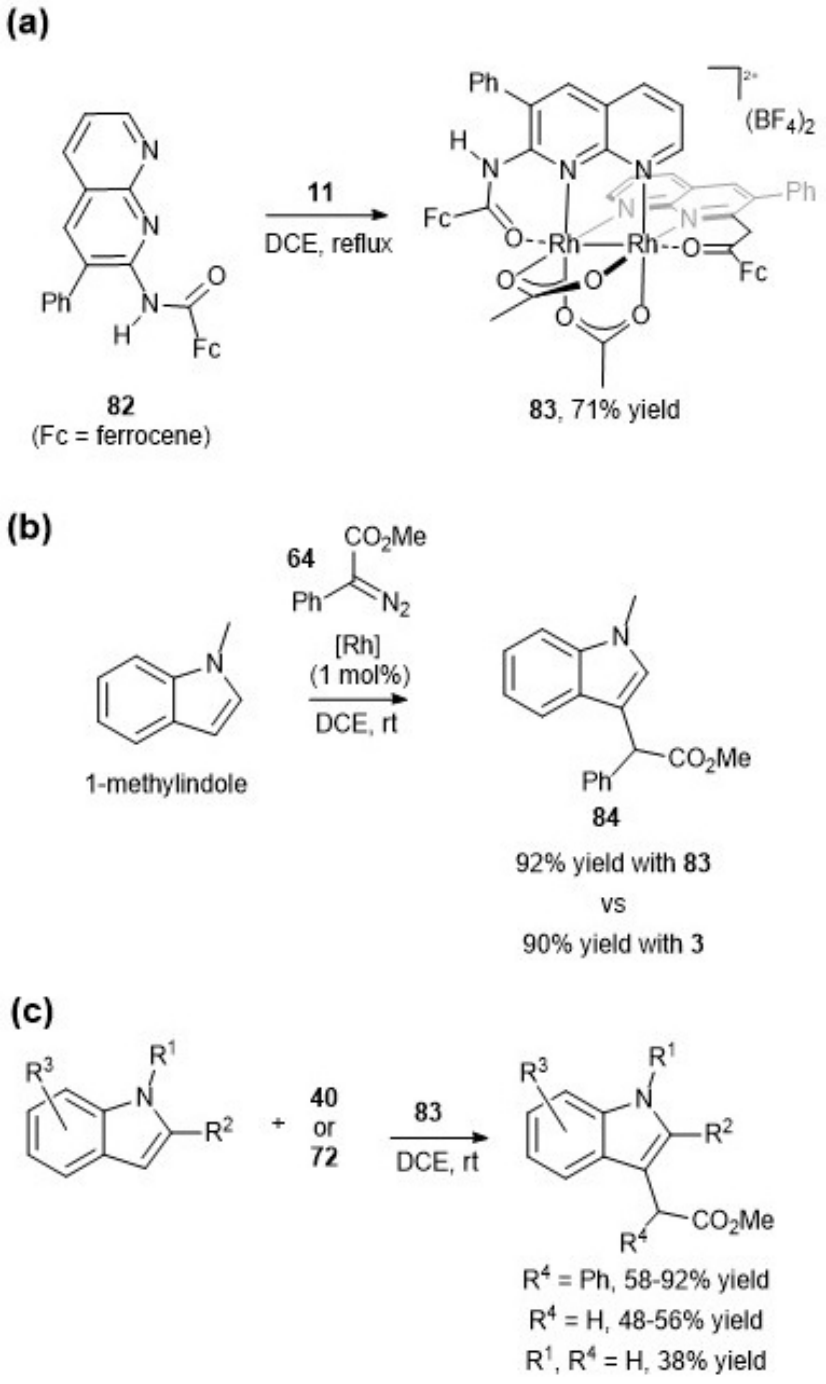

Figure 2.42: (a) Synthesis of complex 83 from ligand 82. (b) C–H insertion of 1-methyl indole with diazo 72 using 83 compared to 3. (c) Range of yields of C–H insertion of functionalized indoles using complex 83.

a 2% difference was observed between 83 and 3 in the reaction when ethyl diazoacetate 40 was used (54% vs 52% yield respectively). Complexes obtained from other naphthyridine ligand derivatives were less active, and this was attributed to the decreased availability of the Rh(II) active site.

Utilizing the optimized reaction conditions, a range of substituted indole substrates were synthesized using diazo 72.[89] Yields of the functionalized indole products were between 58-92% yield (Figure 1.42c) with substitution preferred at the C3 position of the indole ring. When R1 was an allyl group, the C–H insertion reaction at the C3 position was preferred over cyclopropanation. A range of functionalized indoles were also obtained using diazo 40 albeit in lower yields, ranging from 48-56% yield when R^1 was substituted. N–H insertion products were competitive when the indole nitrogen was not substituted (R^1 = H).

In 2019, members of our group leveraged heteroleptic complexes to tether thioether moieties onto Rh(II) paddlewheel complexes in our seminal disclosure.[86,172] The thioether group served as a way to modulate electron density along the Rh–Rh bond by coordinating to axial sites of the complex. The tethered axial thioether groups also biased the reactive site of the complex on what would otherwise be non-equivalent Rh atoms. Carboxylate (phenylthiocarbamoyl benzoate, PhTCB) and carboxamidate-type (methylthiooxazolidinate, MeTOX) ligands functionalized with thioethers were synthesized and incorporated into heteroleptic Rh(II) complexes. Ligand exchange with $Rh_2(OAc)_4$ produced heteroleptic complexes with one or two of the thioether ligands incorporated. Further substitution was prevented due to the blockage of the axial sites by the thioether groups. Due to the presence of one open axial site, the complexes with one-fold ligand exchange were more effective in diazo-mediated reactions (complexes 85, 87, and 88, Figure 1.43a). Heteroleptic complexes 86 and 89 were also synthesized to serve as control complexes to separate effects from the bridging ligand and the pendant thioether group (Figure 1.43a).

The complexes were used as catalysts in the cyclopropanation of styrene derivatives with methyl (*p*-nitrophenyl)diazoacetate 89, in which side products from diazo homocoupling are an issue.[86] Of the complexes tested, 85 was found to be the optimal catalyst in all conditions, besting the mixed carboxamidate/carboxylate 87 and other non-tethered complexes in

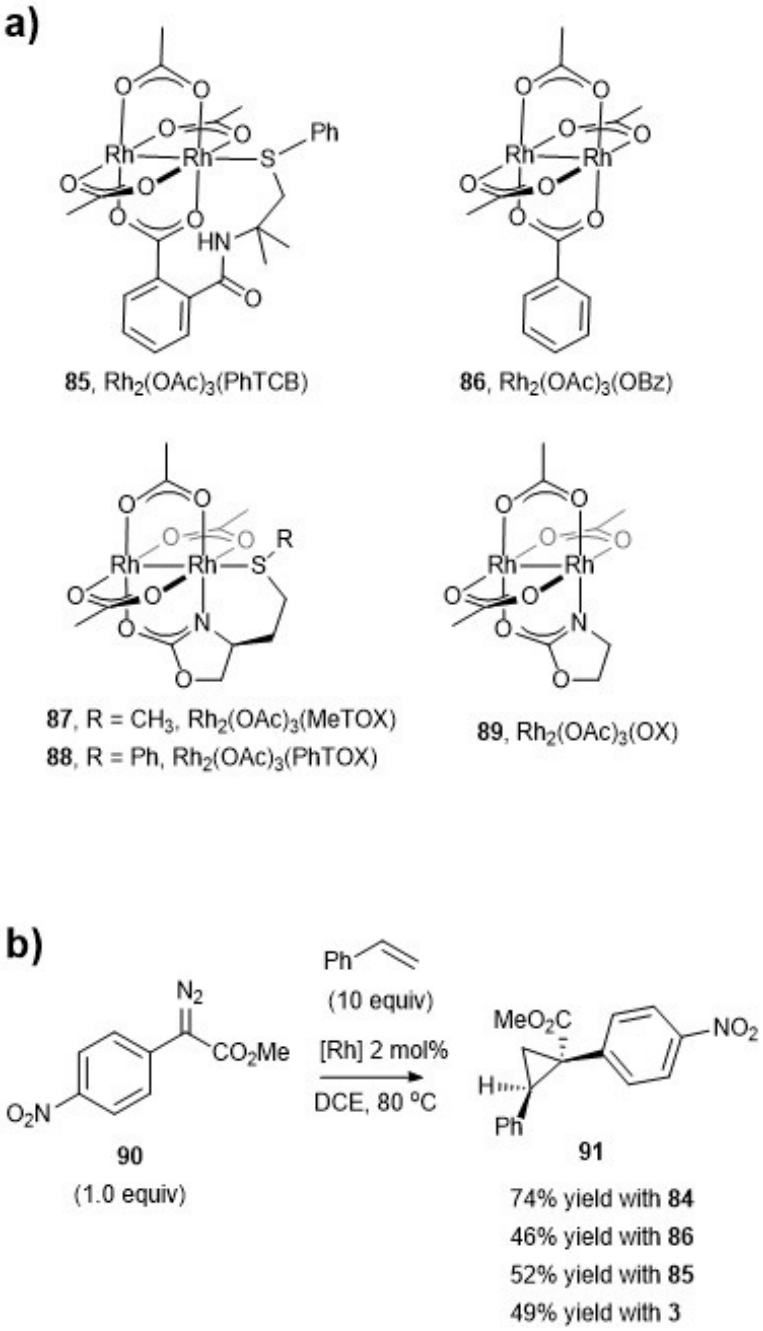

Figure 2.43: Heteroleptic complexes with tethered, axially coordinating thioether ligands (85, 87, and 88) and their control complexes (86 and 89).

yield and selectivity over homocoupling (Fig. 2.43b). Crystal structure, UV/Vis, and electrochemical analysis provided insight into the reactivity of the complexes and suggested that the greater performance of 85 was due to weaker axial coordination of its tethered thioether. In 87, the rigid oxazolidinone bridging ligand allows for an ideal six-membered chelation of the thioether donor group, which creates a more tightly bound thioether group compared to 85. This decreases the electrophilicity of the distal rhodium center and reduces catalyst performance. Electrochemistry data showed that the presence of the axial thioether in 85 resulted in a higher $Rh_2^{4+/5+}$ $E_{1/2}$ value when compared to its non-tethered counterpart 86. The shift to higher redox potentials implied some π-acceptor character of the tethered ligand, since purely σ donating axial ligands shift Rh(II) paddlewheel complexes to lower potentials.[173,174] Overall, complex 85 proved to be the best match for the components in the reaction studies and introduced heteroleptic complexes with tethered thioether coordination as a method to tune Rh(II) paddlewheel complexes.

Very recently, Rej and Chatani introduced sulphonamide and carboxamide bridging ligands with quinolyl or methylthio components.[175] Interestingly, the sulphonamide ligand 91 could coordinate in a neutral chelating fashion or via anionic bridging fashion with tethered axial coordination of the quinolyl nitrogen depending on the number of ligand equivalents (Fig. 2.44a). In screening catalytic activity in the cyclopropanation of styrene derivative 94 with 40, the authors found that the neutral chelated complex 92 had higher activity than complex 93 (60% vs 23% yield, Fig. 2.44b). Complexes 3, 6 and other reported complexes with tethered quinolyl and thiomethyl groups also displayed lower activity than the neutral chelated complex, demonstrating the important role of ligand occupation and lability at rhodium axial sites in diazo-mediated transformations.

2.7 Conclusion

Although heteroleptic dirhodium paddlewheel complexes and axial coordination are not extensively utilized in carbenoid chemistry, this review has outlined the ways in which they can be useful and, in some cases, better than their homoleptic counterparts.

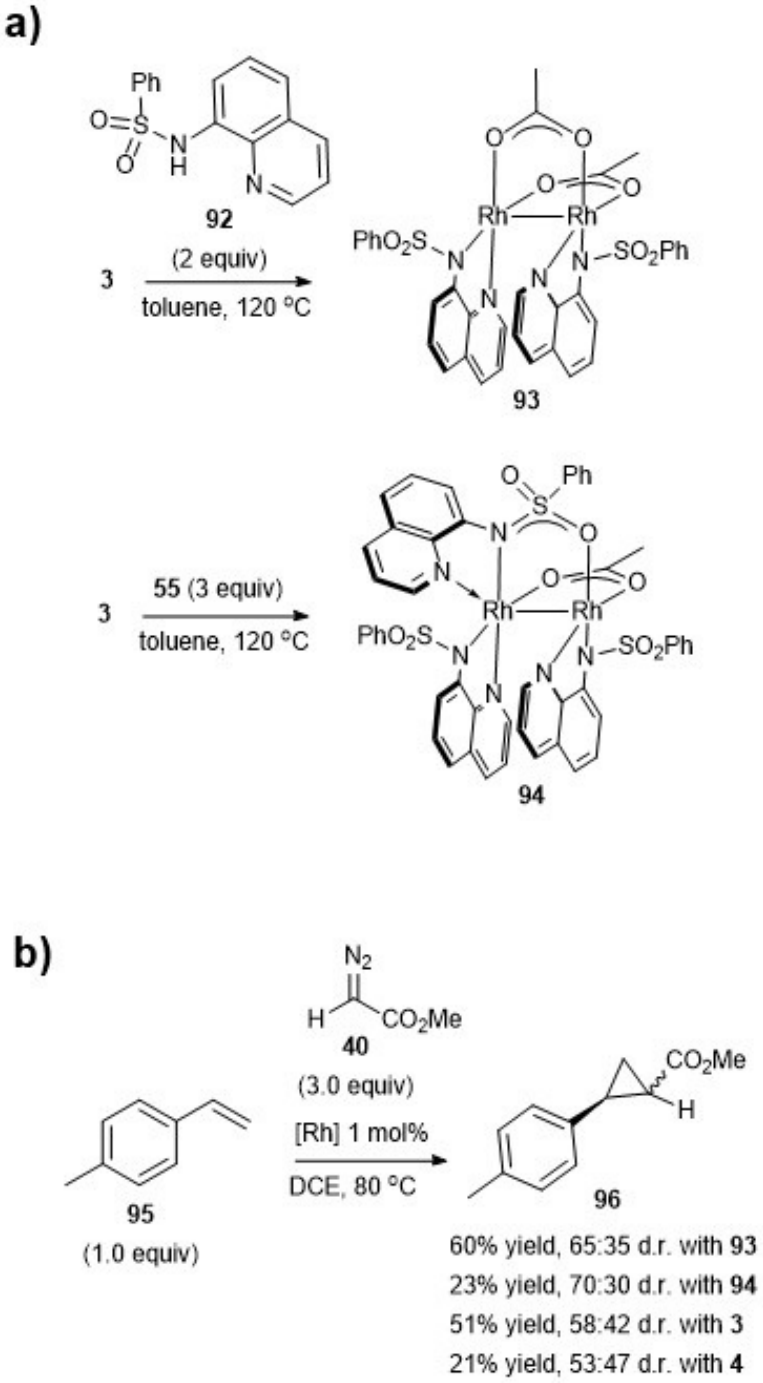

Figure 2.44: a) Synthesis of complex 92 and 93 depending on equivalents of ligand 91. b) Synthesis of cyclopropane 95 using catalysts 92 and 93 compared to conventional Rh(II) catalysts 3 and 6.

An importance in investigating new ligand interactions, immobilisation, and designing artificial metalloenzymes are underscored as methods in which heteroleptic dirhodium(II,II) paddlewheel catalysts succeed in carbenoid transfer reactions. These methods are helping to usher in a new era of dirhodium(II,II) paddlewheel complexes that challenge the need for symmetric environments for highly selective transformations. The biggest challenge that limits the use of heteroleptic dirhodium(II,II) paddlewheel complexes is a lack of a general, high yielding method for their synthesis. To date, only one example of these unique catalysts has been used in total synthesis applications. There are other opportunities for growth in this area and future areas of exploration include leveraging the heteroleptic paddlewheel structure for bifunctional or cooperative catalyst systems.

Chapter 3

Effect of Tethered, Axial Thioether Coordination on Rhodium(II)-Catalyzed Silyl–Hydrogen Insertion

3.1 Disclosure

The following chapter is an adaptation of the journal article W. Sheffield, A. Abshire, and A. Darko. Effect of tethered, axial thioether coordination on rhodium(II)-catalyzed silyl–hydrogen insertion. *Eur. J. Org. Chem.*, 2019(37):6347–6351, 2019. William Sheffield completed the frontier synthesis of the control catalyst, the substrate scope, the UV-vis experiments, the majority of the reactions in catalyst screening, writing of the manuscript, and supplemental information. I completed all of the computational work, assisted with scale-up of the catalyst, separated the *cis* and *trans* isomers of the catalyst 97, and assisted with duplication of some of the results for the catalyst screening, and assisted with the supplemental information. Dr. Ampofo Darko advised the work described herein and assisted with the development of the publication.

3.2 Abstract

The effect of tethering a thioether to a dirhodium(II,II) paddlewheel complex are evaluated in Si–H insertion reactions. This study provides further evidence for the benefits of incorporating thioethers into the rhodium paddlewheel motif. When using a tethered complex, the *in situ* carbenoid formation and subsequent Si–H insertion are not impeded, yields are improved by up to 12 % at elevated temperatures, and selectivity for diazo compounds is greater when compared to non-tethered catalysts. Computational modeling of the complexes is also presented in order to rationalize the results.

3.3 Introduction

Dirhodium paddlewheel complexes, Rh(II), are renowned for being efficient catalysts through the *in situ* formation of reactive rhodium carbenoid species from α-diazo carbonyl compounds, which then promote a wide variety of transformations.[18,26,68] The versatility of these catalysts stems from the ability to efficiently modulate the electrophilicity of the rhodium metals through the exchange of bridging ligands surrounding the bimetallic center (Figure 3.1, left). The axial sites of the bimetallic complex are the reactive sites for the formation of transient carbene species and it is generally accepted that only one of the rhodiums axial sites is involved in catalysis during a reaction.[57] The two Rh atoms also act cooperatively during the reaction, Any electronic changes at one Rh atom is compensated for by the other Rh atom.[166,176] It is this observation that fueled research into incorporating Lewis base (LB) ligands at axial sites to affect the electrophilicity of the distal Rh atom and fine-tune reactivity and/or selectivity.[60]

While adding donating ligands to one Rh axial site has led to new reactivity,[177,178] the strategy is largely detrimental to diazo-mediated reactions.[57,61,164,168,171,179] The reduction in reactivity stems from the need to add excessive amounts of LB to compensate for the inherently weaker interaction at the axial sites.[180] Because LBs are in excess, it becomes difficult to control binding to both Rh centers, which deactivates the catalyst. A strong

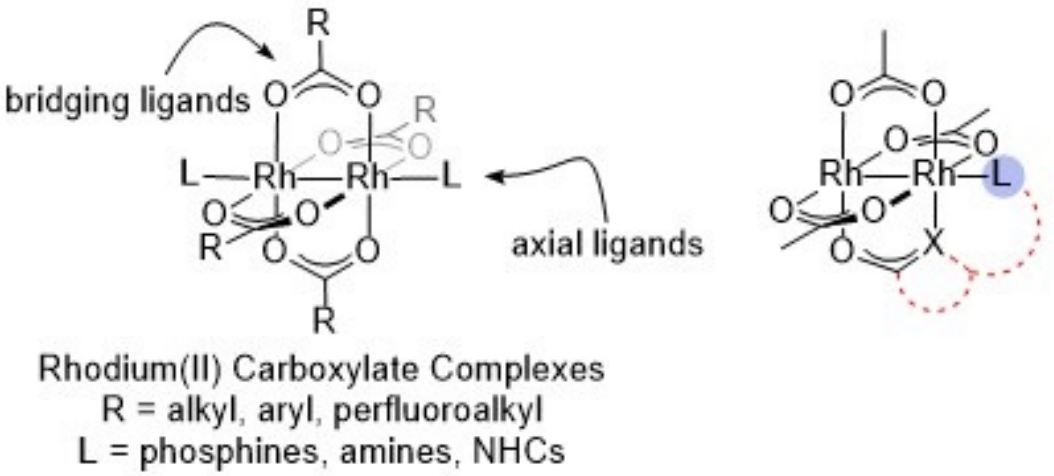

Figure 3.1: Features of a dirhodium carboxylate complex.

σ donor can be used for a stronger interaction, but this leads to a significant decrease in electrophilicity at the other Rh atom, reducing the effectiveness of the diazo decomposition step.[57] We have been interested in tethering LBs to bridging ligands in order to control their coordination to rhodium paddlewheel centers and prevent complications associated with exogenous LBs (Fig. 3.1, right). This design allows for the incorporation of a variety of LBs and a more defined examination of how their coordination influences reactivity and selectivity of the rhodium complex in diazo-mediated reactions.

We recently reported that the incorporation of thioether containing ligands into the rhodium paddlewheel motif improved yields in cyclopropanation reactions when compared to rhodium acetate.[35] The best catalyst in that reaction was the carboxylate-based $Rh_2(OAc)_3$PhTCB 85, while $Rh_2(OAc)_3$MeTOX 87 and $Rh_2(OAc)_2(MeTOX)_2$ 97a/b were sub-optimal catalysts (Fig. 3.2).[35] We reasoned that the more electron-rich nature of carboxamidate-type bridging ligands and the ideal six-membered chelate of the tethered thioether in these complexes rendered them comparatively less suitable for the reaction. We envisioned that catalysts 87 and 97a/b would be better suited for more reactive diazo compounds and substrates.[181] As such, the Si–H insertion reaction with donor/acceptor diazo compounds was chosen due the facile nature of the reaction and as a means to obtain a greater understanding of the role of axially coordinated functional groups.

Rh(II)-catalyzed Si–H insertion with diazo compounds was first reported by Doyle in 1988.[182] Since then, $Rh_2(OAc)_4$ 3 and other Rh(II) catalysts have been shown to give high yields and enantioselectivity of silyl–insertion products.[38,40,144,156,183–185] Among the previous reports, only a study by Ball and Zaykov has considered the influence of axial coordination on the outcome of Si–H insertion.[156] In this article, the authors used kinetic studies to prove that axial coordination of triphenylphosphite improved enantioselectivity of silane insertion with methyl phenyldiazoacetate 72 using dirhodium peptide complexes.[156] Our interests in utilizing tethered thioether ligands in Rh(II) catalysts led us to further explore the effects of axial coordination in silyl–insertion reactions.

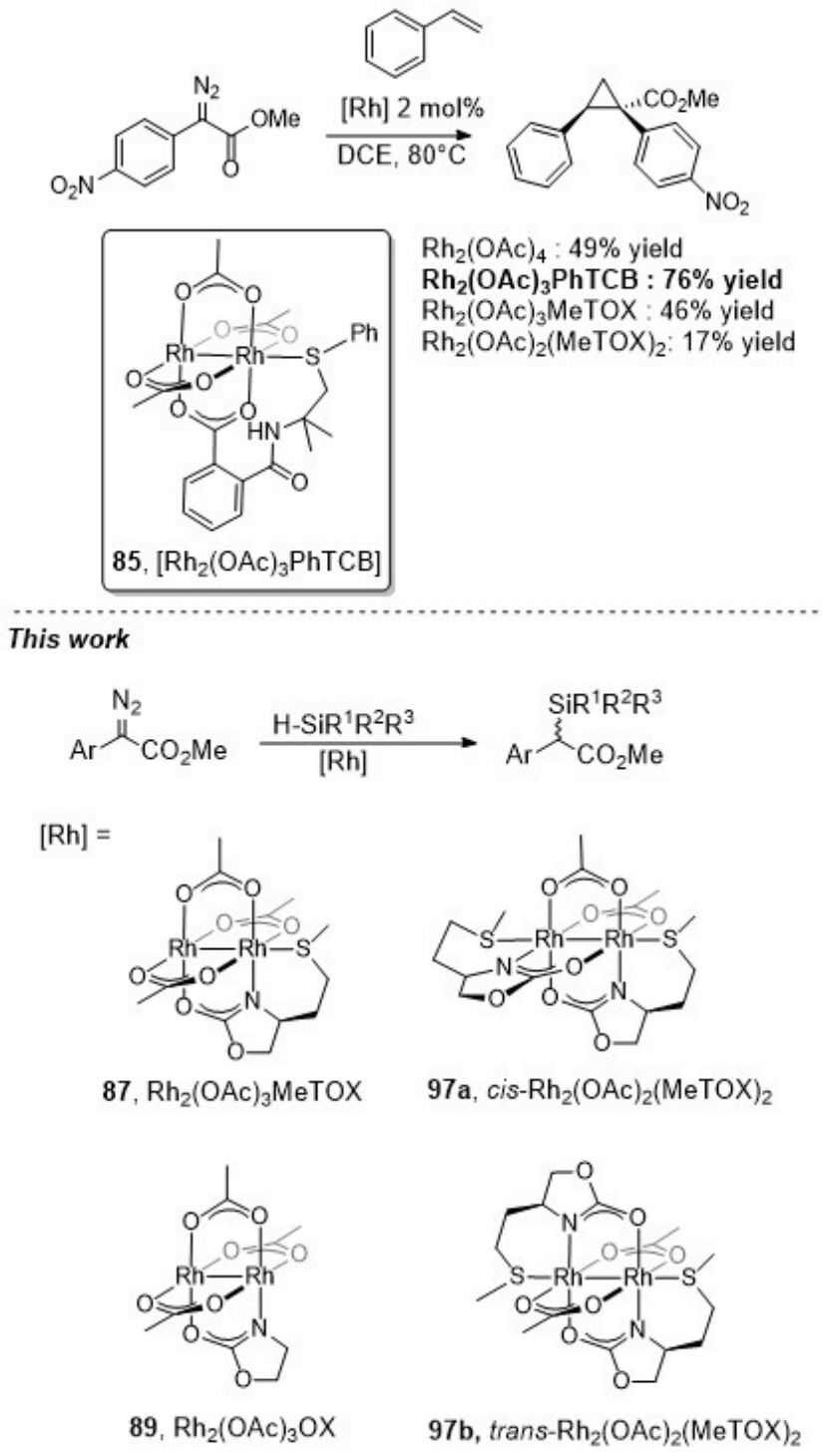

Figure 3.2: (Top) Cyclopropanation with dirhodium complexes featuring tethered, axially coordinated thioether ligands. (Bottom) Investigating silyl–hydrogen insertion reactions using mixed oxazolidinate/carboxylate dirhodium complexes.

3.4 Results and Discussion

3.4.1 Rh(II) Complex Synthesis

Complexes 87, 97a and 97b were synthesized according to our previously disclosed procedures.[35] Complexes 97a and 97b were used together as a 1.5:1 (97a/b) mixture of isomers. To gauge the impact of the thioether tether on catalytic activity, we synthesized complex 89, a mixed-ligand oxazolidinate/carboxylate complex that did not contain an axially coordinated thioether group. Mixed-ligand carboxamidate/carboxylate complexes are scarcely reported in the literature.[69,136] This is most likely due to the lack of control in ligand substitution[186] because of the relatively harsh conditions required to synthesize this family of complexes.[68] Attempts to synthesize and isolate the monooxazolidinone complex 89 proved challenging. Our normal ligand exchange conditions using a Soxhlet apparatus in refluxing conditions failed to provide any ligand substitution. The use of a microwave reactor and high excess of ligand 98, however, allowed us to successfully isolate an adequate amount of the mono-oxazolidinone complex 89 (Fig. 3.3). Attempts to cleanly isolate other multi-substituted products were unsuccessful due to difficulty in isolating the complex mixture of substitution products.[187]

3.4.2 UV-vis Complexes

A UV-vis spectrum of complex 89 with 1 equivalent of diethyl sulfide in dichloroethane was obtained in order to compare the effect of the tethered vs. non-tethered coordination of sulfides on the electronic transitions within the complex. Axial coordination is indicated by a blue shift of the Rh–Rh π^*-to-σ^* HOMO—LUMO band, which is found in the low energy region of Rh(II) UV-vis spectra.[56] We found that the diethyl sulfide ligated version of complex 3 had a very similar λmax of the π^* to σ^* band when compared to complex 87 (576 nm vs. 572 nm). As such, diethyl sulfide was also added to complex 89 in our reaction studies to probe the need for tethered axial coordination.

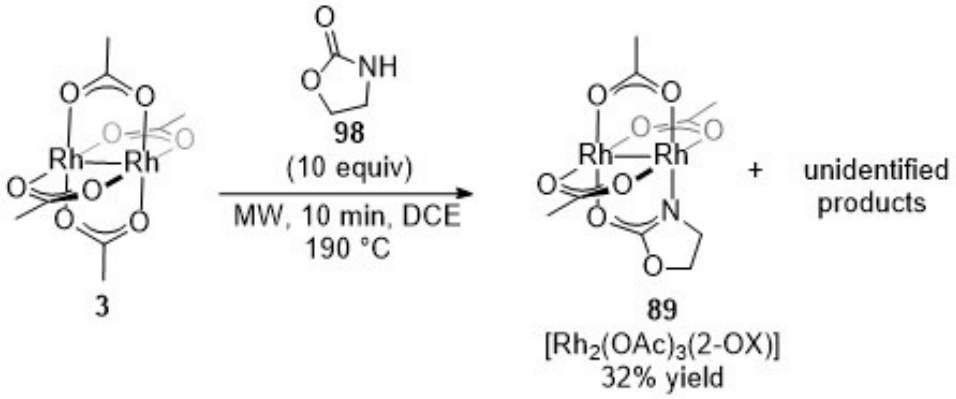

Figure 3.3: Ligand exchange with ligand 97 to produce complex 89.

3.4.3 Si–H Insertion Optimization

Initial catalyst evaluation was conducted using dimethylphenylsilane and 72. Complex 87 was able to efficiently catalyze the carbene insertion into the Si–H bond in ambient conditions with a 73% yield in dichloromethane (DCM). Upon subjecting the complexes 97a and 97b to the same conditions, only 16% yield of the product was observed, even two hours after diazo addition was complete. Complex 89 provided a 70% yield of silane 99a under these conditions and a 72% yield when 2 mol% of diethyl sulfide was added. Performing the reaction in refluxing DCM further improved the yield for complex 87 to 84% and for 97a/b to 25%, but the yields for complex 89 did not improve, even when dimethyl sulfide was added (Table 3.1, entries 4–6). Cooling to 0 °C was detrimental to the performance of complex 87, reducing 99a yield to 50% (Table 3.1, entry 7). Changing solvents to toluene and raising the temperature to 60 °C gave the best yield for complex 87 (89 %, Table 3.1, entry 9), and were used as the optimal conditions to further evaluate the performance of complexes 97a/b and 89. For 97a/b, the optimal conditions dramatically increased the yield of silane 99a to 74 % (Table 3.1, entry 10). The observation that 97a and 97b were more active at elevated temperatures is a strong indication of ligand hemilability.[188] Presumably, the displacement of the thioether ligand by diazo 72 becomes more facile at higher temperatures, enabling catalysis in complexes 97a and 97b. Complex 87 already possesses an open site, allowing it to react much more readily at lower temperatures. Subjecting 89 to the optimized conditions only marginally improved its yield of 99a (77 % yield, Table 3.1, entry 11), which was lower than the yield with complex 87 (compare entries 9 and 11 in Table 3.1). The addition of 2 mol% of diethyl sulfide or (*S*)-MeTOX ligand to complex 89 did not significantly improve yields for 99a (Table 3.1, entries 11 and 12). The UV/Vis results suggested that complex 89 with diethyl sulfide should have similarly reactivity to complex 87. However, the results at higher temperature imply that the diethyl sulfide additive is too weakly coordinated to be of any benefit, indicating that tethering the thioether to the catalyst is most beneficial at elevated temperatures.

Table 3.1: Catalyst screening of Si–H insertion of methyl phenyl diazoacetate.

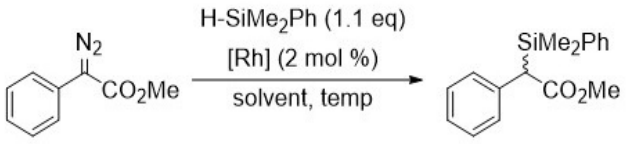

72a **99a**

Entry	[Rh]	Temp. [°C]	Solvent	Yield [%][a]
1	**87**	25	CH_2Cl_2	73
2	**97a/97b**	25	CH_2Cl_2	16[b]
3	**89**	25	CH_2Cl_2	70 (72)[c]
4	**87**	40	CH_2Cl_2	84
5	**97a/97b**	40	CH_2Cl_2	25
6	**89**	40	CH_2Cl_2	72 (69)[c]
7	**87**	0	CH_2Cl_2	50
8	**87**	25	Toluene	78
9	**87**	60	Toluene	89
10	**97a/97b**	60	Toluene	74[d]
11	**89**	60	Toluene	77 (75)[c]
12	**89**	60	Toluene	79[e]

[a] Yields are reported as averages of two runs and were determined by 1 H NMR using mesitylene as an internal standard. [b] Reaction had diazo remaining 2 hours after start of reaction. [c] Yields in parenthesis are when diethyl sulfide (2 mol%) was included as an additive. [d] Separately, 2a and 2b gave average yields of 70 and 73 %, respectively. [e] (*S*)-MeTOX ligand (2 mol%) was included as an additive.

3.4.4 Si–H Insertion Substrate Scope

With optimal conditions in hand, we investigated the scope of the Si–H insertion reaction in the presence of the tethered thioether.

Keeping diazo 72a constant, we tested complexes 87, 97a/b, and 89 with a series of silyl substrates but observed essentially comparable yields between them. Complex 87 was the best catalyst for most substrates tested, but only marginally (99b–e, Table 3.2, entries 1–12). With the exception of triphenylsilane, the silanes in the scope are considered to be more reactive than dimethylphenylsilane.[8] Thus, it seems that the reactive nature of these silanes outweigh any potential benefits in yield afforded by the tethered thioether moiety.

We also sought to investigate the effects afforded from the tethered thioether when electronics were perturbed on the diazo compound and found more notable differences. When a strong withdrawing group is present on the phenyl ring, 87 has lower activity when compared to 89. However, as the donating ability of the diazo became stronger, complex 87 began to perform more effectively (99f–h, Table 3.2, entries 13–18). There was also a larger change in yield when compared to changes in yield for complex 3. For example, the difference in yield of products 99f and 99g was 24 % for complex 87 (Table 3.2, compare entries 13 and 15), while the difference in yield for the same substrates was 8 % for complex 89 (Table 3.2, compare entries 14 and 16). This indicates a greater selectivity for diazo compounds when the tethered thioether group is present.

3.4.5 Mechanistic and Computational Discussion

The enhanced selectivity could be due to the effects that coordinated LBs have on the frontier molecular orbitals on the dirhodium paddlewheel complex. Having ligands coordinated at axial sites has been previously examined computationally in studies that suggest a dramatic increase in the energy of the LUMO of the complex.[56,115] An analysis of the frontier molecular orbitals of complex 87 and 89 seem to agree with this. When the tethered thioether is present, the LUMO energy level is increased by 1.21 eV ($\approx$ 28 kcal/mol, Figure 2.4), along with an increased HOMO-LUMO gap (5.56 eV for 89 vs. 6.47 eV for 87, Figure 2.4). Consequently,

Table 3.2: Si–H insertion substrate scope

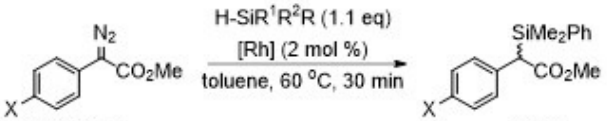

72a: X = H
72b: X = NO_2
72c: X = Br
72d: X = OMe

Entry	Product	[Rh][b]	Yield [%][a]
1	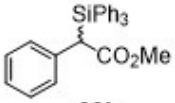	**87**	76
2		**97a/97b**	72
3	**99b**	**89**	70
4	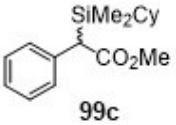	**87**	79
5		**97a/97b**	75
6	**99c**	**89**	77
7	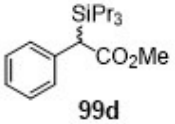	**87**	80
8		**97a/97b**	75
9	**99d**	**89**	77
10	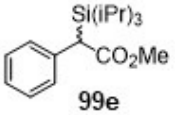	**87**	50
11		**97a/97b**	29
12	**99e**	**89**	54
13	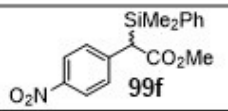	**87**	50
14	**99f**	**89**	64
15	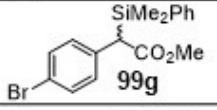	**87**	74
16	**99g**	**89**	72
17	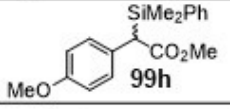	**87**	89
18	**99h**	**89**	79

[a] Yields are reported as averages of two runs and were determined by 1 HNMR using mesitylene as an internal standard.

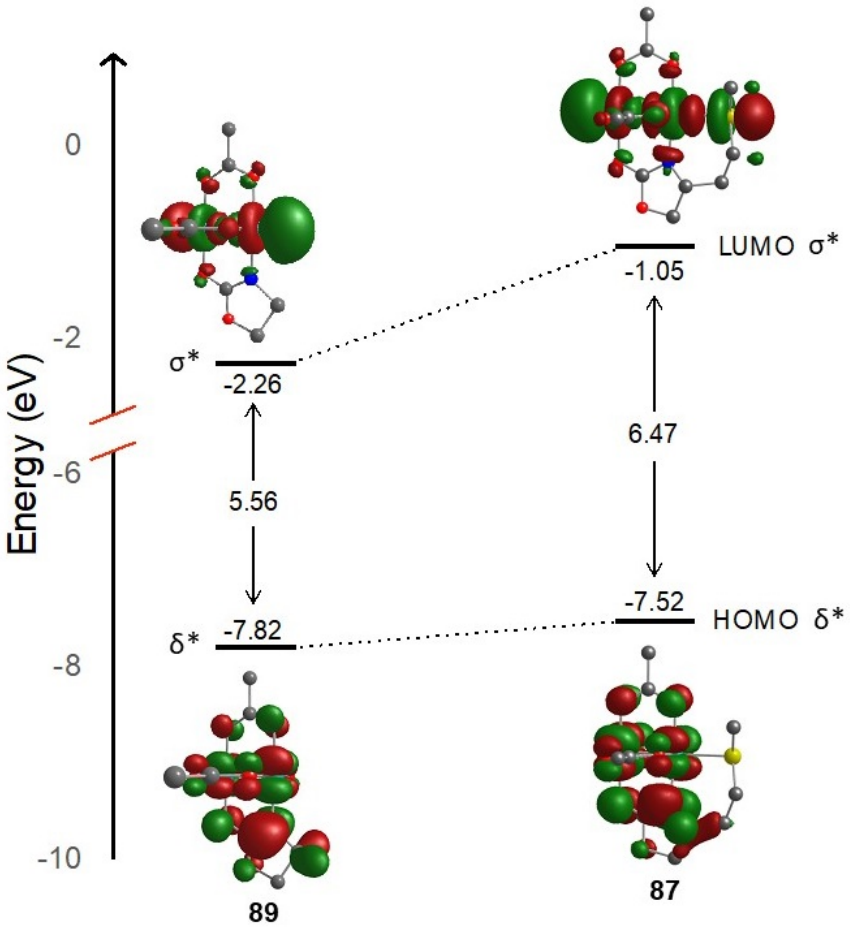

Figure 3.4: Frontier molecular orbital, HOMO-LUMO gap, and frontier orbital perturbation comparison for complexes 87 and 89 calculated at the M06-2X/def2-TZVPP level of theory. Hydrogens were removed for clarity.

the initial step of the nucleophilic attack of the diazo onto the rhodium center is expected to be more difficult (step a, Figure 2.5). This may explain the improved yields at elevated temperatures. The result that complex 87 is still active, albeit less so, at 0 °C suggests that the activity of the complex is more nuanced. Using Berry's three-center/four electron bonding model[56] as an inspiration, it's plausible that the labile nature of the thioether coordination allows an elongation of the Rh–S bond to compensate for the binding of the diazo compound. This was confirmed by calculations performed to understand the energetic profile of the N_2 extrusion event during the formation of carbenoids of 87 and 89 with ethyl diazoacetate discussed in further detail in Chapter 5. Suprisingly, the axial coordinating tether increases the barrier to N_2 by resisting modulation of the electron density of the Rh–Rh bond. This in turn forms a more electron dense Rh–C bond of the carbenoid formed with 89. It was initially though that the thioether ligand can then contract its Rh–S bond to donate electron density to the metal center, facilitating nitrogen extrusion and lengthening the Rh–C bond of the resulting carbene. This is not the case. This "push-pull" relationship of axial ligands on the Rh paddlewheel scaffold has been previously invoked to explain results when *N*-heterocyclic carbenes are used as axial ligands in diazo-mediated reactions.[168] We have found through computational modeling that this proposal does not apply to our system. It was initially proposed the more rigid ligand system used in this study can only "flex" so far, however, and cannot adequately accommodate less nucleophilic diazo compounds such as 72b.[189] It is now proposed that a more nucleophilic carbenoid is needed to overcome the resistance imparted by the axially coordinating thioether. This agrees with the results shown in Table 3.2, as 87 performed worse than 89 in the production of 99f. As the substituent on the phenyl ring of the diazo becomes more donating, as in diazo 72d, the benefits of the thioether are more pronounced due to a better reactivity match.

A comparison of the complete molecular orbital diagram of complex 89 and 87 show they are both calculated to have a calculated electronic configuration of $\sigma^2\pi^4\delta^2\pi^{*4}\delta^{*2}$ (Fig 3.5). The addition of the single oxazoldinone ligand separates the two π^* orbitals in 89 by 0.11 eV. This difference in energy is not changed when σ donation is added into the Rh–Rh bonding framework in 87. An interesting result of σ donation destabilization of all the occupied

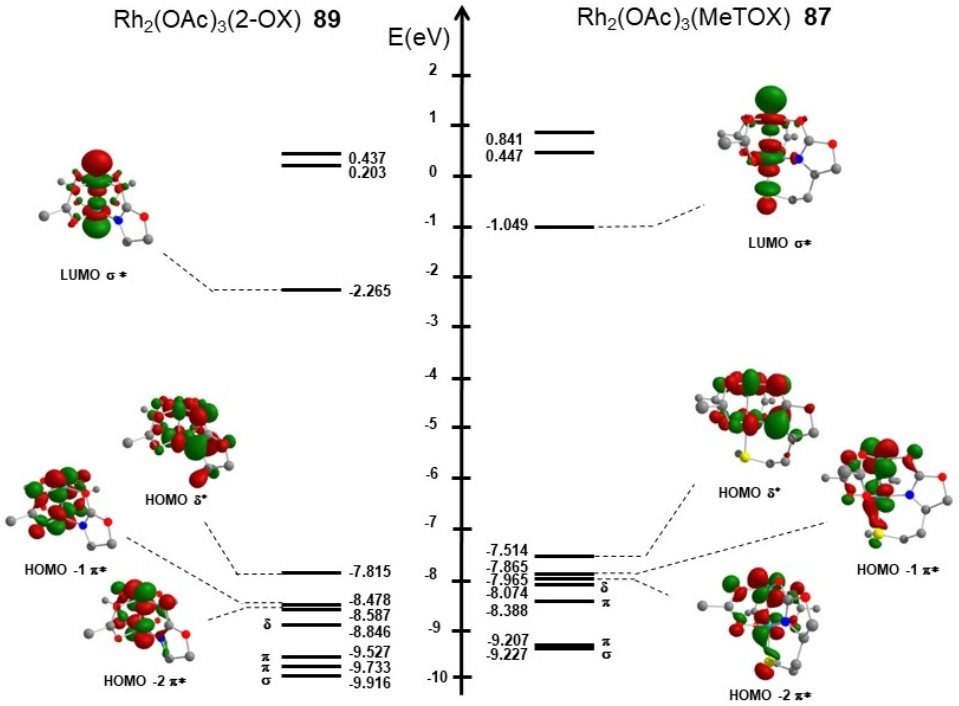

Figure 3.5: Full molecular orbital diagram calculated for 87 and 89 calculated at the M06-2X/def2-TZVPP level of theory. Hydrogens were removed for clarity.

orbitals to higher energies. The σ bonding orbital is destabilized by 0.69 eV due to the the donation of the axially coordinated thioether in the σ^*, resulting in a nearly degenerate σ and π bonding orbital. This conceptually makes sense as donation into antibonding orbitals traditionally weaken the bonding interaction of the corresponding bonding orbital.

3.5 Conclusions

Using Si–H insertion reactions, we have shown that axially coordinated thioethers do give good yields of desired silyl products, achieving yields up to 89 %. In select cases at elevated temperature, the tethered thioether ligands had a positive effect on the catalytic performance of rhodium paddlewheel complexes compared to non-tethered complexes. The effects afforded from the thioether also appear to be more prevalent with more donating diazo substrates. Subsequent calculations have indicated that a more donating diazo compound may be a better reactivity match because the additional σ donation could be needed to overcome the persistent electron density between the Rh atoms when the axially coordinated thioether. This could result in a less endothermic coordination event of the diazo compound when the axially coordinated thioether is present. Calculation of the reaction coordinate diagrams of the electronic perturbation used in the experimental study will further define the nuances that dictate the selectivity imparted by the axially coordinated thioether.

3.6 Experimental

3.6.1 General Considerations

Unless otherwise noted, all reagents were used as received from the manufacturer without further purification. (*S*)-MeTOX derived catalysts were prepared following the procedure outlined previously.[86] Diazo substrates were prepared based on literature procedures.[190–192] All reactions were carried out in reaction vials. Reactions were monitored using thin layer chromatography (TLC) on Sorbent Technologies Silica XG TLC Plates. Column chromatography was performed using either 60 Å, 40-63 μm flash silica or 60 Å, 63-200

μm gravity silica from Sobent Technologies. Microwave assisted reactions were carried out in a closed vessel using a Biotage Initiator+ microwave reactor monitoring the reaction by equipped IR sensor. ^{1}H and ^{13}C NMR spectra were recorded on a Varian Mercury Vx 300 MHz or Varian VNMRS 500 MHz spectrometers. All NMR chemical shifts are reported in ppm on the δ scale. Signals were referenced by residual solvent signal for ^{1}H NMR ($CHCl_3$ = 7.26 ppm) and ^{13}C NMR ($CHCl_3$ = 77.16 ppm). The mass spectra were obtained using either an Exactive Plus OrbitrapTM Mass Spectrometer (Thermo Scientific, San Jose, CA, USA) via direct injection or with a JEOL AccuTOF Mass Spectrometer fitted with a DART interface, run in positive mode. Chiral HPLC analysis was performed on a Shimadzu LC-2030 Prominence-I instrument using a Lux Cellulose-1 column (250 x 4.6 mm, 5 μm): 25 °C; UV detection at 245 nm, 3% isopropanol/hexanes at a 1 mL/min flow rate.

3.6.2 Synthesis of Complex 89

[$Rh_2(OAc)_3$(2-Ox)·2CH_3CN] (89): To four separate 2-5 mL microwave reactor vials, dirhodium tetraacetate (25 mg, 0.057 mmol) and 2-oxazolidinone (49 mg, 0.57 mmol) were added. 1,2-Dichloroethane (5 mL) was then added to the vial, rinsing the sides of the vial of any solid material. A cap was then crimped onto the vial and placed in the microwave reactor. The reactor was set to the following parameters: fixed hold time of 10 minutes; 1 minute pre-stir; low absorbance; temperature 190 °C. After the reaction was complete and cooled, the contents of the microwave vials were combined, and volatiles were removed in vacuo. Purification by column chromatography using gravity silica gel with 1:1 CH_3CN:toluene afforded compound 89 along with a mixture of other ligand substitution products. Compound 89 was obtained as a purple solid (40 mg, 0.066 mmol, 32% yield) ^{1}H NMR (500 MHz, Chloroform-*d*) δ 4.32 (t, J = 8.4 Hz, 2H), 3.71 (dd, J = 8.9, 7.9 Hz, 2H), 2.44 (s, 6H), 2.06 (s, 3H), 1.91 (s, 6H). ^{13}C NMR (126 MHz, Chloroform-*d*) δ 191.90, 190.17, 168.93, 65.62, 49.55, 24.00, 23.43. HRMS (obtained using Orbitrap^{TM}) $[M+H]^+$ m/z calcd for $C_11H_16N_2O_8Rh_2$ ($[Rh_2(OAc)_3(2\text{-}Ox)\cdot CH_3CN]$): 510.9045; found: 510.9084.

3.6.3 Procedure for Si–H Insertion Reactions

Diazo compound (0.4 mL, 0.114 mmol) from a 0.284 M stock solution was added in one portion to an 8 mL reaction vial containing silane (0.125 mmol, 1.1 equiv) and rhodium catalyst (2 mol%). The vial was immediately capped and placed in a pre-heated well plate set to 60 °C and stirred for 30 minutes. Excess solvent was removed by rotary evaporation and the crude material was dissolved in chloroform-*d*. Mesitylene (0.114 mmol, 1.0 equiv) was added as an internal standard. Yields were obtained via ^{1}H-NMR. Chemical shifts of known products were as reported in literature.[193,194]

3.6.4 Silyl Product Yield Calculations

Normalized integration of the methyl proton signal of mesitylene (2.28 ppm) was compared to the integration of the protons assigned to the methyl ester of the products. For products 99e and 99g which had overlapping signals for the methyl ester and methine proton of the stereocenter, the integration of mesitylene was compared to the combined area of both the methyl ester and methine proton signals. For products 99c and 99d, the integration of mesitylene was compared to the methine proton signal. For product 99e, the integration of mesitylene was compared to the methyl signal of the isopropyl group.

3.6.5 Synthesis of Silane Products for Characterization

Methyl 2-(cyclohexyldimethylsilyl)-2-phenylacetate (99c): Scale-up synthesis of product 99c was performed in order to obtain a pure sample of 99c. $Rh_2(OAc)_4$ (2.5 mg, 5.68 µmol) and dimethylphenyl silane (0.0444g, 0.312mmol) were added to a round bottom under ambient conditions. Diazo 72 (0.0500 g, 0.284 mmol) dissolved in 1 mL of methylene chloride was added and the reaction mixture was stirred for 30 minutes. Solvent was then removed by rotary evaporation and the crude material was purified by column chromatography using flash silica gel. Compound 99c was isolated as a colorless oil. ^{1}H NMR (500 MHz, $CDCl_3$) δ 7.35 – 7.32 (m, 2H), 7.30 – 7.25 (m, 3H), 7.19 – 7.14 (m, 1H), 3.68 (s, 3H), 3.51 (s, 1H), 1.75 – 1.59 (m, 6H), 1.26 – 1.02 (m, 5H), 0.65 (tt, J = 12.4, 3.0 Hz, 1H), 0.04 (s, 3H),

-0.09 (s, 3H). ^{13}C NMR (126 MHz, $CDCl_3$) δ 173.76, 136.79, 128.54, 128.24, 125.70, 51.48, 43.68, 28.07, 28.03, 27.44, 27.30, 26.95, 24.41, -5.93, -5.95. HRMS (DART in positive mode) $[M+H]^+$ m/z calcd for $C_{17}H_{26}O_2Si$: 291.1736, found: $[M+H]^+ = 291.1777$.

Methyl 2-(dimethyl(phenyl)silyl)-2-(4-nitrophenyl)acetate (99f): *p*-Nitrophenyl methyl diazo acetate (0.0251g, 0.114 mmol) was added to a reaction vial containing dimethylphenylsilane (0.0170 g, 0.125 mmol) and $Rh_2(OAc)_4$ (1.0 mg, 2.28 μmol). Methylene chloride (0.4 mL) was added by syringe to the reaction mixture and stirred for 30 minutes at 40 °C. Solvent was then removed via rotary evaporation to provide compound 99f (71% by ^{1}H-NMR, 0.081 mmol) and a mixture of byproducts. Attempts to isolate 99f resulted in decomposition of the product during purification. The presence of 99f was determined by using the signal located at 3.61 ppm, which is presumed to be the methyl ester signal. ^{1}H NMR (500 MHz, Chloroform-*d*) δ 8.05 (d, $J = 8.8$ Hz, 2H), 7.37 – 7.30 (m, 7H), 3.76 (s, 1H), 3.61 (s, 3H), 0.37 (d, $J = 3.2$ Hz, 6H). ^{13}C-NMR (126 MHz, Chloroform-*d*) δ 172.07, 146.05, 144.27, 134.18, 134.05, 130.27, 128.89, 128.05, 123.31, 51.77, 46.87, -4.30, -4.40. The presence of 99f within the crude mixture was also detected by mass spectrometry. HRMS (DART in positive mode) $[M+H]^+$ m/z calcd for $C_{17}H_{19}NO_4Si$: 330.1117, found: $[M+H]^+ = 330.1110$.

3.6.6 Computational

All geometry optimizations were completed on Gaussian 09[195] and implemented the density functional theory M06-2X[19] functional with the def2-TZVPP[20] basis set. An ultrafine integration grid was utilized as well as tight convergence criteria. Frequency calculations were performed to verify the stationary points on the potential energy surface were in fact ground state minima. Compound 89 did exhibit a negative frequency at -20.1475 cm^{-1} but is still believed to be the ground state structure. Orbital visualizations were completed with ChemCraft.

Chapter 4

Rh(II)-Catalyzed Si–H Insertion of Nosyl Hydrazone Protected Donor Diazo Compounds

4.1 Disclosure

Chapter three is an adaptation of a manuscript in progress titled "Rh(II)-catalyzed Si–H Insertion of Nosyl-hydrazone Protected Donor Diazo Compounds." I performed the synthesis of some of the hydrazone compounds, the reaction optimization, substrate scope, development of the manuscript, and the development of the supplemental information. Jobe Courtney helped with synthesis of hydrazone compounds and production of catalyst. Dr. Ampofo Darko helped with development of the manuscript and advised all the work described herein.

4.2 Abstract

Dirhodium paddlewheel catalyst are evaluated in silyl–hydrogen insertion reactions of nosyl–hydrazone protected donor-diazo compounds. Donor-diazo compounds are highly reactive and their formation *in situ* from sulphonyl-protected hydrazones has provided a

safer avenue to explored their reactivity. Herein we describe our efforts to evaluate this transformation utilizing catalysts with a mono-substituted tethered, axially coordinating thioether ligand, a mono-substituted heteroleptic control complex, and $Rh_2(OAc)_4$. We found that the heteroleptic control catalyst, $Rh_2(OAc)_3$(2-OX), exhibited the highest activity producing the desired silane in up to 78% yield.

4.3 Introduction

The carbene transfer reaction has greatly increased the synthetic chemist's ability to complete various transformations such as intermolecular and intramolecular cyclizations, X–H insertions (X = C, N, B, O, S, Si, Ge, Sn and P) , and ylide transformations.[14,34,185,196–200] One of the most broadly used carbene precursors is the diazo compounds which can be divided into five separate classes (Fig. 4.1). Donor-donor and donor diazos are described as donor-type while acceptor-acceptor and acceptor diazos are described are acceptor-type. Donor-acceptor and acceptor-type diazos have been broadly investigated in the literature, while donor and donor/donor diazo compounds have had limited impact in carbene transfer reactions due to the dangers of handling the unstable compounds.[200] The donor-type diazo compounds are more commonly explosive as opposed to donor/acceptor and acceptor-type diazos. This makes handling donor-type diazos more difficult.[201] Safe handling requires they must be transported and stored in dilute solutions at low temperatures.

In Rh(II)-catalysis, the diazo coordinates to the one of the rhodiums. This is followed by the extrusion of nitrogen resulting in a metal carbenoid. The metal carbenoid and the diazo precursor have an inverse relationship of reactivity (Fig. 4.2). While the donor-type diazo is highly nucleophilic, the donor-type carbenoid is less reactive and sometimes stable. An example of the donor-donor Rh(II) carbenoids stability is that it is the most common type of Rh(II) carbenoid that has been successfully isolated and crystallized from diazo precursors. Fürstner and coworkers added solutions of bis-(4-methoxyphenyl)diazomethane/CH_2Cl_2 and $Rh_2(tpa)_4/CH_2Cl_2$ under strict inert conditions at -10 °C (Fig. 4.3a).[113] The resulting Rh(II) carbenoid 100 was stable enough to characterize by UV, IR, and NMR. Crystals

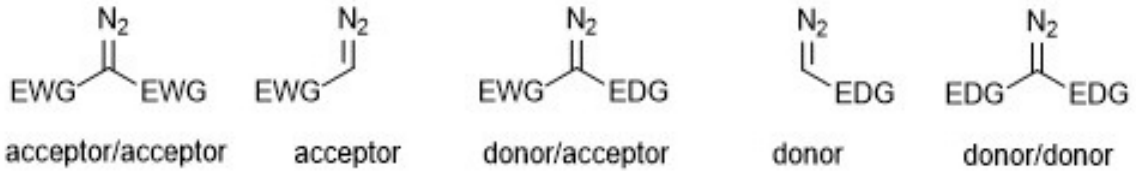

Figure 4.1: Classification of diazo compounds.

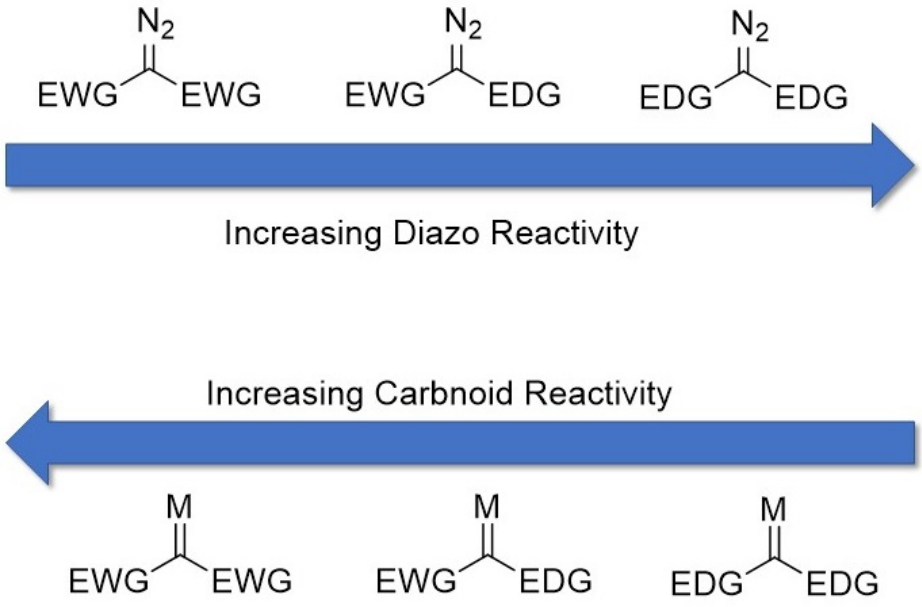

Figure 4.2: The reactivity trend of diazo compounds and metal carbenoids.

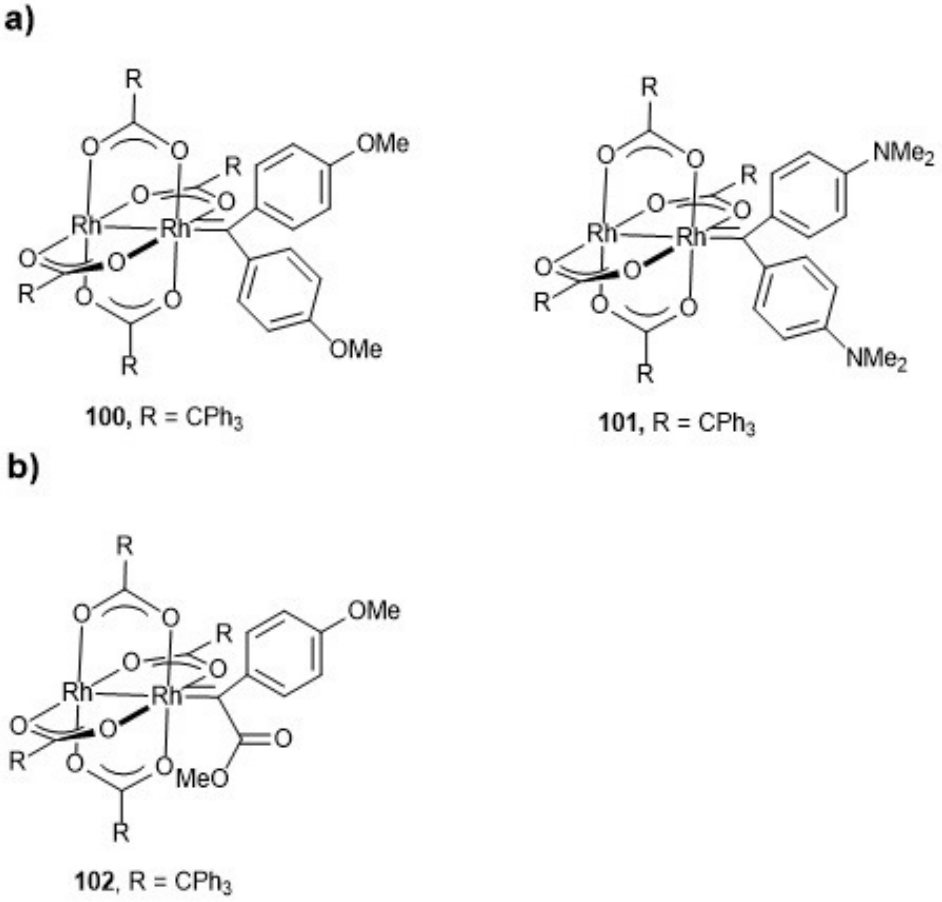

Figure 4.3: a) Rh(II) carbenoids 100 and 101 Fürstner published crystal structures of. b) Rh(II) carbenoid 102 studied spectroscopically be Davies.

were also successfully grown in CH_2Cl_2/toluene and fluorobenzene/toluene/CH_2Cl_2, with the latter providing the best crystals. In a later publication Fürstner and coworkers isolated Rh(II) carbenoid 101 and the $Rh_2(esp)_2$ variant of both carbenoids.[202] Interestingly, they also managed to obtain crystals of a traditional donor-acceptor diazo using the $Rh_2(esp)_4$ complex.[202]

Prior to Fürstner's initial disclosure, only spectroscopic evidence of these normally fleeting intermediates was provided by Davies, Berry, and coworkers.[28] They accomplished this characterization by decomposing methyl (4-methoxyphenyl)diazoacetate, a donor/acceptor diazo, with $Rh_2(tpa)_4$ in CH_2Cl_2. Interestingly, the metal carbenoid formed in ambient conditions and excess diazo had a reported halflife of 10 seconds (Fig. 4.3b). The same metal carbenoid formed under strict anhydrous and anaerobic conditions with substoichiometric diazo could be stored in CH_2Cl_2 or $CHCl_3$ for up to 20 hours.

Due to the unstable nature of donor-type diazos, chemist have long sought alternative precursors. The precursors developed can be separated into two classes: diazo and non-diazo. The substrates that form diazos *in situ* are hydrazones and triazoles with hydrazones being the most implemented in the literature. Hydrazones have the advantage of degrading over time, limiting the build of the reactive diazo in solution. Unprotected hydrazones can be oxidized to a diazo. Hydrazones protected with the nosyl group degrade at room temperature when subjected to basic conditions while hydrazones with the tosyl group also need elevated temperatures.[203] Hydrazones decompose into diazos in moderate base and polar aprotic solvent at elevated temperature (Fig. 4.4a).[204] If a proton source is present, it is believed that the formation of a cation is favored (Fig. 4.4b). This cation can experience rearrangement to form an olefin. If a strong base is present with protic solvent, it changes the mechanism to what is known as the Shapiro reaction resulting in an olefin product (Fig. 4.4c). At times the protic Bamford-Stevens reaction and the Shapiro reaction result in different products due to the differing mechanisms (compare Fig. 4.4b and c). Triazoles experience a thermally driven Dimroth rearrangement into a diazo with a β-imine moiety which must be desired in the final product or designed to be removed in subsequent synthetic

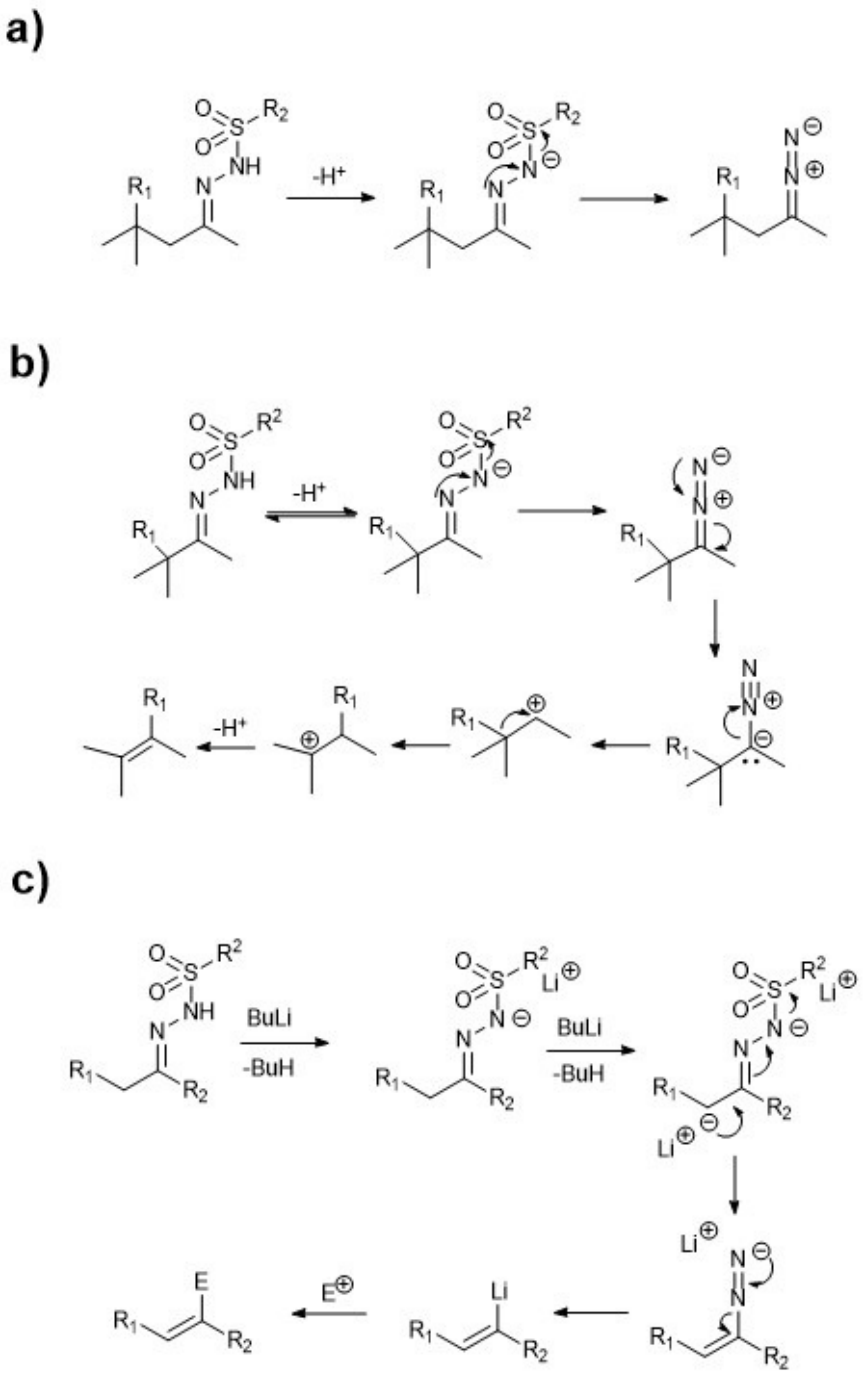

Figure 4.4: a) Proposed mechanism of Bamford-Stevens reaction in polar aprotic solvent using a moderate base. b) Proposed mechanism of Bamford-Stevens reaction in polar protic solvent using a strong base. c) Proposed mechanism of the Shapiro reaction.

steps.[205] Non-diazo precursors include allenes, cyclopropenes, cycloheptatrienes, propargyl esters and ethers, enynes, enynones and were not considered in the study.[200]

4.3.1 Donor-type Diazo Compounds in Si–H and Related Group 14 Insertion Reactions

The emergence of donor diazo carbene transfer reactions is relatively new when compared with the acceptor-type and donor/acceptor diazos. The first report of a donor diazo in a Si–H related reaction in was as recent as 2017. A disclosure from Bi *et al.* reported the insertion of donor-type carbenes into Si–H, Ge–H, and Sn–H bonds (Fig. 4.5a).[206] During the catalyst screening, 5 mol% of $Rh_2(OAc)_4$ was used with the optimal conditions and yielded 25 % of the silane product. The remaining transformations were performed at 30% catalyst loading with silver (I) triflate. The silver (I) triflate catalyst proved tolerant of many functional groups while smoothly inserting into the group 12 atom–hydrogen bonds in high yield, though aliphatic hydrazones failed to convert into the desired silane by this method. The following year, Che *et al.* reported Si–H, Ge–H, and Sn–H insertions utilizing an iron porphyrin catalyst(Fig. 4.5b).[207] This was achieved with a meager 2 mol% of catalyst and showcased the insertion into primary, secondary, and tertiary Si–H bonds.

In 2018, Wang *et al.*[208] published a Pd(0)-catalyzed Si–H insertion from *N*-tosyl-hydrazones. They demonstrated a broad scope with functional group tolerance. Interestingly, it is proposed the reaction proceeds through an alternate mechanism from the previously accepted Si–H insertion mechanism (Fig. 4.6). The proposed mechanism begins with oxidative addition of Si–H onto the Pd(0) resulting in a Pd(II) species. Then, either the silane or hydride migrates to the carbenic carbon. Finally, reductive elimination results in the product and return of the catalyst to the initial Pd(0) species. This method was also able to avoid β-hydride migration that has been experienced in the previous reports of Si–H insertion.

The first chiral iteration of the Si–H insertion with donor/donor diazos was reported by Franz et. al. in collaboration with Shaw (Fig. 4.7a).[209] In the study, they used a chiral

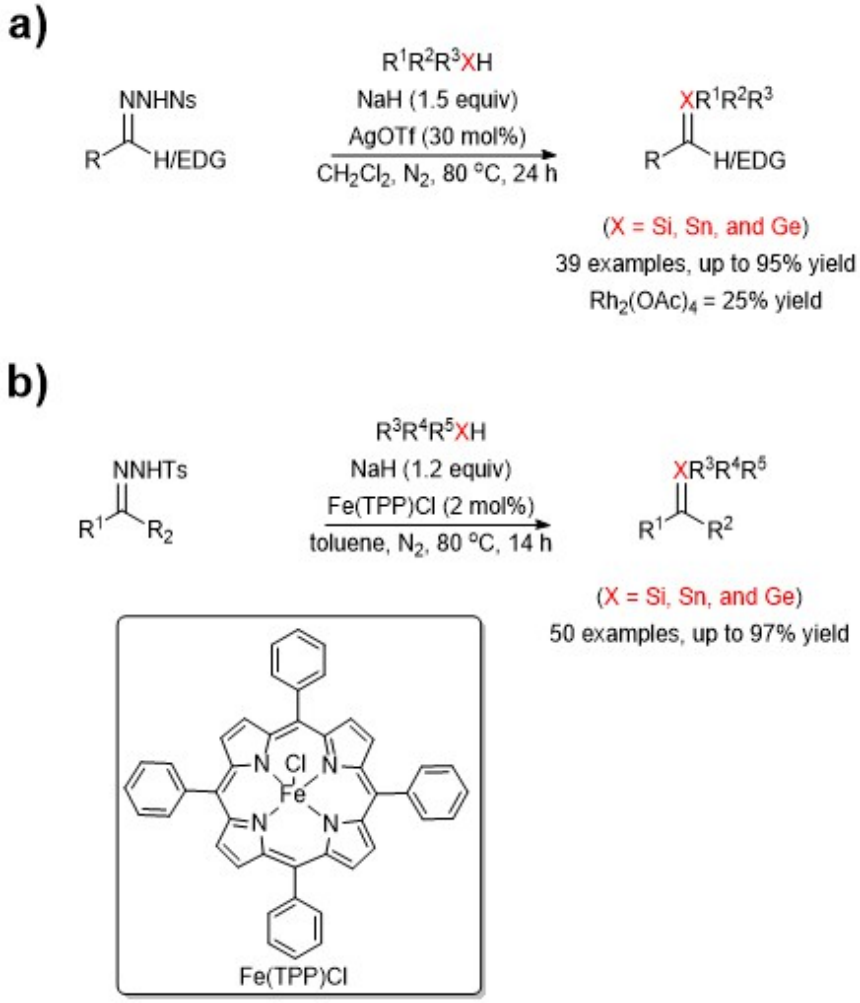

Figure 4.5: a) Silver(I) triflate catalyzed Si–H insertion of nosyl-protected hydrazones. b) Iron porphyrin catalyzed Si–H insertion of tosyl-protected hydrazones.

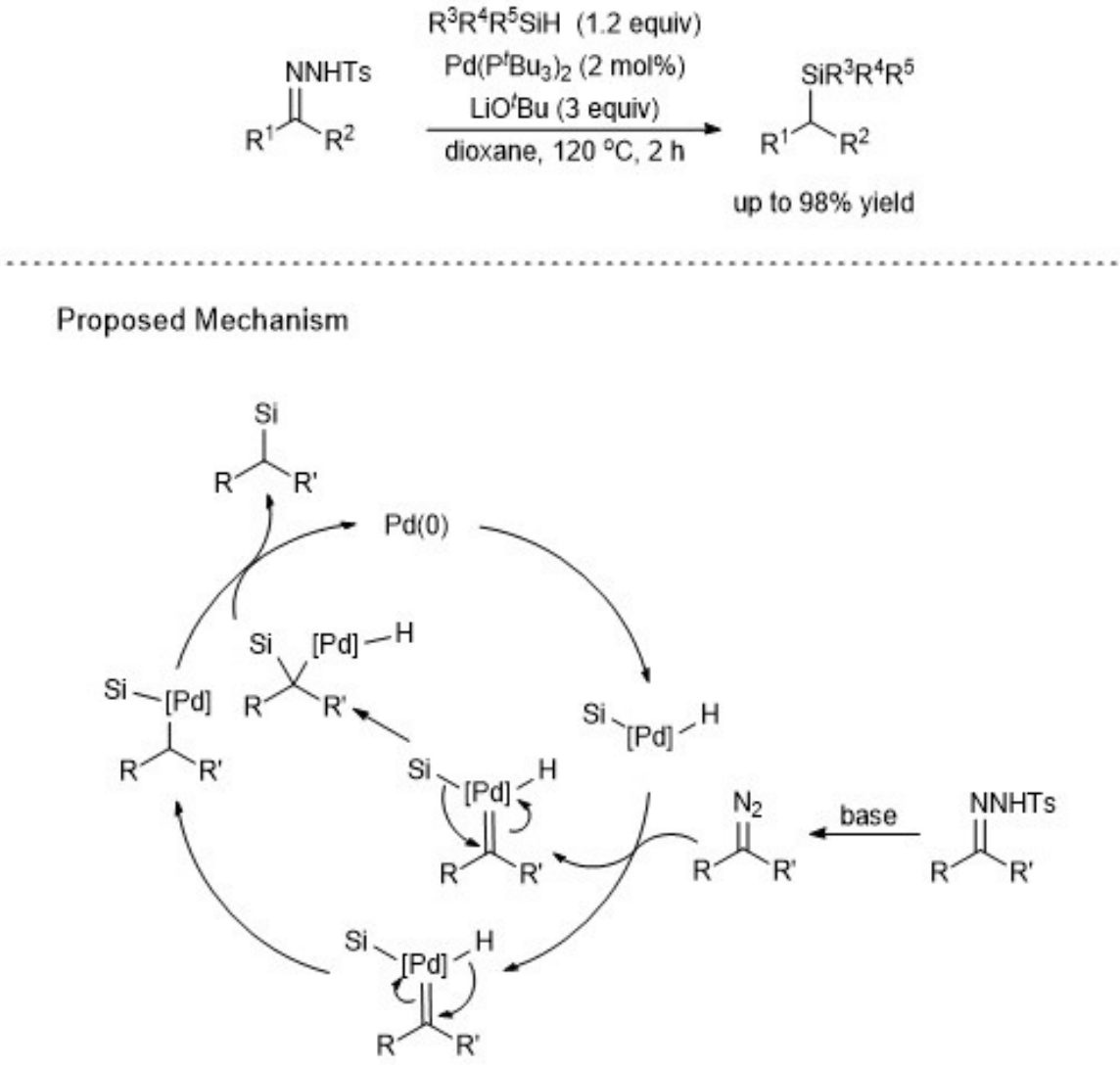

Figure 4.6: Palladium catalyzed Si-H insertion of tosyl-protected hydrazones with proposed mechanism.

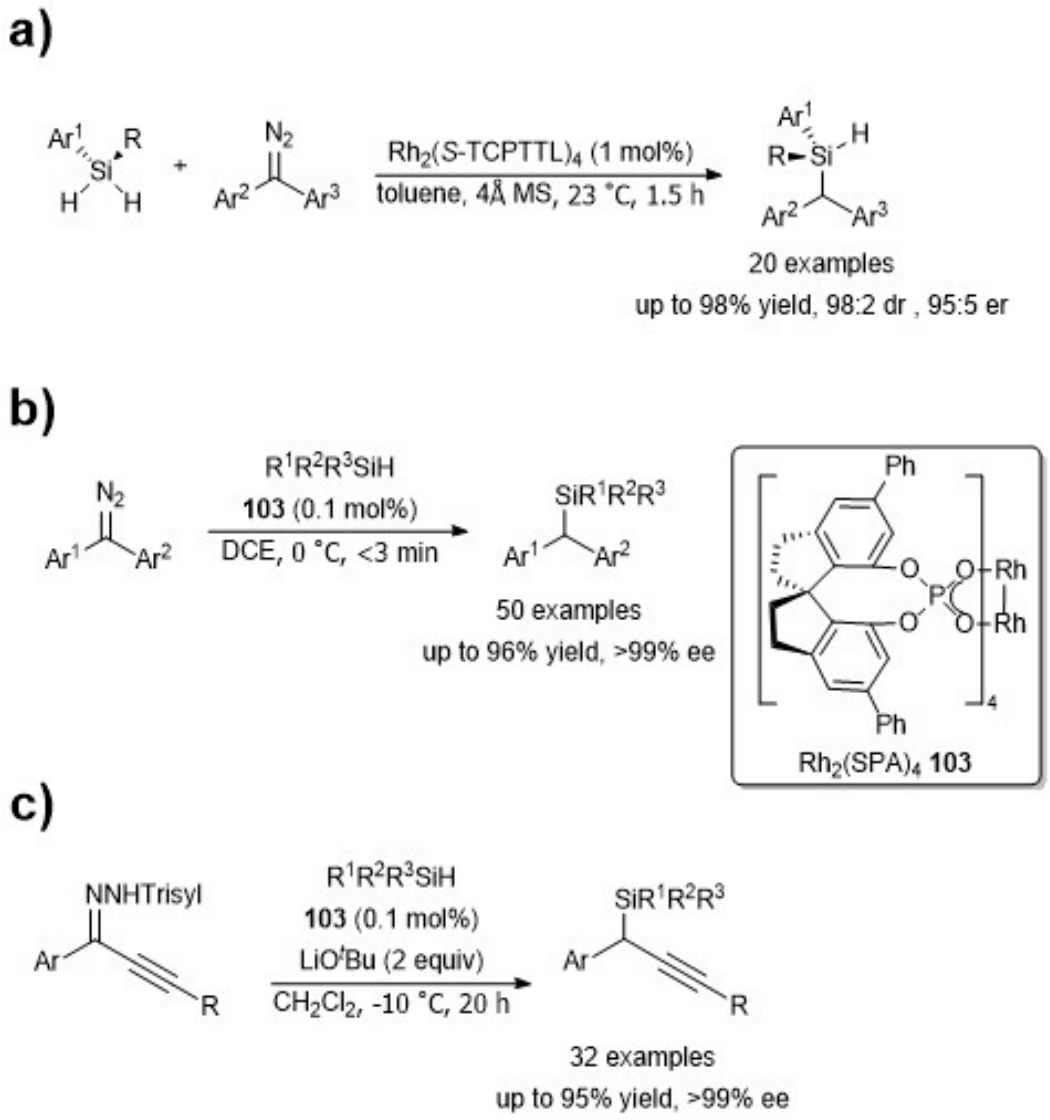

Figure 4.7: a) First example of Rh(II)-catalyzed Si–H insertion of diaryl diazo compounds with chiral silanes. b) Enantioselective Si–H insertion diaryl diazo compounds with chiral Rh(II) spiro-phosphate complex 103. c) Enantioselective Si–H insertion of trisyl-protected alkynyl hydrazones with complex 103.

homoleptic rhodium catalyst in tandem with silicon-stereogenic silanes to promote selectivity. When using symmetric diazos the enantiomeric ratio of the products suffered. They were able to rectify this by implementing a prochiral diazo, achieving up to 98:2 enantiomeric ratio in up to 98% yield. Azide and silyoxide formation were both side reactions experienced but were shown to be reduced by using a bulkier diazo and by adding 4Å-sieves respectively. Kinetic experiments were also conducted indicating the insertion step is the rate determining step .

Zhou *et al.* demonstrated how the electronics of a diaryl diazo could dictate the enantioselectivity of Si–H insertions.[210] They exhibited a linear correlation of the log(er) values and the Hammett parameters. The best catalyst of the chiral rhodium catalyst tested was ligated with chiral spiro phosphate ligands and could catalyze the insertion at a low 0.1 mol% catalyst loading (Fig. 4.7b). Kinetic experiments resulted in a kinetic isotope effect of 1.5 indicating the rate determining step is also the insertion step of the reaction. These results were also corroborated by a computational study. The study demonstrated that differences in the electronics of the diazo substituents correlated to differences in transition state energy.

In a subsequent publication, Zhou *et al.* overcame an unwanted intramolecular cyclization product and overhydrosilyation in their Rh(II)-catalyzed Si–H insertion reactions of sulphonyl protected alkynylhydrazones (Fig. 4.7c).[211] A series of chiral spiro phosphate rhodium catalyst were tested. The unsubstituted chiral spiro phosphate rhodium complex 103 exhibited the highest enantioselectivity when compared to substituted variants. The enantioselectivity was further increased by reducing the temperature to -10 °C. The intramolecular cyclization issue was overcome by exchanging the tosyl protecting group with a trisyl, 2,4,6-triisopropylphenylsulphonyl, protecting group. It was found that the oversilylation was silane dependent. Bulky silanes, such as triethylsilane and diphenylmethylsilane afforded the product high yield and enantioselectivity. The reaction was also highly functional group tolerant.

Although Rh(II) paddlewheel complexes are used quite prevalently for insertion reactions, few reports of Si–H insertion with donor-type diazos using Rh(II) paddlewheel complexes

have been reported. In our previous work, we described Rh(II) paddlewheel complexes with tethered, axially coordinated ligands (TACLs) as efficient Si–H insertion catalysts with donor/acceptor diazo compounds. In our studies, we noticed higher yields for electron rich aryl diazo acetates and were intrigued at the possibility of expanding Si–H insertion using Rh(II) TACLs complexes to donor-type carbenes. We describe our results herein.

4.4 Results and Discussion

4.4.1 Si–H Insertion Optimization

We began our reaction optimization by screening solvents with the nosyl-protected hydrazone[206] 104a, 1.5 equivalents of sodium hydride, 0.5 mol% of our previously developed catalyst, $Rh_2(OAc)_3$(MeTOX) 87, 104a, and 5 equivalents of dimethylphenylsilane at 25 °C for 24 hours. The thioether tethered catalyst converted the hydrazone to the desired silane in only 12% yield in dichloromethane (Table 4.1, Entry 1). The use of acetonitrile as the reaction solvent increased the yield to 20% yield, while a 10% yield was obtained in tetrahydrofuran (Table 4.1, Entry 2 and 3 respectively). We then evaluated 1,2-dichloroethane as the reaction solvent and found it was also a poor solvent to facilitate this transformation (7% yield, Table 4.1, Entry 4). Switching to 1,4-dioxane, however, resulted in a vast increase in yield to 60% (Table 4.1, Entry 5). We then turned our attention to screening other poorly coordinating bases. The use of potassium *t*-butoxide slightly decreased the yield to 56% compared to sodium hydride (Table 4.1, Entry 6). Cesium carbonate produced similar results to potassium *t*-butoxide, producing 57% yield of the desired product (Table 4.1, Entry 7). Sodium hexamethyldisilazane (NaHMDA) facilitated the decomposition of the hydrazone starting material to the reactive diazo intermediate the best, and the yield of the desired product was further increased to 71%. Increasing the reaction temperature did not have a positive effect on the yields of the insertion reaction. When the reaction was performed at 40 °C, the yield decreased by 11% (60% yield, Table 4.1, Entry 9). Other Rh(II) catalysts, with and without the tethered, axial coordinating thioether, were also tested. Changing the

Table 4.1: Reaction optimization of Si–H insertion of hydrazone 104a with dimethylphenylsilane over a 24hrs.

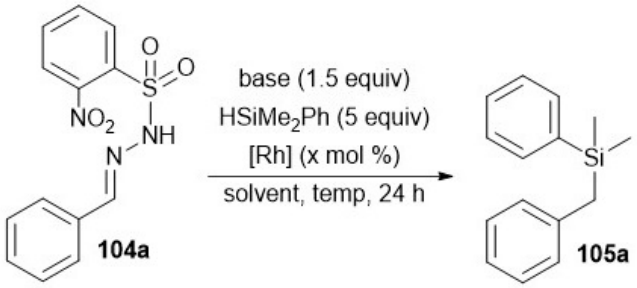

Entry	[Rh] (mol %)	Base	Solvent	Temp (°C)	Yield (%)
1	**87** (5)	NaH	CH_2Cl_2	25	12
2	**87** (5)	NaH	Acetonitrile	25	20
3	**87** (5)	NaH	THF	25	10
4	**87** (5)	NaH	DCE	25	7
5	**87** (5)	NaH	1,4-Dioxane	25	60
6	**87** (5)	KO*t*-Bu	1,4-Dioxane	25	56
7	**87** (5)	Cs_2CO_3	1,4-Dioxane	25	57
8	**87** (5)	NaHMDS	1,4-Dioxane	25	71
9	**87** (5)	NaHMDS	1,4-Dioxane	40	60
10	**87** (5)	NaHMDS	1,4-Dioxane	80	50
11	$Rh_2(OAc)_3$(PhTOX) (5)	NaHMDS	1,4-Dioxane	25	67
12	**3** (5)	NaHMDS	1,4-Dioxane	25	74
13	**89** (5)	NaHMDS	1,4-Dioxane	25	78
14	**3** (2)	NaHMDS	1,4-Dioxane	25	11
15	**89** (2)	NaHMDS	1,4-Dioxane	25	11
16	**87** (2)	NaHMDS	1,4-Dioxane	25	29

substituent on the thioether to phenyl by using 107 slightly reduced the yield by 4% (67% yield, Table 4.1, Entry 13). The benchmark Rh(II) catalyst 3, however, improved the yield to 74% yield (Table 1, Entry 11) and the heteroleptic complex 89 further increased the yield to 78% yield (Table 4.1, Entry 12). The optimization studies here show that the combination of dioxane as the solvent and NaHMDS as the base had greater impact on the reaction than the catalyst. It is worthy to note that when the catalyst loading was lowered to 2 mol%, 87 outperformed both 3 and 89 (Table 4.1, compare Entries 14-16).

4.4.2 Si–H Insertion Substrate Scope

With the optimal conditions in hand, we moved forward to investigate the scope of reactivity with para-substituted, nosyl-protected hydrazones to evaluate functional group tolerance and electronic effects of this substitution. The para-methyl substituent afforded the comparable yield of silane 105b to the model substrate (75% yield, Fig. 4.8). Substitution of the model substrate with a para-hydroxy group greatly suppressed the conversion to silane 105c (12% yield, Fig. 4.8). The competitive and relatively facile O–H insertion reaction is suspected to be the cause of the low yield.[212] The substrate with the para-cyano substitutuent afforded 46% yield of the silane product 105d. The cyano group has the ability to axial coordinate and could potentially poison the catalyst or slow the rate of reaction.[165,213,214] The electron withdrawing para-nitro substitutuent also gave fair yields, affording only 48% of the silane product 105e. The presence of the product from diazo homocoupling was observed by ^{1}H NMR and TLC. Substitution of a halogen at the para-position of the substrate produced good yields. The para-chloro substituted hydrazone 104f afforded 70% of silane product 105f and the para-fluoro substituted hydrazone 104g substrate afforded 72% of silane product 105g. The electron releasing para-methoxy substituent negatively affected the conversion of the diazo to 105h. This could be due to the further stabilization of the carbenoid intermediate by the methoxy group, resulting in decreased reactivity of the carbenoid.

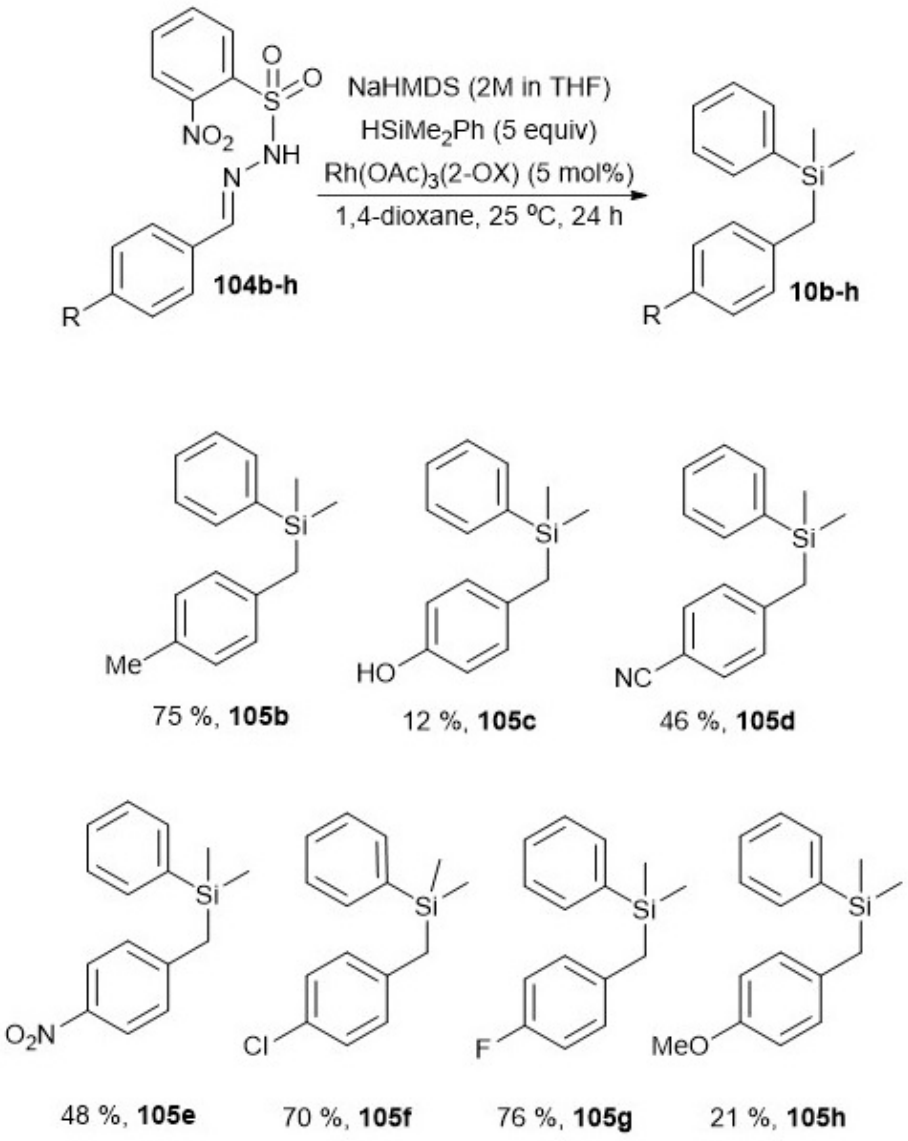

Figure 4.8: Hydrazone substrate scope of Si–H insertion

4.4.3 Discussion

Ethereal solvents have been previously used in carbene transfer reactions as both a solvent and a reactant. Hu *et al.* disclosed that ethereal solvents increased enantiomeric excess while maintaining high yields when compared to chlorinated solvents in Rh(II)-catalyzed intramolecular C–H insertion reactions.[215,216] In the formation of β-lactams toward the synthesis of (-)-Rolipram, 1,4-dioxane was found to be the optimal solvent.[216] In the pursuit of macrocycles, Lacour *et al.* used 1,4-dioxane as both a solvent and reactant.[217] They propose the 1,4-dioxane attacks the Rh(II)-carbenoid releasing the catalyst forming a free ylide. This ylide then experiences a [3+6+3+6] cyclization with another free ylide to form the desired macrocycle. Interestingly, in a subsequent publication Lacour *et al.* used *in-situ* IR and UV-vis titration experiment to determine the reactive catalyst species in solution is the mono-1,4-dioxane adduct of the rhodium catalyst.[163] They found through speciation studies that only 0.4-2.3% of the mono-adduct existed in solution.[163] This result could explain the need for a high catalyst loading in our system. The Lacour studies show that the 1,4-dioxane interacts with both the catalyst and the carbene bound to the catalyst. In various Rh(II)-catalyzed transformations[218–222] 1,4-Dioxane has been the optimal solvent to facilitate the Bamford-Stevens degradation of a hydrazone to the reactive diazo compound *in situ*. This is the first instance of its use in Rh(II)-catalyzed Si–H insertion. To our knowledge, this is also the first instance of the utilization of nosyl-protected hydrazones as a diazo precursor in Rh(II)-catalyzed Si–H insertions producing good yields.

4.5 Conclusion

In summary, we have found that nosyl-protected hydrazones coupled NaHMDS as a base and dioxane as the solvent are suitable conditions to facilitate Rh(II)-catalyzed Si–H insertion reactions. Although $Rh_2(OAc)_3$(2-OX) 89 slightly increased the yield when compared to other tested catalyst, the combination of base and solvent had the greatest positive effect on this transformation. Elevated temperatures had a negative impact on the transformation. Rhodium catalyst with TACL's faired better at lower catalyst loading than those without.

Lastly, the transformation was sensitive to functional group change at the para-position. The positive results of this study highlights that Rh(II)-catalyst are viable in Si–H insertions with hydrazone protected donor diazos and should inspire the development of more strategies to broaden the scope of this reaction.

4.6 Experimental Procedures

4.6.1 General Considerations

Unless otherwise noted, all reagents were purchased and used as received from the manufacturer without further purification. Complex 87, 89 and $Rh_2(OAc)_3$(PhTOX) were synthesized via an established literature procedures.[223] 1,2-dichloroethane (DCE), CH_2Cl_2 (DCM), tetrahydrofuran (THF), 1,4-diaoxane and acetonitrile (ACN) were used as recieved from vendors unless otherwise noted. Reactions were monitored using thin layer chromatography (TLC) on Sorbent Technologies Silica XG TLC Plates. Ligands were purified with column chromatography using 60 Å, 40-63 μm silica from Sorbent Technologies. ^{1}H and ^{13}C NMR spectra were recorded on a Varian Mercury Vx 300 MHz or Bruker AVANCE NEO 500 MHz spectrometers. All NMR chemical shifts are reported in ppm on the δ scale. Signals were referenced by residual solvent signal for ^{1}H NMR ($CHCl_3$ = 7.26 ppm, DMSO = 2.50 ppm) and ^{13}C NMR ($CHCl_3$ = 77.16 ppm, DMSO = 39.52 ppm. The mass spectra for all compounds, unless otherwise specified, were obtained using an AccuTOF Mass spectrometer equipped with a DART ionization apparatus. Hydrazones were made from established literature procedures.[206]

***N*-(4-hydroxybenzylidene)-2-nitrobenzenesulfonohydrazide:** orange solid; ^{1}H NMR (500 MHz, DMSO) δ 11.78 (s, 1H, S-NH-N), 9.90 (s, 1H, -O–H), 8.04-8.03 (m, 1H, Ar–H), 8.01 – 7.97 (m, 1H, Ar–H), 7.96 (s, 1H, N=CH-), 7.90 – 7.85 (m, 2H, Ar–H), 7.40 (d, J = 8.7, 2H, Ar–H), 6.76 (d, J = 8.7, 2H, Ar–H); ^{13}C NMR (125 MHz, DMSO) δ 159.6, 148.2, 147.9, 134.6, 132.5, 131.1, 130.4, 128.7, 124.4, 124,4, 115.61

4.6.2 Procedure for Silane Synthesis

Hydrazone compound (0.065 mmol, 1 equiv, 0.75mL) from a stock solution was added in one portion to an 2-5 mL microwave reaction vial fitted with stirbar. Base (0.098 mmol, 1.5 equiv), rhodium catalyst (5 mol%, 0.5mL) from a stock solution, and dimethylphenylsilane(0.328 mmol, 5 equiv) were added sequentially.. The vial was immediately capped, crimped, and placed in a pre-heated well plate set to 25 °C and stirred for 24 hr. The reaction mixture was then filtered through a 1 cm x 0.5 cm column of silica to remove sulphone salt. 20 mL of CH_2Cl_2 was used to elute the material into a 50 mL roundbottom flask. Excess solvent was removed by rotary evaporation and the crude material was dissolved in chloroform-*d*. Mesitylene (0.065 mmol, 1.0 equiv) or dimethyl carbonate (0.065 mmol, 1.0 equiv) were added as an internal standard. Yields were obtained via ^{1}H-NMR. Chemical shifts of known products were as reported in literature.[206,207]

(4-chlorobenzyl)dimethyl(phenyl)silane: colorless oil; ^{1}H NMR (500 MHz, Chloroform-*d*) δ 7.44-7.42 (m, 2H, Ar–H), 7.37-7.33 (m, 3H, Ar–H), 7.13 (d, J = 8.4, 2H, Ar–H), 6.83 (d, J = 8.4, 2H, Ar–H), 2.26 (s, 2H, -CH_2-), 0.25 (s, 6H, -CH_3); ^{13}C NMR (125 MHz, Chloroform-*d*) δ 138.4, 138.1, 133.8, 129.9, 129.7, 129.3, 128.7, 128.3, 127.9, 25.9, -3.42

4-((dimethyl(phenyl)silyl)methyl)phenol: colorless oil; ^{1}H NMR (500 MHz, Chloroform-*d*) δ 7.46-7.44 (m, 2H, Ar–H), 7.36-7.32 (m, 3H, Ar–H), 6.79 (d, J = 8.6, 2H, Ar–H), 6.83 (d, J = 8.6, 2H, Ar–H), 2.22 (s, 2H, -CH_2-), 0.23 (s, 6H, -CH_3); ^{13}C NMR (125 MHz, Chloroform-*d*) δ 152.6, 138.7, 133.9, 131.8, 129.4, 129.2, 128.7, 115.2, 25.0, -3.33

4.6.3 Silyl Product Yield Calculations

Normalized integration of the methyl proton signal of mesitylene (2.28 ppm) or dimethyl carbonate (3.79 ppm) were compared to the integration of the protons assigned to the methylene of the silane products.

Chapter 5

Tuning Rh(II)-Catalyzed Cyclopropanation with Tethered Thioether Ligands

5.1 Disclosure

This chapter is an adaptation of D. Cressy, C. Zavala, A. Abshire, W. Sheffield, and A. Darko. Tuning Rh(II)-catalysed cyclopropanation with tethered thioether ligands. Dalton Trans., 49(44):15779–15787.2020 This publication was firsts authored by Dr. Derek Cressy. He contributed to the development of the synthesis, characterization, x-ray structure elucidation, catalyst screening, UV-Vis, electrochemical analysis, and manuscript preparation. Dr. Cristian Zavala was responsible for catalytic testing and aided in manuscript preparation. I was responsible for all calculations and figures for calculations, ligand scale-up, and helping with development of the supplemental information. William Sheffield aided in characterization and manuscript preparation. Dr. Ampofo Darko advised the work and aided with manuscript preparation.

5.2 Abstract

Dirhodium(II,II), Rh(II), paddlewheel complexes have high utility in diazo-mediated cyclopropanation reactions and ethyl diazoacetate is one of the most commonly used diazo compounds in this reaction. In this study, we report our efforts to use tethered thioether ligands to tune the reactivity of Rh(II)-carbene mediated cyclopropanation of olefins with ethyl diazoacetate. Microwave methods enabled the synthesis of a family of Rh(II) complexes in which tethered thioether moieties were coordinated to axial sites of the complex. Different tether lengths and thioether substituents were screened to optimise cyclopropane yields and minimise side product formation. Furthermore, good yields were obtained when equimolar diazo and olefin were used. Structural and spectroscopic investigation revealed that tethered thioethers changed the electronic structure of the rhodium core, which was instrumental in the performance of the catalysts. Computational modelling of the catalysts provided further support that the tethered thioethers were responsible for increased yields.

5.3 Introduction

Dirhodium(II,II) paddlewheel, Rh(II), complexes have become ubiquitous in carbene chemistry since the Teyssié group first demonstrated that they were capable of decomposing diazo compounds (Fig. 5.1).[18,55,196] The resulting Rh(II)-carbene is capable of a wide range of reactions including C–H and X–H (X = O, N, S, Si, B) insertion reactions, ylide transformations, and cyclopropanation, which have made it a versatile synthetic tool.[14,34,185,196–199] Despite their wide utility, a common problem is the formation of side products due to competitive carbene dimerization (homocoupling).[68,224] Carbenoids derived from ethyl diazoacetate 40 are particularly prone to side products derived from carbene dimerization[225,226] and a well-used strategy to suppress dimer formation is to use an excess, typically 5-10 equivalents, of the substrate. This method can be problematic, however, in cases where precious substrates or late-stage applications are concerned.[227]

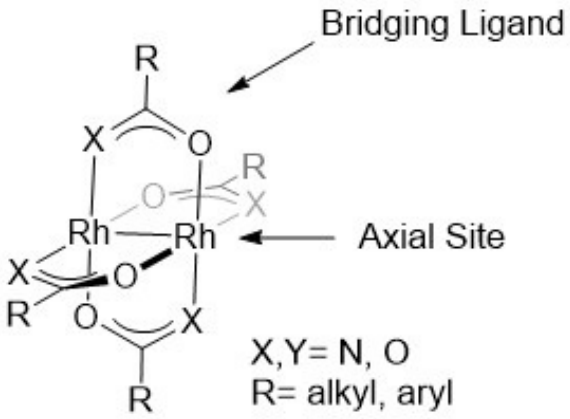

Figure 5.1: General structure of Rh(II) carboxylate (X = O) and carboxamidate (X = N) complexes.

While bridging ligand design is a major focus in the development of Rh(II) complexes,[26,27,36,43,65,81,116,228,229] we hypothesized that axial sites on the complex can be used to modulate Rh-carbene reactivity such that side products due to dimerization could be minimized. Early studies of the axial sites of Rh(II) complexes focused on the role of solvents and other Lewis bases and their effect on the Rh–Rh bond.[165,166,176] It was observed that coordination to the axial site occurs sequentially wherein the first equivalent binds stronger than the second due to the cooperative ability of the two Rh atoms.[230] Applying these fundamental studies to benefit catalytic performance has been somewhat ambiguous but has received attention as an alternative method to exogenous ligands for tuning Rh(II) catalysts.[60] It was clear that solvents such as acetonitrile (MeCN) decreased yields in catalytic applications by binding to the axial site and inhibiting catalysis.[165,213,214] There are situations, though, in which Lewis base additives have improved yields[158,231] and selectivity[61,164,232] in diazo-mediated reactions. In these instances, axial coordination of the additives was believed to be playing a role. The addition of exogenous ligands, however, is complicated by the inherent weakness of axial site coordination of neutral donors. As a result, the coordination exists in solution as an equilibrium, leading to uncertainty as to whether axial coordination is involved in the catalytically active species.[156] One strategy to circumvent the issue is to add a large excess of additive to increase the probability of axial coordination during catalysis.[163] Another method that has been explored is to implement a strong σ donor, such as *N*-heterocyclic carbenes,[168,170] that will irreversibly bind to the axial site. Both of these strategies often lead to decreased catalyst performance or result in only marginal benefits in Rh(II)-carbene reactions.

To better utilize and enhance the effect of axial coordination on Rh(II) complexes, we have developed bridging ligands with tethered thioether moieties that are capable of axial coordination. Incorporation of a tether increases the local concentration of the axial coordinating group and gives significantly more control over the coordination to the axial site. The ligand design was inspired by similar scaffolds reported by Bera[89] and Ball,[155] in which tethered axial coordination resulted in interesting results in α-diazocarbonyl mediated C–H insertion and cyclopropanation. Initial reports of our bespoke Rh(II) complexes

proved that they were proficient in cyclopropanation[86] and Si–H insertion reactions[172] with donor/acceptor carbenes (Fig. 5.2). Most importantly, we demonstrated that dimerization could be minimized by incorporating tethered, axially coordinated thioether groups. In the examples where cyclopropanation was concerned, excess substrate was required for adequate yields. Charette and co-workers were able to obtain good yields with 2 equivalents of alkene using conventional Rh(II) complexes in a biphasic system,[233] but reports of good yields using equimolar alkene to diazo in Rh(II)-mediated intermolecular cyclopropanation reactions remain scarce.[14] To address this gap, we sought to fine-tune catalyst performance by varying tether lengths and thioether substituents on our oxazolidinone-based scaffold. Herein, we report the microwave-assisted synthesis of heteroleptic Rh(II) complexes comprised of oxazolidinone bridging ligands equipped with tethered thioether groups of varying tether lengths and substituents. The complexes were utilized to maximize yields in the cyclopropanation of alkenes with 40. Further analysis of the complexes by UV-Vis, cyclic voltammetry, and computational chemistry was conducted to explain the observed reactivity.

5.4 Results and Discussion

A challenge for the study of our axially coordinated catalysts is the need to synthesize heteroleptic complexes. Traditionally, homoleptic complexes are obtained through sequential substitution of the acetate bridging ligands of dirhodium acetate with the desired ligand.[68] Full ligand substitution is driven by the removal of displaced acetate through trapping methods. When using this strategy to produce heteroleptic complexes, results are hampered by a complex statistical mixture of products.[65,116] Alternatively, one can start with a dirhodium precursor with bridging ligands of varying aptitude for dissociation.[69,87] Corey used this method to synthesize heteroleptic imidazolidinate complexes, however, the number of isomers was further complicated by the orientation of the N and O atoms around each Rh atom.[69,234] We observed that the incorporation of the thioethers on our ligand scaffold significantly reduced the number of products in heteroleptic complex synthesis.[86] Each ligand substitution either slowed or blocked further ligand substitution such that only products from

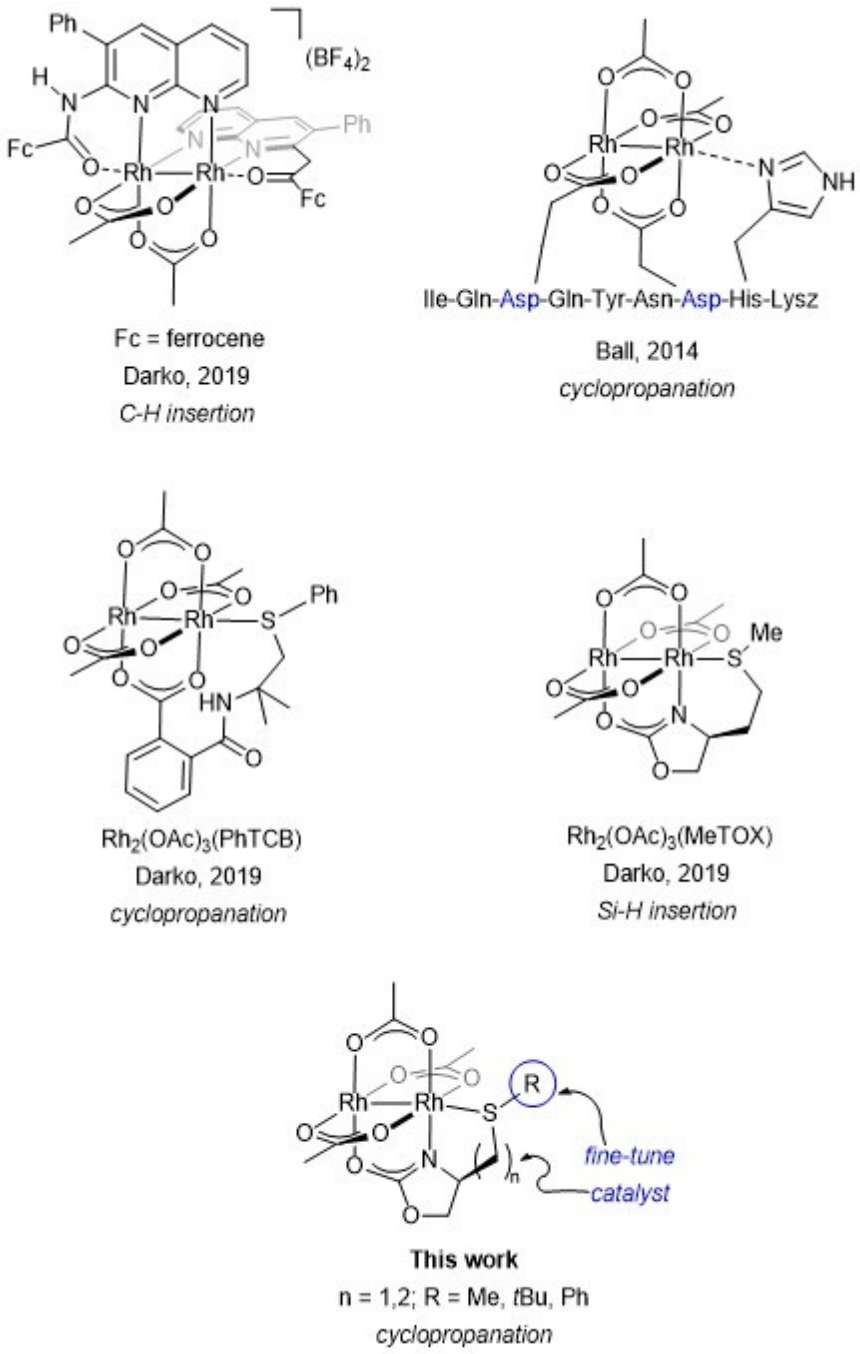

Figure 5.2: Dirhodium complexes with tethered, axial coordination in diazo-mediated applications.

mono- and bis-tethered adducts were produced. Reaction times were a bit sluggish in the case of the oxazolidinate scaffold, so we turned to microwave synthesis to accelerate the process.

5.4.1 Microwave Ligation Optimization

Microwave conditions have previously been implemented for expediting the synthesis of homoleptic dirhodium paddlewheel complexes,[235,236] and we were attracted to the microwave synthesis of each complex, even in small amounts, to facilitate rapid access to a range of catalysts for reaction studies. The synthesis of catalysts 87[86] and 97a/b from ligand 106a and rhodium acetate was used for initial optimization studies. Product formation was initially observed in low yields at 160 °C (Table 5.1, entry 2). Prolonged time at 160 °C did not dramatically improve yields (Table 5.1, entries 3 and 4). Increased temperatures led to an increase in complexes 87 and 97a/b, with preferred formation of 87 (Table 5.1, entry 5). A series of solvents with varied coordinating ability were then screened (Table 5.1, entries 5–9). Ethanol gave a high percent conversion (Table 5.1, entry 7) but provided low yields of 87 and 97a/b along with the presence of a grey solid. It has been reported that ethanol facilitates the reduction of Rh(II) to Rh metal, which would explain the grey solid residue in the reaction vessel.[237] As observed with other ligand exchange conditions, the weakly coordinating solvents 1,2-dichloroethane (DCE) and chlorobenzene (PhCl) produced the highest yields (Table 5.1, entries 5 and 9). Although they gave similar yields, DCE was used in further reactions due to its convenience in reaction workup. A further increase in temperature to 190 °C afforded the optimal conversion and product yield while producing the desired mono-complex 87 preferentially to the bis-complexes 97a and 97b (Table 5.1, entry 10). Continuing to increase the temperature did not significantly improve yields (Table 5.1, entry 11).

Table 5.1: Optimization of microwave synthesis parameters for Rh(II) complex synthesis

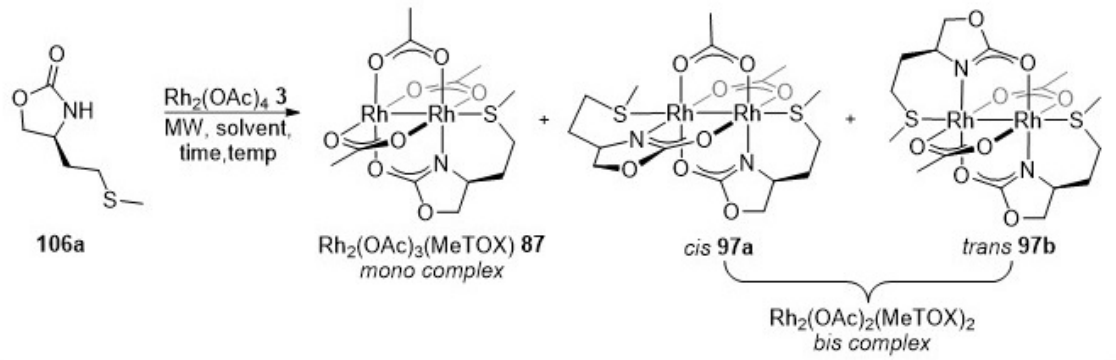

Entry	Solvent	Time [min]	Temp. [°C]	Yield **87** [%][a]	Yield **97a/b** [%] [a]	Conv. [%][a]
1	DCE	10	140	1	0	3
2	DCE	10	160	6	1	7
3	DCE	10	160	13	3	18
4	DCE	30	160	17	5	23
5	DCE	10	180	22	7	46
6	THF	10	180	4	2	9
7	EtOH	10	180	14	7	79
8	MeCN	10	180	18	5	29
9	PhCl	10	180	21	5	27
10	DCE	10	190	33	16	52
11	DCE	10	200	33	17	53

[a] Yield and conversion determined by HPLC.

5.4.2 Microwave Ligation Scope

Other oxazolidinone ligands were synthesized from serine and aspartic acid, providing tether lengths of one and two methylene units, respectively (106b–d, Fig. 5.3). Ligand exchange reactions using the optimized microwave conditions furnished complexes 2–9 (Fig. 5.3). The mono-substituted complexes formed preferentially in all cases, but the ratio of mono-to-bis increased according to donating strength of the thioether substituent. More specifically, the stronger donating *t*-butyl group in ligand 106b furnished a 3 : 1 ratio of complexes 106 to 106a/b compared with 1.3 : 1 for 107 to 107a/b, in which the sulfur substituent was phenyl. Higher overall yields were obtained when the tether length was one methylene unit compared to two methylene units, as evidenced by comparing yields of complexes from ligand 106a to those from ligand 108d. It is worthy to note that while ligands with pendant thioethers proceeded readily with one equivalent of the ligand under microwave conditions, synthesis of mixed ligand oxazolidinate/carboxylate complexes without axial coordination required excess ligand to drive the reaction forward,[69,172] suggesting that the tethered thioether facilitates ligand exchange.

5.4.3 Crystallography of Complexes

We have previously reported the X-ray structure for complex 87,[86] and we were able to obtain suitable crystals for X-ray analysis for complex 107 via slow evaporation of a 1 : 1 mixture of acetonitrile and toluene (Fig. 5.4). Despite our efforts, we were unable to obtain X-ray quality crystals of the other new complexes. Unlike complex 82, $Rh_2(OAc)_3$(PhTOX) 107 does not form an oligomeric chain in the solid state. Instead, the asymmetric unit is comprised of four distinct paddlewheel units in which the second axial site is occupied by acetonitrile. A stereogenic centre is created at the sulphur atom upon coordination to the Rh centre.[238–241] As a result, a mixture of diastereomers are present, (SC, RS) and (SC, SS), due to the sulphur stereogenic centre and the S configuration at the asymmetric carbon on the bridging oxazolidinate (Fig. 5.4). Of the four paddlewheel units, two are (SC, RS) and two structures are (SC, SS), with minor structural variations between them. Representatives

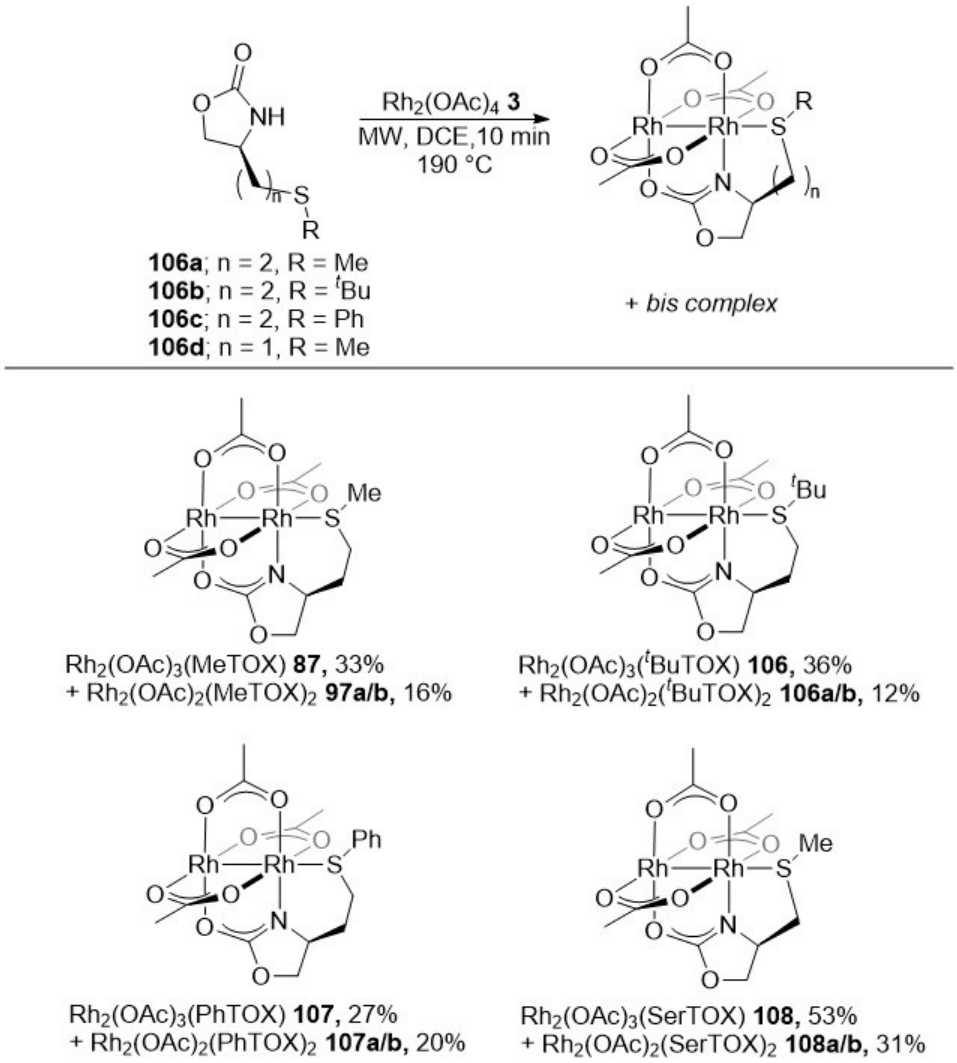

Figure 5.3: Complexes synthesized *via* microwave method.

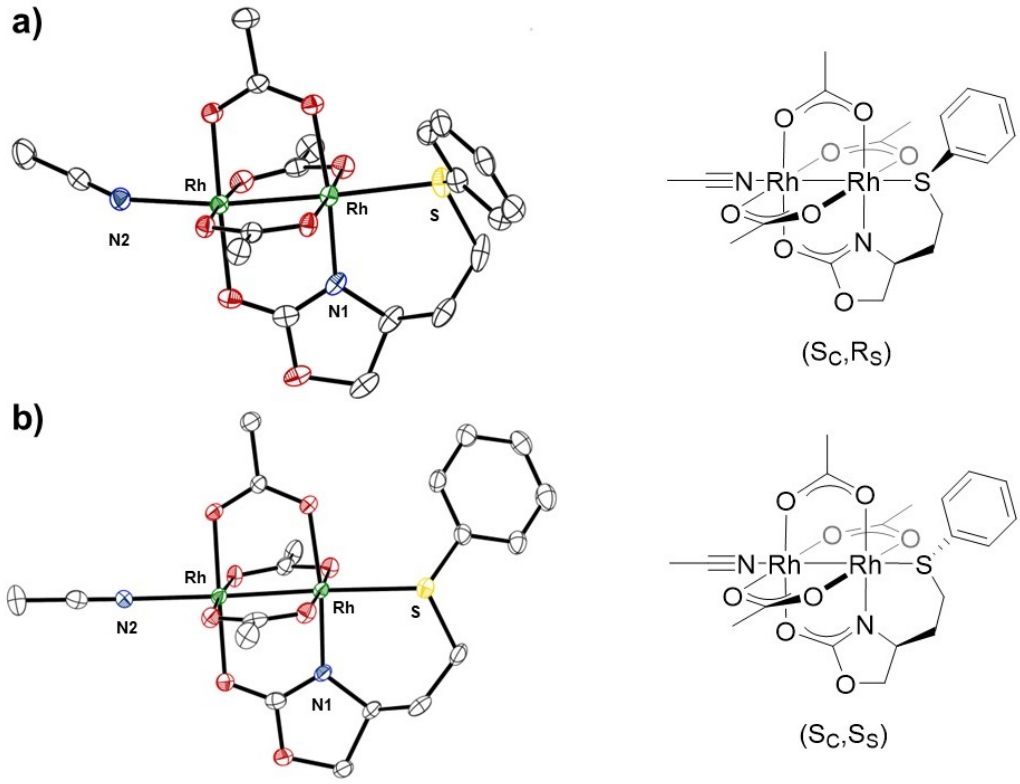

Figure 5.4: X-Ray structure of complex 107 with thermal ellipsoids at 50% probability. Only two of the four molecules in the asymmetric unit is shown. Selected bond lengths and angles as an average of the four structures of the asymmetric unit: Rh–Rh 2.42 Å, Rh–S 2.50 Å, Rh–N_2 2.24 Å, Rh–Rh–S 175.5°.

of each pair are shown in Fig. 5.4. The Rh–Rh bond distances for each paddlewheel unit does not vary (average of 2.4217(5) Å) and is within the general range for Rh–Rh bonds in paddlewheel complexes, which are typically between 2.35–2.45 Å.[51] The Rh–S bond distances of complex 107 range between 2.4730(12)–2.5195(12) Å. The observation that the Rh–S bonds are not constant suggests that the phenyl thioether axial ligand is in a fluxional state and is a weaker donor than the methyl sulphide in 87, in which the intramolecular Rh–S bond is 2.48 Å.[86] The Rh–N_2 bond distance varies little and averages 2.236(4)Åbetween the paddlewheel structures, but pairs of the structures have differences in Rh–Rh–N angles. The (SC, RS) pair has slightly bent Rh–Rh–N angles of 171°, while the (SC, SS) pair has almost linear Rh–Rh–N angles of 175°. The variations are most likely a consequence of packing effects, but they give insight into the structural flexibility of the complex.

5.4.4 UV-vis of Complexes

In general, axially coordinated molecules bind to the σ^* orbital of the Rh–Rh centre, which perturbs the π^* to σ^* HOMO–LUMO gap. This is manifested by shifts in the visible region of their UV-vis spectrum.[56] Fig. 5.5 shows the overlaid UV-vis spectra of the mono-complexes 87, 106, 107, and 108. The colours of the mono-complexes are shades of violet and the local maxima of their bands in the visible region are clustered between 572 nm to 582 nm. The similarity between them suggests that varying the tether length (between 1 or 2 methylene units) or varying the thioether substituent (Me, ^{t}Bu, or Ph) does not significantly alter the HOMO–LUMO energy gap of the complex (Fig. 5.5).

5.4.5 Cyclopropanation Optimization

We initially explored the reactivity of the various rhodium catalysts in the cyclopropanation of styrene with 40 using optimal conditions from our previous studies.[86] We anticipated that performing the reactions with excess styrene would likely result in high yields of the cyclopropane product for most of the catalysts. Therefore, to better distinguish the performance of the catalysts, reactions were conducted with equimolar amounts of styrene

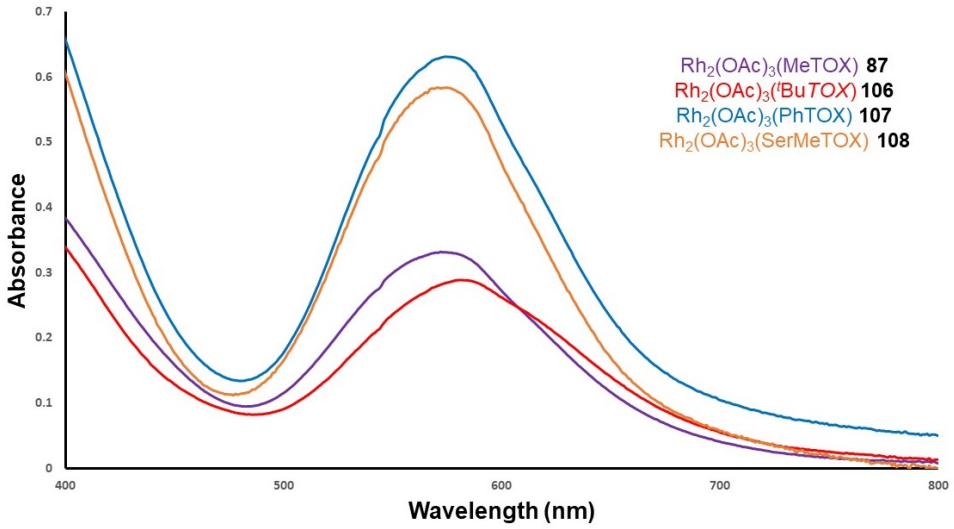

Figure 5.5: UV-vis spectrum of complexes 87, 106, 107, and 108.

to 40 (Table 5.2). In this way, selectivity between carbene dimerization and cyclopropanation could be evaluated. In contrast to previous work in our group demonstrating low reactivity for catalyst 2 with donor/acceptor diazo compounds in the cyclopropanation of styrene,[86] it was a very competent catalyst when 40 was used, providing 63% yield of cyclopropane 41/42 and trace yields of dimer products (Table 5.2, entry 1). The length of the tether only had a minor influence on the yield of 41/42, but the change resulted in increased dimer formation (Table 5.2, compare entries 1 and 2). The thioether substituent had a more pronounced effect on cyclopropane yield. Complex 107, with a phenyl substituent on the thioether, provided the highest cyclopropane yield of the series (71%, Table 5.2, entry 3), while the complexes with alkyl substituents on the thioether (complexes 87, 106, and 108) gave essentially comparable yields (Table 5.2, entries 1–4). Except for complex 108, the mono-substituted tethered complexes had only trace amounts of dimer products. All of the tethered complexes outperformed 97a/b in cyclopropane yield (Table 5.2, entry 5). $Rh_2(OAc)_3$(2-OX) 89 was also tested to eliminate the possibility that the bridging oxazolidinate ligand was responsible for the yield increases. However, 89 also obtained cyclopropane 109 in a lower yield compared to the tethered complexes, further implicating the tethered thioether as the reason for increased yields (Table 5.2, entry 6). As observed in our previous work, the mixed bis-substituted complexes 97a/b exhibited greatly diminished catalytic activity (Table 5.2, entry 7).[86,172] In this reaction, some carbene dimerization was observed along with a high percentage of unreacted 40. The dual tether of the bis-complex likely blocks both axial sites, requiring displacement before catalysis is possible and thereby reducing reaction yield. dimerization yields were more of an issue for non-tethered complexes when catalyst loading was reduced, but the side product was kept minimal when complex 107 was used, although a drop in cyclopropanation yield was observed (Table 5.2 entries 8–11). At 0.1 mol% of catalyst, complex 107 provided a 53% yield of 41/42 with 3% of the dimer products, while 89 gave a 30% yield of 41/42 and 17% yield of dimer products (Table 5.2 entry 10 and 11). This result is evidence that the thioether tether may assist with catalyst turnover, an issue that is present when 40 is used as the diazo precursor.[242]

Table 5.2: Catalyst screening for the cyclopropanation of styrene with 40.

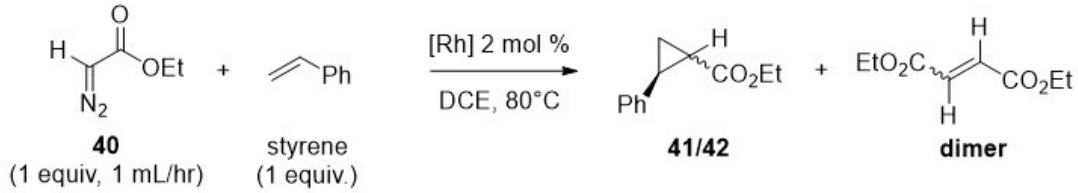

40 (1 equiv, 1 mL/hr) + styrene (1 equiv.) → **41/42** + **dimer**

Entry	[Rh]	Yield **41/42** [%] [a]	Yield **dimer** [%] [a]
1	**87**	63	<1
2	**108**	59	8
3	**107**	71	<1
4	**106**	57	<1
5	**3**	33	3
6	**89**	38	3
7	**97a/b**	19	8
8[b]	**107**	62	1
9[b]	**89**	36	11
10[c]	**107**	53	3
11[c]	**89**	30	17

[a] Yields determined by GC and averaged over 2 runs. [b] 1 mol% catalyst. [c] 0.1 mol% catalyst.

5.4.6 Cyclopropanation Scope

A substrate scope was conducted for the cyclopropanation reaction using 2 mol% of complex 107 (Fig. 5.6). Styrene derivatives 109-114 generally maintained good yields at 1 equivalent of olefin and high yields of cyclopropane when 5 equivalents were used. 4-*tert*-butylstyrene provided similar yields of product 111 compared to styrene, while 4-chlorostyrene gave a slightly lower yield of compound 110. This is consistent with inductive withdrawing effects of the Cl resulting in a less nucleophilic olefin. Introduction of steric hindrance *via* disubstituted olefins also resulted in good to excellent yields, albeit slightly lower than monosubstituted olefins (112 and 113, Fig. 5). Nonstyrene derivatives 114 and 115 performed well in the reaction when 5 equivalents of olefin were used. Using 5 equivalents of the electron-rich ethyl vinyl ether afforded quantitative amounts of cyclopropane 114, but only 31% yield at 1 equivalent. We hypothesized that volatility of the vinyl ether was partly to blame for the low yield. Performing the experiment at room temperature slightly increased the yield to a 43% yield of 114. The synthetically challenging norbornene afforded moderate yields of its respective cyclopropane (compound 115) at 5 equivalents, but low yield at 1 equivalent. In all cases, the diastereomeric ratio of the cyclopropanes did not differ markedly from that observed in the literature.[14] This was anticipated as 40 generally gives low diastereoselectivities in Rh(II)-carbene cyclopropanation reactions (Fig. 5.6).[123,243,244]

5.4.7 Cyclic Voltometry of Complexes

Cyclic voltammetry experiments were performed to probe the effect of the tethered thioether ligands on the electronics at the Rh metal centres. Early studies demonstrated that the variance of the $Rh_2^{4+/5+}$ oxidation potential could be used as a metric for the strength of axial coordination.[213] Our analysis was conducted in 0.1 M [TBA][PF_6] in dichloromethane. Fig. 5.7 is a stack of the cyclic voltammograms of the Rh(II) complexes. Each of the complexes displayed a reversible, or quasi-reversible, oxidation event assigned to the $Rh_2^{4+/5+}$ couple. Oxidation potentials of the mono-complexes followed the trend that increased σ donating ability of the tethered thioether corresponded to a higher oxidation potential (Fig.

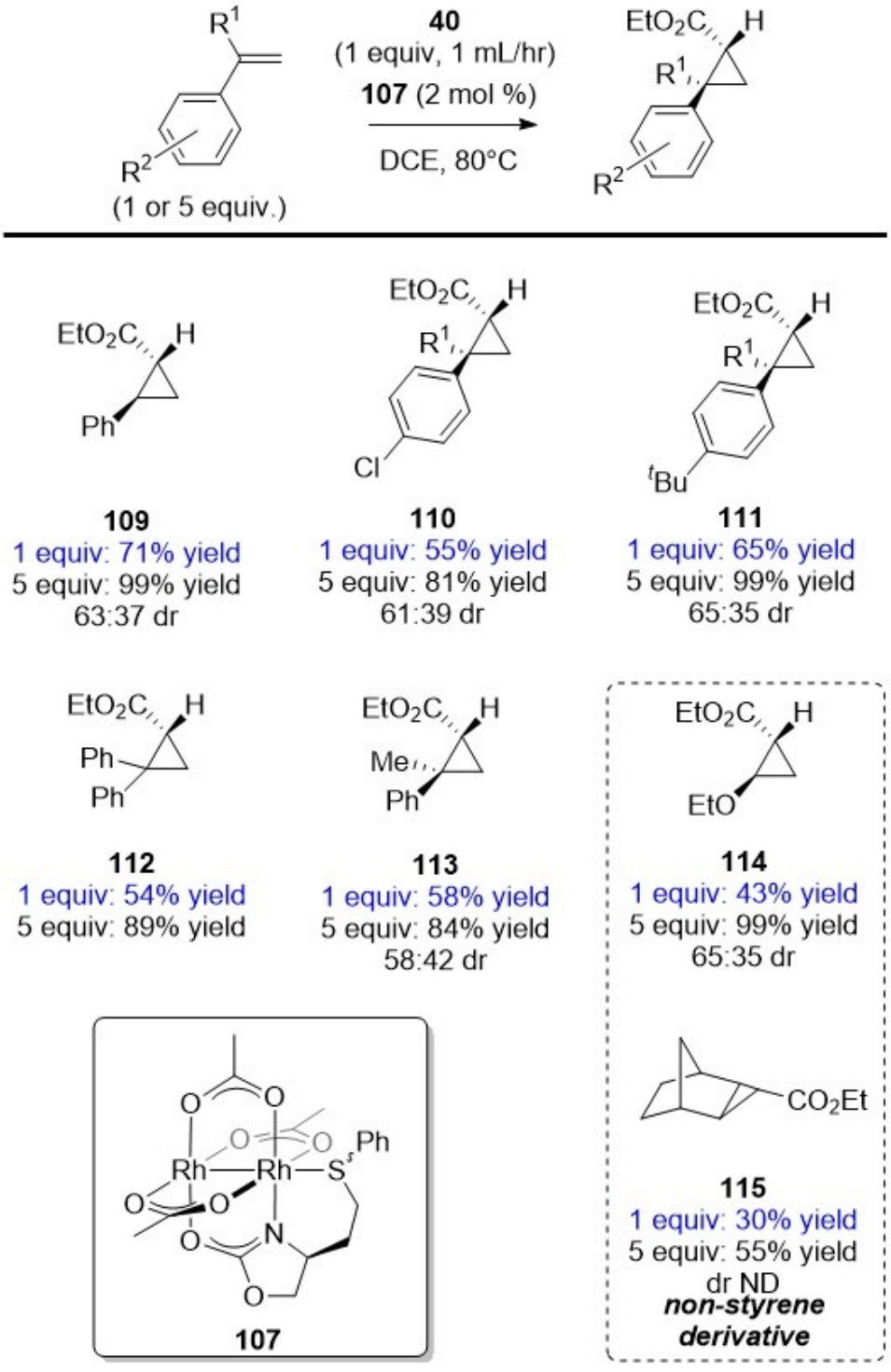

Figure 5.6: 107-catalyzed cyclopropanation with 40. Yields are averaged over 2 runs and calculated by ^{1}H NMR except for compounds 109 and 114. Performed at 25 °C.

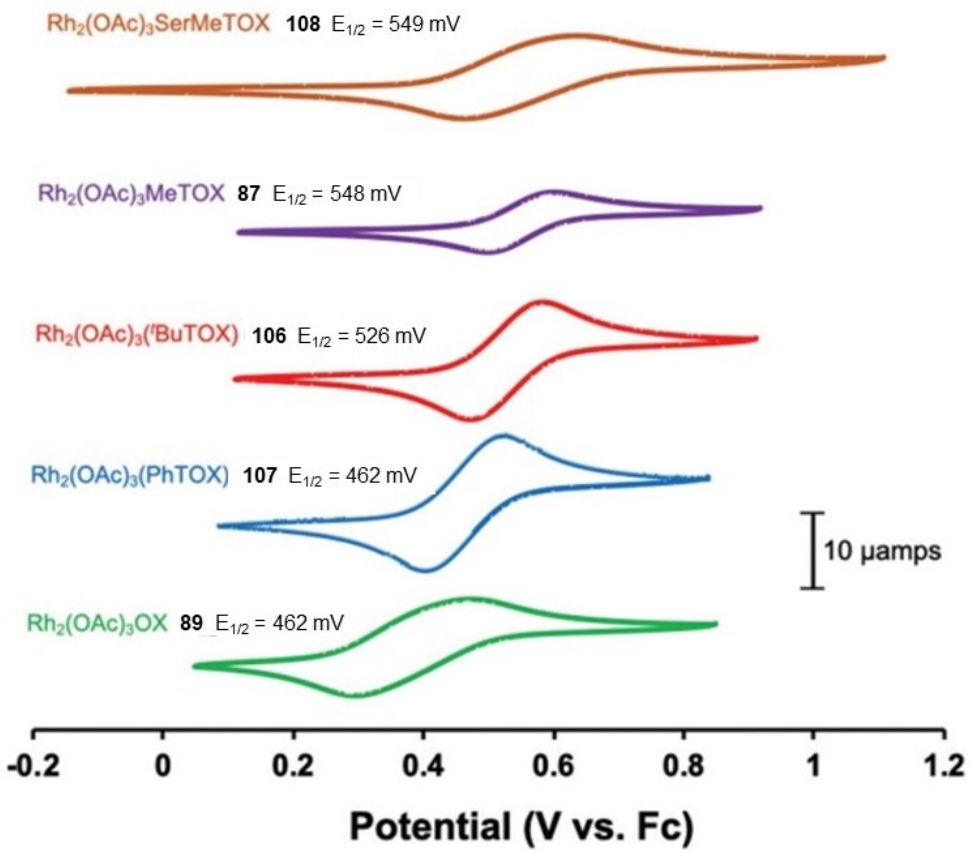

Figure 5.7: Cyclic voltammograms of complexes 87, 89, 106, 107, and 108. Electrolyte comprised of 0.1 M [TBA][PF6] in DCM (scan rate of 100 mV s^{-1}).

5.7). This is contrary to previous studies in which the sequential addition of exogenous axial ligands resulted in a lower oxidation potential.[214] This increased oxidation potential, though unexpected, is not unprecedented. We have shown this trend to be the case with respect to $Rh_2(OAc)_3$PhTCB complexes (PhTCB = phenylthiocarbamoyl benzoate), which also contains a tethered thioether and showed a $Rh_2^{4+/5+}$ $E_{1/2}$ value 36 mV higher than $Rh_2(OAc)_3$OBz (OBz = benzoate).[86] It is worth noting that the same trend was not observed when the CV experiments of complexes 87, 106, 107, and 108 were conducted in MeCN, confirming that the electrochemical study of the complexes is sensitive to coordinating solvents.

5.4.8 Computational Study of Metal Carbenoids

DFT calculations were employed as a means of further understanding the electronic structure of the complexes. Theoretical calculations of the precursor complexes, as well as their carbene complexes with EDA, were calculated at the M06-2X/def2-TZVPP level of theory. According to Berry's three centre/four electron (3c/4e) bonding model, the addition of axial ligands has the most impact in the energy of the Rh–Rh σ^* orbital, which is the LUMO of the complex.[56] The out-of phase combination of the axial ligand's lone pair σ orbitals interact with the Rh–Rh σ^* orbital and raise the energy of the Rh–Rh σ^* LUMO. When comparing complex 107 to $Rh_2(OAc)_3$OX 89, the most dramatic change was in the destabilization of the Rh–Rh σ^* LUMO due to their interaction with the thioether lone pairs (Fig. 5.8). The extent of destabilization is greater with 2[172] than 107, hence, stronger axial interactions lead to greater destabilization, which is in agreement with the 3c/4e model.[56] The effect of the axial ligands also raises the energy of the Rh–Rh π^* HOMO, but this energy destabilization is minor compared to that of the LUMO. The combined effects lead to larger HOMO–LUMO gaps for the complexes with tethered thioethers when compared to 89.

Upon analysis of the LUMO of the carbene species, we found interesting differences in the electronic structure of the tethered complexes (Fig. 5.9). The LUMO of Rh-carbene 116 comprises of an interaction of the p orbital of the carbene with a filled Rh–Rh π^* orbital, which is normally the case with axially free rhodium complexes.[245] The extent of π

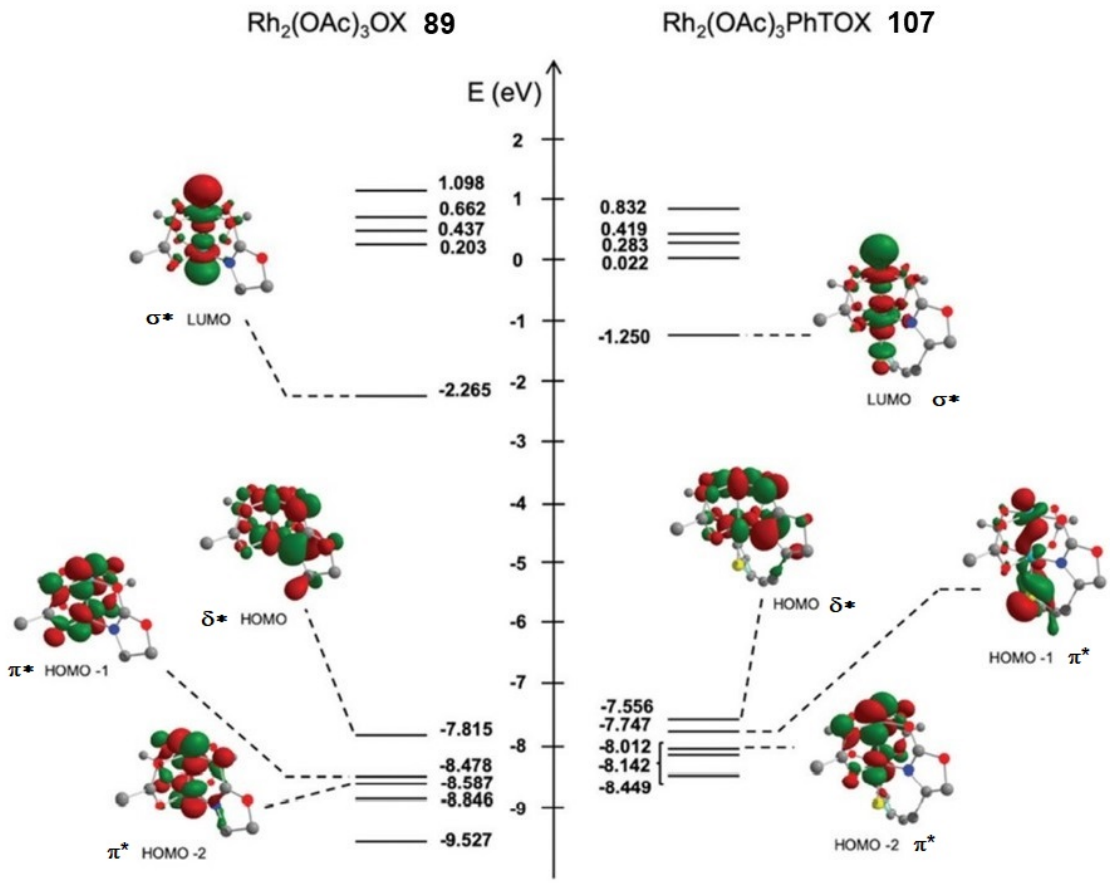

Figure 5.8: Molecular orbitals of complex 107 in comparison to 89 calculated at the M06-2X/def2-TZVPP level of theory.

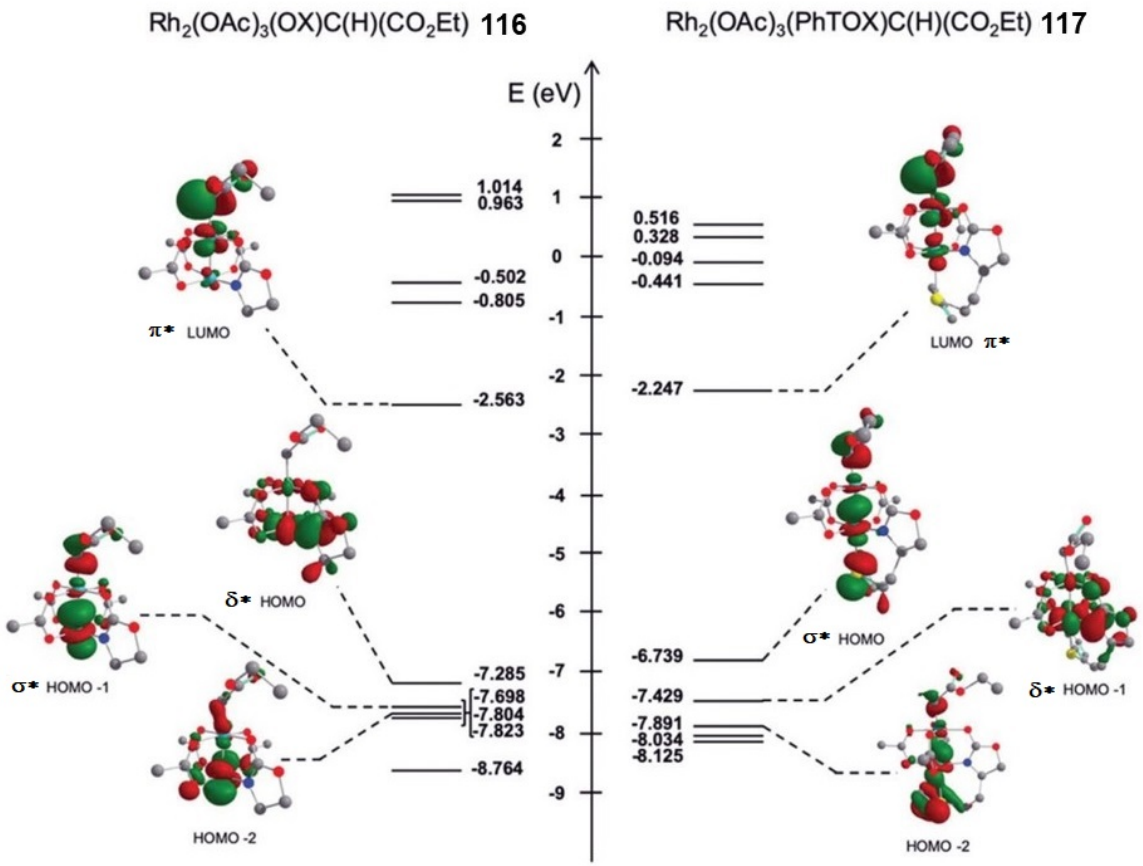

Figure 5.9: Calculated orbitals and energies of 40 carbenoid species 116 and 117. Calculated at the M06-2X/def2-TZVPP level of theory.

backbonding decreases the electrophilicity of the carbene, but this interaction is polarized towards the Rh, leading to "super electrophilic" carbenes.[56,246] In the case of the tethered thioether carbene complex 117, the LUMO seems to include a mixed electronic environment at the Rh core—π symmetry at the Rh–C and σ symmetry at the Rh–S. Such mixing of σ and π components in metal–metal bonding has been reported for triruthenium extended metal-atom chains (EMACs) in which bending of the linear structure introduces mixing of σ and π orbitals in the Ru_3 core.[247] In our case, the calculated S–Rh–Rh (176°) and Rh–Rh–C (168°) angles in 18 deviate from linearity compared to 17 (Rh–Rh–C ∼177°) and this reduction in symmetry may be the driving force for the interaction of the σ and π orbitals. A result of this distortion is an increase in the energy of the LUMO orbital of 117 compared to 116. Although this is not a dramatic increase in energy (0.316 eV or 7.29 kcal mol^{-1}), it opens the possibility of further perturbing the Rh(II)-carbene LUMO energy with distal axial coordination.

The more significant energy destabilization occurs in the HOMO of the carbene complexes with tethered thioether ligands. The HOMO of the carbene from tethered complex 117 is comprised of a Rh–Rh σ-bonding orbital with significant carbene character. Out-of-phase σ interactions characterize both the interaction of the tethered thioether and carbene with the Rh centre. In contrast, in the untethered complex 116, the HOMO is a Rh–Rh π^* orbital with no carbene character. It is plausible that the difference in the HOMOs is an important factor in the enhanced reactivity of the complexes with tethered thioether ligands. A similar change in the electronic character of the HOMO was observed when carboxylate paddlewheel complexes with Rh–Rh and Rh–Bi metal centres were compared. Fürstner and co-workers observed extreme electrophilicity of Rh–Bi acceptor carbene complexes and implicated 3c/4e interactions in the σ framework as the major contributor.[246] Davies and co-workers also observed similar qualitative orbital topologies with Rh–Bi donor/acceptor carbene complexes and proposed that the HOMO of the Rh–Bi complex should result in a more nucleophilic carbenoid.[248] It is generally accepted that cyclopropanation occurs via a concerted, but asynchronous process that is initiated by nucleophilic attack on the carbene carbon by the olefin.[249] We speculate that since the HOMO of the tethered complexes partially lies on the

carbene carbon, it could more readily facilitate the formation of the cyclopropane ring over other competing pathways.

Further support for σ interactions in the HOMO as a major factor is provided by the calculated bond distances for the carbene species, in which the tethered complex 117 possesses an elongated Rh–C bond in comparison to the untethered carbene complex 116 (Table 5.3). Natural population analysis of the carbene complexes shows increased electron density at the carbene carbon of 117 compared to 116 (0.095 vs. 0.174 respectively, Table 5.3), meaning that the tethered thioether can modulate the electron density at the distal carbene. It was initially thought that this modulation of electron density could account for the reactivity and be a factor in reducing the barrier for the rate-limiting diazo extrusion step,[57,249] thereby increasing catalyst turnover. This led us to study the reaction coordinate diagram of the diazo decomposition step of this reaction. We also calculated the natural population and the Wiberg index of the Rh–Rh–C and S–Rh–Rh–C bonding framework of the intermediates to inform us on changes in electron density and bond strengths along the reaction coordinate diagram.

The first event of diazo decomposition is the coordination of the diazo compound to the Rh(II) complex. The coordination of 40 is exothermic by -5.8 kcal/mol for complex 3, and -4.6 kcal/mol for complex 89 (Fig. 5.10). For complex 87, however, a 1.4 kcal/mol increase in the barrier was found. The thioether coordination in 87 was also found to increase the barrier of N_2 extrusion to 23.9 kcal/mol compared to 19.2 kcal/mol for complex 3 and 18.4 kcal/mol for 89. This result is interesting because it indicates that the reason for the increased reactivity of the complexes with tethered, axially coordinating thioethers is either the cyclopropanation step is energetically favored or homocoupling coupling is energetically disfavored. Also of note, the barrier of N_2 extrusion for 87 is lower than for complex 3. This, coupled with the low amount of dimer detected in the catalyst screening, increases the evidence that the more nucleophilic carbene could be responsible for the increased reactivity. The Natural Population Analysis indicated the electron density was equally distributed over both rhodium atoms on 3. The introduction of the oxazoldinone ligand slightly biased the electron distribution toward the rhodium with the nitrogen bonded to it (Rh_a, Table 5.4).

Table 5.3: Bond lengths and Natural Population Analysis of carbenoids 116 and 117.

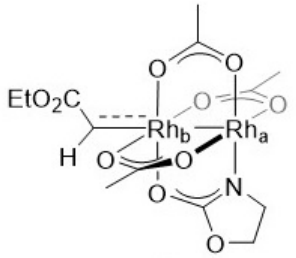

116

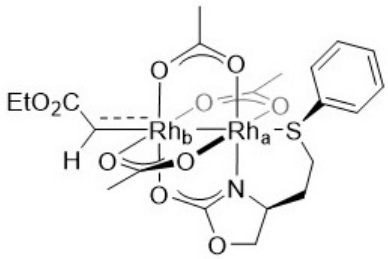

117

Natural Population Analysis			Bond Distances (Å)		
	116	**117**		**116**	**117**
Rh_a	0.523	0.407	Rh_a-Rh_b	2.47	2.45
Rh_b	0.625	0.592	Rh_b-$C_{carbene}$	1.86	1.91
$C_{carbene}$	0.174	0.095	Rh_a-S		2.76
S		0.394			

Table 5.4: Natural Population Analysis and Wiberg index values for the calculated mechanism of N_2 extrusion of 40 with complexes 3, 87, and 89.

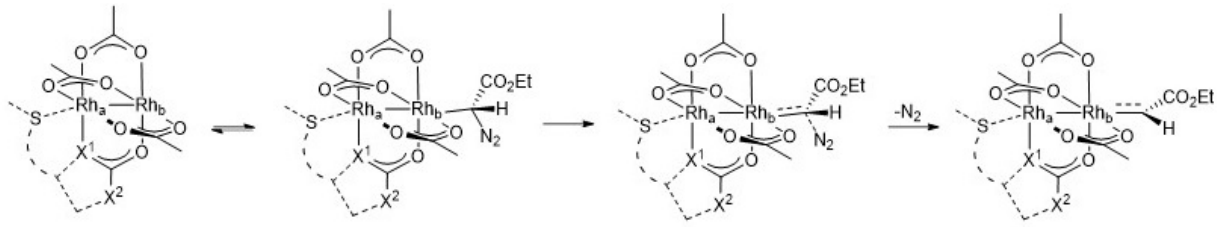

Catalyst | Catalyst·**40** coordinated | Catalyst·**40** transition state | Catalyst·**40** carbenoid

	Natural Population Analysis				Wiberg Index		
Catalyst·**40**	S	Rh_a	Rh_b	C	S-Rh	Rh-Rh	Rh-C
3		0.81616	0.81616			0.9174	
3·40 Coordinated		0.77578	0.65317	-0.40848		0.8003	0.2936
3·40 TS		0.64854	0.58645	0.06703		0.6165	0.8601
3·40 Carbenoid		0.61506	0.59687	0.17329		0.5672	1.1599
89		0.77653	0.87409			0.9075	
89·40 Coordinated		0.69324	0.66974	-0.3982		0.7859	0.2891
89·40 TS		0.56497	0.60147	0.04858		0.6043	0.8197
89·40 Carbenoid		0.52593	0.61679	0.17719		0.546	1.1588
87	0.49873	0.45877	0.76402		0.5105	0.7586	
87·40 Coordinated	0.43320	0.46709	0.64787	-0.40342	0.4134	0.7750	0.0055
87·40 TS	0.36118	0.42017	0.57183	0.02099	0.2910	0.6675	0.7124
87·40 Carbenoid	0.35950	0.41037	0.57993	0.08773	0.2893	0.6029	1.0289

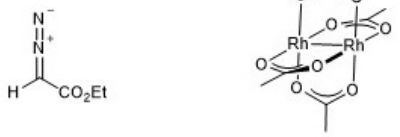

EDA **40** | $Rh_2(OAc)_4$ **3** | $Rh_2(OAc)_3$(2-OX) **89** | $Rh_2(OAc)_3$(2-OX) **89**

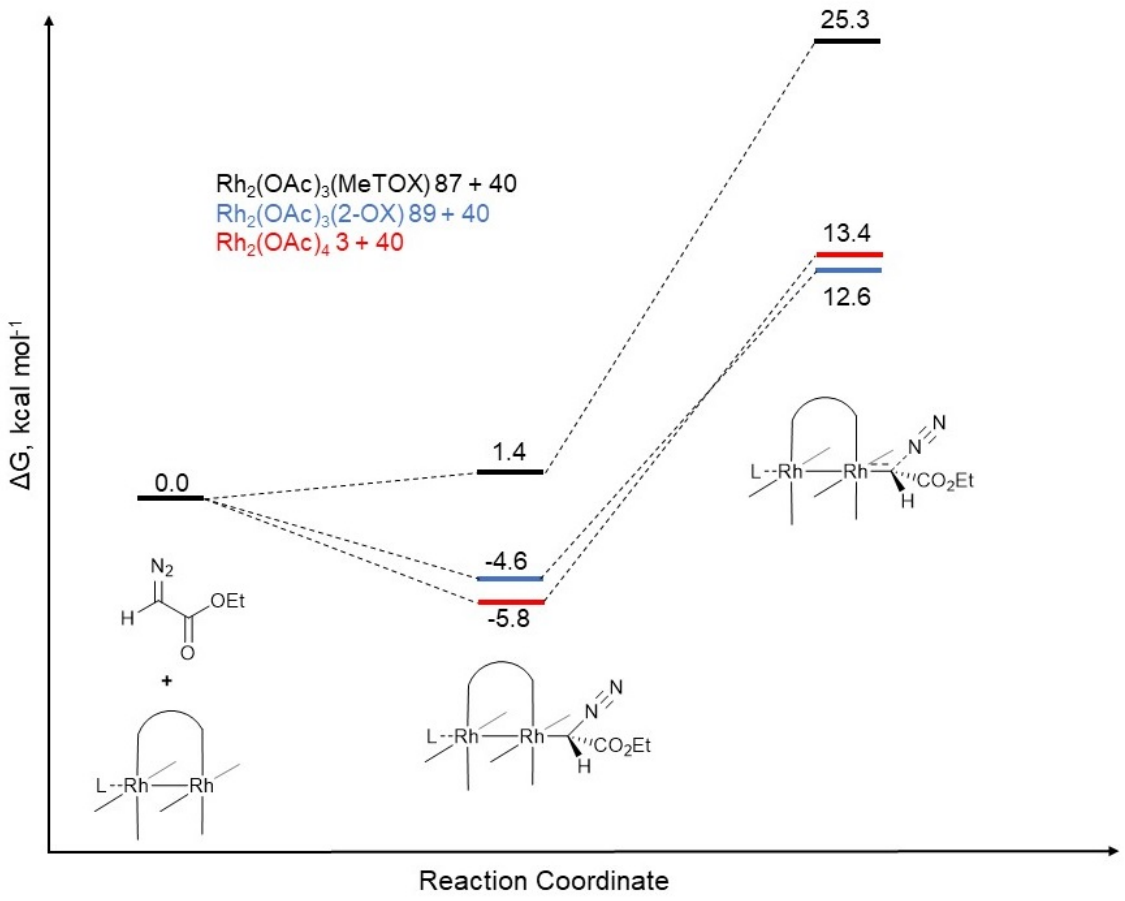

Figure 5.10: Comparison of the coordination and transition state energy differences during the extrusion of N_2 of 40 with complexes 3, 87, and 89 calculated at the M06-2x/def2-TZVP level of theory.

The donation of the thioether further exaggerates this bias on complex 87. Upon coordination of 40 to 3, the added electron density is increased on Rh_b while Rh_a acts like an electron sink to help delocalize the donated electron density from 40. This effect is also present when 40 coordinates to 89. Interestingly, when 40 coordinates to 87, the electron density on Rh_a decreases but the electron density the sulfur atom increases indicating the sulpher atom is helping modulate the electron density on Rh_a At the transition state of N_2 extrusion, the electron density distribution is inverted between Rh_a and Rh_b on complex 89 making Rh_b the more electron deficient of the two. The electron distribution trend on complexes 3 and 87 remained the same throughout. When inspecting the carbenoid complexes, the electron density is much greater on the carbene carbon when the carbenoid is formed with complex 87 than it is when it formed either complex 3 or 89. The Wiberg bond index is consistent with the results of the Natural Population Analysis. The absence of the thioether on complexes 2 and 89 allows for a weaker Rh–Rh bond. This is apparent by the increased difference in Wiberg bond index in complexes 3 and 89 (0.35 for 3 and 0.36 for 89, Table 5.4) which possess thioether coordination, compared to complex 87 (0.16, Table 5.4). The carbenoid formed with 87 thus maintains a stronger Rh–Rh bond, resulting in a weaker Rh–C bond in its carbenoid compared to carbenoids formed with complexes 3 and 89, 1.03 versus 1.16 respectively.

The Natural Population Analysis indicated the electron density was equally distributed over both rhodium atoms on 3. The introduction of the oxazoldinone ligand slightly biased the electron distribution toward the rhodium with the nitrogen bonded to it, Rh_a. The donation of the thioether further exaggerates this bias on complex 87. Upon coordination of 40 to 3, the added electron density is increased on Rh_b while Rh_a acts like an electron sink to help delocalize the donated electron density from 40. This effect is also present when 40 coordinates to 89. Interestingly, when 40 coordinates to 87 the electron density on Rh_a decreases but the electron density the sulfur atom increases. At the transition state of N_2 extrusion, the electron density distribution inverted between Rh_a and Rh_b on complex 89 making Rh_b the more electron deficient of the two. The electron distribution trend on complexes 3 and 87 remained the same. When inspecting the carbenoid complexes, the

electron density is much greater on the carbene carbon when the carbenoid is formed with complex 87 than it is when it formed either complex 3 or 89. The Wiberg bond index is consistent with the results of the Natural Population Analysis. The absence of the thioether on complexes 2 and 89 allows for a greater weakening of the Rh–Rh bond. This is apparent by the increased difference in Wiberg bond index between the complexes with thioether coordination, 3 and 89, and complex 87, a difference of 0.35 and 0.36 versus 0.16 respectively. As a result of the carbenoid formed with 87 maintaining a stronger Rh–Rh bond, the Rh–C bond is weaker than it is in the carbenoids formed with complexes 3 and 89, 1. 03 versus 1.16 respectively.

5.5 Conclusions

In conclusion, heteroleptic dirhodium(II) paddlewheel complexes containing axially coordinated thioether ligands were synthesized using a microwave-assisted approach. We have demonstrated that catalyst synthesis and reactivity is influenced by the tether length and the substituent of the thioether. The tethered complexes achieved higher yields than their non-tethered counterparts in the cyclopropanation of styrene with ethyl diazoacetate, even demonstrating good yields with equimolar amounts of styrene substrate. Electronic studies and computational methods provided insight into the effect of the donating strength of the tethered ligands on the observed reactivity. The calculations were of particular relevance, revealing the importance of the effect of the tethered thioether on the HOMO of the Rh(II)-carbene complexes. The calculated reaction coordinate diagrams of the N_2 extrusion revealed the coordination of the thioether increases the energy needed for coordination. Natural Population Analysis calculations suggest axial coordination of the thioether makes the distal rhodium resistant to the increased electron density which also results in more electron density localized on the carbon of the carbene. Efforts to further understand the interplay between the donating ability of the tether and reactivity in Rh(II)-carbene mediated reactions are currently being explored by a collaborator.

5.6 Experimental

5.6.1 General Considerations

Unless otherwise noted, all reagents were purchased and used as received from the manufacturer without further purification. Ligand 1a and 1d were synthesized via established literature procedures.[250,251] Methyl phenyl diazoacetate was prepared from benzylic acid according to established procedures.[252] Hexanes, tetrahydrofuran (THF), diethyl ether, CH_2Cl_2, and acetonitrile (ACN) were dried with columns packed with alumina using an Inert PureSolv Micro Solvent Purification System and stored over molecular sieves. Reactions were monitored using thin layer chromatography (TLC) on Sorbent Technologies Silica XG TLC Plates. Column chromatography was performed using 60 Å, 40-63 μm silica from Sorbent Technologies. ^{1}H and ^{13}C NMR spectra were recorded on a Varian Mercury Vx 300 MHz, Varian VNMRS 500 MHz, or Varian VNMRS 600 MHz spectrometers. All NMR chemical shifts are reported in ppm on the δ scale. Signals were referenced by residual solvent signal for ^{1}H NMR ($CDCl_3$ = 7.26 ppm, acetone = 2.05 ppm, acetonitrile = 1.94 ppm) and ^{13}C NMR ($CDCl_3$ = 77.16 ppm, d6-acetone = 206.26 ppm, d3-acetonitrile = 1.32 ppm). HPLC analysis was performed on a Shimadzu LC-2030 Prominence-I instrument using a C_{18} column. The mass spectra for all compounds, unless otherwise specified, were obtained using an AccuTOF Mass spectrometer equipped with a DART ionization apparatus. UV-Visible data was obtained in a 10 mm quartz cell using a Cary 5000 spectrophotometer.

5.6.2 Ligand Synthesis

(*S*)-4-(2-(*tert*-butylthio)ethyl)oxazolidine-2-one (106b): To a flame dried 5 mL flask equipped with a stir bar was (*S*)-2-(2-oxooxazolidin-4-yl)ethyl 4-methylbenzenesulfonate[86] (0.43 g, 1.5 mmol) followed by 2-methyl-2-propanethiol (1.5 mL, 13 mmol). The reagents were then dissolved in 6 mL acetone and refluxed at 45 °C for 24 hours. The reaction was allowed to cool to room temperature, then concentrated *in vacuo*. The resulting mixture was dissolved in 10 mL DI water and extracted twice with 5 mL dichloromethane. The combined

organic layers were then washed with 5 mL brine solution, followed by 5 mL saturated sodium bicarbonate solution. The organics were separated and dried over anhydrous Na_2SO_4, filtered, and concentrated. The crude mixture was then purified by column chromatography (25% EtOAc/Hexanes to 50% EtOAc/Hexanes) to afford 106b as a pale-yellow oil (0.1181 g, 0.58 mmol, 39% yield). ^{1}H NMR (500 MHz, Chloroform-*d*) δ 5.81 (s, 1H), 4.56 – 4.47 (m, 1H), 4.07 – 3.96 (m, 2H), 2.63 – 2.54 (m, 2H), 1.93 – 1.81 (m, 2H), 1.32 (s, 9H). ^{13}C NMR (126 MHz, Chloroform-*d*) δ 159.46, 70.24, 52.29, 42.69, 35.05, 30.97, 24.62. Calculated m/z: $[M+H]^+$ = 204.1014, found m/z: $[M+H]^+$ = 204.1069

(*S*)-4-(2-(phenylthiol)oxazolidin-2-one (106c): To a flame dried 5 mL flask equipped with a stir bar was added (S)-2-(2-oxooxazolidin-4-yl)ethyl 4-methylbenzenesulfonate[86] (0.10 g, 0.36 mmol) followed by thiophenol (0.5 mL, 0.54 mmol). The reagents were then dissolved in 1 mL acetone and refluxed for 4 hours. The reaction was allowed to cool to room temperature, then concentrated in vacuo. The resulting mixture was dissolved in 2 mL DI water and extracted twice with 2 mL dichloromethane. The organics were combined and washed with 1 mL brine solution, followed by 1 mL saturated sodium bicarbonate solution. The organics were separated, dried over anhydrous Na_2SO_4, filtered, and concentrated. The crude mixture was then purified by column chromatography (2.5% MeOH/DCM) to afford 106c as a yellow oil (68 mg, 0.29 mmol, 84% yield). ^{1}H NMR (500 MHz, Chloroform-*d*) δ 7.38 – 7.21 (m, 4H), 5.73 – 5.65 (m, 1H), 4.55 – 4.47 (m, 1H), 4.09 – 3.99 (m, 2H), 2.97 (td, J = 7.0, 2.5 Hz, 2H), 1.99 – 1.83 (m, 2H). ^{13}C NMR (126 MHz, Chloroform-*d*) δ 159.18, 134.88, 129.88, 129.20, 126.79, 51.63, 34.33, 30.21. Calculated m/z: $[M+H]^+$ = 224.0701, found m/z: $[M+H]^+$ = 224.0691

5.6.3 General Microwave Conditions

All microwave reactions were conducted in sealed reaction vials with a Biotage Initiator+ equipped with an IR sensor for determination of reaction temperature. Power input was adjusted by the instrument achieve and maintain the desired reaction temperature. Reaction times are presented as hold times, not total reaction time. Synthesis of

$Rh_2(OAc)_3$(MeTOX) (87), $Rh_2(OAc)_2$(MeTOX)$_2$ (97a/b), and $Rh_2(OAc)_3$(2-OX) (89) were confirmed by comparison of NMR spectra from our previous work.[86,172]

5.6.4 General Procedure for Microwave Reactions

General Procedure for Microwave Reactions A 2-5 mL microwave vial equipped with a magnetic stir bar was charged with dirhodium acetate (15 mg, 34 mmol) and the desired ligand (34 mmol). The edges of the flask were rinsed with 4 mL 1,2-dichloroethane (DCE). The vial was then capped and heated at 190 °C for 10 minutes. The mixture was allowed to cool to RT, transferred to a round-bottom flask using DCM, and concentrated *in vacuo*. The crude mixture was then purified by column chromatography using a 1:1 toluene/MeCN mobile phase. Bis substituted products eluted first as a mixture of *cis* and *trans* isomers. The bis fractions were then recrystallised in MeCN to remove excess oxazolidinone starting material. Mono products eluted next with no further purification needed. $Rh_2(OAc)_4$ eluted last. The product distribution for the ligand exchange reaction with ligand 106a was quantified via HPLC using 75% 1:1 MeCN:MeOH with 0.1% TFA/25% water with 0.1%TFA on a C_{18} column. Calibration curves were generated for 2, 97a/b, $Rh_2(OAc)_4$. The yields for complexes 106-108 and related bis complexes were determined by isolated material.

$Rh_2(OAc)_3$(^{t}BuTOX) (106): R_f: 0.46. ^{1}H NMR (500 MHz, Chloroform-*d*) δ 4.45 – 4.39 (m, 1H), 3.76 – 3.65 (m, 1H), 3.11 (ddd, J = 12.7, 5.4, 2.7 Hz, 1H), 2.97 (td, J = 2.4, 3.0 Hz, 1H), 2.11 (dddd, J = 14.7, 5.4, 3.0, 1.3 Hz, 1H), 1.99 (s, 3H), 1.87 (s, 3H), 1.84 (s, 3H), 1.84 – 1.76 (m, 1H), 1.66 (s, 10H). ^{13}C NMR (126 MHz, Chloroform-*d*) δ 190.82, 190.79, 189.00, 167.23, 70.04, 58.95, 49.59, 31.96, 29.15, 29.03, 24.07, 23.90, 23.34. Calculated m/z: $[M+H]^+$ = 585.9489 , found m/z: $[M+H]^+$ 585.9444. Anal. Calcd for $C_{15}H_{25}NO_8Rh_2S$: C, 30.79; H, 4.31; N, 2.39; S, 5.48. Found: C, 32.80; H, 4.79; N, 2.42; S, 5.18.

$Rh_2(OAc)_2$(^{t}BuTOX)$_2$ (106a/b): R_f: 0.93. ^{1}H NMR (500 MHz, Chloroform-*d*) δ 4.31 – 4.25 (m, 1H), 3.74 – 3.54 (m, 2H), 3.19 (m, J = 13.1, 5.7, 2.5 Hz, 1H), 2.97 (m, J = 12.2, 9.1, 2.8 Hz, 1H), 1.99 (m, J = 17.5, 5.6, 2.8, 1.3 Hz, 1H), 1.90 (s, 2H), 1.85 (s, 1H), 1.81 – 1.72 (m, 1H), 1.65 (s, 10H). ^{13}C NMR (126 MHz, Chloroform-*d*) δ 189.25, 69.62, 59.84, 59.74, 48.19, 48.01, 32.70, 32.64, 29.84, 29.78, 29.75, 28.95, 23.94, 23.71. Calculated m/z:

$[M+H]^+$ = 729.0257, found m/z: $[M+H]^+$ = 729.0233. Anal. Calcd for $C_{22}H_{38}N_2O_8Rh_2S_2$: C, 36.27; H, 5.27; N, 3.85; S, 8.81. Found: C, 39.08; H, 5.88; N, 3.62; S, 8.04.

$Rh_2(OAc)_3$(PhTOX) (107)p: R_f: 0.46. ^{1}H NMR (500 MHz, Chloroform-*d*) δ 7.93 – 7.89 (m, 2H), 7.44 – 7.40 (m, 3H), 4.45 – 4.38 (m, 1H), 3.83 – 3.73 (m, 2H), 3.55 (ddd, J = 13.1, 5.8, 2.3 Hz, 1H), 3.37 (ddd, J = 13.1, 11.8, 2.5 Hz, 1H), 2.18 (dddd, J = 14.8, 6.0, 2.6, 1.4 Hz, 1H), 2.02 (dddd, J = 14.6, 12.1, 9.9, 2.4 Hz, 1H), 1.96 (s, 3H), 1.88 (s, 3H), 1.81 (s, 3H). ^{13}C NMR (126 MHz, Chloroform-*d*) δ 191.27, 190.97, 189.55, 167.73, 133.00, 131.05, 129.04, 128.54, 69.89, 59.09, 37.26, 31.16, 23.94, 23.91, 23.35 Calculated m/z: $[M+H]^+$ = 605.9176 , found m/z: $[M+H]^+$ 605.9180. Anal. Calcd for $C_{17}H_{21}NO_8Rh_2S$: C, 33.74; H, 3.50; N,2.32; S, 5.30. Found: C, 37.79; H, 4.40; N, 2.51.

$Rh_2(OAc)_2$(PhTOX)$_2$ (107a/b): R_f: 0.85. ^{1}H NMR (500 MHz, Chloroform-*d*) δ 7.95 – 7.84 (m, 2H), 7.42 – 7.29 (m, 3H), 4.41 – 4.07 (m, 2H), 3.77 – 3.61 (m, 3H), 3.43 – 3.30 (m, 1H), 2.12 – 1.93 (m, 3H), 1.89 (s, 1H), 1.86 (s, 1H). ^{13}C NMR (126 MHz, Chloroform-*d*) δ 189.65, 168.30, 131.41, 131.06, 128.91, 127.86, 69.39, 59.67, 37.09, 31.53, 23.64 Calculated m/z: $[M+H]^+$ = 768.9632, found m/z: $[M+H]^+$ = Anal. Calcd for $C_{26}H_{30}N_2O_8Rh_2S_2$: C, 40.64; H, 3.94; N, 3.65; S, 8.35. Found: C, 41.49; H, 4.24; N, 3.45; S, 7.73.

$Rh_2(OAc)_3$(SerMeTOX) (108)f: R_f 0.63. ^{1}H NMR (500 MHz, Chloroform-*d*) δ 4.69 (t, J = 8.0 Hz, 1H), 4.11 (m, J = 11.4, 10.2, 7.8, 3.5 Hz, 1H), 3.98 (dd, J = 10.4, 8.2 Hz, 1H), 2.86 (dd, J = 12.2, 3.5 Hz, 1H), 2.55 (s, 3H), 2.26 (t, J = 12.0 Hz, 1H), 2.03 (s, 3H), 1.84 (d, J = 5.4 Hz, 6H). ^{13}C NMR (126 MHz, Chloroform-*d*) δ 192.49, 192.22, 191.04, 72.96, 59.70, 41.16, 24.27, 24.18, 23.77, 16.27. Calculated m/z: $[M+H]^+$ = 529.8863, found m/z: $[M+H]^+$ = 529.3375. Anal. Calcd for $C_{11}H_{17}NO_8Rh_2S$: C, 24.97; H, 3.25; N,2.65; S, 6.06. Found: C, 29.71; H, 4.26; N, 2.74.

$Rh_2(OAc)_2$(SerMeTOX)$_2$ (108a/b): R_f: 0.95. ^{1}H NMR (500 MHz, Chloroform-*d*) δ 4.71 – 4.59 (m, 1H), 4.00 – 3.89 (m, 1H), 2.84 (m, J = 12.2, 5.8, 3.4 Hz, 1H), 2.59 (d, J = 9.2 Hz, 1H), 2.52 (d, J = 5.8 Hz, 2H), 2.31 – 2.18 (m, 1H), 1.97 – 1.90 (m, 3H). ^{13}C NMR (126 MHz, Chloroform-*d*) δ 190.32, 167.65, 72.29, 59.69, 23.72, 15.76. Calculated m/z: $[M+H]^+$ = 616.9006 , found m/z: $[M+H]^+$ = 616.8975. Anal. Calcd for $C_{14}H_{22}N_2O_8Rh_2S_2$: C, 27.29; H, 3.61; N, 4.45; S, 10.41. Found: C, 28.92; H, 3.91; N, 4.33; S, 9.95.

5.6.5 General Procedure for the Cyclopropanation of Olefin Substrates with 107

Under an atmosphere of N_2, a 25 mL Schlenk flask equipped with a magnetic stir bar was flame dried and charged with olefin (1.0 or 5.0 equiv. with respect to ethyl diazoacetate), 107 (2 mol%), and DCE (0.5 mL). The solution was then heated to 80 °C, followed by slow addition of ethyl diazoacetate (1.7 mL, 0.17 mmol, 1.0 equiv.) by syringe pump (1 mL/hr). After addition was complete, the reaction solution was filtered through 1.5-inch silica plug and eluted with 4 mL of DCM. The eluent was then concentrated *in vacuo* with a rotary evaporator. 10 μL of mesitylene was then added as an internal standard for ^{1}H NMR determination of cyclopropane product yield and diastereoselectivity.

5.6.6 Computational

The geometry optimizations utilized for the molecular orbital energies were completed on Gaussian 09[195] and implemented the density functional theory M06-2X[19] functional with the def2-TZVPP[20] basis set. Due to resource constraints the transition states were calculated using the def2-TZVP[20] basis set. The Natural Population Analysis and Wiberg Bond Index calculations were performed using NBO3 program in Gaussian 09 also utilizing the M06-2x/def2-TZVP level of theory. An ultrafine integration grid was utilised as well as tight convergence criteria. Frequency calculations were performed to verify the stationary points on the potential energy surface were in fact ground state minima. Negative frequencies were calculated for $Rh_2(OAc)_3(Ox)$ at -20.1475 cm^{-1}, $Rh_2(OAc)_3(PhTOX)$ at -4.6272 cm^{-1}, $Rh_2(OAc)_4C(H)(CO_2Et)$ at -19.8149 cm^{-1}, $Rh_2(OAc)_2(OX)C(H)(CO_2Et)$ at -10.6252 cm^{-1}, and $Rh_2(OAc)_3(MeTOX)C(H)(CO_2Et)$ at -3.5171 cm^{-1} but is still believed to be the ground state structure. Orbital visualisations were completed with ChemCraft. Transition state structures were confirmed by a negative frequency representing the C-N bond breaking, -241.12 cm^{-1} for the decomposition of 40 with 3, -256.89 cm^{-1} with 89, and -239.16 cm^{-1} with 87. Transition state structures need to be refined as the all produced small negative frequencies from a twisting methyl twisting mode. The magnitude of these negative

vibrational frequencies, between 0 and -15.00 cm^{-1}, indicates the structures are close and all trends evaluated will be consistent with the trends calculated with structure completely void of of these small negative frequencies.

Chapter 6

Chiral Rh(II) Complexes with Tethered, Axially Coordinated Ligands (TACLs) Improve Asymmetric Cyclopropanation with Methyl Phenyldiazoacetate

6.1 Disclosure

This chapter was adapted from a manuscript in preparation titled "Chiral Rh(II,II) Complexes with Tethered, Axially Coordinated Ligands (TACLs) Improve Asymmetric Cyclopropanation with Methyl Phenyldiazoacetate." First authorship will be shared by Dr. Cristian Zavala and myself. Dr. Cristian Zavala contributed the frontier synthesis and characterization of chiral complexes, catalytic screening of complexes, preparation of the manuscript, and preparation of the supplemental information. I contributed to the scale-up of the ligands, isolation and characterization of the Rh_2(*S*-PTTL)$_3$(1*S*-Ph-PhTCB) complex,

development of the manuscript, and development of the supplemental information. Dr. Ampofo Darko advised the work.

6.2 Abstract

Rh(II) paddlewheel complexes have been extensively studied in asymmetric carbene transfer reactions. The development of chiral bridging ligands is the most commonly explored way to enhance enantioselectivity. The effects and utilization of axial coordination have been less explored. A tethered axial coordinating ligand can conceivably leverage non-covalent and steric interactions at the axial site. The synthesis of chiral axially coordinating ligands and their exchange onto chiral Rh(II) paddlewheel complexes is described herein. It was determined that axial coordinating ligands with a chiral tether can improve the enantioselectivity of the cyclopropanation of styrene and methyl phenyldiazoacetate.

6.3 Introduction

The cyclopropane moiety exhibits unique properties that make them highly sought after in the pharmaceutical and natural products industries.[17,253,254] As a result, chemo- and stereoselective transformations are imperative for the synthesis of cyclopropane containing pharmaceuticals or bioactive natural products.[255] The catalytic formation of cyclopropanes *via* transition-metal carbene transfer reactions is one of the most common strategies and has been extensively studied for decades.[18,26,256–258] Dirhodium(II,II), Rh(II), paddlewheel catalysts are among the most effective catalysts used in diazo-mediated cyclopropanation reactions.

Rh(II)-paddlewheel complexes are highly efficient at carbene transfer reactions with many types of diazo species.[259] Stereoselective cyclopropanation reactions with Rh(II) complexes can be achieved by using diverse bridging ligand architectures. Early studies led by the Doyle lab demonstrated the effectiveness of Rh(II)-carboxamidates in intramolecular cyclopropanations of allylic diazos (Fig. 6.1a).[13,55] Chiral Rh(II)-carboxylates based on

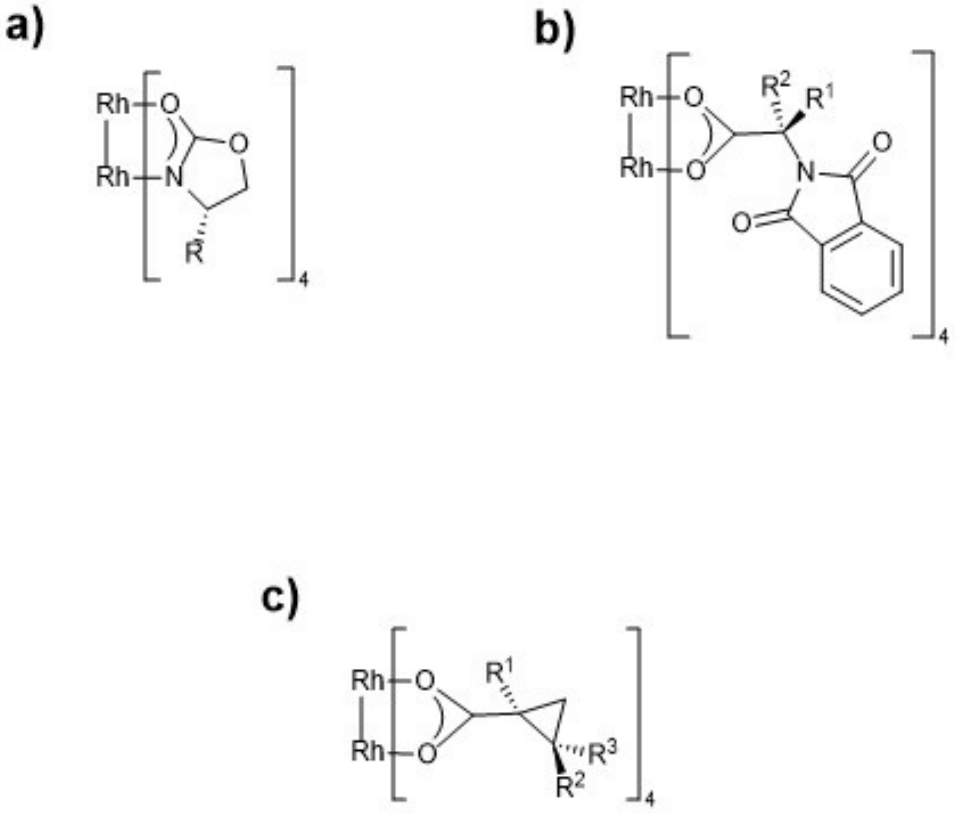

Figure 6.1: a) General structure of chiral Rh(II) carboxamidate complex. b) General structure of Rh(II) carboxylate complex with phthalimide-protected amino acid ligands. c) General structure of Rh(II) carboxylate with chiral cyclopropyl ligands.

phthalimide-protected amino acids are generally efficient at asymmetric induction of various diazo types, but are most proficient at acceptor/acceptors (Fig. 6.1b).[26,27,49] By far the most impressive complexes for stereoselective carbene transfer reactions of donor/acceptor diazos are the Rh(II) complexes developed by the Davies lab (Fig. 6.1c).[26,44,49] Recently, Davies and co-workers have developed their "third generation" of carboxylate complexes that contain triarylcyclopropanecarboxylate (TPCP) bridging ligands (Figure). These complexes contain cyclopropane rings with sterically crowding aryl groups that give the catalyst the conformational rigidity necessary for selective transformations.[31,35,260,261]

The control of the stereoselectivity has mainly been accomplished through the development of chiral bridging ligands with large sterically blocking groups. Lately, trends with non-covalent interactions to enable selectivity have been of interest.[61,62,156,158–162] Axial ligand coordination is thought to slow catalysis by blocking the active sites of the catalyst, however, one axial site must be opened for catalysis to take place,[57] with the distal rhodium behaving as an electronic support for the active Rh(II)-carbene. This influence and its role on asymmetric catalysis are not as clear as the bridging ligands in Rh(II) chemistry. The Charette lab has probed the influence of axial coordination in the cyclopropanation of acceptor/acceptor diazos with styrene.[61,262] With the cyclopropanation of α-nitro diazoacetates and styrene, the addition of nitrogenous LBs resulted in increased enantioselectivity, albeit with drops in diastereoselectivity and comparable cyclopropane yields.[61] Additives don't always result in an increase in enantioselectivity, however. In the same study, they also conducted cyclopropanations of styrene and amido diazoacetates, also acceptor/acceptors, and found that most additives either offered no change or decreased enantioselectivity.[61] Indeed, elucidating the influence of the axial position on stereoselectivity is more nuanced than simply adding exogenous ligands. Previously, our group has used Rh(II) complexes with tethered, axially coordinated ligands (TACLs) to control the local concentration of the axially bound LB and more accurately assess its role in catalysis.[86,172,263] We have observed increased yields in cyclopropanation[86,263] reactions when using the TACLs complexes over comparative Rh(II) complexes with no axial tether (Fig. 6.2 Top). Herein, we investigate the influence of the axial tether's stereoelectronics on asymmetric

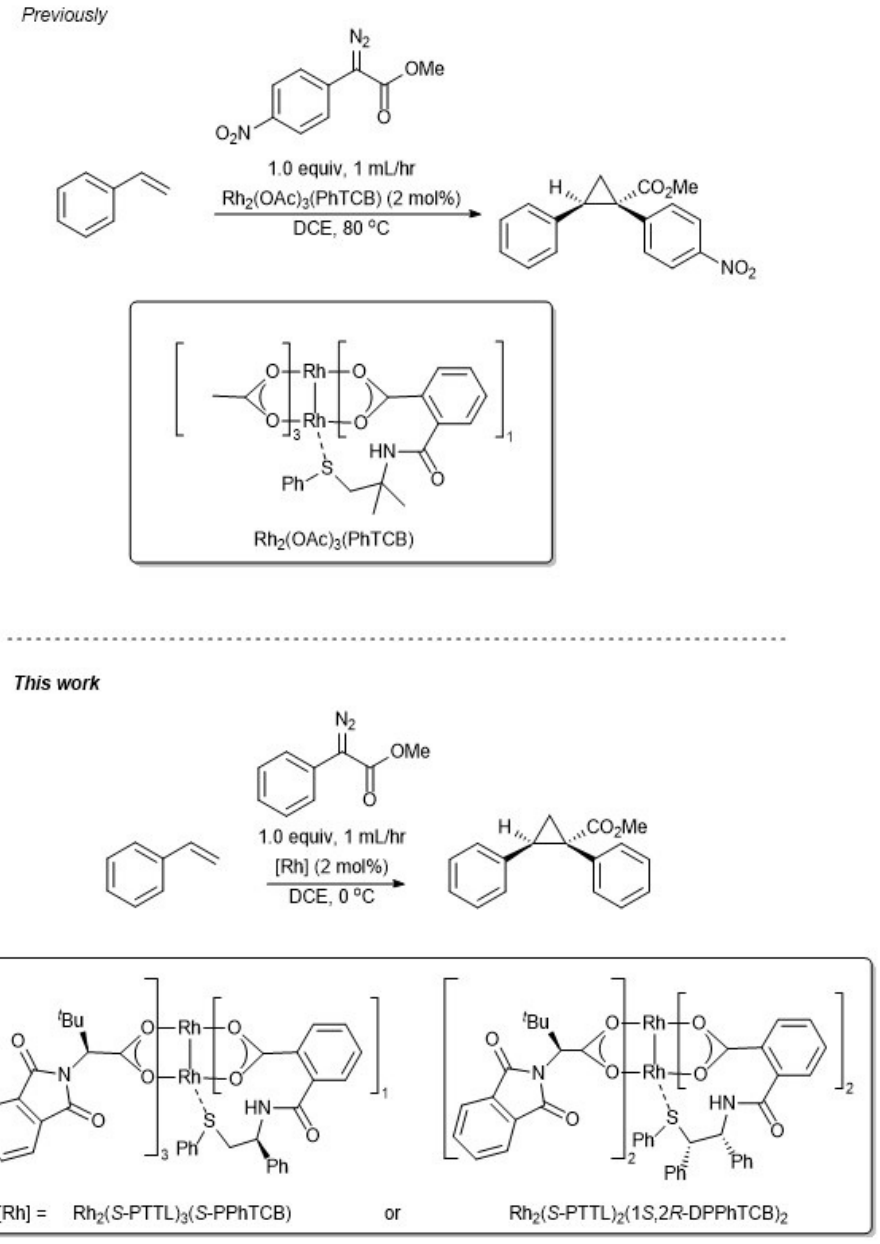

Figure 6.2: (Top) Cyclopropanation with achiral Rh(II)-carboxylate complex featuring a tethered, axially coordinating thioether ligand. (Bottom) Cyclopropanation Chiral Rh(II) complexes with chiral tethered, axially coordinating thioether ligands.

cyclopropanation reactions using chiral heteroleptic Rh(II)-carboxylate complexes with chiral tethered, axially coordinated ligands (Fig. 6.2 Bottom).

6.4 Results and Discussion

6.4.1 Ligand Synthesis

Chiral heteroleptic Rh(II) complexes containing TACLs were synthesized using the carboxylate thiocarbamoyl benzoate (TCB) ligand template from our previously reported studies.[86] The pendant arm of the tether was modified to contain chiral centers that can aid in stereoinduction through non-covalent interactions and perturb the bridging ligand sphere. To this end, ligand 121 was synthesized through Mitsunobu coupling of (1*S*,2*R*)-2-amino-1,2-diphenylethan-1-ol 118 to aziridine 119, followed by nucleophilic ring-opening with thiophenol to provide compound 120. Finally, ring-opening of phthalic anhydride with compound 120 obtained the desired TCB ligand 121 (Fig. 6.3a). Ligand 126 was also synthesized through an aziridine intermediate; however, a few steps were different. Synthesis of (*S*)-2-phenylaziridine 124 was achieved by first isolating an amino alcohol hydrogen sulfate 123 followed by nucleophilic ring-closing in basic conditions to arrive at the subsequent aziridine 124. Using a zinc(II) chloride mediated ring-opening of the aziridine with thiophenol resulted in formation of the aminothioether 125. Aminothioether 125 was then used to ring-open phthalic anhydride to arrive at ligand 126 (Fig. 6.3b).

6.4.2 Complex Synthesis

Phthalimide-protected amino acid derived chiral Rh(II) complexes were chosen as parent complexes for exchange with the tethered ligands due to their versatility in diazo-mediated cyclopropanation reactions and facile synthesis.[26] Specifically, Rh_2(*S*-PTTL)$_4$ has been widely studied and has previously shown success in asymmetric cyclopropanation reactions even when one of the chiral PTTL ligands was exchanged for an achiral ligand.[116] NTTL and PTPA were also used for added variety and the possibility for non-covalent interactions

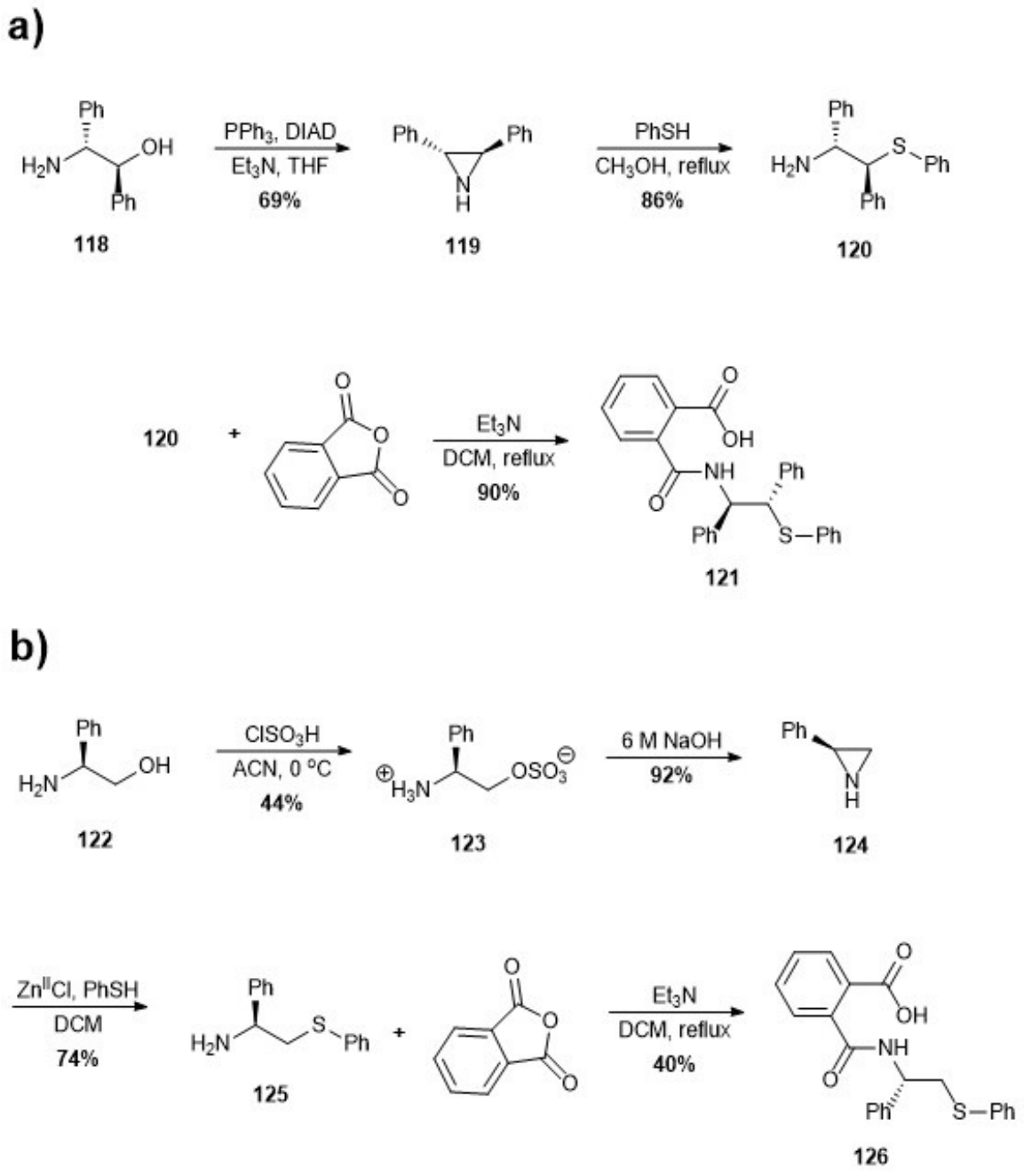

Figure 6.3: a) Synthesis of ligand 121. b) Synthesis of ligand 126.

with the ligand π system. With this in mind, we proceeded to exchange the chiral TCB ligands onto the homoleptic complexes using our previously published conditions.[86] We were able to successfully exchange ligands 121 and 126 unto Rh_2(*S*-PTTL)$_4$. Unfortunately, we were unable to exchange either ligand with the other complexes under similar conditions. Nevertheless, the ability to exchange unto PTTL gave us a comparison of the effect of chirality on a TACL. The parent homoleptic complex and chiral TCB ligands are stirred with Hünig's base in refluxing DCE overnight to furnish the bis-substituted species Rh_2(*S*-PTTL)$_2$(1*S*,2*R*-DPPhTCB)$_2$ 127 as the only product as a *cis*/*trans* mixture in a 10% yield (Fig. 6.4a). The low yield for the bis complex could be a result of bulkiness of the chiral groups on the ligand. When we performed the ligand exchange with glycine derived ligand 126, we obtained 11% of the mono-substituted product 128 as the only isolable complex (Fig. 6.4b).

6.4.3 Asymmetric Cyclopropanation

The effect of the axial tether on enantioinduction was then probed in the asymmetric cyclopropanation of styrene with methyl phenyldiazoacetate (Table 6.1). Enantioselectivity for this cyclopropanation with Rh_2(*S*-PTTL)$_4$ was found to be in agreement with previous attempts in the literature[264,265] with 32% ee observed at 0 °C and 1 mL/hr addition rate of diazo (Table 6.1, entry 1). Cyclopropanation with the naphthyl analog, Rh_2(S-NTTL)$_4$, in the same conditions gave 42% ee, a marked improvement over previous attempts at room temperature in 2,2-DMB (Table 6.1, entry 2).[264,265] The phenylalanine derived complex, Rh_2(*S*-PTPA)$_4$ was also tested and found to exhibit the same enantioselectivity as the Rh_2(*S*-NTTL)$_4$ catalyst, 42 % ee (Table 6.1, entry 3). Cyclopropane yields for the homoleptic catalysts were low to moderate for all the homoleptic complexes tested. To our delight, enantioinduction was improved to 46% with complex 127a/b (Table 6.1, entry 4). Yields for complex 127a/b were lower than the corresponding homoleptic species at 12%. This was most likely due to both axial sites being blocked, which inhibits the active centers, and requiring a dissociation event to occur. Complex 128 gave a comparable ee to Rh_2(*S*-PTTL)$_4$ and increased the yield.

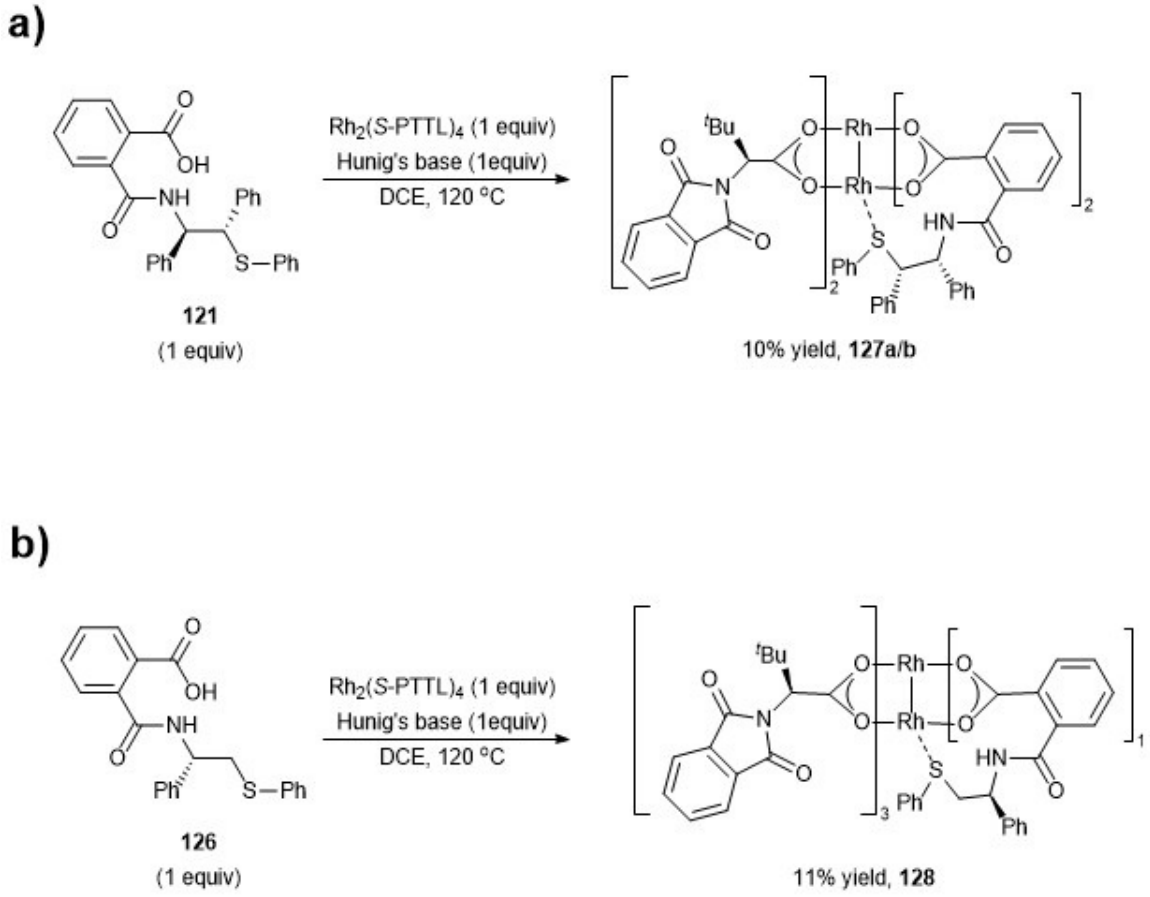

Figure 6.4: a) Synthesis of complexes 127a/b. b) Synthesis of complex 128.

Table 6.1: Asymmetric cyclopropanation of styrene with methyl phenyldiazoacetate.

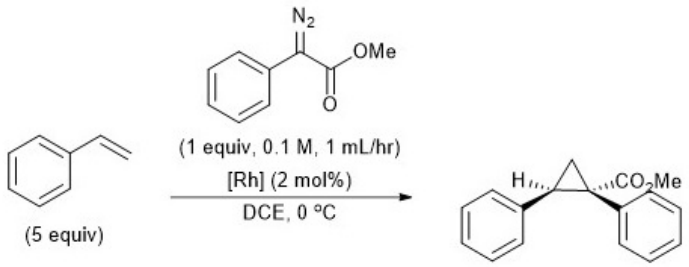

Entry	[Rh]	Yield [%]	% ee
1	Rh_2(*S*-PTTL)$_4$	19	32
2	Rh_2(*S*-NTTL)$_4$	31	42
3	Rh_2(*S*-PTPA)$_4$	35	42
5	**127a/b**	12	46
6	**128**	33	31

6.4.4 Discussion

Predictive models for the observed enantioinduction of Rh(II) phthalimide complexes have primarily focused on the orientations of the sterically bulky groups of the chiral ligands. An early model put forth by Hashimoto and co-workers based on the x-ray structure of Rh_2(*S*-PTPA)$_4$ proposed that the bulky groups are aligned in an "up, up, down, down" C2 configuration leading to two equivalent faces (one at each rhodium). Each of these faces influence the formation of the cyclopropane by blocking certain attack trajectories of the substrate and directing their approach.[266,267] Later, Fox and co-workers reported the x-ray structure of Rh_2(*S*-PTTL)$_4$ and found that the sterically bulky groups adopted an "all-up" C4 configuration. They proposed that the bulky *tert*-butyl groups at one face block access to the axial site and allow all enantioinduction to occur at the phthalimide occupied face. This theory is not entirely accurate as other groups have shown that coordination at the *tert*-butyl face still occurs.[265] The fluxional state of the bulky ligands in solution make it difficult to envision a model to explain the resulting stereoselectivity. However, we do propose the interactions at the axial site could involve π-π interactions on the ligand scaffold that could aid in creating a chiral environment for the substrates.

6.5 Conclusion

In conclusion, we have developed chiral Rh(II) TACLs complexes that give improved enantioselectivity when compared to its parent complex, Rh_2(PTTL)$_4$. A combination of steric factors coupled with non-covalent interactions are a plausible explanation for the increase of selectivity. This result expands the methods in which an increase in enantioselectivity can be achieved. Including tethered, axial ligands on a chiral scaffold have an effect on activity and enantioselectivity depending on the ratio of ligands, mono- and bis-substituted respectively. Different synthetic routes to provide selective formation of *cis* and *trans* isomers and mono-complexes are being explored in our lab currently. We are also attempting to develop synthetic routes that will not limit the chiral ligands that can be applied to the scaffold.

6.6 Experimental Procedures

6.6.1 General Considerations

Unless otherwise noted, all reagents were purchased and used as received from the manufacturer without further purification. Compounds 118 and 119 were synthesized via an established literature procedures.[223] Compounds 123[268], 124[268], and 125[269] were also synthesized according to literature procedures. Methyl phenyl diazoacetate was prepared from benzylic acid according to established procedures.[270] Hexanes, CH_2Cl_2 (DCM), tetrahydrofuran (THF), and acetonitrile (ACN) were dried with columns packed with alumina using an Inert PureSolv Micro Solvent Purification System and stored over molecular sieves. Reactions were monitored using thin layer chromatography (TLC) on Sorbent Technologies Silica XG TLC Plates. Ligands were purified with column chromatography using 60 Å, 40-63 μm silica from Sorbent Technologies. ^{1}H and ^{13}C NMR spectra were recorded on a Varian Mercury Vx 300 MHz or Bruker AVANCE NEO 500 MHz spectrometers. All NMR chemical shifts are reported in ppm on the δ scale. Signals were referenced by residual solvent signal for ^{1}H NMR ($CHCl_3$ = 7.26 ppm, acetone = 2.05 ppm, acetonitrile = 1.94 ppm) and ^{13}C NMR ($CHCl_3$ = 77.16 ppm, acetone = 29.84 ppm, acetonitrile = 1.32 ppm. The mass spectra for all compounds, unless otherwise specified, were obtained using an AccuTOF Mass spectrometer equipped with a DART ionization apparatus.

6.6.2 Ligand Synthesis

2-(((1S,2R)-1,2-diphenyl-2-(phenylthio)ethyl)carbamoyl)benzoic acid (121): To a stirring solution of phthalic anhydride (194 mg, 1.31 mmol) in dry CH_2Cl_2 (8 mL) was added a solution of (1*S*,2*R*)-1,2-diphenyl-2-(phenylthio)ethan-1-amine 3 (400 mg, 1.31) in dry CH_2Cl_2 (8 mL). Triethylamine (18 μL, 10 mol%) was added and the mixture was stirred at reflux for 41 hours. Reaction was cooled to room temperature and a 20 mL portion of DI water was added. The resulting solution was extracted 3 X 70 mL EtOAc. The organic

portions were combined, dried over anhydrous Na_2SO_4, then concentrated in vacuo to a white solid without further purification (535 mg, 1.18 mmol, 90% yield). ^{1}H NMR (500 MHz, acetone-*d6*): δ 8.04 (s, 1H, Ar–H), 7.78 (d, 1H, Ar–H), 7.58-7.08 (m, 17H, Ar–H), 6.93 (d, 1H, Ar–H), 5.72 (t, 1H, N–CH–C), 4.94 (d, 1H, –CH–S); ^{13}C NMR (125 MHz, acetone-*d6*) δ 168.7, 167.8, 140.8, 139.1, 135.7, 133.0, 132.1, 131.2, 130.8, 130.2, 129.7, 129.6, 129.1, 128.9, 128.9, 128.6, 128.3, 128.1, 127.9, 59.6, 58.4; HRMS (EI) *m/z*: calcd. for $C_{28}H_{24}NO_3S$ ($[M+H]^+$) 454.1477, found 454.1523.

(*S*)-2-((1-phenyl-2-(phenylthio)ethyl)carbamoyl)benzoic acid (126): To a stirring solution of phthalic anhydride (388 mg, 2.62 mmol) in dry CH_2Cl_2 (15 mL) was added a solution of (*S*)-1-phenyl-2-(phenylthio)ethan-1-amine 8 (600 mg, 2.62) in dry CH_2Cl_2 (15 mL). Triethylamine (36 μL, 10%) was added and the mixture was stirred at reflux for 20 hours. Reaction was cooled to room temperature and a 20 mL portion of DI water was added. The resulting solution was extracted 3 X 50 mL EtOAc. The organic portions were combined, dried over anhydrous Na_2SO_4, then concentrated in vacuo to a yellow residue. Recrystallized by dissolving in hot EtOAc and adding hexanes then placing in a freezer. (93.5 mg, 0.248 mmol, 40% yield). ^{1}H NMR (500 MHz, acetone-*d6*): δ 7.86 (s, 1H, Ar–H), 7.52-7.41 (m, 7H, Ar–H), 7.32-7.21 (m, 7H, Ar–H), 4.77 (dd, J = 2.53, 1H, Ph–CH-), 4.00 (dd, J = 7.31, 1H, –CHH–), 3.86 (dd, J = 4.92, 1H, –CHH–); ^{13}C NMR (125 MHz, acetone-*d6*) δ 169.9, 167.9, 140.9, 139.3, 137.1, 135.9, 132.2, 132.0, 131.3, 130.9, 130.8, 130.2, 129.9, 129.8, 129.7, 129.3, 129.2, 129.2, 129.1, 128.6, 128.3, 127.6, 127.3, 127.0, 126.2, 51.8, 45.5; HRMS (EI) *m/z*: calcd. for $C_{22}H_{20}NO_3S$ ($[M+H]^+$) 378.1158, found 378.1148.

6.6.3 Complex Synthesis

Rh_2(*S*-PTTL)$_2$(1*S*,2*R*-DPPhTCB)$_2$ (127a/b): To a stirring solution of Rh_2(*S*-PTTL)$_4$ (100 mg, 0.08 mmol, 1 equiv.) in 10 mL dry DCE was added 4 (40 mg, 0.088 mmol) in a Schlenk tube with a Young's tap. Hünig's base (15.4 μL, 0.088 mmol) was then added. The tube was then sealed and the mixture heated to 120 °C and stirred overnight. The resulting solution was concentrated in vacuo and the products separated via a Biotage Selekt automated column using a EtOAc:hexanes gradient on a 10 g Biotage Sfär column. First

the Rh_2(S-PTTL)4 is separated using 1:1 hexane/EtOAc as the eluent. This is then followed by 9:1 toluene/ACN as the eluent to afford the bis-substituted complex 5 as a mixture of cis and trans isomers. Blue-green solid (13 mg, 0.008 mmol, 10% yield). ^{1}H NMR (500 MHz, CD_3CN): δ 7.70 (s, 9H, Ar–H), 7.68 (d, 5H, Ar–H), 7.33 (d, 6H, Ar–H), 7.20 (m, 15H, Ar–H), 7.08 (t, 3H, Ar–H), 6.86 (t, 8H, Ar–H), 6.56 (d, 1H, Ar–H), 4.92 (d, 2H, N–CH–C), 4.56 (d, 2H, –CH–S), 4.40 (s, 2H, NH), 4.22 (t, 2H, (CO^+)CH–N), 0.83 (s, 18H, $C(CH_3)_3$); ^{13}C NMR (125 MHz, $CDCl_3$): δ 168.0, 138.2, 133.8, 132.3, 129.9, 129.5, 128.9, 128.4, 128.3, 128.3, 128.1, 127.8, 127.8, 123.5, 65.8, 61.8, 58.4, 35.6, 29.0, 28.2; HRMS (EI) *m/z*: calcd. for $C_{84}H_{73}N_4O_{14}Rh_2S_2$ ($[M+H]^+$) 1631.2675, found 1631.2770.

Rh_2(*S*-PTTL)$_3$(*S*-PPhTCB) (128): To a stirring solution of Rh_2(*S*-PTTL)$_4$ (564 mg, 0.41mmol, 1 equiv.) in 50 mL dry DCE was added 9 (189 mg, 0.5 mmol) in a Schlenk tube with a Young's tap. Hünig's base (87 μL, 0.5 mmol) was then added. The tube was then sealed, and the mixture heated to 120 °C and stirred overnight. The resulting solution was concentrated *in vacuo* and the products separated via a Biotage Selekt automated column using a EtOAc:hexanes gradient on a 25 g Biotage Sfär column. The mono-substituted complex 11 isolated as a Blue-green solid (61 mg, 0.045 mmol, 11% yield). ^{1}H NMR (500 MHz, CD_3CN): δ 8.58-8.54 (m, 1H, Ar–H), 8.10-8.04 (m, 1H, Ar–H), 7.84 (dd, J = 3.88, 2H, Ar–H), 7.87-7.47 (m, 14H, Ar–H), 7.36 (d, J = 7.91, 1H, Ar–H), 7.18-7.01 (m, 3H, Ar–H), 6.81-6.70 (m, 3H, Ar–H), 6.49 (d, J = 6.12, 2H, Ar–H), 6.03 (dt, J = 7.5, 3H, Ar–H), 5.76 (d, J = 7.76, 2H, Ar–H), 5.07 (s, 1H, (CO_2)CH–N), 4.67 (s, 1H, (CO_2)CH–N), 4.47 (s, 1H, (CO_2)CH–N), 4.16 (dd, J = 9.45, 1H, N–CH–C), 3.59 (d, J = 5.11, 1H, CH–CHH–S), 3.11 (dt, J = 5.13, 1H, CH–CHH–S), 1.27 (s, 9H, $C(CH_3)_3$), 1.03 (s, 9H, $C(CH_3)_3$), 0.72 (s, 9H, $C(CH_3)_3$); ^{13}C NMR (125 MHz, $CDCl_3$): δ 189.6, 188.0, 187.0, 186.5, 168.3, 168.1, 165.4, 139.3, 136.1, 134.0, 133.7, 133.1, 132.9, 132.6, 132.2, 132.0, 131.8, 130.5, 130.1, 128.4, 128.0, 127.7, 127.6, 127.3, 126.8, 126.7, 125.9, 124.9, 123.4, 123.2, 63.0, 62.6, 60.6, 58.7, 41.5, 36.2, 35.2, 34.5, 28.8, 28.2, 28.1, 28.0, 27.9. HRMS (EI) *m/z*: calcd. for $C_{84}H_{73}N_4O_{14}Rh_2S_2$ ($[M+H]^+$) 1631.2675, found 1631.2770.

6.6.4 Aysmmetric Cyclopropanation

Under an atmosphere of argon, a 25 mL Schlenk flask equipped with a magnetic stir bar was flame dried and charged with styrene (96.82 μL, 0.845 mmol), complex 5 (5.5 mg, 0.0034 mmol), and DCE (0.5 mL). The solution was then cooled to 0 °C, followed by slow addition of methyl phenyldiazoacetate (30 mg, 0.17 mmol) as a 0.1 M solution in DCE by syringe pump (1 mL/hr). After addition was complete, the reaction solution was filtered through 1.5-inch silica plug and eluted with 4 mL DCM. The eluent was then concentrated *in vacuo* with a rotary evaporator. Yields were calculated by ^{1}H NMR using mesitylene as an internal standard. Normalized integration of the methyl protons of mesitylene (2.26 ppm) was compared to the integration of the diastereotopic proton of the methylene unit of the cyclopropane. Enantioselectivity was determined by chiral HPLC analysis. Chiral HPLC analysis was performed on a Shimadzu LC-2030 Prominence-I instrument using a Chiralcel OJ-H column with a flow rate of 1 mL/min and 2% IPA/Hexanes mobile phase.

Chapter 7

Conclusion

Rh(II) complexes are a privileged class of catalyst in carbene transfer reactions. The effects of LBs coordinated at the axial site have recently interested the research community. Previously, the coordination of a LB to the axial site was thought to hinder catalysis. Presented within this dissertation are many instances where this is not the case. Although not clearly defined, axial coordination can be leveraged to increase the activity and selectivity of Rh(II) catalyst. The work presented herein includes my efforts to help define the role of axial coordination in Rh(II)-mediated carbene transfer reactions, specifically in Si–H insertions and cyclopropanations.

In Chapter 2, Rh(II) complexes with TACLs were tested in Si–H insertion reaction of donor/acceptor diazo compounds. We synthesized a mono-substituted heteroleptic complex, $Rh_2(OAc)_3$(2-OX), to isolate the effects of the tethered axial coordinating thioether on catalysis. In this study, we found that the tether did not hinder catalysis in the Si–H insertion of donor/acceptor diazo compounds unless it was bis-substituted. It was shown that $Rh_2(OAc)_3$(MeTOX) was more selective toward Si–H reactions with more nucleophilic donor/acceptor diazo compounds. This result was reasoned by the effect the coordinated thioether complex has on the frontier orbitals of the complex. The HOMO and LUMO of the complex were destablized resulting in a large energy increase of the LUMO and an increased HOMO-LUMO gap. We propose that the labile nature of the thioether coordination allows

for the elongation of the Rh–S bond to compensate for the binding of the more nucleophilic diazo compound.

The work presented in Chapter 3 was inspired by the results of Chapter 2. We sought to expand the use Rh(II) paddlewheel complexes in Si–H insertion reactions with donor diazo compounds by utilizing Rh(II) paddlewheel complexes with TACLs. Due to the instability of donor diazo compounds, we opted to use nosyl-protected benzylhydrazones as diazo precursors. When screening catalyst, it was found that the complexes with TACLs were not as active as the complexes without. This trend inverted when the catalyst loading was reduced, although the yield suffered in both cases. It was also concluded that the combination of base and solvent had the greatest effect on the system, NaHMDS and 1,4-dioxane respectively. When inspecting the scope of diazo compound reactivity, it was seen that Si–H insertion is hindered by competing reactions and donating substituents, but provided good to fair yields otherwise.

Chapter 4 highlights our efforts to streamline the diversification of the axial tether by implementing microwave syntheses. The synthesized complexes were then investigated in the cyclopropanation of olefins with ethyl diazoacetate to understand how changes to the tether length and substituent of axially coordinated thioether modulated reactivity. It was found that complexes mono-substituted with a TACL gave higher yields than those without, and even provided good yields with equimolar amounts of substrates. The ability to affect the reactivity by changing tether length and substituent on the thioether was also confirmed. Interestingly, calculations elucidated that the HOMO of the carbene was destablized due to the axial coordination of the thioether. This is proposed to be a contributing factor to the increased activity of the catalyst. The elongation of the Rh–S bond length also provided evidence that the tether helps accommodate the increase of electron density of the distal Rh center. Also, shown is the axial tether increases the activation energy of N_2 extrusion due to the increased strength of the Rh–Rh bond.

Finally, Chapter 5 demonstrates how chiral TACLs can be designed and applied to asymmetric cyclopropanation reactions. In this study, chiral TACLs were successfully synthesized and substituted onto $Rh_2(S\text{-PTTL})_4$. It was found that the mono-substituted

complex with a β-phenyl substituent to the thioether increased activity while retaining enantioselectivity in the cyclopropanation of styrene with methyl diazoacetate when compared to $Rh_2(S\text{-PTTL})_4$. The bis-substituted complex with α,β-phenyl substituents increased the enantioselectivity but experienced a reduced yield. We propose that steric and non-covalent interactions close to the axial site are responsible for the increased enantioselectivity.

Bibliography

[1] F. Ye and L.-W. Xu. A glimpse and perspective of current organosilicon chemistry from the view of hydrosilylation and synthesis of silicon-stereogenic silanes. *Synlett*, 32:1281–1288, 2021. 1, 5

[2] T. Hiyama. Organosilicon and relating organotin chemistry. page 373. John Wiley & Sons, Inc. 2, 5, 8

[3] I. Fleming and A. Pearce. Controlling the outcome of a carbocation-initiated cyclization. *J. Chem. Soc., Perkin Trans. 1*, page 251, 1981. 2

[4] T. Komiyama, Y. Minami, and T. Hiyama. Recent advances in transition-metal-catalyzed synthetic transformations of organosilicon reagents. *ACS Catal.*, 7:631–651, 2017. 2, 5

[5] A. Sugiyama, Y.-y. Ohnishi, M. Nakaoka, Y. Nakao, H. Sato, S. Sakaki, Y. Nakao, and T. Hiyama. Why does fluoride anion accelerate transmetalation between vinylsilane and palladium(II)–vinyl complex? theoretical study. *J. Am. Chem. Soc.*, 130:12975–12985, 2008. 5

[6] C. Amatore, L. Grimaud, G. Le Duc, and A. Jutand. Three roles for the fluoride ion in palladium-catalyzed Hiyama reactions: Transmetalation of [ArPdFL$_2$] by Ar'Si(OR)$_3$. *Angew. Chem., Int. Ed.*, 53:6982–6985, 2014. 5

[7] Y. Kong and D. Mu. Recent progress in transition metal-catalyzed hydrosilane-mediated C–H silylation. *Chem. - Asian J.*, 17:e202200104, 2022. 5, 8

[8] Y. Landais, L. Parra-Rapado, D. Planchenault, and V. Weber. Mechanism of metal-carbenoid insertion into the Si–H bond. *Tetrahedron Lett.*, 38:229–232, 1997. 5, 102

[9] Z. Xu, W.-S. Huang, J. Zhang, and L.-W. Xu. Recent advances in transition-metal-catalyzed silylations of arenes with hydrosilanes: C–X bond cleavage or c–h bond activation synchronized with Si–H bond activation. *Synthesis*, 47:3645–3668, 2015. 8

[10] X. Zhang, J. Fang, C. Cai, and G. Lu. Recent advances in synthesis of organosilicons via radical strategies. *Chin. Chem. Lett.*, 32:1280–1292, 2021. 8

[11] Z. Casar. Synthetic approaches to contemporary drugs that contain the cyclopropyl moiety. *Synthesis*, 52:1315–1345, 2020. 10

[12] T. T. Talele. The "cyclopropyl fragment" is a versatile player that frequently appears in preclinical/clinical drug molecules. *J. Med. Chem.*, 59:8712–8756, 2016. 10

[13] H. Lebel, J.-F. Marcoux, C. Molinaro, and A. B. Charette. Stereoselective cyclopropanation reactions. *Chem. Rev.*, 103:977–1050, 2003. 10, 165

[14] H. M. L. Davies and E. G. Antoulinakis. Intermolecular metal-catalyzed carbenoid cyclopropanations. *Org. React.*, 57:1–326, 2001. 10, 18, 112, 131, 134, 145

[15] J. Lee, H. Kim, and J. K. Cha. A new variant of the Kulinkovich hydroxycyclopropanation. Reductive coupling of carboxylic esters with terminal olefins. *J. Am. Chem. Soc.*, 118:4198, 1996. 10

[16] Y. Duan, B. Zhou, J.-H. Lin, and J.-C. Xiao. Diastereoselective Johnson-Corey-Chaykovsky trifluoroethylidenation. *Chem. Commun.*, 51:13127–13130, 2015. 10

[17] W. Wu, Z. Lin, and H. Jiang. Recent advances in the synthesis of cyclopropanes. *Org. Biomol. Chem.*, 16:7315–7329, 2018. 10, 165

[18] M. P. Doyle and D. C. Forbes. Recent advances in asymmetric catalytic metal carbene transformations. *Chem. Rev.*, 98:911–935, 1998. 13, 94, 131, 165

[19] Y. Zhao and D. G. Truhlar. The M06 suite of density functionals for main group thermochemistry, thermochemical kinetics, noncovalent interactions, excited states, and transition elements: Two new functionals and systematic testing of four M06-class functionals and 12 other functionals. *Theor. Chem. Acc.*, 120:215–241, 2008. 13, 110, 162

[20] F. Weigend and R. Ahlrichs. Balanced basis sets of split valence, triple zeta valence and quadruple zeta valence quality for H to Rn: Design and assessment of accuracy. *Phys. Chem. Chem. Phys.*, 7:3297–3305, 2005. 13, 14, 110, 162

[21] W. Kohn and L. J. Sham. Self-consistent equations including exchange and correlation effects. *Phys. Rev.*, 140:A1133–A1138, 1965. 14

[22] P. Hohenberg and W. Kohn. Inhomogeneous electron gas. *Phys. Rev.*, 136:B864–B871, 1964. 14

[23] K. B. Wiberg. Application of the Pople-Santry-Segal complete neglect of differential overlap method to the cyclopropyl-carbinyl and cyclobutyl cation and to bicyclobutane. *Tetrahedron*, 24:1083, 1968. 14

[24] F. Weinhold, C. R. Landis, and E. D. Glendening. What is NBO analysis and how is it useful? *Int. Rev. Phys. Chem.*, 35:399–440, 2016. 14

[25] A. E. Reed and F. Weinhold. Natural bond orbital analysis of near-hartree–fock water dimer. *J. Chem. Phys*, 78:4066–4073, 1983. 14

[26] H. M. L. Davies and B. T. Parr. *Rhodium Carbenes*, volume 7, pages 363–403. John Wiley & Sons, Inc, Hoboken, New Jersey, 2013. 18, 20, 94, 133, 165, 167, 169

[27] Y. Deng, H. Qiu, H. D. Srinivas, and M. P. Doyle. Chiral dirhodium(II) catalysts for selective metal carbene reactions. *Curr. Org. Chem.*, 20:61–81, 2016. 18, 133, 167

[28] K. P. Kornecki, J. F. Briones, V. Boyarskikh, F. Fullilove, J. Autschbach, K. E. Schrote, K. M. Lancaster, H. M. L. Davies, and J. F. Berry. Direct spectroscopic

characterization of a transitory dirhodium donor-acceptor carbene complex. *Science*, 342:351–354, 2013. 116

[29] C. Werle, R. Goddard, P. Philipps, C. Fares, and A. Fürstner. Structures of reactive donor/acceptor and donor/donor rhodium carbenes in the solid state and their implications for catalysis. *J. Am. Chem. Soc.*, 138:3797–3805, 2016. 18

[30] S. Singha, M. Buchsteiner, G. Bistoni, R. Goddard, and A. Fürstner. A new ligand design based on london dispersion empowers chiral bismuth-rhodium paddlewheel catalysts. *J. Am. Chem. Soc.*, 143:5666–5673, 2021. 18

[31] B. Wei, J. C. Sharland, P. Lin, S. M. Wilkerson-Hill, F. A. Fullilove, S. McKinnon, D. G. Blackmond, and H. M. L. Davies. *In situ* kinetic studies of Rh(II)-catalyzed asymmetric cyclopropanation with low catalyst loadings. *ACS Catal.*, 10:1161–1170, 2020. 167

[32] K. O. Marichev, J. T. Ramey, H. Arman, and M. P. Doyle. Highly regio-, diastereo-, and enantioselective rhodium-catalyzed intramolecular cyclopropanation of (*Z*)-1,3-dienyl aryldiazoacetates. *Org. Lett.*, 19:1306–1309, 2017. 18

[33] H. M. L. Davies. Finding opportunities from surprises and failures. Development of rhodium-stabilized donor/acceptor carbenes and their application to catalyst-controlled C–H functionalization. *J. Org. Chem.*, 84:12722–12745, 2019. 18

[34] H. M. L. Davies and D. Morton. Guiding principles for site selective and stereoselective intermolecular C–H functionalization by donor/acceptor rhodium carbenes. *Chem. Soc. Rev.*, 40:1857–1869, 2011. 112, 131

[35] K. Liao, W. Liu, Z. L. Niemeyer, Z. Ren, J. Bacsa, D. G. Musaev, M. S. Sigman, and H. M. L. Davies. Site-selective carbene-induced C–H functionalization catalyzed by dirhodium tetrakis(triarylcyclopropanecarboxylate) complexes. *ACS Catal.*, 8:678–682, 2018. 18, 96, 98, 167

[36] C. Qin and H. M. L. Davies. Role of sterically demanding chiral dirhodium catalysts in site-selective C–H functionalization of activated primary C–H bonds. *J. Am. Chem. Soc.*, 136:9792–9796, 2014. 133

[37] S. M. Wilkerson-Hill and H. M. L. Davies. *Rhodium(II) Tetracarboxylate-Catalyzed Enantioselective C–H Functionalization Reactions*, book section 13, pages 343–372. Wiley-VCH Verlag GmbH & Co. KGaA, 2019. 18

[38] R. T. Buck, M. P. Doyle, M. J. Drysdale, L. Ferris, D. C. Forbes, D. Haigh, C. J. Moody, N. D. Pearson, and Q.-L. Zhou. Asymmetric rhodium carbenoid insertion into the Si–H bond. *Tetrahedron Lett.*, 37:7631–7634, 1996. 18, 96

[39] H. Keipour, V. Carreras, and T. Ollevier. Recent progress in the catalytic carbene insertion reactions into the silicon–hydrogen bond. *Org. Biomol. Chem.*, 15:5441–5456, 2017.

[40] S. Kitagaki, M. Kinoshita, M. Takeba, M. Anada, and S. Hashimoto. Enantioselective Si-H insertion of methyl phenyldiazoacetate catalyzed by dirhodium(II) carboxylates incorporating *N*-phthaloyl-(*S*)-amino acids as chiral bridging ligands. *Tetrahedron: Asymmetry*, 11:3855–3859, 2000. 18, 96

[41] R. M. Savizky and D. J. Austin. *Rhodium(II)-Catalyzed 1,3-Dipolar Cycloaddition Reactions*, book section 19, pages 433–454. Wiley-VCH Verlag GmbH & Co. KGaA, 2005. 18

[42] N. De, D. Ko, and E. J. Yoo. In *Rhodium(II)-catalyzed 1,3- and 1,5-Dipolar Cycloaddition*, pages 471–486. Wiley-VCH Verlag GmbH & Co. KGaA, 2019. 18

[43] F. G. Adly. On the structure of chiral dirhodium(II) carboxylate catalysts: Stereoselectivity relevance and insights. *Catalysts*, 7:347, 2017. 18, 20, 133

[44] F. G. Adly, H. Bollard, M. G. Gardiner, and A. Ghanem. Chiral dirhodium(II) carboxylates: New insights into the effect of ligand stereo-purity on catalyst structure and enantioselectivity. *Catalysts*, 8:268–282, 2018. 167

[45] F. G. Adly and A. Ghanem. Chiral dirhodium(II) carboxylates and carboxamidates as effective chemzymes in asymmetric synthesis of three-membered carbocycles. *Chirality*, 26:692–711, 2014. 18

[46] N. R. Candeias, C. A. M. Afonso, and P. M. P. Gois. Making expensive dirhodium(II) catalysts cheaper: Rh(II) recycling methods. *Org. Biomol. Chem.*, 10:3357–3378, 2012. 20, 65, 67

[47] Z. T. Ball. Designing enzyme-like catalysts: A rhodium(II) metallopeptide case study. *Acc. Chem. Res.*, 46:560–570, 2013. 20, 31, 72

[48] R. Hrdina. Dirhodium(II,II) paddlewheel complexes. *Eur. J. Inorg. Chem.*, 2021: 501–528, 2021. 20

[49] J. Hansen and H. M. L. Davies. High symmetry dirhodium(II) paddlewheel complexes as chiral catalysts. *Coord. Chem. Rev.*, 252:545–555, 2008. 21, 167

[50] H. T. Chifotides and K. R. Dunbar. Rhodium compounds. In *Rhodium compounds*, pages 465–589. Springer, 2005. 20, 21, 27

[51] F. A. Cotton, C. A. Murillo, and R. A. Walton. *Multiple Bonds Between Metal Atoms, Third Edition*. Springer, New York, NY, 3rd edn edition, 2005. Caplus AN 2006:216477 (Book). 20, 36, 141

[52] D. J. Timmons and M. P. Doyle. Chiral dirhodium(II) catalysts and their applications. pages 591–632. Springer, 2005. 20

[53] A. Padwa, D. J. Austin, A. T. Price, M. A. Semones, M. P. Doyle, M. N. Protopopova, W. R. Winchester, and A. Tran. Ligand effects on dirhodium(II) carbene reactivities. Highly effective switching between competitive carbenoid transformations. *J. Am. Chem. Soc.*, 115:8669–80, 1993. 20

[54] A. Padwa, D. J. Austin, S. F. Hornbuckle, M. A. Semones, M. P. Doyle, and M. N. Protopopova. Control of chemoselectivity in catalytic carbenoid reactions.

Dirhodium(II) ligand effects on relative reactivities. *J. Am. Chem. Soc.*, 114:1874–1876, 1992. 20

[55] M. P. Doyle. Perspective on dirhodium carboxamidates as catalysts. *J. Org. Chem.*, 71:9253–9260, 2006. 20, 131, 165

[56] J. F. Berry. The role of three-center/four-electron bonds in superelectrophilic dirhodium carbene and nitrene catalytic intermediates. *Dalton Trans.*, 41:700–713, 2012. 20, 37, 39, 42, 44, 98, 102, 105, 141, 148, 151

[57] M. C. Pirrung, H. Liu, and J. Morehead, Andrew T. Rhodium chemzymes: Michaelis-Menten kinetics in dirhodium(II) carboxylate-catalyzed carbenoid reactions. *J. Am. Chem. Soc.*, 124:1014–1023, 2002. 20, 94, 96, 152, 167

[58] H. K. Kisan and R. B. Sunoj. Axial coordination dichotomy in dirhodium carbenoid catalysis: A curious case of cooperative asymmetric dual-catalytic approach toward amino esters. *J. Org. Chem.*, 80:2192–2197, 2015. 21, 86

[59] B. Lu, X. Liang, J. Zhang, Z. Wang, Q. Peng, and X. Wang. Dirhodium(II)/xantphos-catalyzed relay carbene insertion and allylic alkylation process: Reaction development and mechanistic insights. *J. Am. Chem. Soc.*, 143:11799–11810, 2021.

[60] A. F. Trindade, J. A. S. Coelho, C. A. M. Afonso, L. F. Veiros, and P. M. P. Gois. Fine tuning of dirhodium(II) complexes: Exploring the axial modification. *ACS Catal.*, 2: 370–383, 2012. 94, 133

[61] D. Marcoux, V. N. G. Lindsay, and A. B. Charette. Use of achiral additives to increase the stereoselectivity in Rh(II)-catalyzed cyclopropanations. *Chem. Commun.*, 46:910–912, 2010. 21, 80, 86, 94, 133, 167

[62] V. N. G. Lindsay, W. Lin, and A. B. Charette. Experimental evidence for the all-up reactive conformation of chiral rhodium(II) carboxylate catalysts: Enantioselective synthesis of *cis*-cyclopropane α-amino acids. *J. Am. Chem. Soc.*, 131:16383–16385, 2009. 21, 80, 167

[63] A. DeAngelis, D. T. Boruta, J.-B. Lubin, I. Plampin, James N., G. P. A. Yap, and J. M. Fox. The chiral crown conformation in paddlewheel complexes. *Chem. Commun.*, 46:4541–4543, 2010. 21

[64] A. DeAngelis, O. Dmitrenko, G. P. A. Yap, and J. M. Fox. Chiral crown conformation of Rh_2(*S*-PTTL)$_4$: Enantioselective cyclopropanation with α-alkyl-αdiazoacetate. *J. Am. Chem. Soc.*, 131:7230–7231, 2009. 21

[65] V. N. G. Lindsay and A. B. Charette. Design and synthesis of chiral heteroleptic rhodium(II) carboxylate catalysts: Experimental investigation of halogen bond rigidification effects in asymmetric cyclopropanation. *ACS Catal.*, 2:1221–1225, 2012. 21, 24, 27, 45, 133, 134

[66] J. L. Bear, J. Kitchens, and I. Willcott, M. Robert. Kinetic study of the reaction of rhodium(II) acetate with trifluoroacetic acid. *J. Inorg. Nucl. Chem.*, 33:3479–3486, 1971. 24

[67] R. S. Lifsey, X. Q. Lin, M. Y. Chavan, M. Q. Ahsan, K. M. Kadish, and J. L. Bear. Reaction of rhodium(II) acetate with *N*-phenylacetamide: Substitution products and geometric isomers. *Inorg. Chem.*, 26:830–836, 1987. 24

[68] M. P. Doyle, M. A. McKervey, and T. Ye. *Modern Catalytic Methods for Organic Synthesis with Diazo Compounds: From Cyclopropanes to Ylides*. Wiley, New York, 1998. 24, 94, 98, 131, 134

[69] Y. Lou, T. P. Remarchuk, and E. J. Corey. Catalysis of enantioselective [2+1]-cycloaddition reactions of ethyl diazoacetate and terminal acetylenes using mixed-ligand complexes of the series $Rh_2(RCO_2)_n(L_4\text{-}n)$. Stereochemical heuristics for ligand exchange and catalyst synthesis. *J. Am. Chem. Soc.*, 127:14223–14230, 2005. 24, 27, 31, 62, 98, 134, 138

[70] T. P. Zhu, M. Q. Ahsan, T. Malinski, K. M. Kadish, and J. L. Bear. Electrochemical studies of a series of dirhodium(II) complexes with acetate and acetamidate bridging ligands. *Inorg. Chem.*, 23:2–3, 1984. 24

[71] K. Takeda, T. Oohara, M. Anada, H. Nambu, and S. Hashimoto. A polymer-supported chiral dirhodium(II) complex: Highly durable and recyclable catalyst for asymmetric intramolecular C–H insertion reactions. *Angew. Chem., Int. Ed.*, 49:6979–6983, 2010. 27

[72] A. R. Chakravarty, F. A. Cotton, D. A. Tocher, and J. H. Tocher. Structural and electrochemical characterization of the novel *ortho*-metalated dirhodium(II) compounds $Rh_2(O_2CMe)_2[Ph_2P(C_6H_4)]_2{\cdot}2L$. *Organometallics*, 4:8–13, 1985. 27, 53

[73] A. R. Chakravarty, F. A. Cotton, and D. A. Tocher. *ortho*-metalation at dimetallic centers: Syntheses and x-ray characterizations of $Os_2(OAc)_2[Ph_2P(C_6H_4)]_2Cl_2$ and $Rh_2(OAc)_2[Ph_2P(C_6H_4)]_2(2AcOH)$. *J. Chem. Soc., Chem. Commun.*, pages 501–502, 1984. 27, 53

[74] F. Estevan, P. Lahuerta, J. Perez-Prieto, S.-E. Stiriba, and M. A. Ubeda. New rhodium(II) catalysts for selective carbene transfer reactions. *Synlett*, pages 1121–1122, 1995. 27, 53

[75] F. Estevan, P. Lahuerta, J. Perez-Prieto, M. Sanau, S.-E. Stiriba, and M. A. Ubeda. Ligand effects on the chemoselectivity of *ortho*-metalated rhodium(II) catalyzed α-diazo ketone transformations. *Organometallics*, 16:880–886, 1997. 27, 53

[76] F. Estevan, J. Lloret, M. Sanau, and M. A. Ubeda. Enantio- and diastereocontrol in intermolecular cyclopropanation reaction of styrene catalyzed by dirhodium(II) complexes with bulky *ortho*-metalated aryl phosphines: Catalysis in water as solvent. study of a (+)-nonlinear effect. *Organometallics*, 25:4977–4984, 2006. 57

[77] P. Lahuerta, I. Pereira, J. Perez-Prieto, M. Sanau, S. E. Stiriba, and D. F. Taber. *ortho*-metalated dirhodium(II)-catalyzed α-diazocarbonyl transformation. diastereoselective

cyclopropanation of menthyl-α-diazo-β-keto ester and C–H insertion of α-diazo ester. *J. Organomet. Chem.*, 612:36–45, 2000. 53, 57

[78] J. Lloret, F. Estevan, P. Lahuerta, P. Hirva, J. Perez-Prieto, and M. Sanau. Dirhodium(II) compounds with bridging thienylphosphines: Studies on reversible P,C/P,S coordination. *Chem. Eur. J.*, 15:7706–7716, 2009. 27, 57

[79] P. Lahuerta, J. Paya, M. A. Pellinghelli, and A. Tiripicchio. Fast *ortho*-metalation reactions in binuclear dirhodium compounds. Syntheses and molecular structures of a monometalated compound and two doubly metalated compounds with head-to-head configurations. *Inorg. Chem.*, 31:1224–1232, 1992. 27

[80] P. Lahuerta, J. Paya, X. Solans, and M. A. Ubeda. *ortho*-metalation reactions in binuclear dirhodium compounds. Molecular structure and reactivity of a monometalated compound with the phosphine P(o-ClC_6H_4)(C_6H_5)$_2$. *Inorg. Chem.*, 31, 1992. 27

[81] D. F. Taber, R. P. Meagley, J. P. Louey, and A. L. Rheingold. Molecular complex design: Bridging the tetrakiscarboxylatodirhodium core. *Inorg. Chim. Acta*, 239:25–28, 1995. 27, 133

[82] R. P. Bonar-Law, T. D. McGrath, N. Singh, J. F. Bickley, and A. Steiner. Dinuclear complexes as connectors for carboxylates. self-assembly of a molecular box. *Chem. Commun.*, pages 2457–2458, 1999. 27

[83] J. F. Bickley, R. P. Bonar-Law, C. Femoni, E. J. MacLean, A. Steiner, and S. J. Teat. Dirhodium(II) carboxylate complexes as building blocks. synthesis and structures of square boxes with tilted walls. *Dalton*, pages 4025–4027, 2000. 31

[84] J. Bickley, R. Bonar-Law, T. McGrath, N. Singh, and A. Steiner. Dirhodium(II) carboxylate complexes as building blocks. *cis*-chelating dicarboxylic acids designed to bridge the dinuclear core. *New J. Chem.*, 28:425–433, 2004. 27

[85] F. P. Calo and A. Fürstner. A heteroleptic dirhodium catalyst for asymmetric cyclopropanation with α-stannyl α-diazoacetate. "stereoretentive" Stille coupling with formation of chiral quarternary carbon centers. *Angew. Chem., Int. Ed.*, 59:13900–13907, 2020. 31, 62, 65

[86] B. G. Anderson, D. Cressy, J. J. Patel, C. F. Harris, G. P. A. Yap, J. F. Berry, and A. Darko. Synthesis and catalytic properties of dirhodium paddlewheel complexes with tethered, axially coordinating thioether ligands. *Inorg. Chem.*, 58:1728–1732, 2019. 31, 88, 107, 134, 136, 138, 141, 143, 148, 158, 159, 160, 167, 169, 171

[87] S. C. Martin, M. B. Minus, and Z. T. Ball. Chemical posttranslational modification with designed rhodium(II) catalysts. *Methods Enzymol*, 580:1–19, 2016. 31, 134

[88] G. Pimblett, C. D. Garner, and W. Clegg. Synthesis, crystal structure, and spectroscopic properties of bis-μ-acetato-bis[tris(acetonitrile)molybdenum(II)](4Mo-Mo) and bis[tris(acetonitrile)rhodium(II)](Rh–Rh) tetrafluoroborate, and bis-μ-acetato-bis[bis(acetonitrile)(pyridine)rhodium(II)](Rh-Rh) tetrafluoroborate. *J. Chem. Soc., Dalton Trans.*, pages 1257–63, 1986. 31

[89] M. Sarkar, P. Daw, T. Ghatak, and J. K. Bera. Amide-functionalized naphthyridines on a Rh(II)–Rh(II) platform: Effect of steric crowding, hemilability, and hydrogen-bonding interactions on the structural diversity and catalytic activity of dirhodium(II) complexes. *Chem. Eur. J.*, 20:16537–16549, 2014. 31, 86, 88, 133

[90] C. S. Campos-Fernandez, X. Ouyang, and K. R. Dunbar. A homologous series of redox-active, dinuclear cations with the bridging ligand 2-(2-pyridyl)-1,8-naphthyridine. *Inorg. Chem.*, 39:2432–2433, 2000.

[91] B. Saha, S. M. W. Rahaman, A. Sinha, and J. K. Bera. Contrasting reactivity of 2-mesityl-1,8-naphthyridine (Mes–NP) with singly-bonded [RhII–RhII] and [RuI–RuI] compounds. *Aust. J. Chem.*, 64:583–589, 2011. 31

[92] J. D. Aguirre, D. A. Lutterman, A. M. Angeles-Boza, K. R. Dunbar, and C. Turro. Effect of axial coordination on the electronic structure and biological activity of dirhodium(II,II) complexes. *Inorg. Chem.*, 46:7494–7502, 2007. 31

[93] H. T. Chifotides, D. A. Lutterman, K. R. Dunbar, and C. Turro. Insight into the photoinduced ligand exchange reaction pathway of *cis*-$[Rh_2(O_2CCH_3)_2(CH_3CN)_6]^2+$ with a DNA model chelate. *Inorg. Chem.*, 50:12099–12107, 2011. 31

[94] H. T. Bonge and T. Hansen. Computational comparison of $Rh_2(esp)_2$ and $Rh_2(o_2ch)_4$ as catalysts in a carbenoid reaction. *Tetrahedron Lett.*, 51:5298–5301, 2010. 36

[95] H. T. Bonge and T. Hansen. Computational study of cyclopropanation reactions with halodiazoacetates. *J. Org. Chem.*, 75:2309–2320, 2010.

[96] L. R. Collins, M. van Gastel, F. Neese, and A. Fürstner. Enhanced electrophilicity of heterobimetallic Bi–Rh paddlewheel carbene complexes: A combined experimental, spectroscopic, and computational study. *J. Am. Chem. Soc.*, 140:13042–13055, 2018.

[97] G. Costantino, R. Rovito, A. Macchiarulo, and R. Pellicciari. Structure of metal-carbenoid intermediates derived from the dirhodium(II) tetracarboxylate mediated decomposition of α-diazocarbonyl compounds: A DFT study. *J. Mol. Struct.: THEOCHEM*, 581:111–115, 2002.

[98] M. P. Doyle, L. J. Westrum, W. N. E. Wolthuis, M. M. See, W. P. Boone, V. Bagheri, and M. M. Pearson. Electronic and steric control in carbon-hydrogen insertion reactions of diazoacetoacetates catalyzed by dirhodium(II) carboxylates and carboxamides. *J. Am. Chem. Soc.*, 115:958–964, 1993.

[99] J. Hansen, J. Autschbach, and H. M. L. Davies. Computational study on the selectivity of donor/acceptor-substituted rhodium carbenoids. *J. Org. Chem.*, 74:6555–6563, 2009.

[100] J. Hansen, B. Li, E. Dikarev, J. Autschbach, and H. M. L. Davies. Combined experimental and computational studies of heterobimetallic Bi–Rh paddlewheel

carboxylates as catalysts for metal carbenoid transformations. *J. Org. Chem.*, 74: 6564–6571, 2009. 36, 43

[101] E. Nakamura, N. Yoshikai, and M. Yamanaka. Mechanism of C-H bond activation/C-C bond formation reaction between diazo compound and alkane catalyzed by dirhodium tetracarboxylate. *J. Am. Chem. Soc.*, 124:7181–7192, 2002. 37

[102] S. C. A. H. Pierrefixe and F. M. Bickelhaupt. Hypervalence and the delocalizing versus localizing propensities of H^{-3}, Li^{-3}, CH^{-5} and SiH^{-5}. *Struct. Chem.*, 18:813–819, 2007. 39

[103] R. G. Pearson. Electronic spectra and chemical reactivity. *J. Am. Chem. Soc.*, 110: 2092, 1988. 39

[104] L. Dubicki and R. L. Martin. Metal-metal bond in binuclear rhodium(II) acetate monohydrate. *Inorg. Chem.*, 9:673, 1970. 42

[105] J. Norman, Joe G. and H. J. Kolari. Strength and *trans* influence of the rhodium-rhodium bond in rhodium(II) carboxylate dimers. *J. Am. Chem. Soc.*, 100:791, 1978. 42

[106] B. E. Bursten and F. A. Cotton. Electronic structure of phosphine adducts of tetrakis(carboxylato) dirhodium(II). Pronounced influence of axial ligands. *Inorg. Chem.*, 20:3042, 1981. 42

[107] T. Kawamura, K. Fukamachi, and S. Hayashida. ESR study of the cation radical of $Rh_2(O_2CEt)_4(pph_3)_2$; A σ electron radical. *J. Chem. Soc., Chem. Commun.*, page 945, 1979. 42

[108] T. Kawamura, K. Fukamachi, T. Sowa, S. Hayashida, and T. Yonezawa. Electronic structure of the rhodium-rhodium bond in $rh_2(O_2CR)_2(PY_3)_2$ by electron spin resonance study of their cation radicals. *J. Am. Chem. Soc.*, 103:364, 1981. 42

[109] P. Mougenot, J. Demuynck, and M. Benard. Diaquatetrakis(carboxylato)dirhodium(1+) $Rh_2(O_2CR)_4(H_2O)^{2+}$: Theoretical confirmation of the $\sigma^2\pi^4\delta^2\delta^{*2}\pi^{*3}$ ground state. *Chem. Phys. Lett.*, 136:279, 1987. 42

[110] H. Nakatsuji, J. Ushio, K. Kanda, Y. Onishi, T. Kawamura, and T. Yonezawa. Electronic structure of dirhodium tetracarboxylate complexes by the *ab initio* SCF MO method. *Chem. Phys. Lett.*, 79:299–304, 1981. 42

[111] F. A. Cotton, E. V. Dikarev, and X. Feng. Unligated dirhodium tetra(trifluoroacetate): Preparation, crystal structure and electronic structure. *Inorg. Chim. Acta*, 237:19–26, 1995. 42

[112] D. L. Lichtenberger, J. R. Pollard, M. A. Lynn, F. A. Cotton, and X. Feng. Metal-metal bonding in Rh_2(tfa): Extensive metal-ligand orbital mixing promoted by filled fluorine orbitals. *J. Am. Chem. Soc.*, 122:3182–3190, 2000. 42

[113] C. Werlé, R. Goddard, and A. Fürstner. The first crystal structure of a reactive dirhodium carbene complex and a versatile method for the preparation of gold carbenes by rhodium-to-gold transmetalation. *Angew. Chem., Int. Ed.*, 54:15452–15456, 2015. 43, 112

[114] H. K. Kisan and R. B. Sunoj. Axial coordination dichotomy in dirhodium carbenoid catalysis: A curious case of cooperative asymmetric dual-catalytic approach toward amino esters. *J. Org. Chem.*, 80:2192–2197, 2015. 44

[115] C. J. Laconsay, A. Pla-Quintana, and D. J. Tantillo. Effects of axial solvent coordination to dirhodium complexes on the reactivity and selectivity in C–H insertion reactions: A computational study. *Organometallics*, 2021. 44, 102

[116] D. T. Boruta, O. Dmitrenko, G. P. A. Yap, and J. M. Fox. Rh_2(*S*-PTTL)$_3$TPA-a mixed-ligand dirhodium(II) catalyst for enantioselective reactions of α-alkyl-α-diazo esters. *Chem. Sci.*, 3:1589–1593, 2012. 47, 48, 133, 134, 169

[117] A. DeAngelis, R. Panish, and J. M. Fox. Rh-catalyzed intermolecular reactions of α-alkyl-α-diazo carbonyl compounds with selectivity over β-hydride migration. *Acc. Chem. Res.*, 49:115–127, 2016. 47

[118] T. Goto, Y. Natori, K. Takeda, H. Nambu, and S. Hashimoto. Catalytic enantioselective C–H functionalization of indoles with α-diazopropionates using chiral dirhodium(II) carboxylates: Asymmetric synthesis of the (+)-α-methyl-3-indolylacetic acid fragment of acremoauxin A. *Tetrahedron: Asymmetry*, 22:907–915, 2011. 48

[119] R. A. Panish, S. R. Chintala, and J. M. Fox. Mixed-ligand chiral rhodium(II) catalyst enables the enantioselective total synthesis of piperarborenine B. *Angew. Chem., Int. Ed.*, 55:4983–4987, 2016. 48

[120] F. Estevan, P. Lahuerta, J. Perez-Prieto, I. Pereira, and S.-E. Stiriba. Reactivity and selectivity of *ortho*-metalated rhodium(II) complexes in C–H insertion reactions of α-diazo compounds. *Organometallics*, 17:3442–3447, 1998. 53

[121] P. Lahuerta, J. Perez-Prieto, S.-E. Stiriba, and M. A. Ubeda. Novel unsymmetrical *ortho*-metalated dirhodium(II) catalysts: Trans influence of the axial ligand. *Tetrahedron Lett.*, 40:1751–1754, 1999.

[122] D. F. Taber, S. C. Malcolm, K. Bieger, P. Lahuerta, M. Sanau, S.-E. Stiriba, J. Perez-Prieto, and M. A. Monge. Synthesis, structure, and reactivity of the first enantiomerically pure *ortho*-metalated rhodium(II) dimer. *J. Am. Chem. Soc.*, 121: 860–861, 1999. 53, 57

[123] M. Barberis, J. Perez-Prieto, P. Lahuerta, and M. Sanau. Enantiocontrol in the intermolecular cyclopropanation reaction catalyzed by dirhodium(II) complexes with ortho-metalated aryl phosphine ligands. *Chem. Commun.*, pages 439–440, 2001. 145

[124] F. Estevan, K. Herbst, P. Lahuerta, M. Barberis, and J. Perez-Prieto. Chiral dirhodium(II) catalysts with *ortho*-metalated aryl phosphine ligands: Synthesis and

application for enantioselective C–H insertion of α-diazo ketones. *Organometallics*, 20: 950–957, 2001.

[125] M. Barberis, J. Perez-Prieto, K. Herbst, and P. Lahuerta. Chiral dirhodium(II) catalysts with ortho-metalated arylphosphine ligands: Synthesis and application to the enantioselective cyclopropanation of α-diazo ketones. *Organometallics*, 21:1667–1673, 2002. 57

[126] P. Hirva, P. Lahuerta, and J. Perez-Prieto. Structural and electronic trends in *ortho*-metalated dirhodium(II) complexes. *Theor. Chem. Acc.*, 113:63–68, 2005. 53, 57

[127] A. J. Catino, R. E. Forslund, and M. P. Doyle. Dirhodium(II) caprolactamate: An exceptional catalyst for allylic oxidation. *J. Am. Chem. Soc.*, 126:13622–13623, 2004. 53

[128] M. P. Doyle, W. R. Winchester, J. A. A. Hoorn, V. Lynch, S. H. Simonsen, and R. Ghosh. Dirhodium(II) tetrakis(carboxamidates) with chiral ligands. structure and selectivity in catalytic metal-carbene transformations. *J. Am. Chem. Soc.*, 115:9968–9978, 1993. 57

[129] Y. Lou, M. Horikawa, R. A. Kloster, N. A. Hawryluk, and E. J. Corey. A new chiral Rh(II) catalyst for enantioselective [2 + 1]-cycloaddition. Mechanistic implications and applications. *J. Am. Chem. Soc.*, 126:8916–8918, 2004. 57, 62

[130] A. Caballero, A. Prieto, M. M. Diaz-Requejo, and P. J. Perez. Metal-catalyzed olefin cyclopropanation with ethyl diazoacetate: Control of the diastereoselectivity. *Eur. J. Inorg. Chem.*, pages 1137–1144, 2009. 57

[131] P. Hirva, J. Esteban, J. Lloret, P. Lahuerta, and J. Perez-Prieto. Determination of equilibrium constants and computational interaction energies for adducts of $[Rh_2(RCO_2)_4 - n(PC)_n]$ (n = 0-2) with Lewis bases. *Inorg. Chem.*, 46:2619–2626, 2007. 57

[132] N. McCarthy, M. A. McKervey, T. Ye, M. McCann, E. Murphy, and M. P. Doyle. A new rhodium(II) phosphate catalyst for diazo carbonyl reactions including asymmetric synthesis. *Tetrahedron Lett.*, 33:5983–5986, 1992. 57, 59

[133] M. C. Pirrung and J. Zhang. Asymmetric dipolar cycloaddition reactions of diazo compounds mediated by a binaphtholphosphate rhodium catalyst. *Tetrahedron Lett.*, 33:5987–5990, 1992. 57

[134] R. Hrdina, L. Guenee, D. Moraleda, and J. Lacour. Synthesis, structural analysis, and catalytic properties of tetrakis(binaphthyl or octahydrobinaphthyl phosphate) dirhodium(II,II) complexes. *Organometallics*, 32:473–479, 2013. 59

[135] D. M. Hodgson and S. Man. Synthesis of the anti-HIV agent (-)-hyperolactone C by using oxonium ylide formation-rearrangement. *Chem. - Eur. J.*, 17:9731–9737, 2011. 59

[136] J. M. Nichols, Y. Liu, P. Zavalij, L. Isaacs, and M. P. Doyle. Diphenylglycoluril as a novel ligand architecture for dirhodium(II) carboxamidates. *Inorg. Chim. Acta*, 361: 3309–3314, 2008. 62, 98

[137] H. K. A. C. Coolen, P. W. N. M. van Leeuwen, and R. J. M. Nolte. Synthesis and conformational behavior of rhodium(I) metallohosts derived from diphenylglycoluril. *J. Org. Chem.*, 61:4739–4747, 1996. 62

[138] V. S. I. Sprakel, M. C. Feiters, W. Meyer-Klaucke, M. Klopstra, J. Brinksma, B. L. Feringa, K. D. Karlin, and R. J. M. Nolte. Oxygen binding and activation by the complexes of PY^2- and TPA-appended diphenylglycoluril receptors with copper and other metals. *Dalton Trans.*, pages 3522–3534, 2005.

[139] R. Lee, Y. Yang, G. K. Tan, C.-H. Tan, and K.-W. Huang. A novel heteroleptic paddlewheel diruthenium bicyclic guanidinate complex: Synthesis, structure, and scope. *Dalton Trans.*, 39:723–725, 2010. 62

[140] D. E. Bergbreiter, M. Morvant, and B. Chen. Catalytic cyclopropanation with transition metal salts of soluble polyethylene carboxylates. *Tetrahedron Lett.*, 32:2731–2734, 1991. 65

[141] M. P. Doyle, M. Y. Eismont, D. E. Bergbreiter, and H. N. Gray. Enantioselective metal carbene transformations with polyethylene-bound soluble recoverable dirhodium(II) 2-pyrrolidone-5(S)-carboxylates. *J. Org. Chem.*, 57:6103–5, 1992. 65

[142] K. M. Chepiga, Y. Feng, N. A. Brunelli, C. W. Jones, and H. M. L. Davies. Silica-immobilized chiral dirhodium(II) catalyst for enantioselective carbenoid reactions. *Org. Lett.*, 15:6136–6139, 2013. 67

[143] H. M. L. Davies, P. Bruzinski, D. K. Hutcheson, N. Kong, and M. J. Fall. Asymmetric cyclopropanations by rhodium(II) N-(arylsulfonyl)prolinate catalyzed decomposition of vinyldiazomethanes in the presence of alkenes. Practical enantioselective synthesis of the four stereoisomers of 1-amino-2-phenylcyclopropanecarboxylic acid. *J. Am. Chem. Soc.*, 118:6897–6907, 1996. 67

[144] H. M. L. Davies, T. Hansen, J. Rutberg, and P. R. Bruzinski. Rhodium(II) (S)-N-(arylsulfonyl)prolinate catalyzed asymmetric insertions of vinyl- and phenylcarbenoids into the Si–H bond. *Tetrahedron Lett.*, 38:1741–1744, 1997. 96

[145] H. M. L. Davies. Dirhodium tetra(N-arylsulfonylprolinates) as chiral catalysts for asymmetric transformations of vinyl- and aryldiazoacetates. *Eur. J. Org. Chem.*, pages 2459–2469, 1999.

[146] H. M. L. Davies and C. Venkataramani. Dirhodium tetraprolinate-catalyzed asymmetric cyclopropanations with high turnover numbers. *Org. Lett.*, 5:1403–1406, 2003.

[147] H. M. L. Davies and G. H. Lee. Dirhodium(II) tetra(N-(dodecylbenzenesulfonyl)prolinate) catalyzed enantioselective cyclopropenation of alkynes. *Org. Lett.*, 6:1233–1236, 2004. 67

[148] E. G. Moschetta, S. Negretti, K. M. Chepiga, N. A. Brunelli, Y. Labreche, Y. Feng, F. Rezaei, R. P. Lively, W. J. Koros, H. M. L. Davies, and C. W. Jones. Composite polymer/oxide hollow fiber contactors: Versatile and scalable flow reactors for heterogeneous catalytic reactions in organic synthesis. *Angew. Chem., Int. Ed.*, 54: 6470–6474, 2015. 67

[149] C.-J. Yoo, D. Rackl, W. Liu, C. B. Hoyt, B. Pimentel, R. P. Lively, H. M. L. Davies, and C. W. Jones. An immobilized-dirhodium hollow-fiber flow reactor for scalable and sustainable C–H functionalization in continuous flow. *Angew. Chem., Int. Ed.*, 57: 10923–10927, 2018. 67, 70

[150] D. Rackl, C.-J. Yoo, C. W. Jones, and H. M. L. Davies. Synthesis of donor/acceptor-substituted diazo compounds in flow and their application in enantioselective dirhodium-catalyzed cyclopropanation and C–H functionalization. *Org. Lett.*, 19:3055–3058, 2017. 70

[151] P. Srivastava, H. Yang, K. Ellis-Guardiola, and J. C. Lewis. Engineering a dirhodium artificial metalloenzyme for selective olefin cyclopropanation. *Nat. Commun.*, 6:7789, 2015. 70, 72

[152] J. C. Lewis. Beyond the second coordination sphere: Engineering dirhodium artificial metalloenzymes to enable protein control of transition metal catalysis. *Acc. Chem. Res.*, 52:576–584, 2019. 70

[153] H. Yang, P. Srivastava, C. Zhang, and J. C. Lewis. A general method for artificial metalloenzyme formation through strain-promoted azide-alkyne cycloaddition. *ChemBioChem*, 15:223–227, 2014. 70

[154] J. Zhao, D. G. Bachmann, M. Lenz, D. G. Gillingham, and T. R. Ward. An artificial metalloenzyme for carbene transfer based on a biotinylated dirhodium anchored within streptavidin. *Catal. Sci. Technol.*, 8:2294–2298, 2018. 72

[155] R. Sambasivan, W. Zheng, S. J. Burya, B. V. Popp, C. Turro, C. Clementi, and Z. T. Ball. A tripodal peptide ligand for asymmetric Rh(II) catalysis highlights unique features of on-bead catalyst development. *Chem. Sci.*, 5:1401–1407, 2014. 72, 74, 133

[156] A. N. Zaykov and Z. T. Ball. Kinetic and stereoselectivity effects of phosphite ligands in dirhodium catalysis. *Tetrahedron*, 67:4397–4401, 2011. 72, 80, 86, 96, 133, 167

[157] R. Sambasivan and Z. T. Ball. Determination of orientational isomerism in rhodium(II) metallopeptides by pyrene fluorescence. *Org. Biomol. Chem.*, 10:8203–8206, 2012. 74

[158] T. D. Nelson, Z. J. Song, A. S. Thompson, M. Zhao, A. DeMarco, R. A. Reamer, M. F. Huntington, E. J. J. Grabowski, and P. J. Reider. Rhodium-carbenoid-mediated intermolecular O–H insertion reactions: A dramatic additive effect. Application in the synthesis of an ascomycin derivative. *Tetrahedron Lett.*, 41:1877–1881, 2000. 74, 86, 133, 167

[159] D. C. Wynne, M. M. Olmstead, and P. G. Jessop. Supercritical and liquid solvent effects on the enantioselectivity of asymmetric cyclopropanation with tetrakis[1-[(4-*tert*-butylphenyl)sulfonyl]-(2*S*)-pyrrolidinecarboxylate]dirhodium(II). *J. Am. Chem. Soc.*, 122:7638–7647, 2000. 76

[160] H. Saito, R. Iwai, T. Uchiyama, M. Miyake, and S. Miyairi. Chiral induction by cinchona alkaloids in the rhodium(II)-catalyzed O–H insertion reaction. *Chem. Pharm. Bull.*, 58:872–874, 2010. 76, 86

[161] D. Marcoux, S. Azzi, and A. B. Charette. $TfNH_2$ as achiral hydrogen-bond donor additive to enhance the selectivity of a transition metal catalyzed reaction. Highly enantio- and diastereoselective rhodium-catalyzed cyclopropanation of alkenes using α-cyano diazoacetamide. *J. Am. Chem. Soc.*, 131:6970–6972, 2009. 80

[162] H. Lebel, H. Piras, and J. Bartholomeues. Rhodium-catalyzed stereoselective amination of thioethers with *N*-mesyloxycarbamates. DMAP and bis(DMAP)CH_2Cl_2 as key additives. *Angew. Chem., Int. Ed.*, 53:7300–7304, 2014. 83, 86, 167

[163] D. Poggiali, A. Homberg, T. Lathion, C. Piguet, and J. Lacour. Kinetics of Rh(II)-catalyzed α-diazo-β-ketoester decomposition and application to the [3+6+3+6] synthesis of macrocycles on a large scale and at low catalyst loadings. *ACS Catal.*, 6: 4877–4881, 2016. 83, 127, 133

[164] V. N. G. Lindsay, C. Nicolas, and A. B. Charette. Asymmetric rh(II)-catalyzed cyclopropanation of alkenes with diacceptor diazo compounds: *p*-Methoxyphenyl ketone as a general stereoselectivity controlling group. *J. Am. Chem. Soc.*, 133:8972–8981, 2011. 86, 94, 133

[165] R. S. Drago, J. R. Long, and R. Cosmano. Comparison of the coordination chemistry and inductive transfer through the metal-metal bond in adducts of dirhodium and dimolybdenum carboxylates. *Inorg. Chem.*, 21:2196–2202, 1982. 86, 125, 133

[166] C. Bilgrien, R. S. Drago, G. C. Vogel, and J. Stahlbush. Trans influence across a rhodium-rhodium bond. Effect of a series of lewis bases on the stretching frequency of coordinated carbon monoxide. *Inorg. Chem.*, 25:2864–2866, 1986. 86, 94, 133

[167] L. Zhao, Y. Wang, Z. Ma, and Y. Wang. Dirhodium(II)-catalyzed carbonylation peroxidation of α,β-unsaturated esters: Mechanistic insight into the role of aryl aldehydes. *Inorg. Chem.*, 56:8166–8174, 2017. 86

[168] L. F. R. Gomes, A. F. Trindade, N. R. Candeias, P. M. P. Gois, and C. A. M. Afonso. Intramolecular C–H insertion using NHC-dirhodium(II) complexes: The influence of axial coordination. *Tetrahedron Lett.*, 49:7372–7375, 2008. 86, 94, 105, 133

[169] A. F. Trindade, P. M. P. Gois, L. F. Veiros, V. Andre, M. T. Duarte, C. A. M. Afonso, S. Caddick, and F. G. N. Cloke. Axial coordination of NHC ligands on dirhodium(II) complexes: Generation of a new family of catalysts. *J. Org. Chem.*, 73:4076–4086, 2008.

[170] L. F. R. Gomes, A. F. Trindade, N. R. Candeias, L. F. Veiros, P. M. P. Gois, and C. A. M. Afonso. Cyclization of diazoacetamides catalyzed by *N*-heterocyclic carbene dirhodium(II) complexes. *Synthesis*, pages 3519–3526, 2009. 133

[171] Q.-S. Ye, X.-N. Li, Y. Jin, J. Yu, Q.-W. Chang, J. Jiang, C.-X. Yan, J. Li, and W.-P. Liu. Synthesis, crystal structures and catalytic activity of tetrakis(acetato)dirhodium(II) complexes with axial picoline ligands. *Inorg. Chim. Acta*, 434:113–120, 2015. 86, 94

[172] W. Sheffield, A. Abshire, and A. Darko. Effect of tethered, axial thioether coordination on rhodium(II)-catalyzed silyl-hydrogen insertion. *Eur. J. Org. Chem.*, 2019:6347–6351, 2019. 88, 134, 138, 143, 148, 160, 167

[173] H. Jacobsen, H. B. Kraatz, T. Ziegler, and P. M. Boorman. A new look at an old ligand: Surprises with thioethers. A density functional study. *J. Am. Chem. Soc.*, 114: 7851–60, 1992. 90

[174] H. B. Kraatz, H. Jacobsen, T. Ziegler, and P. M. Boorman. π-acidity of thioethers and selenoethers: Truth or fiction? A comparative density functional study. *Organometallics*, 12:76–80, 1993. 90

[175] S. Rej and N. Chatani. Effect of sulfonamide and carboxamide ligands on the structural diversity of bimetallic Rh(II)–Rh(II) cores: Exploring the catalytic activity of these newly synthesized Rh_2 complexes. *Inorg. Chem.*, 60:3534–3538, 2021. 90

[176] R. S. Drago, J. R. Long, and R. Cosmano. Metal synergism in the coordination chemistry of a metal-metal bonded system: tetrakis(μ-butyrato)-dirhodium(II). *Inorg. Chem.*, 20:2920–7, 1981. 94, 133

[177] Z. Ma and Y. Wang. Dirhodium(II)/P(t-Bu)$_3$ catalyzed tandem reaction of α,β-unsaturated aldehydes with arylboronic acids. *Org. Biomol. Chem.*, 16:7470–7476, 2018. 94

[178] J. Tan, Y. Kuang, Y. Wang, Q. Huang, J. Zhu, and Y. Wang. Axial tri-*tert*-butylphosphane coordination to $Rh_2(OAc)_4$: Synthesis, structure, and catalytic studies. *Organometallics*, 35:3139–3147, 2016. 94

[179] X. Xu, P. Y. Zavalij, and M. P. Doyle. Catalytic asymmetric syntheses of quinolizidines by dirhodium-catalyzed dearomatization of isoquinolinium/pyridinium methylides-The role of catalyst and carbene source. *J. Am. Chem. Soc.*, 135:12439–12447, 2013. 94

[180] G. G. Christoph and Y. B. Koh. Metal-metal bonding in dirhodium tetracarboxylates. Trans influence and dependence of the rhodium-rhodium bond distance upon the nature of the axial ligands. *J. Am. Chem. Soc.*, 101:1422–34, 1979. 94

[181] A. Ford, H. Miel, A. Ring, C. N. Slattery, A. R. Maguire, and M. A. McKervey. Modern organic synthesis with α-diazocarbonyl compounds. *Chem. Rev.*, 115:9981–10080, 2015. 96

[182] V. Bagheri, M. P. Doyle, J. Taunton, and E. E. Claxton. A new and general synthesis of α-silyl carbonyl compounds by silicon-hydrogen insertion from transition metal-catalyzed reactions of diazo esters and diazo ketones. *J. Org. Chem.*, 53:6158–6160, 1988. 96

[183] R. Sambasivan and Z. T. Ball. Metallopeptides for asymmetric dirhodium catalysis. *J. Am. Chem. Soc.*, 132:9289–9291, 2010. 96

[184] J. Wu and J. S. Panek. Total synthesis of (-)-virginiamycin M2: Application of crotylsilanes accessed by enantioselective Rh(II) or Cu(i) promoted carbenoid Si–H insertion. *J. Org. Chem.*, 76:9900–9918, 2011.

[185] H. Keipour, V. Carreras, and T. Ollevier. Recent progress in the catalytic carbene insertion reactions into the silicon–hydrogen bond. *Org. Biomol. Chem.*, 15:5441–5456, 2017. 96, 112, 131

[186] C. Welch, Q. Tu, T. Wang, C. Raab, P. Wang, X. Jia, X. Bu, D. Bykowski, B. Hohenstaufen, and M. Doyle. Observations of rhodium-containing reaction

intermediates using HPLC with ICP-MS and ESI-MS detection. *Adv. Synth. Catal.*, 348:821–825, 2006. 98

[187] M. Q. Ahsan, I. Bernal, and J. L. Bear. Reaction of tetrakis(acetato)dirhodium with acetamide: crystal and molecular structure of tetrakis(acetamido)diaquadirhodium trihydrate. *Inorg. Chem.*, 25:260–265, 1986. 98

[188] P. Braunstein and F. Naud. Hemilability of hybrid ligands and the coordination chemistry of oxazoline-based systems. *Angew. Chem., Int. Ed.*, 40:680–699, 2001. 100

[189] Z. Qu, W. Shi, and J. Wang. A kinetic study on the pairwise competition reaction of α-diazo esters with rhodium(II) catalysts: Implication for the mechanism of rh(II)-carbene transfer. *J. Org. Chem.*, 66:8139–8144, 2001. 105

[190] H. M. L. Davies, T. Hansen, and M. R. Churchill. Catalytic asymmetric C–H activation of alkanes and tetrahydrofuran. *J. Am. Chem. Soc.*, 122:3063–3070, 2000. 107

[191] S. Muthusamy and M. Sivaguru. Atom-economical access to highly substituted indenes and furan-2-ones *via* tandem reaction of diazo compounds and propargyl alcohols. *Org. Lett.*, 16:4248–4251, 2014.

[192] T. Miyazaki, S. Kasai, Y. Ogiwara, and N. Sakai. Indium-catalyzed reductive sulfidation of esters by using thiols: An approach to the diverse synthesis of sulfides. *Eur. J. Org. Chem.*, 2016:1043–1049, 2016. 107

[193] Y. Z. Zhang, S.-F. Zhu, L.-X. Wang, and Q.-L. Zhou. Copper-catalyzed highly enantioselective carbenoid insertion into Si–H bonds. *Angew. Chem., Int. Ed.*, 47: 8496–8498, 2008. 109

[194] L. A. Dakin, P. C. Ong, J. S. Panek, R. J. Staples, and P. Stavropoulos. Speciation and mechanistic studies of chiral copper(I) Schiff base precursors mediating asymmetric carbenoid insertion reactions of diazoacetates into the Si–H bond of silanes. *Organometallics*, 19:2896–2908, 2000. 109

[195] M. J. Frisch, G. W. Trucks, H. B. Schlegel, G. E. Scuseria, M. A. Robb, J. R. Cheeseman, G. Scalmani, V. Barone, G. A. Petersson, H. Nakatsuji, X. Li, M. Caricato, A. V. Marenich, J. Bloino, B. G. Janesko, R. Gomperts, B. Mennucci, H. P. Hratchian, J. V. Ortiz, A. F. Izmaylov, J. L. Sonnenberg, F. Williamsand Ding, F. Lipparini, F. Egidi, J. Goings, B. Peng, A. Petrone, T. Henderson, D. Ranasinghe, V. G. Zakrzewski, J. Gao, N. Rega, G. Zheng, W. Liang, M. Hada, M. Ehara, K. Toyota, R. Fukuda, J. Hasegawa, M. Ishida, T. Nakajima, Y. Honda, O. Kitao, H. Nakai, T. Vreven, K. Throssell, J. A. Montgomery Jr., J. E. Peralta, F. Ogliaro, M. J. Bearpark, J. J. Heyd, E. N. Brothers, K. N. Kudin, V. N. Staroverov, T. A. Keith, R. Kobayashi, J. Normand, K. Raghavachari, A. P. Rendell, J. C. Burant, S. S. Iyengar, J. Tomasi, M. Cossi, J. M. Millam, M. Klene, C. Adamo, R. Cammi, J. W. Ochterski, R. L. Martin, K. Morokuma, O. Farkas, J. B. Foresman, and D. J. Fox. Gaussian 09 rev. a.02, 2009. 110, 162

[196] R. Paulissen, H. Reimlinger, E. Hayez, A. J. Hubert, and P. Teyssie. Transition metal catalyzed reactions of diazo compounds. II. insertion in the hydroxylic bond. *Tetrahedron Lett.*, page 2233, 1973. 112, 131

[197] K. M. Chepiga, C. Qin, J. S. Alford, S. Chennamadhavuni, T. M. Gregg, J. P. Olson, and H. M. L. Davies. Guide to enantioselective dirhodium(II)-catalyzed cyclopropanation with aryldiazoacetates. *Tetrahedron*, 69:5765–5771, 2013.

[198] D. Gillingham and N. Fei. Catalytic X–H insertion reactions based on carbenoids. *Chem. Soc. Rev.*, 42:4918–4931, 2013.

[199] Y. Pang, Q. He, Z.-Q. Li, J.-M. Yang, J.-H. Yu, S.-F. Zhu, and Q.-L. Zhou. Rhodium-catalyzed B–H bond insertion reactions of unstabilized diazo compounds generated *in situ* from tosylhydrazones. *J. Am. Chem. Soc.*, 140:10663–10668, 2018. 131

[200] D. Zhu, L. Chen, H. Fan, Q. Yao, and S. Zhu. Recent progress on donor and donor-donor carbenes. *Chem. Soc. Rev.*, 49:908–950, 2020. 112, 118

[201] S. P. Green, K. M. Wheelhouse, A. D. Payne, J. P. Hallett, P. W. Miller, and J. A. Bull. Thermal stability and explosive hazard assessment of diazo compounds and diazo transfer reagents. *Org. Process Res. Dev.*, 24:67–84, 2020. 112

[202] C. Werle, R. Goddard, P. Philipps, C. Fares, and A. Fürstner. Structures of reactive donor/acceptor and donor/donor rhodium carbenes in the solid state and their implications for catalysis. *J. Am. Chem. Soc.*, 138:3797–3805, 2016. 116

[203] Z. Liu, K. Raveendra Babu, F. Wang, Y. Yang, and X. Bi. Influence of sulfonyl substituents on the decomposition of *N*-sulfonylhydrazones at room temperature. *Org. Chem. Front.*, 6:121–124, 2019. 116

[204] M. Ghavre. Bamford-Stevens and Shapiro reactions in organic synthesis. *Asian J. Org. Chem.*, 9:1901–1923, 2020. 116

[205] P. Anbarasan, D. Yadagiri, and S. Rajasekar. Recent advances in transition-metal-catalyzed denitrogenative transformations of 1,2,3-triazoles and related compounds. *Synthesis*, 46:3004–3023, 2014. 118

[206] Z. Liu, Q. Li, Y. Yang, and X. Bi. Silver(I)-promoted insertion into X–H (X = Si, Sn, and Ge) bonds with *N*-nosylhydrazones. *Chem. Commun.*, 53:2503–2506, 2017. 118, 123, 128, 129

[207] E.-H. Wang, Y.-J. Ping, Z.-R. Li, H. Qin, Z.-J. Xu, and C.-M. Che. Iron porphyrin catalyzed insertion reaction of *N*-tosylhydrazone-derived carbenes into X–H (X = Si, Sn, Ge) bonds. *Org. Lett.*, 20:4641–4644, 2018. 118, 129

[208] Z. Liu, J. Huo, T. Fu, H. Tan, F. Ye, M. L. Hossain, and J. Wang. Palladium(0)-catalyzed C(sp^3)–Si bond formation *via* formal carbene insertion into a Si–H bond. *Chem. Commun.*, 54:11419–11422, 2018. 118

[209] J. R. Jagannathan, J. C. Fettinger, J. T. Shaw, and A. K. Franz. Enantioselective Si–H insertion reactions of diarylcarbenes for the synthesis of silicon-stereogenic silanes. *J. Am. Chem. Soc.*, 142:11674–11679, 2020. 118

[210] L.-L. Yang, D. Evans, B. Xu, W.-T. Li, M.-L. Li, S.-F. Zhu, K. N. Houk, and Q.-L. Zhou. Enantioselective diarylcarbene insertion into Si–H bonds induced by electronic properties of the carbenes. *J. Am. Chem. Soc.*, 142:12394–12399, 2020. 122

[211] L.-L. Yang, J. Ouyang, H.-N. Zou, S.-F. Zhu, and Q.-L. Zhou. Enantioselective insertion of alkynyl carbenes into Si–H bonds: An efficient access to chiral propargylsilanes and allenylsilanes. *J. Am. Chem. Soc.*, 143:6401–6406, 2021. 122

[212] Y. Yang, B. Lu, G. Xu, and X. Wang. Overcoming O–H insertion to para-selective C–H functionalization of free phenols: Rh(II)/Xantphos catalyzed geminal-difunctionalization of diazo compounds. *ACS Cent. Sci.*, 8:581–589, 2022. 125

[213] K. Das, K. M. Kadish, and J. L. Bear. Substituent and solvent effects on the electrochemical properties of tetra-μ-carboxylato-dirhodium(II). *Inorg. Chem.*, 17: 930, 1978. 125, 133, 145

[214] M. Y. Chavan, T. P. Zhu, X. Q. Lin, M. Q. Ahsan, J. L. Bear, and K. M. Kadish. Axial-ligand-dependent electrochemical and spectral properties of a series of acetate- and acetamidate-bridged dirhodium complexes. *Inorg. Chem.*, 23:4538, 1984. 125, 133, 148

[215] Z. Du, Z. Chen, Z. Chen, X. Yu, and W. Hu. Dirhodium-catalyzed enantioselective C–H insertion of *N*-(2-benzyloxyethyl)-*N*-(*tert*-butyl)diazoacetamide and its application for the synthesis of chiral GABOB. *Chirality*, 16:516–519, 2004. 127

[216] W.-J. Liu, Z.-L. Chen, Z.-Y. Chen, and W.-H. Hu. Dirhodium catalyzed intramolecular enantioselective C–H insertion reaction of *N*-cumyl-*N*-(2-*p*-anisylethyl)diazoacetamide: synthesis of (-)-rolipram. *Tetrahedron: Asymmetry*, 16: 1693–1698, 2005. 127

[217] W. Zeghida, C. Besnard, and J. Lacour. Rhodium(II)-catalyzed one-pot four-component synthesis of functionalized polyether macrocycles at high concentration. *Angew. Chem., Int. Ed.*, 49:7253–7256, 2010. 127

[218] Y. Li, Z. Huang, X. Wu, P.-F. Xu, J. Jin, Y. Zhang, and J. Wang. Rh(II)-catalyzed [2,3]-sigmatropic rearrangement of sulfur ylides derived from *N*-tosylhydrazones and sulfides. *Tetrahedron*, 68:5234–5240, 2012. 127

[219] P. Q. Le and J. A. May. Hydrazone-initiated carbene/alkyne cascades to form polycyclic products: Ring-fused cyclopropenes as mechanistic intermediates. *J. Am. Chem. Soc.*, 137:12219–12222, 2015.

[220] R. Lingayya, M. Vellakkaran, K. Nagaiah, and J. B. Nanubolu. Rhodium(II)-catalyzed carbenoid insertion of *N*-tosylhydrazones into amide N-H bonds: An efficient approach to *N*3-benzyl/alkyl-2-arylquinazolinones. *Adv. Synth. Catal.*, 358:81–89, 2016.

[221] F. Medina, C. Besnard, and J. Lacour. One-step synthesis of nitrogen-containing medium-sized rings *via* α-imino diazo intermediates. *Org. Lett.*, 16:3232–3235, 2014.

[222] N. Su, J. A. Theorell, D. J. Wink, and T. G. Driver. Copper-catalyzed formation of α-alkoxycycloalkenones from *N*-tosylhydrazones. *Angew. Chem., Int. Ed.*, 54:12942–12946, 2015. 127

[223] H.-G. Cheng, L.-Q. Lu, T. Wang, J.-R. Chen, and W.-J. Xiao. Design of chiral sulfoxide-Schiff base hybrids and their application in Cu-catalyzed asymmetric Henry reactions. *Chem. Commun.*, 48:5596–5598, 2012. 128, 175

[224] J. H. Hansen, B. T. Parr, P. Pelphrey, Q. Jin, J. Autschbach, and H. M. L. Davies. Rhodium(II)-catalyzed cross-coupling of diazo compounds. *Angew. Chem., Int. Ed.*, 50:2544, 2011. 131

[225] H. M. L. Davies, L. M. Hodges, J. J. Matasi, T. Hansen, and D. G. Stafford. Effect of carbenoid structure on the reactivity of rhodium-stabilized carbenoids. *Tetrahedron Lett.*, 39:4417–4420, 1998. 131

[226] I. Dragutan, V. Dragutan, and F. Verpoort. Carbenoid transfer in competing reactions catalyzed by ruthenium complexes. *Appl. Organomet. Chem.*, 28:211–215, 2014. 131

[227] X. Liu, J. Liu, J. Zhao, S. Li, and C.-C. Li. Toward the total synthesis of eurifoloid A. *Org. Lett.*, 19:2742–2745, 2017. 131

[228] S. Miah, A. M. Z. Slawin, C. J. Moody, S. M. Sheehan, J. Marino, Joseph P., M. A. Semones, A. Padwa, and I. C. Richards. Ligand effects in the rhodium(II) catalyzed reactions of diazoamides and diazoimides. *Tetrahedron*, 52:2489, 1996. 133

[229] P. Panne and J. M. Fox. Rh-catalyzed intermolecular reactions of alkynes with α-diazoesters that possess β-hydrogens: Ligand-based control over divergent pathways. *J. Am. Chem. Soc.*, 129:22–23, 2007. 133

[230] R. S. Drago, S. P. Tanner, R. M. Richman, and J. R. Long. Quantitative studies of chemical reactivity of tetra-μ-butyrato-dirhodium(II) complexes. *J. Am. Chem. Soc.*, 101:2897, 1979. 133

[231] H. M. L. Davies and A. M. Walji. Asymmetric intermolecular C–H activation, using immobilized dirhodium tetrakis((*S*)-*N*-(dodecylbenzenesulfonyl)-prolinate) as a recoverable catalyst. *Org. Lett.*, 5:479–482, 2003. 133

[232] S. C. Martin, F. Vohidov, H. Wang, S. E. Knudsen, A. A. Marzec, and Z. T. Ball. Designing selectivity in dirhodium metallopeptide catalysts for protein modification. *Bioconjugate Chem.*, 28:659–665, 2017. 133

[233] R. P. Wurz and A. B. Charette. Transition metal-catalyzed cyclopropanation of alkenes in water: Catalyst efficiency and *in situ* generation of the diazo reagent. *Org. Lett.*, 4: 4531–4533, 2002. 134

[234] M. P. Doyle, C. E. Raab, G. H. P. Roos, V. Lynch, and S. H. Simonsen. (4,0)-dirhodium(II) tetrakis[methyl 1-acetyl-2-oxoimidazolidine-4(*S*)-carboxylate]. Implications for the mechanism of ligand exchange reactions. *Inorg. Chim. Acta*, 266:13–18, 1997. 134

[235] O. F. Gonzalez-Belman, Y. Varela, M. Flores-Alamo, K. Wrobel, S. Gutierrez-Granados, J. M. Peralta-Hernandez, J. O. C. Jimenez-Halla, and O. Serrano.

Microwave-assisted synthesis and characterization of $[Rh_2(OAc)_4(L)_2]$ paddlewheel complexes: A joint experimental and computational study. *Int. J. Inorg. Chem.*, pages 1–12, 2017. 136

[236] G. F. Keaney and J. L. Wood. Rhodium perfluorobutyramide ($Rh_2(pfm)_4$): A synthetically useful catalyst for olefin aziridination. *Tetrahedron Lett.*, 46:4031–4034, 2005. 136

[237] S. A. Johnson, H. R. Hunt, and H. M. Neumann. Preparation and properties of anhydrous rhodium(II) acetate and some adducts thereof. *Inorg. Chem.*, 2:960, 1963. 136

[238] M. M. Major, G. Roevid, S. Balogh, A. Benyei, G. Lendvay, D. Frigyes, J. Bakos, and G. Farkas. Double stereoselective coordination of chiral N,S ligands: Synthesis, coordination chemistry and utilization in Pd-catalyzed allylic alkylation. *Appl. Organomet. Chem.*, 33:1–14, 2019. 138

[239] D.-H. Bao, H.-L. Wu, C.-L. Liu, J.-H. Xie, and Q.-L. Zhou. Development of chiral spiro P–N–S ligands for iridium-catalyzed asymmetric hydrogenation of β-alkyl-β-ketoesters. *Angew. Chem., Int. Ed.*, 54, 2015.

[240] M. J. Page, J. Wagler, and B. A. Messerle. Pyridine-2,6-bis(thioether) (SNS) complexes of ruthenium as catalysts for transfer hydrogenation. *Organometallics*, 29:3790–3798, 2010.

[241] A. M. Masdeu-Bulto, M. Dieguez, E. Martin, and M. Gomez. Chiral thioether ligands: Coordination chemistry and asymmetric catalysis. *Coord. Chem. Rev.*, 242:159–201, 2003. 138

[242] P. Pelphrey, J. Hansen, and H. M. L. Davies. Solvent-free catalytic enantioselective C–C bond forming reactions with very high catalyst turnover numbers. *Chem. Sci.*, 1: 254–257, 2010. 143

[243] M. P. Doyle, M. Protopopova, P. Muller, D. Ene, and E. A. Shapiro. Effective uses of dirhodium(II) tetrakis[methyl 2-oxopyrrolidine-5(R or S)-carboxylate] for highly enantioselective intermolecular cyclopropenation reactions. *J. Am. Chem. Soc.*, 116: 8492, 1994. 145

[244] N. Watanabe, H. Matsuda, H. Kuribayashi, and S.-i. Hashimoto. Dirhodium(II) tetrakis[3(S)-phthalimido-2-piperidinonate]: A novel dirhodium(II) carboxamidate catalyst for asymmetric cyclopropanation. *Heterocycles*, 42:537, 1996. 145

[245] E. Nakamura, N. Yoshikai, and M. Yamanaka. Mechanism of C–H bond activation/C–C bond formation reaction between diazo compound and alkane catalyzed by dirhodium tetracarboxylate. *J. Am. Chem. Soc.*, 124:7181–7192, 2002. 148

[246] L. R. Collins, M. van Gastel, F. Neese, and A. Fürstner. Enhanced electrophilicity of heterobimetallic Bi–Rh paddlewheel carbene complexes: A combined experimental, spectroscopic, and computational study. *J. Am. Chem. Soc.*, 140:13042–13055, 2018. 151

[247] P. J. Mohan, V. P. Georgiev, and J. E. McGrady. Periodic trends in electron transport through extended metal atom chains: Comparison of $Ru_3(dpa)_4(NCS)_2$ with its first-row analogues. *Chem. Sci.*, 3:1319–1329, 2012. 151

[248] Z. Ren, T. L. Sunderland, C. Tortoreto, T. Yang, J. F. Berry, D. G. Musaev, and H. M. L. Davies. Comparison of reactivity and enantioselectivity between chiral bimetallic catalysts: Bismuth-rhodium and dirhodium-catalyzed carbene chemistry. *ACS Catal.*, 8:10676–10682, 2018. 151

[249] D. T. Nowlan, T. M. Gregg, H. M. L. Davies, and D. A. Singleton. Isotope effects and the nature of selectivity in rhodium-catalyzed cyclopropanations. *J. Am. Chem. Soc.*, 125:15902–15911, 2003. 151, 152

[250] M. P. Sibi, D. Rutherford, P. A. Renhowe, and B. Li. Investigations of a nucleophilic alaninol synthon derived from serine. *J. Am. Chem. Soc.*, 121:7509–7516, 1999. 158

[251] G. S. Basarab, M. R. Gowravaram, S. I. Hauck, and F. Zhou. Preparation of spiro[oxazino[4,3-a]isoxazolo[4,5-g]quinoline-pyrimidine]trione compounds and methods for treating bacterial infections, 2014. 158

[252] D.-R. Hou, J. H. Reibenspies, and K. Burgess. New, optically active phosphine oxazoline (JM-phos) ligands: Syntheses and applications in allylation reactions. *J. Org. Chem.*, 66:206–215, 2001. 158

[253] M.-R. Sun, H.-L. Li, M.-Y. Ba, W. Cheng, H.-L. Zhu, and Y.-T. Duan. Cyclopropyl scaffold: A generalist for marketed drugs. *Mini-Rev. Med. Chem.*, 21:150–170, 2021. 165

[254] T. T. Talele. The "cyclopropyl fragment" is a versatile player that frequently appears in preclinical/clinical drug molecules. *J. Med. Chem.*, 59:8712–8756, 2016. 165

[255] J. Börgel and T. Ritter. Late-stage functionalization. *Chem*, 6:1877–1887, 2020. 165

[256] J. W. Herndon. The chemistry of the carbon-transition metal double and triple bond: Annual survey covering the year 2018. *Coord. Chem. Rev.*, 401:213051, 2019. 165

[257] G. T. Gurmessa and G. S. Singh. Recent progress in insertion and cyclopropanation reactions of metal carbenoids from α-diazocarbonyl compounds. *Res. Chem. Intermed.*, 43:6447–6504, 2017.

[258] A. Abshire, D. Moore, J. Courtney, and A. Darko. Heteroleptic dirhodium(II,II) paddlewheel complexes as carbene transfer catalysts. *Org. Biomol. Chem.*, 19:8886–8905, 2021. 165

[259] G. Bartoli, G. Bencivenni, and R. Dalpozzo. Asymmetric cyclopropanation reactions. *Synthesis*, 46:979–1029, 2014. 165

[260] K. Liao, Y.-F. Yang, Y. Li, J. N. Sanders, K. N. Houk, D. G. Musaev, and H. M. L. Davies. Design of catalysts for site-selective and enantioselective functionalization of non-activated primary C–H bonds. *Nat. Chem.*, 10:1048–1055, 2018. 167

[261] C. Qin, V. Boyarskikh, J. H. Hansen, K. I. Hardcastle, D. G. Musaev, and H. M. L. Davies. D_2-symmetric dirhodium catalyst derived from a 1,2,2-triarylcyclopropanecarboxylate ligand: Design, synthesis and application. *J. Am. Chem. Soc.*, 133:19198–19204, 2011. 167

[262] D. Marcoux and A. B. Charette. *trans*-directing ability of amide groups in cyclopropanation: Application to the asymmetric cyclopropanation of alkenes with diazo reagents bearing two carboxy groups. *Angew. Chem., Int. Ed.*, 47:10155–10158, 2008. 167

[263] D. Cressy, C. Zavala, A. Abshire, W. Sheffield, and A. Darko. Tuning Rh(II)-catalysed cyclopropanation with tethered thioether ligands. *Dalton Trans.*, 49:15779–15787, 2020. 167

[264] F. G. Adly, J. Maddalena, and A. Ghanem. $Rh_2(S\text{-}1,2\text{-}NTTL)_4$: A novel $Rh_2(S\text{-}PTTL)_4$ analog with lower ligand symmetry for asymmetric synthesis of chiral cyclopropylphosphonates. *Chirality*, 26:764–774, 2014. 171

[265] F. G. Adly, M. G. Gardiner, and A. Ghanem. Design and synthesis of novel chiral dirhodium(II) carboxylate complexes for asymmetric cyclopropanation reactions. *Chem. - Eur. J.*, 22:3447–3461, 2016. 171, 174

[266] M. Anada, S. Kitagaki, and S. Hashimoto. Double stereodifferentiation in intramolecular C–H insertion reaction toward the synthesis of 1β-methylcarbapenem antibiotics. *Heterocycles*, 52:875–883, 2000. 174

[267] H. Tsutsui, M. Matsuura, K. Makino, S. Nakamura, M. Nakajima, S. Kitagaki, and S. Hashimoto. Enantioselective tandem formation and [2,3]-sigmatropic rearrangement of cyclic propargylic oxonium ylides catalyzed by dirhodium(II) tetrakis[*N*-phthaloyl-(*S*)-*tert*-leucinate]. *Isr. J. Chem.*, 41:283–295, 2002. 174

[268] X. Li, N. Chen, and J. Xu. An improved and mild Wenker synthesis of aziridines. *Synthesis*, pages 3423–3428, 2010. 175

[269] J. Wu, X.-L. Hou, and L.-X. Dai. An efficient procedure for cleavage of aziridines with various thiols promoted by $ZnCl_2$. *J. Chem. Soc., Perkin Trans. 1*, pages 1314–1317, 2001. 175

[270] H. Keipour, A. Jalba, L. Delage-Laurin, and T. Ollevier. Copper-catalyzed carbenoid insertion reactions of α-diazoesters and α-diazoketones into Si–H and S-H bonds. *J. Org. Chem.*, 82:3000–3010, 2017. 175

Appendices

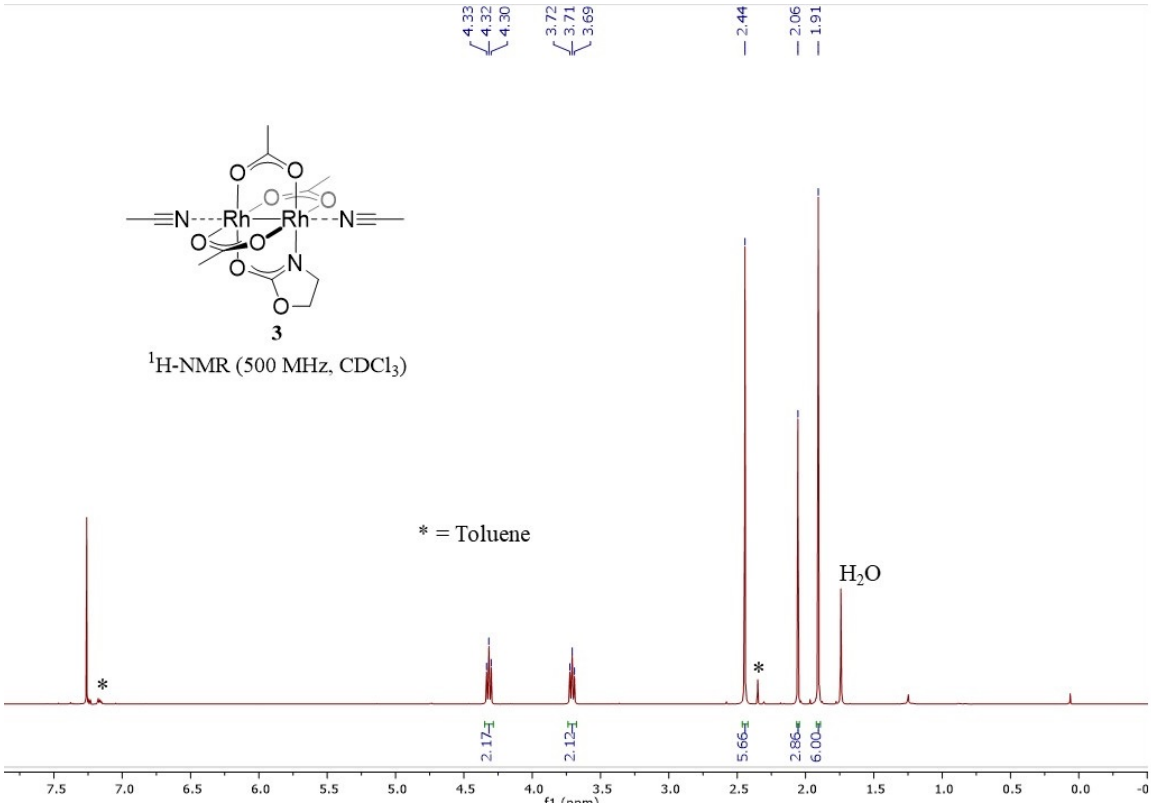

Figure 1: ^{1}H NMR of complex 89.

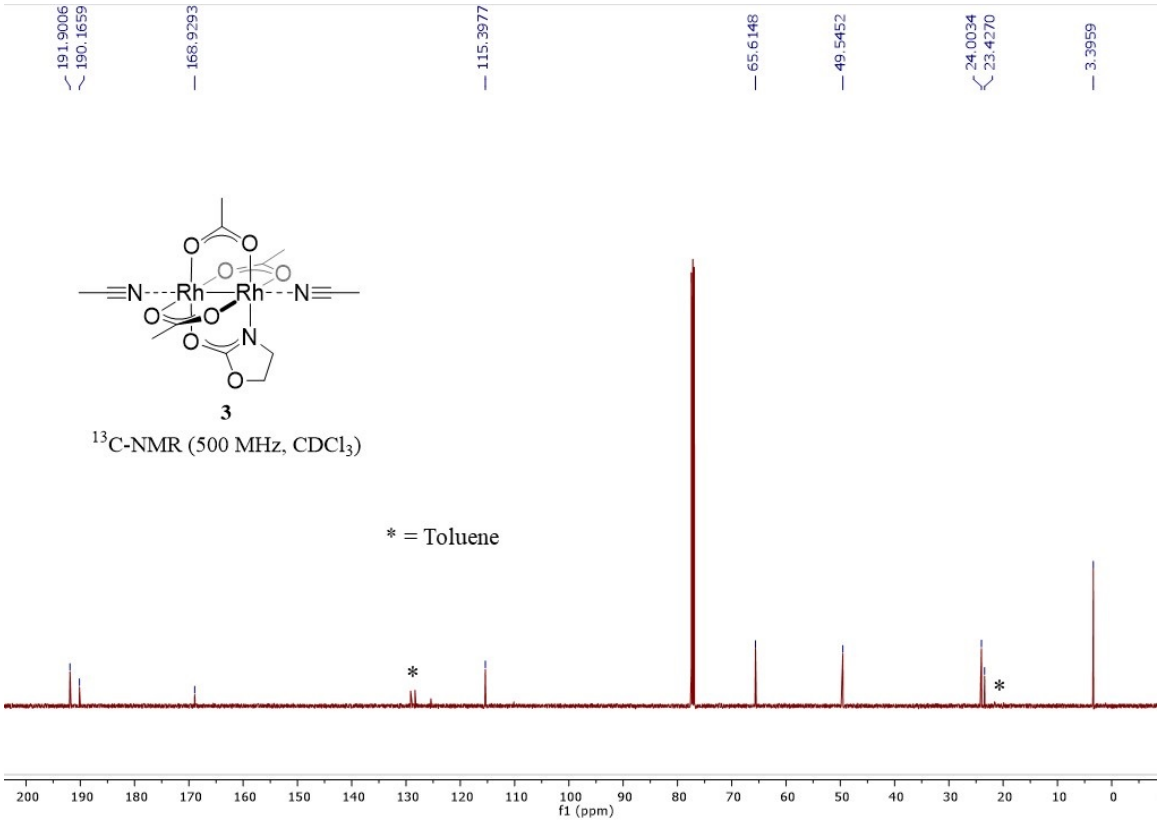

Figure 2: ^{13}C NMR of complex 89.

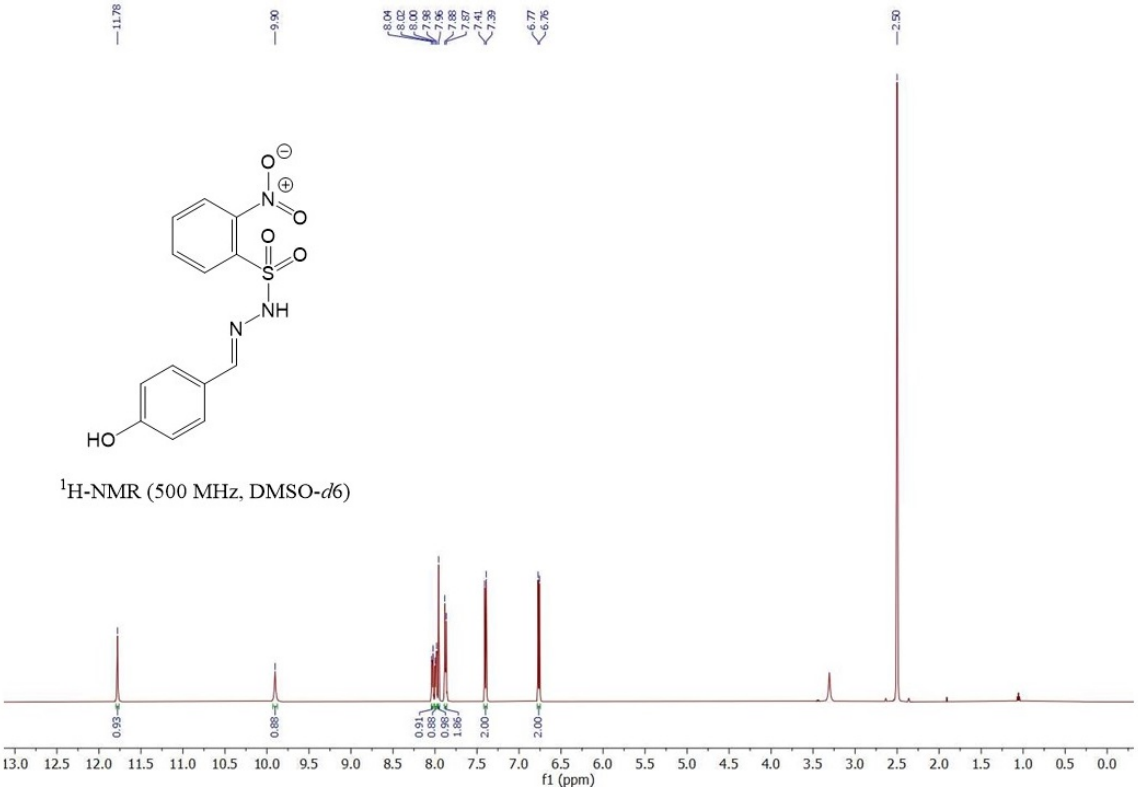

Figure 3: ^{1}H NMR of complex 104c.

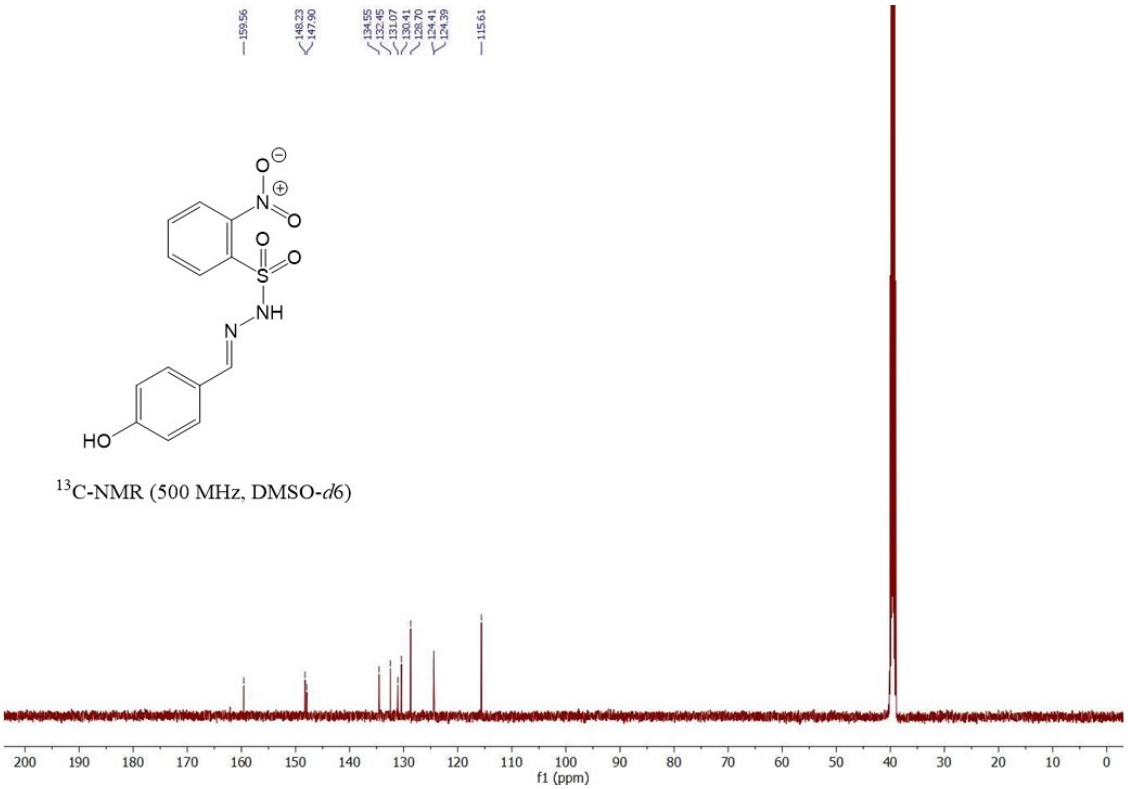

Figure 4: ^{13}C NMR of complex 104c.

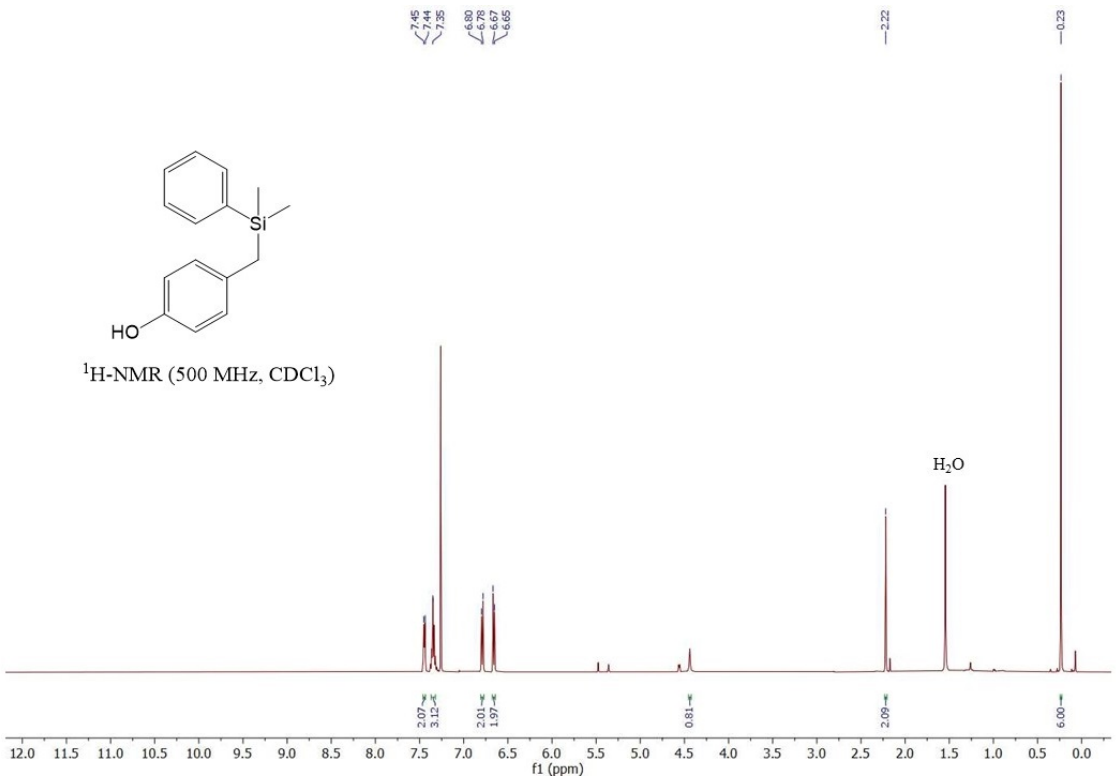

Figure 5: ^{1}H NMR of complex 105c.

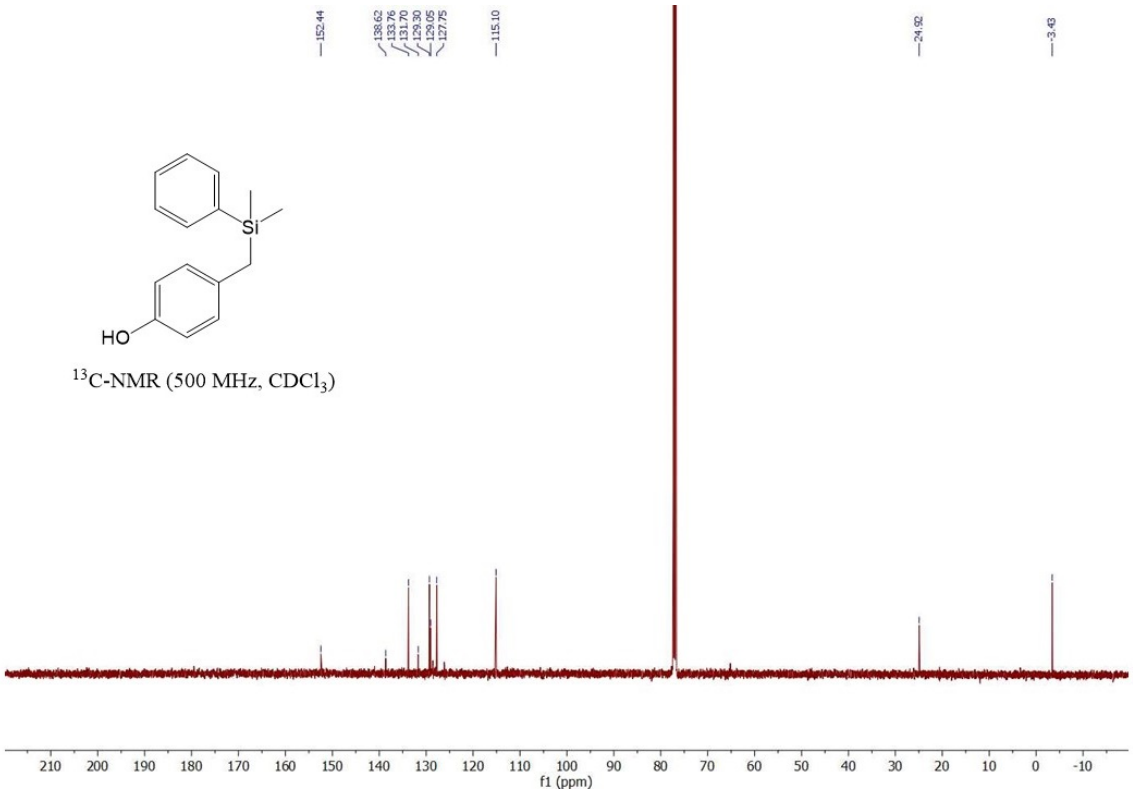

Figure 6: ^{13}C NMR of complex 105c.

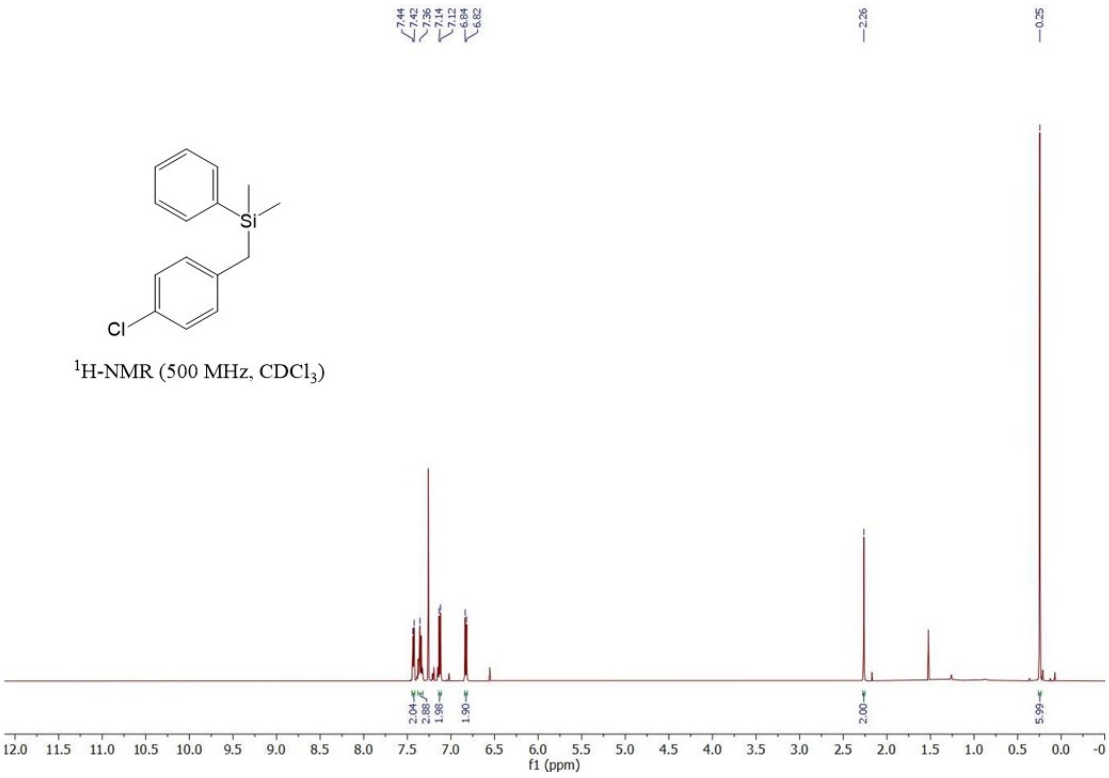

Figure 7: ^{1}H NMR of complex 105f.

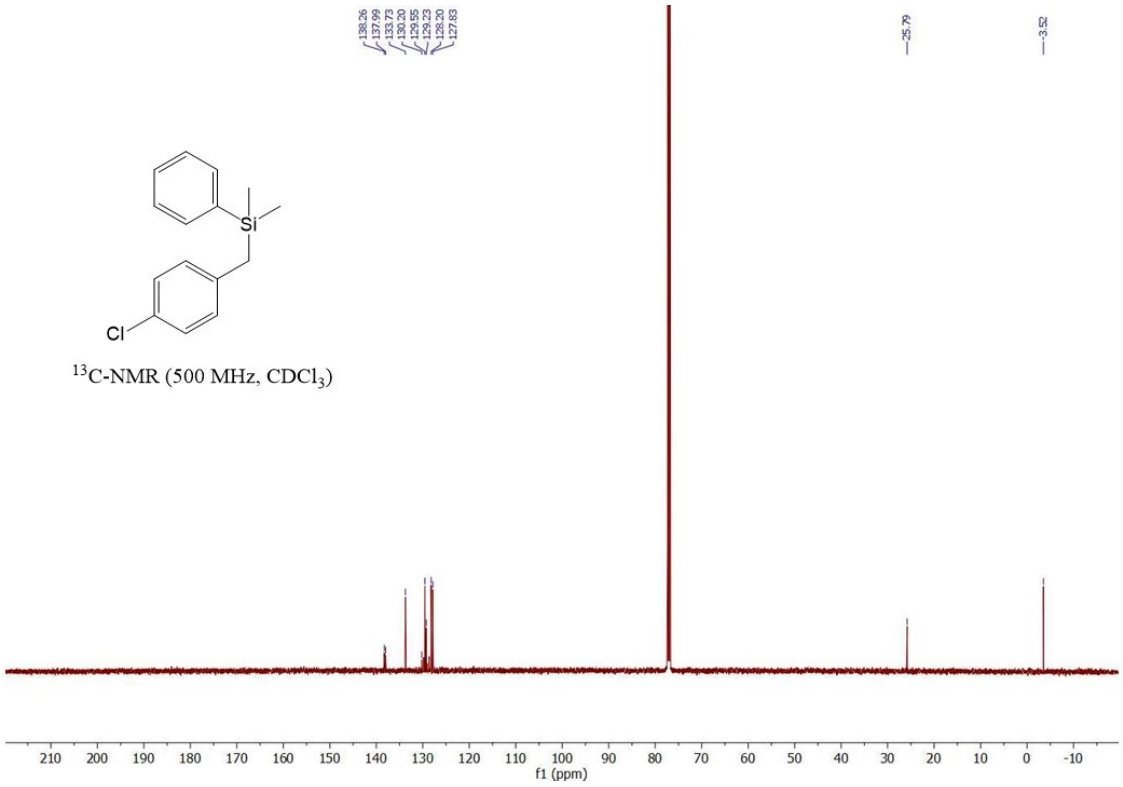

Figure 8: ^{13}C NMR of complex 105f.

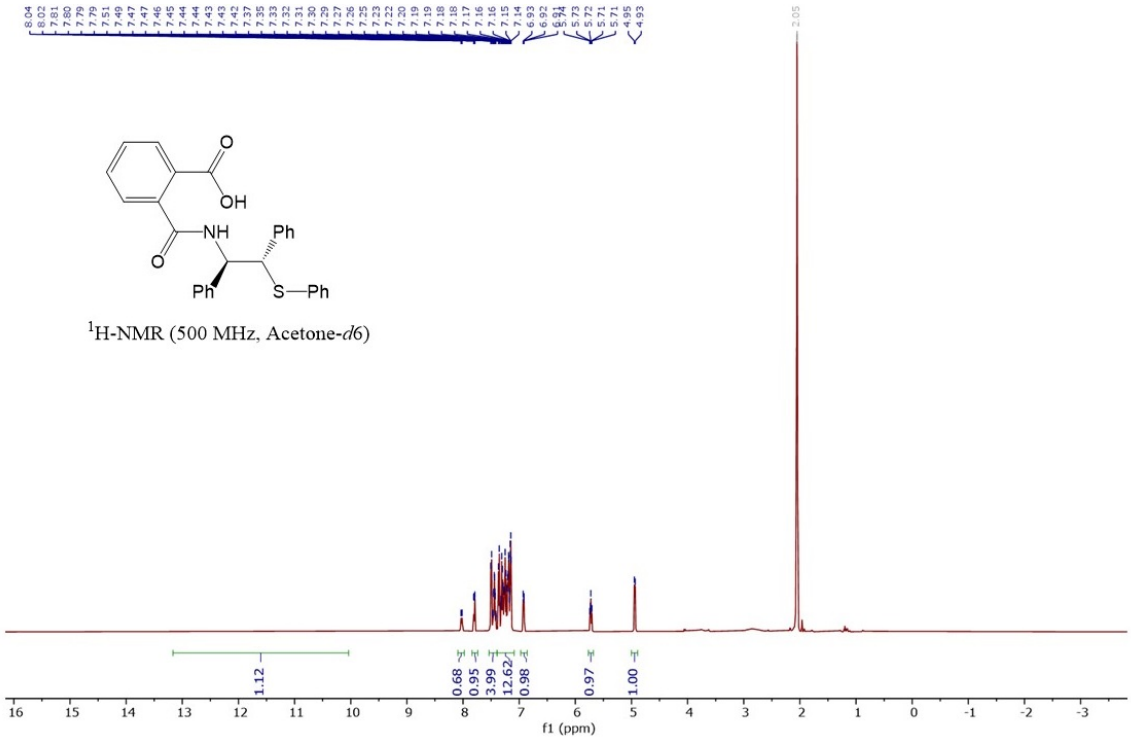

Figure 9: ^{1}H NMR of compound 121.

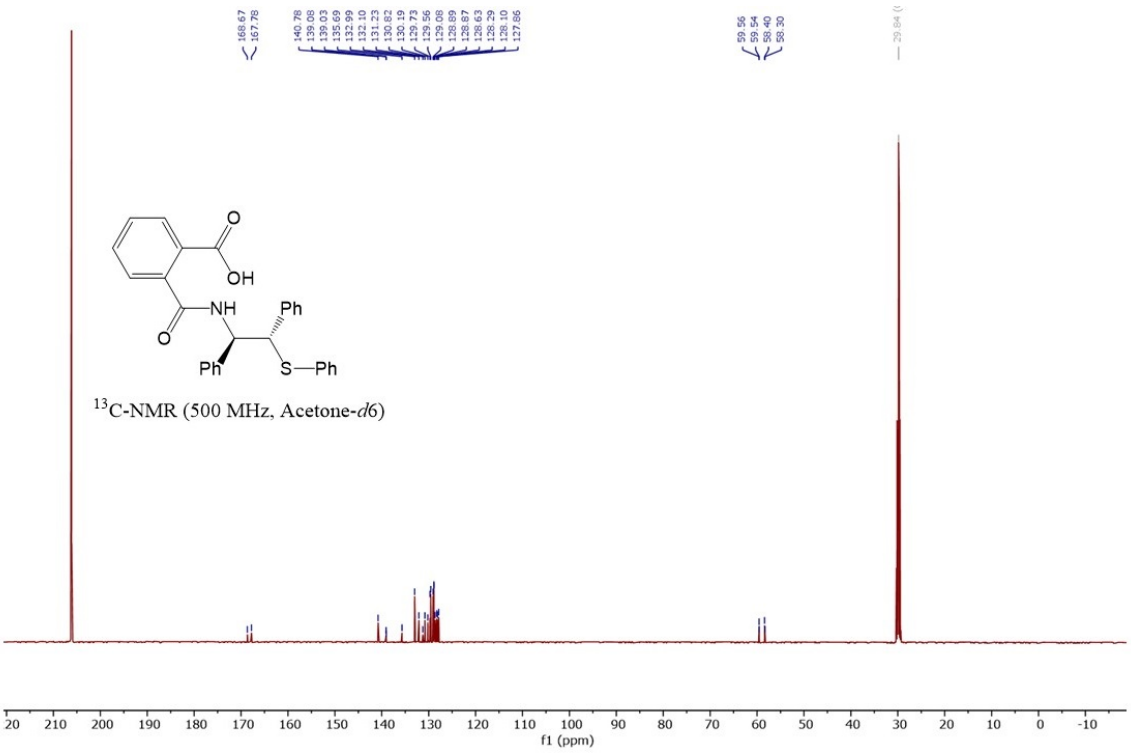

Figure 10: ^{13}C NMR of compound 121.

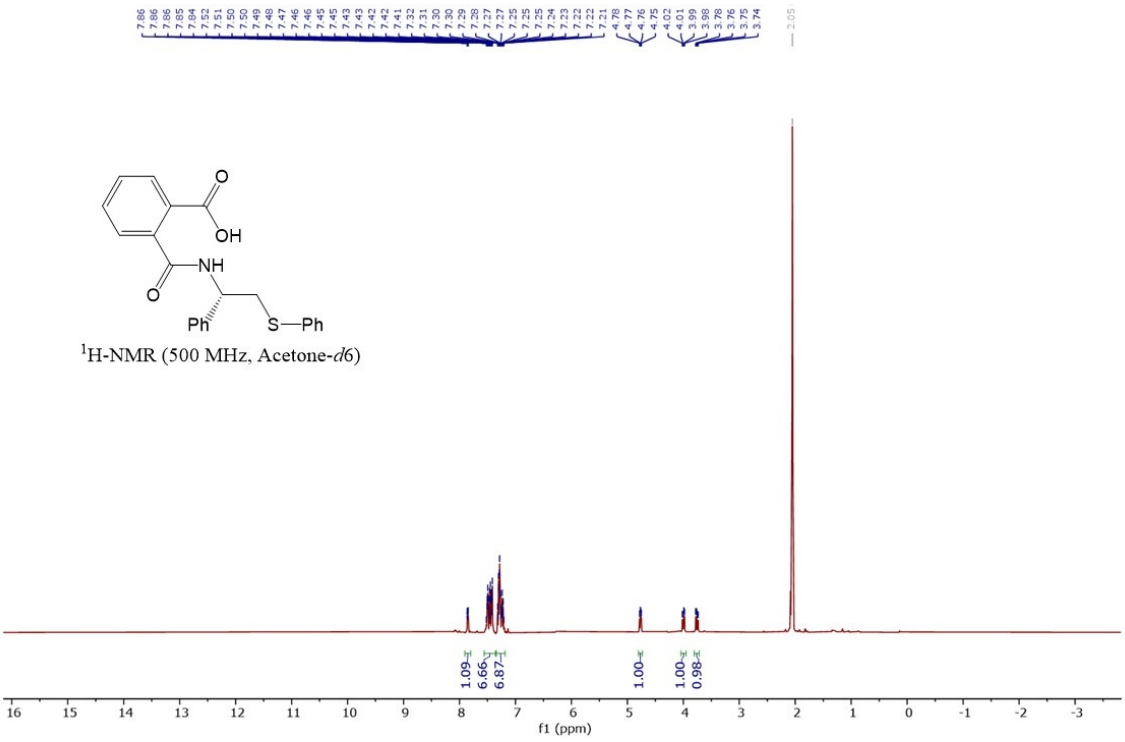

Figure 11: ^{1}H NMR of complex 126.

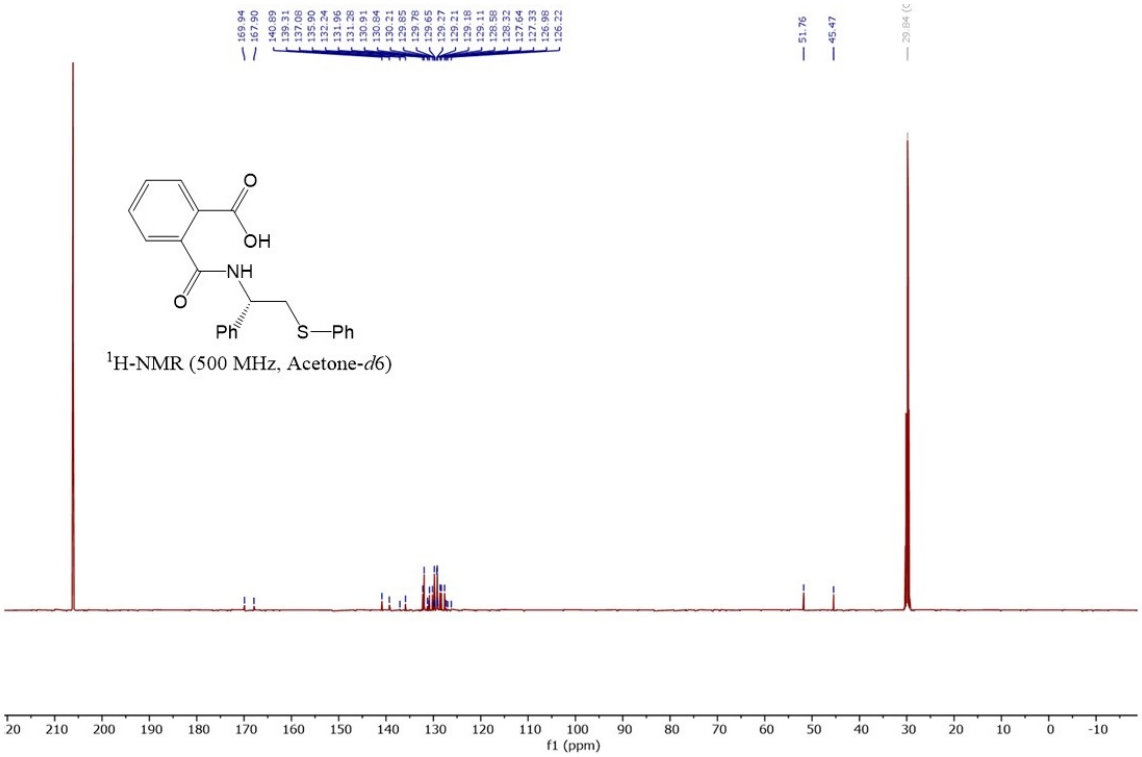

Figure 12: ^{13}C NMR of complex 126.

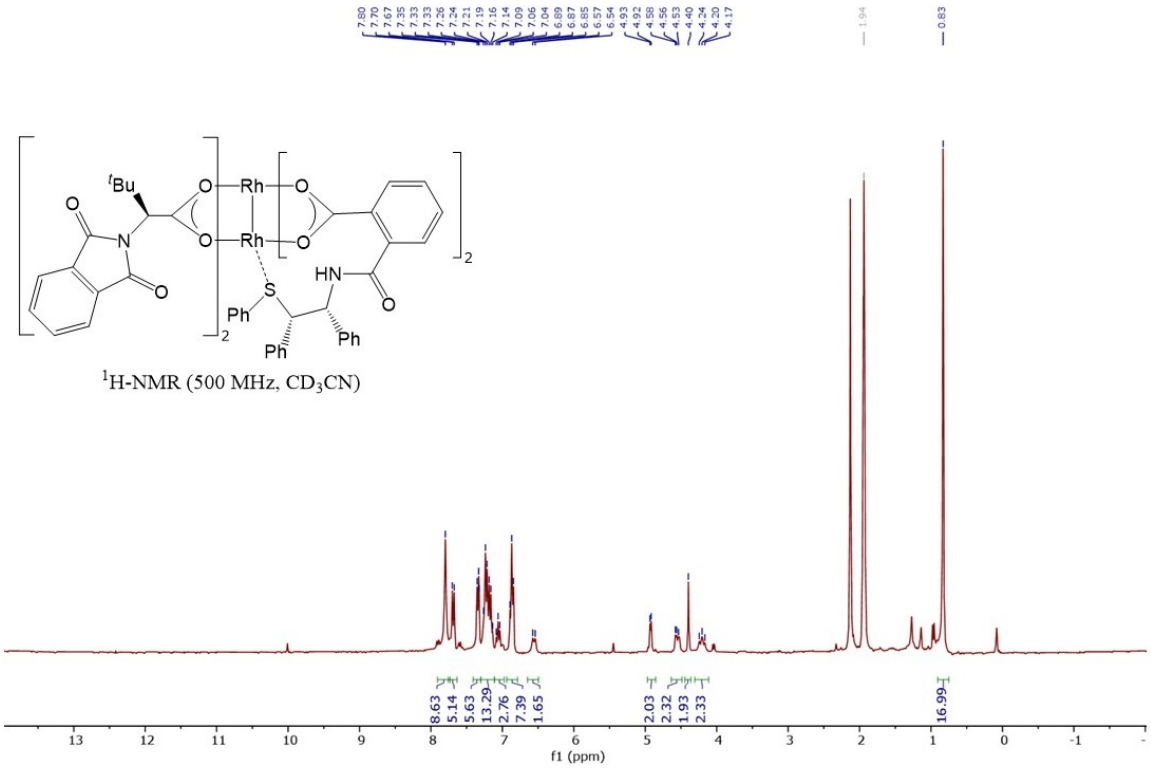

Figure 13: ^{13}C NMR of complex 127a/b.

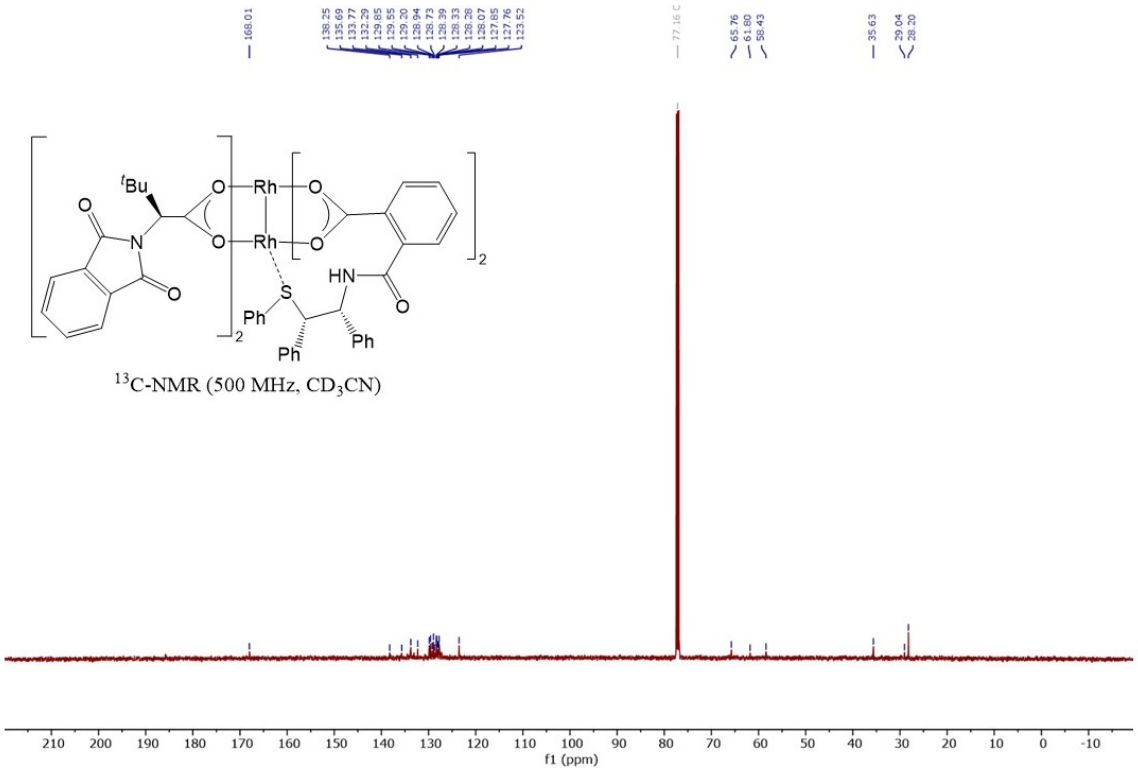

Figure 14: ^{1}H NMR of complex 127a/b.

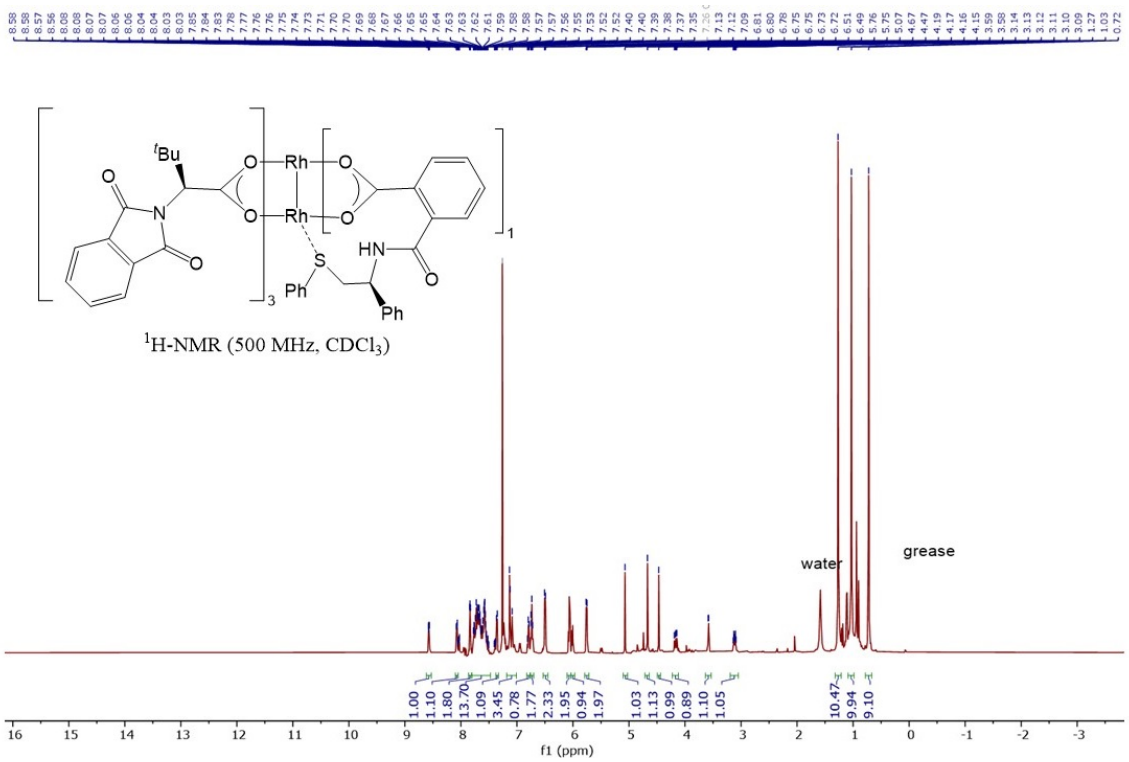

Figure 15: ^{1}H NMR of complex 128.

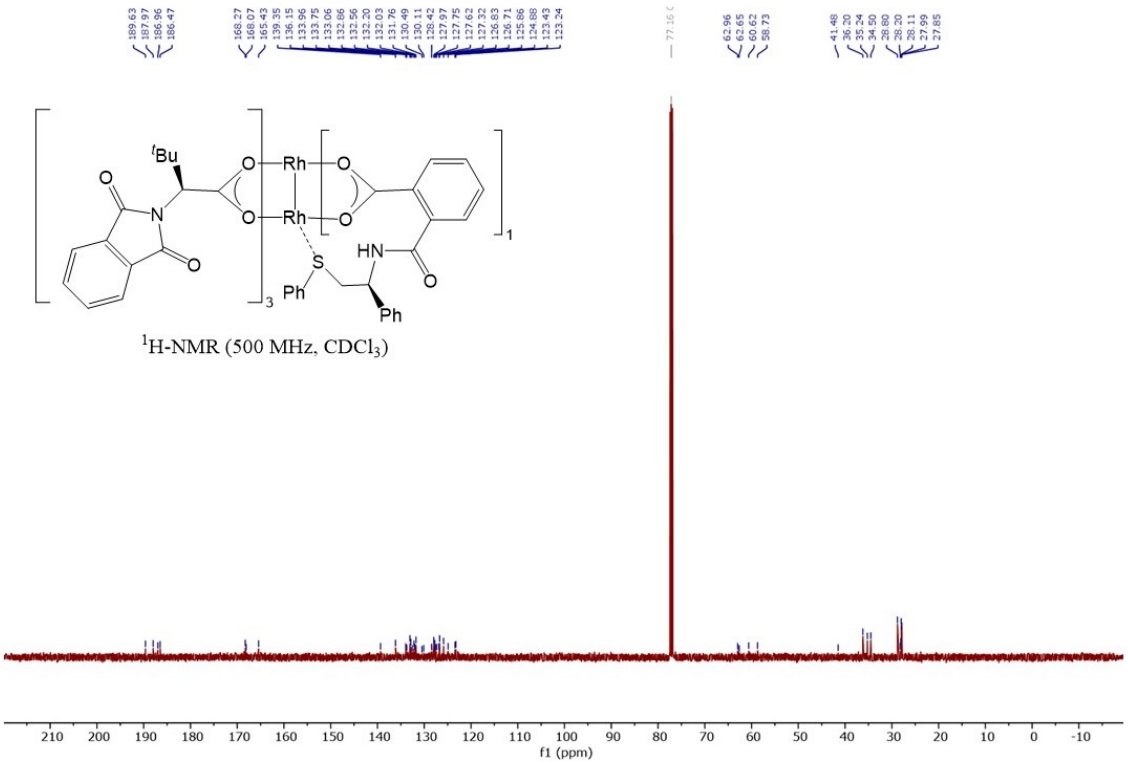

Figure 16: ^{13}C NMR of complex 128.

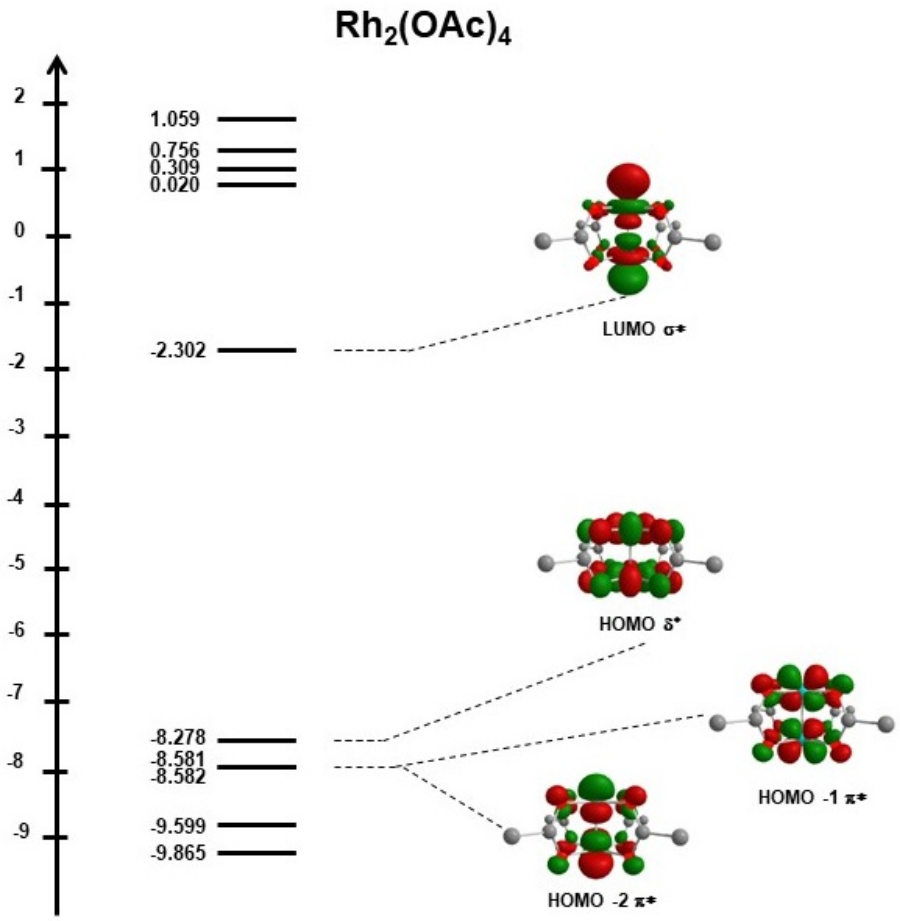

Figure 17: Molecular orbital diagram of 3

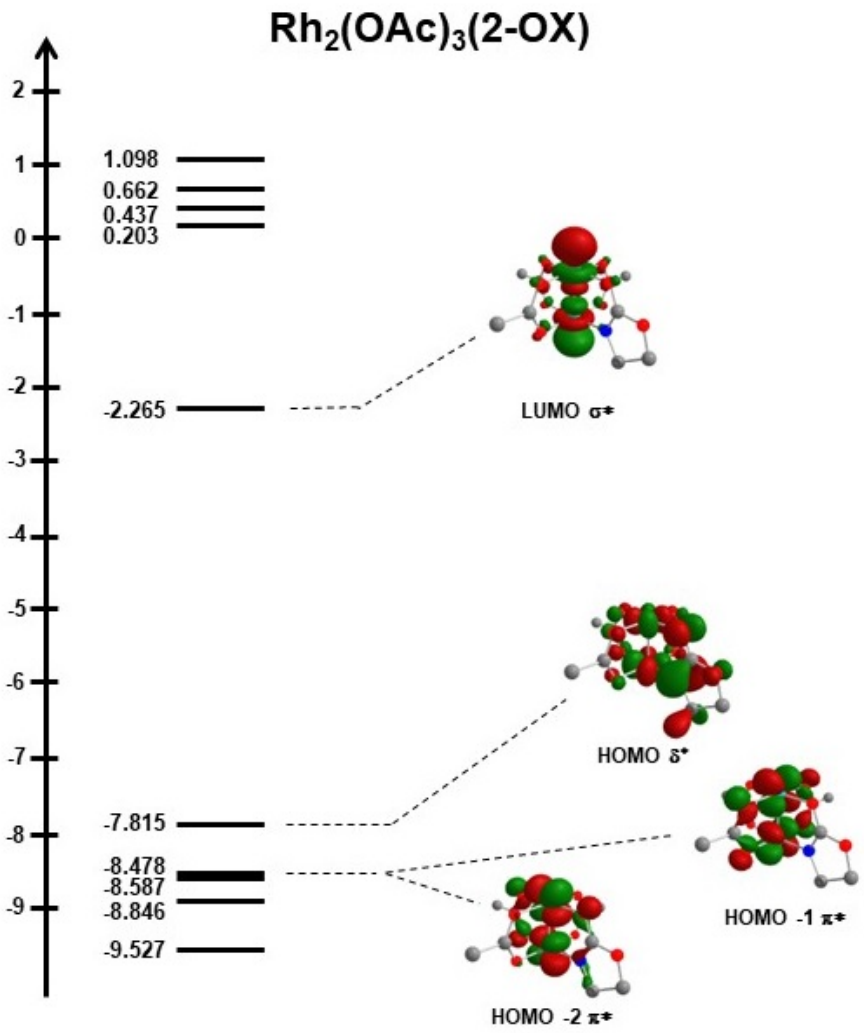

Figure 18: Molecular orbital diagram of 89

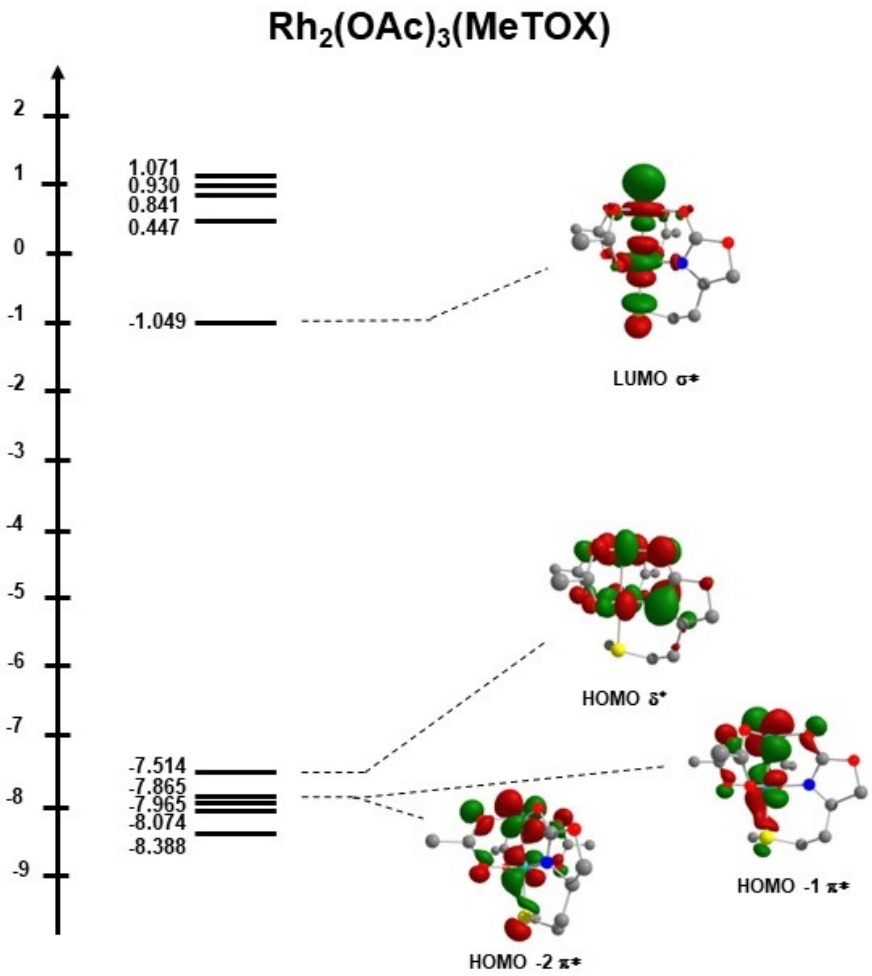

Figure 19: Molecular orbital diagram of 87

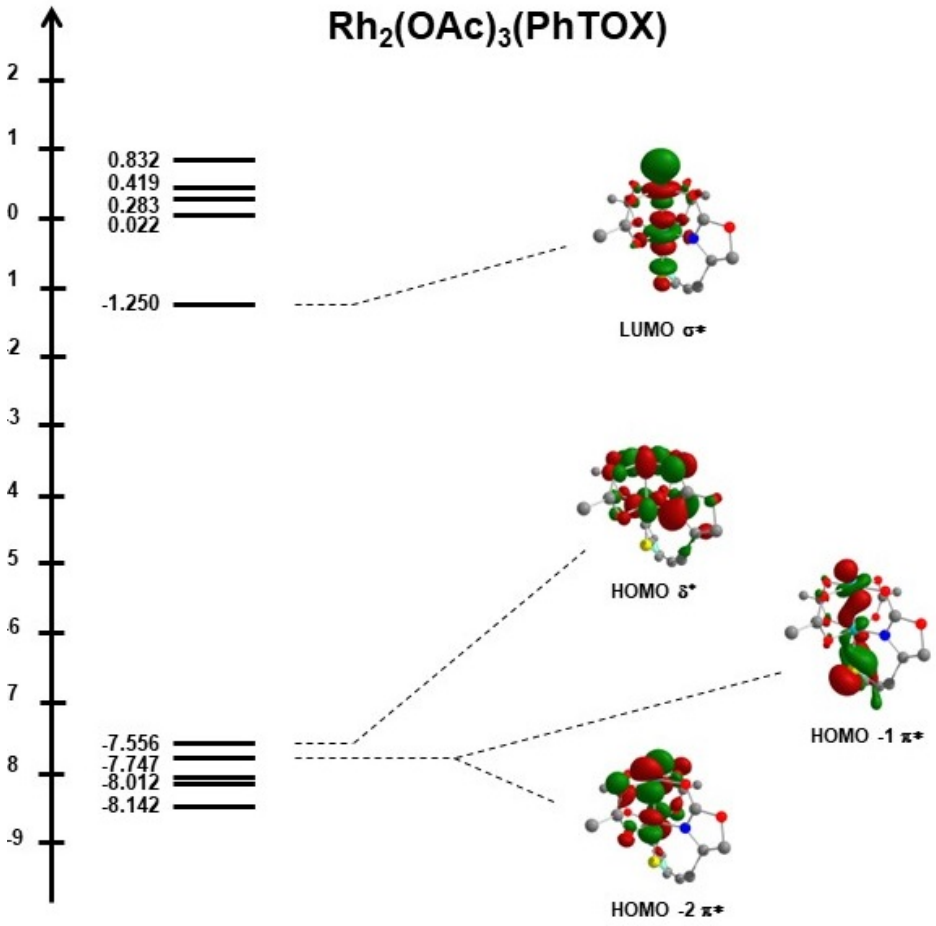

Figure 20: Molecular orbital diagram of 107

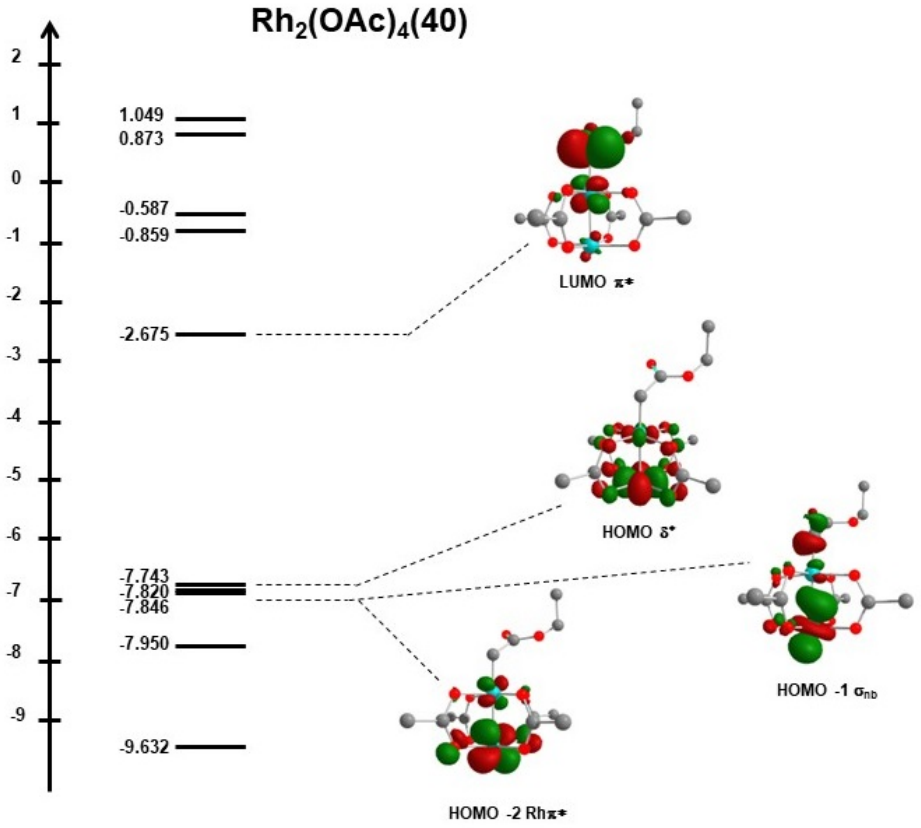

Figure 21: Molecular orbital diagram of carbenoid formed from 3 and 40

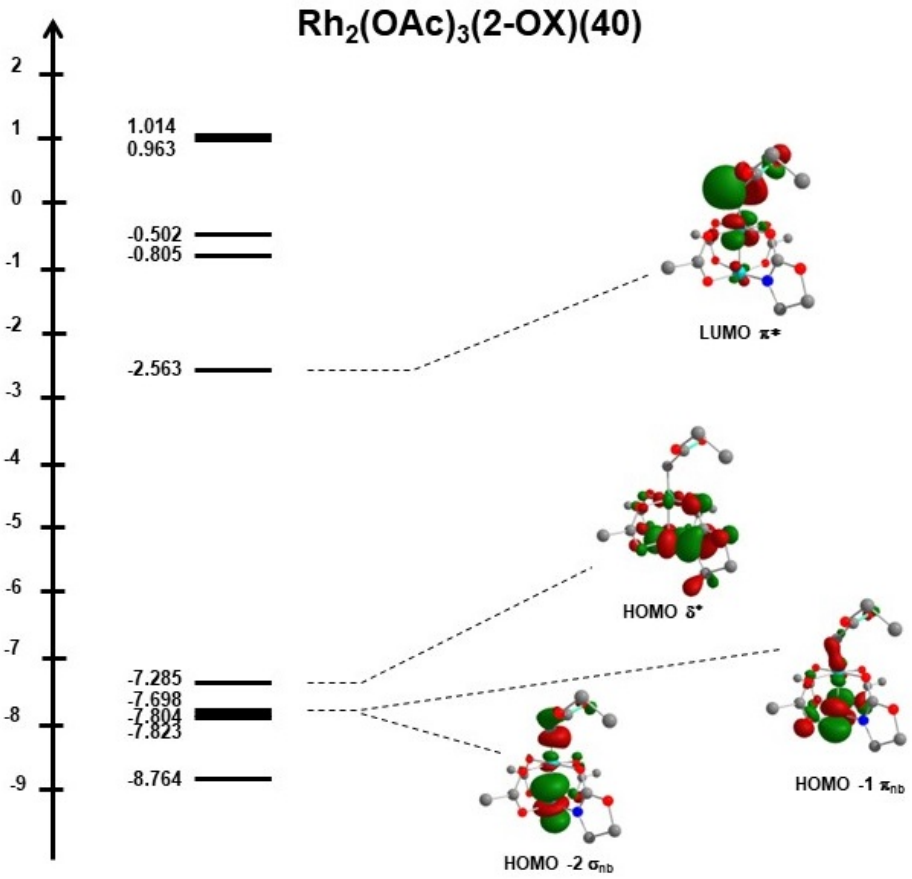

Figure 22: Molecular orbital diagram of carbenoid formed from 89 and 40

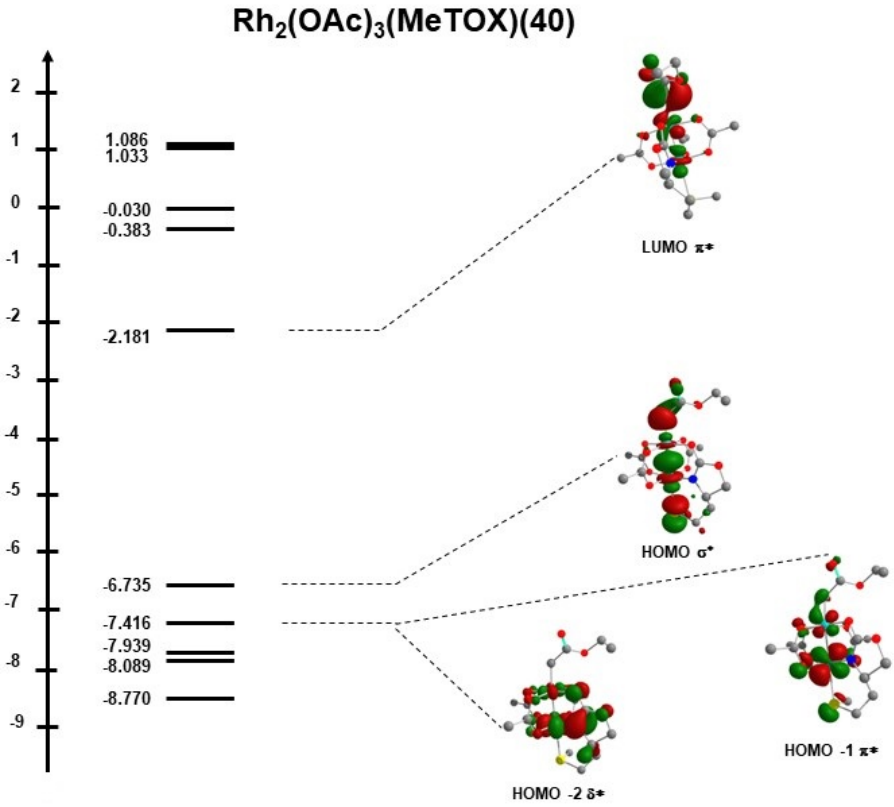

Figure 23: Molecular orbital diagram of carbenoid formed from 87 and 40

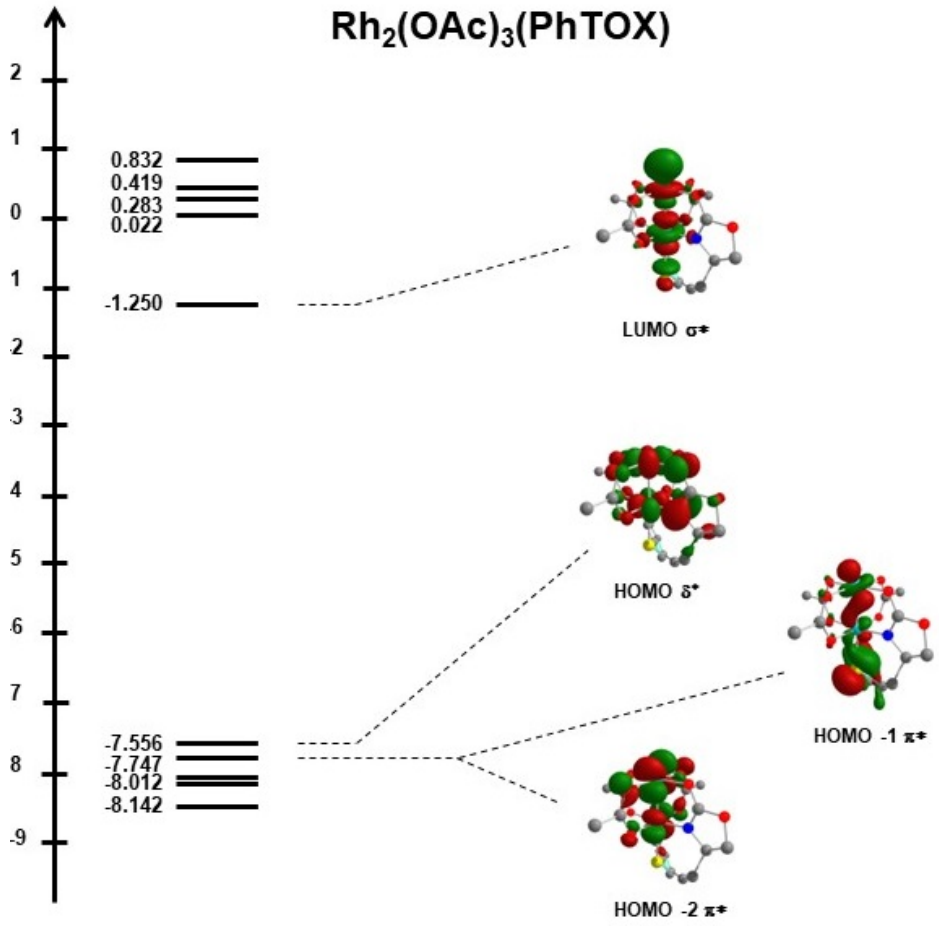

Figure 24: Molecular orbital diagram of carbenoid formed from 107 and 40

Vita

Anthony D. Abshire was born in Gulfport, Mississippi in 1985 to parents Mark and Diane Abshire. He graduated from Pearl High School in Pearl, Mississippi in 2003. After high school Anthony worked the next 7 years in various fields of construction, mainly focused around welding and sheet metal. In 2010, Anthony began his college career at Mississippi Gulf Coast Community College where he received an associate's degree. He then transferred to The University of Southern Mississippi in 2013 where he obtained his American Chemical Society certified Bachelor of Science with a minor in mathematics. In the Donahue Research Group, he worked as an undergraduate research assistant on the total synthesis of Palhinine A under the advisement of Dr. Matthew Donahue. He won multiple awards for his research during this time: 1st place at Southeastern Undergraduate Research Conference, 1st place at the University of Southern Mississippi's Undergraduate Research Symposium, and 2nd place at the Mississippi Academy of Science's Research Symposium. He was also awarded the Eagle SPUR research grant to help fund his research project.

In 2016, Anthony began his graduate school career at the University of Tennessee where he studied organic chemistry under the advisement of Dr. Ampofo Darko. During his time as a graduate student, Anthony mentored many undergraduate researchers and presented work at the Southeastern Regional Meeting of the American Chemical Society. He first authored a review paper and contributed work toward two other publications. He also has two other first author publications in preparation on his work from his graduate career.